

The Novel Role of Epidermal Growth Factor (EGF) in the regulation of ion channels in the Calu-3 submucosal cell line

Craig S. Clements BSc MSc

A Thesis Presented to
Faculty of Medicine and Health Sciences, Norwich Medical School
University of East Anglia

In Fulfilment of the Requirements of the University of East Anglia for the Degree of
Doctor of Philosophy

September 2012



© This copy of thesis has been supplied on the condition that anyone who consults it is understood to recognise that its copyright rests with the author and that no quotation from the thesis, nor any information derived from it, may be published without the author's prior written consent.

Declaration

I hereby declare that the work in this thesis is my own work and effort and that it has not been submitted anywhere for any award. Where other sources of information have been used, they have been acknowledged.

Signature: 

Date: 6th September, 2012

Abstract

Cystic fibrosis transmembrane conductance regulator (CFTR) is a cell membrane bound chloride ion channel regulated by cyclic AMP-dependent phosphorylation and levels of intracellular ATP. Mutations in this channel, such as the common deletion of phenylalanine at residue 508 (CFTR Δ F508), leads to a decrease in chloride transport seen in the disease condition cystic fibrosis (CF). The mutant CFTR is not processed in the normal way and consequently not delivered to the cell membrane. Currently, the effect of growth factors such as epidermal growth factor (EGF) on ion transport in the airway has not been previously researched and is consequently unknown. Therefore the aim of this thesis is to determine (i) if EGF has an effect on ion transport in the submucosal cell line Calu-3, (ii) what the mechanisms are behind this, and (iii) if the effect of EGF was due to induction of gelatinase activity or a transactivation process. Functional investigations looking at ion transport were carried out by using short circuit current. This technique was complemented by traditional molecular biology techniques such as RT-PCR, Western blotting, flow cytometry and gelatin zymography. The level of EGF, a potent inducer of gelatinases, is known to be elevated in the lungs during tissue repair in CF. Calu-3 cells preincubated with EGF on the basolateral membrane increased initial current at one hour via a EGFR-PI3K-PKC- δ -KCNN4/KCNQ1 signalling pathway. Similarly, preincubation with EGF also decreased forskolin induced short circuit current compared to untreated monolayers at 1 to 3 hours, with a recovery at 24 hours. The decreases were found to be dependent on the activation of KCNQ1 since chromanol 293B, a specific inhibitor for KCNQ1, restored the short circuit current back to untreated levels. Stimulation of the β_2 adrenergic receptors with salbutamol were not reduced using metalloproteinase inhibitor, GM-6001 and EGFR inhibitor, AG1478. This suggested that stimulation of β_2 adrenergic receptors does not lead to transactivation of EGFR via activation of sheddases and the release of EGF ligand. β_3 adrenergic receptors are present in Calu-3, but produce negligible currents when stimulated. It was concluded that EGF induced potassium channel activation led to a change in chloride driving force. This activation of potassium channels has previously been linked to wound repair in the airway during disease. The implications of this study suggest that manipulation of the

EGF signalling pathway and / or potassium channel activity in the lungs may be beneficial in disease conditions such as CF for increasing chloride transport.

Papers and Conference Abstracts

The following is a list of published works resulting from the work in this thesis.

Papers:

Clements CS and Winpenny JP (2012) *EGF activates basolateral potassium channels and increases chloride driving force in the Calu-3 cell line.* J Physiol (In prep)

Clements CS and Winpenny JP (2012) *EGF inhibits stimulated CFTR short circuit current in the Calu-3 cell line.* J Physiol (In prep)

Conference Abstracts:

Clements CS, Gavrilovic J, Winpenny JP (2010) *Epidermal growth factor (EGF) increases matrix metalloproteinase (MMP) activity and cystic fibrosis transmembrane conductance regulator (CFTR) chloride current in the Calu-3 cell line.* Proc Physiol Soc 19, PC53.

Abstract accepted and presented as a poster to The Physiological Society at the Physoc Manchester 2010 conference. Shortlisted by The Physiological Society for best poster prize.

Clements CS and Winpenny JP (2012) *EGF activates basolateral potassium channels in the Calu-3 cell line.* Proc Physiol Soc 27, PC98.

Abstract accepted and presented as a poster to The Physiological Society at the Physoc Edinburgh 2012 conference.

Table of Contents

ABSTRACT	3
PAPERS AND CONFERENCE ABSTRACTS	5
TABLE OF CONTENTS	6
LIST OF FIGURES	12
LIST OF TABLES.....	14
LIST OF ABBREVIATIONS.....	15
ACKNOWLEDGMENTS.....	17
CHAPTER 1 LITERATURE REVIEW	18
1.1 Types of Chloride Channels.....	18
1.1.1 Ligand-gated chloride channels.....	18
1.1.1.1 GABA _A receptor (GABA _{AR}).....	18
1.1.1.2 GABA _A -rho receptor (GABA _A -p).....	18
1.1.1.3 Glycine receptor (GlyR)	19
1.1.2 Voltage gated chloride channels (VGCLC).....	19
1.1.3 Volume-sensitive chloride channels (VSCC).....	20
1.1.4 Stretch-activated chloride channels.....	21
1.1.5 Calcium activated chloride channel (CaCC) candidates	21
1.1.5.1 Chloride channel, Calcium-activated (CLCA)	21
1.1.5.2 Bestrophins (BESTs).....	22
1.1.5.3 Anoctamins (ANOs)	24
1.1.6 Cystic fibrosis transmembrane conductance regulator (CFTR)	26
1.1.6.1 Domain Structure of CFTR	26
1.1.6.2 Gating of CFTR is controlled by phosphorylation by protein kinases	28
1.1.6.3 Regulation via β_2 adrenergic receptor.....	29
1.1.6.4 Regulation via β_1 and β_3 adrenergic receptors	30
1.1.6.5 Regulation via G Protein Coupled Receptors (GPCRs)	30
1.2 Physiology of the Lung.....	32
1.2.1 Lung structure	32
1.2.2 Lung function	34
1.2.3 Underlying tissue of the lung	34
1.2.4 Calu-3 cells as a model for lung ion transport	36
1.2.4.1 Channels present in Calu-3	36
1.3 Cystic Fibrosis (CF).....	39
1.3.1 Cystic Fibrosis in the lung.....	39

1.3.1.1	High-salt hypothesis.....	40
1.3.1.2	Low-volume hypothesis	40
1.3.2	Cystic fibrosis in the pancreas.....	41
1.3.3	Cystic fibrosis and the reproductive system	42
1.3.3.1	Congenital absence of the vas deferens (CAVD)	42
1.3.3.2	Congenital absence of the uterus and vagina (CAUV).....	42
1.3.4	Current treatments available for cystic fibrosis.....	43
1.3.5	Treatments currently in development for cystic fibrosis	43
1.3.5.1	Gene therapy	43
1.3.5.2	CFTR correctors and potentiators.....	44
1.3.5.3	Alternative ion channel therapy.....	45
1.4	Matrix Metalloproteinases: A potential pharmacological target for treating Cystic Fibrosis?	
49		
1.4.1	What are matrix metalloproteinases (MMPs)?	49
1.4.2	Subfamilies of matrix metalloproteinases	52
1.4.2.1	Matrilysins	53
1.4.2.2	Collagenases and Stromelysins.....	53
1.4.2.3	Gelatinases	53
1.4.2.4	Membrane-type Matrix Metalloproteinases (MT-MMPs).....	53
1.4.3	General regulation of matrix metalloproteinases	54
1.4.3.1	Tissue Inhibitors of Metalloproteinases (TIMPs).....	54
1.4.3.2	Subfamilies of TIMPs	55
1.4.3.3	Synthetic inhibitors	55
1.4.4	MMP Regulation in Airway Epithelial cells.....	56
1.4.5	Role of MMPs under specific disease conditions	58
1.4.5.1	Cystic Fibrosis.....	58
1.4.5.2	Asthma	59
1.4.5.3	Chronic Obstructive Pulmonary Disease	59
1.4.5.4	Pancreatitis	60
1.4.6	Known interactions of MMPs with ion channels	61
1.4.6.1	Cystic fibrosis transmembrane conductance regulator (CFTR).....	61
1.4.6.2	Chloride channel, Calcium activated (CLCA)	61
1.4.6.3	Calcium activated chloride channels (CaCC)	62
1.4.6.4	CIC Proteins	62
1.4.6.5	Potassium ion channels	63
1.5	Epidermal Growth Factor: Inducer of Matrix Metalloproteinases	64
1.5.1	EGF and EGFR in lung disease	66
1.5.2	EGF and potassium ion transport in other tissues.....	67
1.5.3	Potassium channels in the lung	69
1.6	Purpose of Study, Hypothesis and Aims	70

CHAPTER 2	MATERIALS AND METHODS	72
2.1	Cell culture	72
2.1.1	Preparation of culture media.....	72
2.1.2	Initial seeding and maintenance	72
2.1.3	Trypsinization and splitting procedure	73
2.1.4	Freezing down procedure	73

2.2 Reverse Transcriptase Polymerase Chain Reaction (RT-PCR)	74
2.2.1 RNA extraction.....	74
2.2.2 Preparation of samples for reverse transcription.....	75
2.2.3 Preparing the ethidium bromide gel.....	79
2.2.4 Imaging the gels and densitometry.....	79
2.2.5 Band extraction and sequencing	79
2.2.6 Obtaining and solubilising the gel slice.....	79
2.2.7 Loading sample into spin columns	80
2.2.8 Elution of DNA	81
2.3 Western Blotting.....	82
2.3.1 Preparation of solutions	82
2.3.2 Protein extraction and quantification	82
2.3.2.1 RIPA buffer extraction	82
2.3.2.2 Hot SDS buffer extraction	83
2.3.2.3 NP-40 buffer extraction	83
2.3.3 Protein separation.....	83
2.3.4 Protein Transfer	84
2.3.4.1 Wet transfer technique	84
2.3.4.2 Semi-dry technique	84
2.3.5 Antibody treatment.....	85
2.3.6 Signal detection	85
2.4 Flow Cytometry.....	86
2.4.1 Cell counting	86
2.4.2 Cell viability with propidium iodide	87
2.4.3 Cell growth and serum starvation	87
2.5 Gelatin Zymography.....	88
2.5.1 Preparation of solutions	89
2.5.2 Preparing samples.....	90
2.5.3 Running the samples.....	90
2.5.4 Staining the gel	90
2.6 Short Circuit Current.....	91
2.6.1 Tissue culturing.....	91
2.6.2 Preparation of Ussing chamber	91
2.6.3 Compensating for voltage and fluid resistance.....	94
2.7 How the data were analysed	96
2.8 Experimental Design	96
2.9 Statistical Analysis.....	97
CHAPTER 3 FUNCTIONAL CHARACTERISATION AND GENE EXPRESSION OF CL⁻ CHANNELS IN THE CALU-3 CELL LINE	99
3.1 Introduction.....	99
3.2 Results.....	100
3.2.1 Determining transepithelial resistance.....	100

3.2.2	Calu-3 Vehicle Controls	101
3.2.3	Forskolin characterisation in Calu-3	103
3.2.4	UTP Characterisation in Calu-3	106
3.2.5	Endogenous levels of chloride channel gene and protein expression in three cell lines	109
3.2.5.1	CFTR is expressed in Calu-3 cells.....	109
3.2.5.2	BEST genes are expressed in the Calu-3 cell line	109
3.2.5.3	Anoctamin genes are expressed in epithelial cell lines	111
3.2.6	CFTR fragments detected in Calu-3 cells.....	113
3.2.6.1	BEST1 protein is expressed in the Calu-3 cell line.....	114
3.3	Discussion	115
3.3.1	Forskolin responses are biphasic and sustained.....	115
3.3.2	CFTR regulatory domain fragments detected in Calu-3 cells.....	116
3.3.3	UTP responses were transient and dependent on basolateral potassium channels	116
3.3.4	Bestrophins are expressed in Calu-3, CFPAC and A549.....	117
3.3.5	Anoctamins are expressed in Calu-3, CFPAC and A549.....	118
CHAPTER 4	INDUCTION OF METALLOPROTEINASES AND THEIR EFFECT	
ON SHORT CIRCUIT CURRENT.....		120
4.1	Introduction.....	120
4.2	Results.....	122
4.2.1	Determining Optimal Cell Growth using Carboxyfluorescein succinimidyl ester (CFSE)....	122
4.2.2	Calu-3 cells are viable with PMA incubation.....	126
4.2.3	Detecting gelatinase function with gelatin zymography.....	129
4.2.3.1	PMA incubation for 24 and 48 hours induces gelatinase function	129
4.2.3.2	PMA and EGF incubation for 24 and 48 hours induces gelatinase function	131
4.2.3.3	PMA and EGF incubation with GM-6001 for 24 and 48 hours reduces gelatinase function	133
4.2.4	MMP-2 is detected in Calu-3 conditioned media	135
4.2.5	Acute addition of GM-6001 does not affect I_{SC} across Calu-3 monolayers.....	136
4.2.6	Negligible GM-6001 acute response in A549 monolayers	138
4.2.7	Acute addition of recombinant MMP-2 does not decrease I_{SC} across Calu-3 monolayers .	139
4.2.8	Negligible recombinant MMP-2 response in A549 monolayers.....	140
4.2.9	Acute addition of anti-MMP-2 does not affect I_{SC} across Calu-3 monolayers	141
4.2.10	Negligible anti-MMP-2 and anti-IgG response in A549	143
4.2.11	Acute addition EGF increases I_{SC} across Calu-3 monolayers	145
4.2.12	Negligible EGF response in A549 monolayers	147
4.2.13	Blocking Potassium Channels and EGF acute addition in Calu-3 monolayers	148
4.2.14	Blocking Potassium Channels and EGF acute addition in A549 monolayers.....	150
4.2.15	A549 Vehicle Controls	152
4.2.16	Negligible Forskolin response in A549 monolayers	153
4.3	Discussion	154
4.3.1	Calu-3 cells can grow at high seeding densities.....	154
4.3.2	Calu-3 cells are viable in low serum	155
4.3.3	MMP-2 and 9 are functional in the conditioned media of Calu-3.....	155
4.3.4	MMP-2 protein is present in Calu-3 and A549 cells	156
4.3.5	Effect of MMP-2 and EGF on I_{SC}	156

CHAPTER 5 EFFECTS OF EGF TREATMENT ON INITIAL SHORT CIRCUIT CURRENT 159

5.1 Introduction.....	159
5.2 Results.....	160
5.2.1 Addition of Epidermal Growth Factor (EGF) to the Calu-3 monolayers leads to an increase in initial I_{SC}	160
5.2.2 The EGF stimulated increase in initial I_{SC} is prevented by inhibition of the EGF receptor (EGFR) 162	
5.2.3 Protein kinase inhibitors prevent EGF-stimulated increases in initial I_{SC}	163
5.2.4 Potassium channel blockers reduce EGF-stimulated increases in initial I_{SC}	165
5.2.5 The potassium channels KCNQ1, KCNA2, KCNA3 and KCNN4 are expressed in the Calu-3 cell line 167	
5.2.6 U0126 pretreatment reduces initial EGF stimulated I_{SC} in EGF preincubated Calu-3 monolayers	168
5.3 Discussion	170
5.3.1 EGF increases initial I_{SC} in intact Calu-3 monolayers.....	170
5.3.2 EGF increases initial I_{SC} in Calu-3 via PI3K-PKC- δ -KCNN4/KCNQ1 dependent pathway .170	
5.3.3 EGF increases in initial I_{SC} in intact Calu-3 monolayers are abolished by U0126 pretreatment.....	175
5.3.4 Potassium channels are expressed in Calu-3	175

CHAPTER 6 EFFECTS OF EGF TREATMENT ON UTP RESPONSE..... 176

6.1 Introduction.....	176
6.2 Results.....	177
6.2.1 Addition of Epidermal Growth Factor (EGF) to the Calu-3 monolayers leads to an increase in UTP-stimulated I_{SC}	177
6.2.2 Permeabilisation removes EGF-induced UTP stimulated I_{SC} in Calu-3	178
6.2.3 EGF treatment and chloride channel gene expression in Calu-3 cells.....	180
6.2.4 EGF treatment and chloride channel gene expression in Calu-3 cells.....	184
6.3 Discussion	186
6.3.1 EGF increases intracellular Ca^{2+} over 24 hours and UTP induced CaCC activation	186
6.3.2 EGF elevates UTP induced CaCC responses via Ca^{2+} activated potassium channels	187
6.3.3 Effect of EGF on chloride channel transcription	189
6.3.4 BEST1 protein is present in Calu-3 cells	189

CHAPTER 7 EFFECTS OF EGF ON FORSKOLIN STIMULATION

7.1 Introduction.....	190
7.2 Results.....	193
7.2.1 EGF preincubation decreases forskolin response in intact Calu-3 monolayers.....	193
7.2.2 EGFR inhibition does not prevent EGF-induced decreases in forskolin stimulated I_{SC}	195
7.2.3 Protein kinase inhibitors do not prevent EGF-induced decreases in forskolin stimulated I_{SC} 196	
7.2.4 Chromanol 293B rescues EGF-induced decreases in forskolin stimulated I_{SC}	198

7.2.5	U0126 prevents recovery of EGF induced decreases in forskolin stimulated I_{SC} at 24 hours 200	
7.2.6	Does EGF work via transactivation of the β_2 adrenergic receptor?.....	202
7.2.7	β_3 adrenergic receptor - a minor regulator of ion transport in Calu-3?.....	205
7.2.8	How is the β_3 adrenergic receptor regulated in Calu-3?.....	207
7.2.9	Beta Receptors 1, 2 and 3 are expressed in the Calu-3 cell line	209
7.3	Discussion	210
7.3.1	EGF pretreatment suppresses forskolin stimulation in Calu-3 monolayers	210
7.3.2	Chromanol 293B pretreatment restores forskolin response in EGF treated Calu-3 monolayers	212
7.3.3	The EGF induced decrease in forskolin stimulated I_{SC} at 24 hours is blocked by U0126 ..	213
7.3.4	EGFR transactivation via stimulation of β_2 adrenergic receptor does not occur in Calu-3 monolayers	213
7.3.5	Adenylate cyclase and PI3K blockers prevent β_3 adrenergic receptor induced ion transport in Calu-3 monolayers	214
7.3.6	Beta adrenergic receptors are expressed in Calu-3.....	214
CHAPTER 8 FINAL DISCUSSION		215
8.1	Overview.....	215
8.2	Summary of Findings.....	216
8.2.1	Characterisation of chloride channels in the Calu-3 cell line.....	216
8.2.2	Effect of MMPs on ion transport in the Calu-3 cell line.....	217
8.2.3	EGF signalling increases chloride driving force in the Calu-3 cell line	217
8.2.4	EGF signalling increases UTP response in the Calu-3 cell line	218
8.2.5	Reduction in stimulated I_{SC} after EGF treatment in the Calu-3 cell line	219
8.2.6	Effect of EGF in the Calu-3 cell line is independent of a transactivation process	220
8.2.7	β_3 agonists have negligible effects on Calu-3 monolayers.....	221
8.3	Concluding Remarks	222
8.4	Future Work	222
REFERENCES		225

List of Figures

Figure 1.1 – CFTR open and closed states.	27
Figure 1.2 – Regulation of CFTR via G Protein Coupled Receptors.	31
Figure 1.3 – The physiology of the human lungs.	33
Figure 1.4 – A general overview of the physiology of the tissues on and near the surface of the lung.	35
Figure 1.5 – Overview of Ion transport in Calu-3 cells.	37
Figure 1.6 – Schematic depicting the low volume hypothesis of cystic fibrosis.	41
Figure 1.7 – The domain structure of the matrix metalloproteinases.	52
Figure 1.8 – The interactions leading to the expression of MMP-2 as a result of Collagen I and Thrombin.	57
Figure 1.9 – The interplay between CIC-7, Cathepsin K and MMPs during the resorption of calcified bone and degradation of decalcified bone.	62
Figure 1.10 – Schematic depicting MMP-9 induction via EGF, HB-EGF and TGF- α	64
Figure 1.11 – The effect of neutrophil elastase on lung inflammation.	66
Figure 1.12 – The role of EGF on chloride secretion in the gut.	68
Figure 2.1 – Ussing chamber schematic.	93
Figure 2.2 – Schematic of how to set the voltage clamp.	94
Figure 2.3 – Block diagram of the apparatus used during an Ussing chamber investigation.	95
Figure 3.1 – Calu-3 transepithelial resistance readings.	101
Figure 3.2 – Vehicle control data for Calu-3 monolayers.	102
Figure 3.3 – Characterisation of forskolin response across Calu-3 monolayers.	105
Figure 3.4 – Characterisation of UTP response across Calu-3 monolayers.	107
Figure 3.5 – Characterisation of UTP response across permeabilised Calu-3 monolayers.	108
Figure 3.6 – Endogenous levels of CFTR message in the Calu-3 cell line.	109
Figure 3.7 – Endogenous levels of bestrophin message in the Calu-3, CFPAC and A549 cell lines.	110
Figure 3.8 – Endogenous levels of expression of anoctamin message in Calu-3, CFPAC and A549 cells.	112
Figure 3.9 – Characterisation of CFTR protein expression in the Calu-3 cell line.	113
Figure 3.10 – Characterisation of BEST1 protein expression in the Calu-3 cell line.	114
Figure 4.1 – How the CFSE fluorescence intensity decreases with cell growth.	122
Figure 4.2 – Calu-3 growth is unaffected by seeding density.	124
Figure 4.3 – Calu-3 cell growth is largely unaffected by low / no serum media.	125
Figure 4.4 – Representation of propidium iodide spectra.	126
Figure 4.5 – A549 cells are viable in the presence of PMA over a period of time.	127
Figure 4.6 – Calu-3 cells are viable in the presence of PMA over a period of time.	128
Figure 4.7 – Gelatinase activity is induced by PMA in A549 and Calu-3 cells.	130
Figure 4.8 – Gelatinase activity is induced by PMA and EGF in A549 cells.	131
Figure 4.9 – Gelatinase activity is induced by PMA and EGF in Calu-3 cells.	132
Figure 4.10 – PMA and EGF induced increases in gelatinase activity are inhibited by GM-6001 in A549 cells.	134
Figure 4.11 – Gelatin Zymography of EGF-treated A549 cells inhibited by GM-6001 after 48 hours.	135
Figure 4.12 – Western Blot depicting the presence of MMP-2 within two cell lines using the RIPA extraction method and conditioned media.	135
Figure 4.13 – GM-6001 acute response does not affect I_{SC} across Calu-3 monolayers.	137
Figure 4.14 – Negligible GM-6001 acute response in A549 monolayers.	138
Figure 4.15 – Recombinant MMP-2 acute response does not affect I_{SC} across Calu-3 monolayers.	139
Figure 4.16 – Negligible recombinant MMP-2 response in A549 monolayers.	140
Figure 4.17 – Anti-MMP-2 acute response does not affect I_{SC} across Calu-3 monolayers.	142

Figure 4.18 – Negligible anti-MMP-2 response in A549.	144
Figure 4.19 – EGF acute response increases I_{SC} across Calu-3 monolayers.	146
Figure 4.20 – Negligible EGF response in A549 monolayers.	147
Figure 4.21 – Blocking potassium channels and EGF acute response in Calu-3 monolayers.	149
Figure 4.22 – Negligible EGF response in barium chloride treated A549 monolayers and permeabilised A549 monolayers.	151
Figure 4.23 – Vehicle control data for A549 monolayers.	152
Figure 4.24 – Negligible forskolin response in A549 monolayers.	153
Figure 5.1 – EGF preincubation for 1 hour significantly increases initial I_{SC} in intact, but not permeabilised, Calu-3 monolayers.	161
Figure 5.2 – EGFR inhibitor AG1478 reduces EGF induced increases in starting current.	162
Figure 5.3 – Kinase inhibitors reduce EGF induced increases in starting current.	164
Figure 5.4 – Potassium channel inhibitors reduce EGF induced starting current.	166
Figure 5.5 – KCNQ1, KCNA2, KCNA3 and KCNN4 channel expression in Calu-3 cells	167
Figure 5.6 – ERK inhibitor U0126 reduces EGF induced starting current.	169
Figure 5.7 – Proposed signalling pathways involved in the regulation of chloride transport via EGF.	174
Figure 6.1 – Addition of EGF to the Calu-3 monolayers leads to an increase in UTP-stimulated I_{SC}	178
Figure 6.2 – Permeabilisation removes UTP induced I_{SC} in Calu-3.	179
Figure 6.3 – Bestrophin and CFTR channel expression in response to EGF treatment in Calu-3 cells.	181
Figure 6.4 – Anoctamin expression in response to EGF treatment in Calu-3 cells.	182
Figure 6.5 – Densitometry of chloride channel mRNA in response to EGF preincubation normalised to β -actin.	183
Figure 6.6 – Mean fold change in mRNA expression of chloride channels compared to the unstimulated mRNA baseline.	183
Figure 6.7 – Characterisation of CFTR protein expression in the Calu-3 cell line.	184
Figure 6.8 – BEST1 protein expression is not affected by EGF treatment.	185
Figure 6.9 – Proposed model of EGF regulation of UTP response in Calu-3 cells.	188
Figure 7.1 – Hypothesis of β_2 adrenergic receptor stimulation leading to transactivation of the EGF receptor by sheddases.	192
Figure 7.2 – Short term EGF preincubation decreases forskolin response in intact Calu-3 monolayers.	194
Figure 7.3 – EGFR inhibitor AG1478 does not significantly change EGF induced decreases in forskolin stimulated I_{SC} across Calu-3 monolayers.	195
Figure 7.4 – Kinase inhibitors do not significantly change EGF induced decreases in forskolin stimulated I_{SC} across Calu-3 monolayers.	197
Figure 7.5 – Potassium channel inhibitor chromanol 293B rescues EGF induced decreases in forskolin stimulated I_{SC} across Calu-3 monolayers back to control levels.	199
Figure 7.6 – U0126 further decreases EGF induced decreases in forskolin stimulated I_{SC}	201
Figure 7.7 – Transactivation by the β_2 adrenergic receptor does not occur in Calu-3 monolayers.	204
Figure 7.8 – Dose response to determine of the maximal response to CGP-12177.	206
Figure 7.9 – β_3 adrenergic receptor is potentially regulated by adenylate cyclase and PI3K in Calu-3 cells.	208
Figure 7.10 – Beta receptor expression in Calu-3 cells, showing expression of all three receptors.	209
Figure 7.11 – Proposed model of the effect of EGF treatment on adenylate cyclase in Calu-3 cells.	211
Figure 8.1 – Model for the transmodulation of the EGFR receptor.	223

List of Tables

Table 1.1 – Alternative gene names for bestrophins.	22
Table 1.2 – Alternative gene names for anoctamins.	24
Table 1.3 – Matrix metalloproteinases, their known substrates and tissue expression in humans.	50
Table 1.4 – TIMP summary table.	54
Table 2.1 – Concentration of PCR reaction mix components	75
Table 2.2 – Chloride channel primer information and sequences.	77
Table 2.3 – Primer information – beta adrenergic receptors and potassium channels	78
Table 2.4 – Solutions required for Western blotting.	82
Table 2.5 – Antibodies used for Western blotting.	85
Table 2.6 – Table of solutions required for gelatin zymography.	89
Table 2.7 – Summary of compounds used and their appropriate chambers.	92

List of Abbreviations

This list provides the meanings to some commonly used abbreviations:

16HBE	Human bronchial epithelial cell line
A549	Human alveolar epithelial cell line
AKT	Protein Kinase B
ATP	Adenosine-5'-triphosphate
BAL	Bronchoalveolar lavage
ANO	Anoctamin, chloride channel
β_1 AR	Beta 1 adrenergic receptor
β_2 AR	Beta 2 adrenergic receptor
β_3 AR	Beta 3 adrenergic receptor
BEST	Bestrophin, chloride channel
Calu-3	Lung epithelial cell line derived from adenocarcinoma
cAMP	Cyclic adenosine monophosphate
CBD	Collagen binding domain
CF	Cystic fibrosis
CFPAC	Cystic fibrosis pancreatic adenoma cell line
CFTR	Cystic fibrosis transmembrane conductance regulator, chloride channel
cGMP	Cyclic guanosine monophosphate
CIC	Voltage gated chloride channel
CaCC	Calcium activated chloride channel
COPD	Chronic obstructive pulmonary disease
ECM	Extracellular Matrix
EGF	Epidermal growth factor
EGFR	Epidermal growth factor receptor
ERK	Extracellular signal-regulated kinase
FEV ₁	Forced Expiration Volume in 1 second
GlyR	Glycine receptor
GPCR	G Protein coupled receptor
HEXXH	Zn ²⁺ Binding motif found in the catalytic region of MMPs
I _{sc}	Short Circuit Current

JNK	c-Jun N-terminal kinase
KCNN4	Potassium intermediate/small conductance calcium-activated channel, subfamily N, member 4
KCNA2	Potassium voltage-gated channel subfamily A member 2
KCNA3	Potassium voltage-gated channel, shaker-related subfamily, member 3
KCNQ1	Potassium voltage-gated channel, KQT-like subfamily, member 1
MAPK	Mitogen-activated protein kinase
MEK	Mitogen-activated protein kinase kinase
MMP	Matrix Metalloproteinase
MT-MMP	Membrane-Type Matrix Metalloproteinase
NF- κ B	Nuclear factor-kappa B
NO	Nitric Oxide
NOS2	Inducible nitric oxide synthase
PEF	Peak expiratory flow rate
PI3K	Phosphatidylinositol 3-kinase
PKA	Protein kinase A
PKC	Protein kinase C
PMA	Phorbol 12-myristate 13-acetate
PTX	Pertussis toxin, G _{i/o} antagonist
RRKR	Furin recognition sequence (Arg-Arg-Lys-Arg)
RT-PCR	Reverse-transcriptase Polymerase Chain Reaction
R _{TE}	Transepithelial resistance
SAP	Severe acute pancreatitis
siRNA	Small interfering RNA
TCIPA	Tumor cell-induced platelet aggregation
TGF- α	Transforming growth factor alpha
TGF- β_1	Transforming growth factor beta 1
TIMP	Tissue Inhibitor of Metalloproteinases
TNF- α	Tumour Necrosis Factor alpha
TZD	Thiazolidinedione, PPAR γ activator
UTP	Uridine-5'-triphosphate
V _{TE}	Transepithelial voltage

Acknowledgments

I wish to acknowledge the Norfolk and Norwich Bicentenary Trust for funding this work. I would like to thank my supervisory team, John Winpenny, Jelena Gavrilovic and Darren Sexton, for supervising me during my time at the University of East Anglia.

I would also wish to give many thanks to Matthew Jefferson for his general advice throughout my time at the University, and training with Western blotting. I would also like to thank Kevin McDermott for his help with zymography and encouragement. I would like to thank Richard Kelwick for training me to use the nanodrop and for general encouragement. I'd like to thank Kirsty Kirk for training me in RT-PCR and Western Blotting, and Megan Murray for her help to get me started with zymography. I would also like to thank Roberto Pierini, Ursula Rodgers, Rebecca Roberts, Rose Davidson, Julie Decock and Eleanor Cottam for their general advice and help. I wish to also thank Gabriel Mutungi and Muhammad Hamdi Mahmood for their invaluable technical advice on the EGF and beta receptor signalling pathways and help with experimental brainstorming.

I would also like to give special thanks to Anthony de Mel and Nikhil Awatade for additional support and friendship in the lab. I would like to give special thanks to my fiancée Caroline Searle, for supporting me during the many difficult times, and my mother Joanne Clements and former supervisor Ian Kill and Joanna Bridger of Brunel University, without which I would not have embarked on this research.

Chapter 1 Literature Review

1.1 Types of Chloride Channels

1.1.1 Ligand-gated chloride channels

Ligand-gated chloride channels are a type of ionotropic receptor (Hartmann *et al.*, 2004) that is transmembrane. They respond to the binding of a chemical messenger by opening and closing. There are several types of ligand-gated chloride channels, which include γ -Aminobutyric acid (GABA) gated chloride channels and the Glycine receptor (GlyR). These channels are members of the Cys-loop super-family of similarly structured ligand-gated ion channels (Jansen *et al.*, 2008).

1.1.1.1 $GABA_A$ receptor ($GABA_{AR}$)

The $GABA_A$ receptor ligand is γ -aminobutyric acid, also known as GABA. Once the receptor binds up to two GABA molecules, it can allow chloride ions through its pore, which typically has the function of hyperpolarising neurons (Herbison & Moenter, 2011). This hyperpolarisation results in a reduction in the chance of an action potential occurring via an inhibition of neurotransmission. In humans, the $GABA_A$ receptor is multimeric, consisting of five protein subunits, which can comprise α , β , γ , δ , ϵ , π and θ ; which in turn have various different isoforms. There are six types of α subunit isoforms (GABRA1, GABRA2, GABRA3, GABRA4, GABRA5 and GABRA6), three types of β subunits (GABRB1, GABRB2, GABRB3), three types of γ subunits (GABRG1, GABRG2, GABRG3) as well as a δ subunit (GABRD), an ϵ subunit (GABRE), a π subunit (GABRP), and finally a θ subunit (GABRQ). To result in a $GABA_A$ receptor, these subunits need to combine at least an α and a β subunit (Hevers & Luddens, 1998).

1.1.1.2 $GABA_A$ -rho receptor ($GABA_A$ - ρ)

The $GABA_A$ -rho receptor has a very similar structure to the $GABA_A$ receptor, except that it comprises a combination of $\rho 1$ (GABRR1), $\rho 2$ (GABRR2) and $\rho 3$ (GABRR3) subunits. Functionality-wise, the $GABA_A$ -rho receptor induced chloride responses are more sustained, but slower to initiate than that of the response from $GABA_A$ receptor (Enz & Cutting, 1998).

1.1.1.3 Glycine receptor (GlyR)

The Glycine receptor accepts the amino acid and neurotransmitter glycine in order to bring about chloride current. It is most prominent in the central nervous system. Like the GABA-gated chloride channels, the glycine receptor itself consists of five subunits, each containing α helical transmembrane segments around a central pore. There are four isoforms of the α -subunit (α_{1-4}) of the receptor called GLRA1, GLRA2, GLRA3 and GLRA4, and one form of the β -subunit called GLRB. The mature heteromeric protein consists of either three α_1 subunits and two β -subunits (Kuhse *et al.*, 1993), or four α_1 subunits and one β subunit (Kuhse *et al.*, 1995).

1.1.2 Voltage gated chloride channels (VGCLC)

Voltage gated chloride channels consist of nine members in mammals (Jentsch *et al.*, 1995). They can function either as Cl^- channels at the plasma membrane or as H^+/Cl^- exchangers in intracellular organelles (Dutzler, 2006). The nine homologues of the CIC family in humans are found at either the cell membrane or in the membranes of intracellular organelles. They are involved in processes such as electrical signalling in muscle, epithelial ion transport and the acidification of intracellular compartments (Jentsch *et al.*, 2005). The CIC family have a diverse array of functions, yet all the family shares a conserved molecular structure. This structure consists of a transmembrane transport domain, followed by a cytoplasmic component that is thought to be a key regulator of channel gating (Jentsch *et al.*, 2005). The first CIC channel, CIC-0, was discovered by expression cloning in *Xenopus* oocytes (Jentsch *et al.*, 1990). The structure of CIC found in *Escherichia coli*, EcCIC, is one of the most studied CICs. Initially proposed based on electrophysiological experiments on CIC-0, the 'double barrelled' structure of the CIC channels is reflected in the dimeric structure of EcCIC (Miller, 1982). The gating of CIC-1 and CIC-2, which are found in muscle, is influenced by voltage, extracellular chloride concentration and pH (Chen & Chen, 2001). The voltage-gating of the transmembrane CICs are thought to be conferred by the permeating chloride ion itself to act as the gating charge (Pusch *et al.*, 1995). This differs from voltage dependent cation channels where voltage is generally sensed by the protein domain (Dutzler, 2007). The cytoplasmic domains of the CIC family share conserved molecular structures that contain a pair of cystathionine beta synthase (CBS) motifs. Enzymes, kinases and transmembrane transporters frequently contain

similar motifs that are found as building blocks for regulatory ligand binding domains (Ignoul & Eggermont, 2005). The amino acid length of the cytoplasmic domains of the CIC family varies from 150 residues in CIC-Ka found in the kidney, to 390 residues in CIC-1 found in muscle. This variation is largely due to the linker region that connects the two CBS motifs, and the C-peptide that consists of residues that follow the second CBS motif (CBS2) (Meyer & Dutzler, 2006). In some CIC family members, there are recognition sites for kinases in the linker region, and that channel function is altered by phosphorylation. Such examples include the phosphorylation of CIC-2 by PKA (Cuppoletti *et al.*, 2004b) and the inactivation of CICs by phosphorylation by germinal center kinase III (GCK-3) (Denton *et al.*, 2005). The linker of the CIC-5 transporter contains a recognition site for ubiquitin ligase, which is important for correct targeting of the protein to intracellular compartments. The recognition site on CIC-5 resembles the PY motif, which is crucial for the endocytosis and degradation of epithelial sodium channels. (Schwake *et al.*, 2001).

1.1.3 Volume-sensitive chloride channels (VS^{CC})

Volume-sensitive chloride channels (VS^{CC}) are also known as volume-regulated chloride channels and volume-activated chloride channels. CIC-3 is thought to be a VS^{CC}. When expressed in NIH/3T3 cells, CIC-3 produced a basally active chloride conductance that resembled that of native volume sensitive anion channels (Duan *et al.*, 2001). Native volume sensitive anion secretion in bovine non-pigmented ciliary epithelial (NPCE) cells could be delayed by CIC-3 antisense treatment (Wang *et al.*, 2000). In human gastric epithelial cells, anti-CIC-3 antibodies eliminated CIC-3 response suggesting that CIC-3 may be volume-sensitive chloride channels (Jin *et al.*, 2003). It has been suggested that CIC-3 may play a role in the cell proliferation of vascular smooth muscle cells, relating to its function as a cell volume regulator (Zhou *et al.*, 2005). However, the hypothesis that CIC-3 is a volume sensitive chloride channel is controversial (Li *et al.*, 2000; Shimada *et al.*, 2000; Stobrawa *et al.*, 2001; Weylandt *et al.*, 2001).

1.1.4 Stretch-activated chloride channels

Stretch-activated chloride channels are also known as swell-activated chloride channels, and have various functions in the cardiovascular system, including vascular wall distension (Remillard *et al.*, 2000). Stretch-activated chloride channels can also be activated in disease conditions such as congestive heart failure (Clemo *et al.*, 1999).

1.1.5 Calcium activated chloride channel (CaCC) candidates

Calcium activated chloride channels (CaCCs) were first described in *Xenopus* oocytes where they have a role in the prevention of polyspermy (Miledi, 1982). More recently, CaCCs have been shown to be expressed in epithelial tissue (Kunzelmann *et al.*, 2007). The molecular identification of CaCCs has been subject to developments occurring from 1995 to the present day.

1.1.5.1 Chloride channel, Calcium-activated (CLCA)

The chloride channel, calcium-activated (CLCA) family consists of 4 types in humans, numbered 1 to 4 (Loewen & Forsyth, 2005). Of significance, CLCA2 is expressed in the trachea and mammary gland (Agnel *et al.*, 1999; Gruber *et al.*, 1999), the testis, prostate and uterus (Agnel *et al.*, 1999), and the nasal epithelium (Mall *et al.*, 2003). Originally cloned from the spleen, CLCA3 has subsequently been found to be expressed in the lung, trachea, mammary gland, and thymus (Gruber & Pauli, 1999), as well as the nasal epithelium (Mall *et al.*, 2003). By examining the amino acid sequence of CLCA channels, they are now known to be metal-dependent hydrolases. Hydrolases, which also bind a Zinc ion to facilitate their catalytic activity, have a similar activity to that of Matrix Metalloproteinases. In fact, CLCA shares some notable homologies to MMPs, such as the conserved HEXXH motif that is responsible for binding the zinc ion. Moreover, there was some dispute as to whether CLCA is either secreted or membrane-bound (Pawlowski *et al.*, 2006). Early electrophysiological data using HEK 293 cells transfected with different CLCA homologues identified a transmembrane current that was activated by ionomycin, a calcium ionophore, and blocked with 4,4'-diisothiocyanostilbene-2,2'-disulphonic acid (DIDS) (Gruber *et al.*, 1998). Later work by Gibson *et al.*, 2005 found no transmembrane domains within hCLCA or mCLCA3 when using a bioinformatics

based approach. It also appeared that CLCAs were globular proteins that could be involved in protein-protein interactions. When expressed in HEK293 cells, hCLCA1 and mCLCA3 were detected in the extracellular medium, and that they were constitutively secreted. Cleavage products of hCLCA can be found in the bronchoalveolar lavage (BAL) fluid of asthmatic patients, further suggesting that CLCAs are in fact secreted proteins and not chloride ion channels (Gibson *et al.*, 2005). Later studies by Mundhenk *et al.*, 2006 explored if CLCA proteins could form chloride channels, or had some other function. The 110 kDa translated product of mCLCA3 is processed in the endoplasmic reticulum into two peptides consisting of a 75 kDa N terminal and a 35 kDa carboxyl terminal. These products are glycosylated and remain associated, and were found to be inside secretory vesicles and not associated with the cell membrane. The secreted products form a soluble complex of two glycoproteins, so it was suggested that the secreted CLCAs may act as mediators of chloride channels instead (Mundhenk *et al.*, 2006).

1.1.5.2 Bestrophins (BESTs)

Bestrophins (BESTs) are candidates for calcium activated chloride channels. These channels were so-named after a disease called Best vitelliform macular dystrophy, which the gene for human BEST1 was found to be linked to, and that mutations in the gene consequently led to the development of this and similar diseases. Whether or not the bestrophins function as chloride channels is still disputed, although it is thought that the bestrophins, like CFTR, are able to regulate other ion channels.

Table 1.1 – Alternative gene names for bestrophins.

Gene name	Alternate name	Abbreviated Names	
Bestrophin 1	vitelliform macular dystrophy 2	BEST1	VMD2
Bestrophin 2	vitelliform macular dystrophy 2-like 1	BEST2	VMD2L1
Bestrophin 3	vitelliform macular dystrophy 2-like 3	BEST3	VMD2L3
Bestrophin 4	vitelliform macular dystrophy 2-like 2	BEST4	VMD2L2

Evidence that bestrophins were chloride channels came from a study by Sun *et al.*, 2002 where human BEST1 was overexpressed in HEK cells that showed an induction of chloride currents. The experiment conducted involved a comparison between untransfected and transfected HEK cells using the patch-clamp technique. With

untransfected cells in a micromolar-free calcium intracellular solution, it was seen that the chloride currents were comparatively small compared to the transfected cells, suggesting that the induced chloride current was calcium dependent. To further support the hypothesis that bestrophins are chloride channels, mutagenesis experiments have been carried out where mutations in residues such as W93H in human BEST2 were shown to significantly alter the gating of the channel (Sun *et al.*, 2002). In terms of the quaternary structure, there is a conflict in the literature in the number of subunits they contain. In one study conducted by Sun *et al.*, 2002, it has been estimated to be either a tetramer or a pentamer by co-transfected human BEST1 with Rim3F4 and myc epitopes, and then immunoprecipitating the result. In another by Stanton *et al.*, 2006, hydrodynamic studies were used to determine that pBest1 was in fact a dimer. Both methods used have limitations, since the overexpression of human BEST1 in Sun's study and the use of detergent in Stanton's may over and under estimate the number of subunits respectively (Stanton *et al.*, 2006). Bestrophins are thought to act as chloride channels. Bestrophin 3 is known to be a calcium ion dependent chloride channel which is sensitive to the chloride inhibitor DIDS (Srivastava *et al.*, 2008). It has been demonstrated that all 4 human bestrophins are able to conduct HCO_3^- ions, and mutations in human BEST1 that are responsible for Best's disease such as Y85H, R92C, and W93C abolish this ability, implying that HCO_3^- conductance is altered in the disease state (Qu & Hartzell, 2008). The activation mechanism of bestrophin 3 is not fully understood, but PI3K inhibitors have been shown to activate the protein (Qu *et al.*, 2010). Human bestrophin 4 has shown to be activated by free Ca^{2+} on the cytoplasmic side of excised patches, thus providing evidence that it is a calcium activated chloride channel (Tsunenari *et al.*, 2006).

1.1.5.3 Anoctamins (ANOs)

In 2008 a step change in our understanding of the molecular candidates for CaCCs occurred (Caputo *et al.*, 2008; Schroeder *et al.*, 2008; Yang *et al.*, 2008). The term 'Anoctamin' derives from the fact that they are anion (AN) selective and have eight (OCT) transmembrane segments (Yang *et al.*, 2008). Shown in Table 1.2, there are 10 known anoctamins, and their expression profiles vary from tissue to tissue. However, it is not currently known which of these are CaCCs (Schreiber *et al.*, 2010).

Table 1.2 – Alternative gene names for anoctamins.

Gene name	Alternate name	Abbreviated Names	
Anoctamin 1	transmembrane protein 16A	ANO1	TMEM16A
Anoctamin 2	transmembrane protein 16B	ANO2	TMEM16B
Anoctamin 3	transmembrane protein 16C	ANO3	TMEM16C
Anoctamin 4	transmembrane protein 16D	ANO4	TMEM16D
Anoctamin 5	transmembrane protein 16E	ANO5	TMEM16E
Anoctamin 6	transmembrane protein 16F	ANO6	TMEM16F
Anoctamin 7	transmembrane protein 16G	ANO7	TMEM16G
Anoctamin 8	transmembrane protein 16H	ANO8	TMEM16H
Anoctamin 9	transmembrane protein 16J	ANO9	TMEM16J
Anoctamin 10	transmembrane protein 16K	ANO10	TMEM16K

ANO1 has splice variants (Caputo *et al.*, 2008; Ferrera *et al.*, 2009; Davis *et al.*, 2010; Manoury *et al.*, 2010) and a closely related analogue, ANO2, which can produce similar calcium activated chloride currents (Schroeder *et al.*, 2008; Pifferi *et al.*, 2009; Stephan *et al.*, 2009; Stohr *et al.*, 2009). In particular, ANO1 has been shown to be important and widely expressed in epithelial tissues such as in the airways. Whole-cell patch-clamp experiments carried out on CFPAC-1 cells stimulated with solution containing 600 nM free Ca^{2+} showed outwardly rectifying currents resembling typical CaCC currents. These currents could be inhibited by anti-ANO1 siRNA. This evidence strongly indicated that ANO1 encodes a Ca^{2+} activated Cl^- channel (Caputo *et al.*, 2008). In contrast, the biophysical properties of hBEST1 do not resemble those of Ca^{2+} activated Cl^- current, suggesting that it is not the molecular identity of CaCCs (Sun *et al.*, 2002; Barro Soria *et al.*, 2009). In knockout mice studies with ANO1, it is seen that calcium dependent conductance is reduced in the airway epithelium, along

with a decrease in mucociliary clearance (Rock *et al.*, 2009). ANO1 expression was first demonstrated in human bronchial epithelial cells (Caputo *et al.*, 2008). The expression of ANO1 has also been found in the interstitial cells of Cajal in gastrointestinal muscles (Gomez-Pinilla *et al.*, 2009; Huang *et al.*, 2009; Hwang *et al.*, 2009; Zhu *et al.*, 2009), airway epithelial cells (Ousingsawat *et al.*, 2009; Rock *et al.*, 2009) and vascular smooth muscle cells (Davis *et al.*, 2010).

An investigation carried out by Duran *et al.*, 2012 concerned itself with identifying which of the ANOs were present at the cell membrane. Expression of ANO3 – ANO7 in HEK293 cells did not generate calcium activated chloride currents using whole cell patch clamping. Only ANO1 and ANO2 are trafficked to the cell membrane when using confocal microscopy. ANO7 in the human prostate is predominantly intracellular. Using chimeric approaches, it was determined that chimeras of ANO1 and ANO5/7 were not trafficked to the cell membrane. These data suggested that these intracellular anoctamins could be endoplasmic reticulum proteins (Duran *et al.*, 2012). Besides ANO1 and ANO2, ANO6 was also found to produce a chloride conductance (Kunzelmann *et al.*, 2012). Moreover, previous studies with human bronchial epithelial cells *in vitro* showed upregulation of UTP induced chloride secretion when preincubated with interleukin-4 (IL-4) for 24 hours. These data suggested that IL-4 increased ANO1 gene expression (Galietta *et al.*, 2002). ANO1 protein has been shown to be expressed at the apical membrane of airway epithelial membrane as with CFTR (Ousingsawat *et al.*, 2009). High-throughput screening of chemical libraries has been conducted to find small-molecule activators of ANO1 that could be used as a corrector in alternative ion channel therapy for the treatment of cystic fibrosis (Namkung *et al.*, 2011). ANO1 currents can be blocked by 4,4'-diisothiocyanostilbene-2,2'-disulphonic acid (DIDS) and niflumic acid (Hartzell *et al.*, 2005). Aside from roles as an ion channel, ANO1 has been found to be a regulator of proliferation as studies by Stanich *et al.*, 2011 showed. ANO1 is highly expressed in gastrointestinal stromal tumours. In knockout mice for ANO1, it was seen that there was decreased proliferation in primary cultures derived from the interstitial cells of Cajal. Chloride channel blockers also decreased cell proliferation in primary cultures of the interstitial cells of Cajal and the CFPAC-1 cell line. Mice lacking ANO1 had less phosphorylated retinoblastoma protein compared to controls. Taken together, it was

thought that ANO1 regulates proliferation at the G₁/S phase transition of the cell cycle and may be involved in tumourigenesis (Stanich *et al.*, 2011).

1.1.6 Cystic fibrosis transmembrane conductance regulator (CFTR)

Cystic fibrosis transmembrane conductance regulator (CFTR) is a phosphorylation dependent chloride ion channel, which is generally expressed on the apical surface of lung epithelia (Rosenfeld *et al.*, 1992). CFTR can either act in an absorptive or secretory role, which is greatly dependent on the particular tissue (Kunzelmann, 2001). In the lungs, CFTR is the main transporter of chloride ions. Other than in the lungs, CFTR also plays a major role in the regulation of fluid secretion and ion transport in the pancreas (Marino *et al.*, 1991), gastrointestinal tract (Cuthbert *et al.*, 1994) and sweat glands (Cohn *et al.*, 1991).

1.1.6.1 Domain Structure of CFTR

The gene length for CFTR is approximately 189 kb, is translated into a glycoprotein of 1480 amino acids in length. CFTR is a member of the ATP-binding cassette (ABC) transporter superfamily, and the final folded protein consists of five domains. Figure 1.1 shows the structure of the CFTR protein with two transmembrane domains (TMDs), two cytoplasmic nucleotide binding domains (NBDs) and a regulatory R domain. Each transmembrane domain consists of six alpha helices. TMD1 is located at the N terminal, and is connected to NBD1 at the last alpha helix. NBD1 is connected to the regulatory R domain, which is in turn connected to the first alpha helix of TMD2. NBD2 is located at the C-terminus, and is connected to the last alpha helix of TMD2. The regulatory R domain is unique among ABC transporters and contains many phosphorylation sites (Riordan *et al.*, 1989)

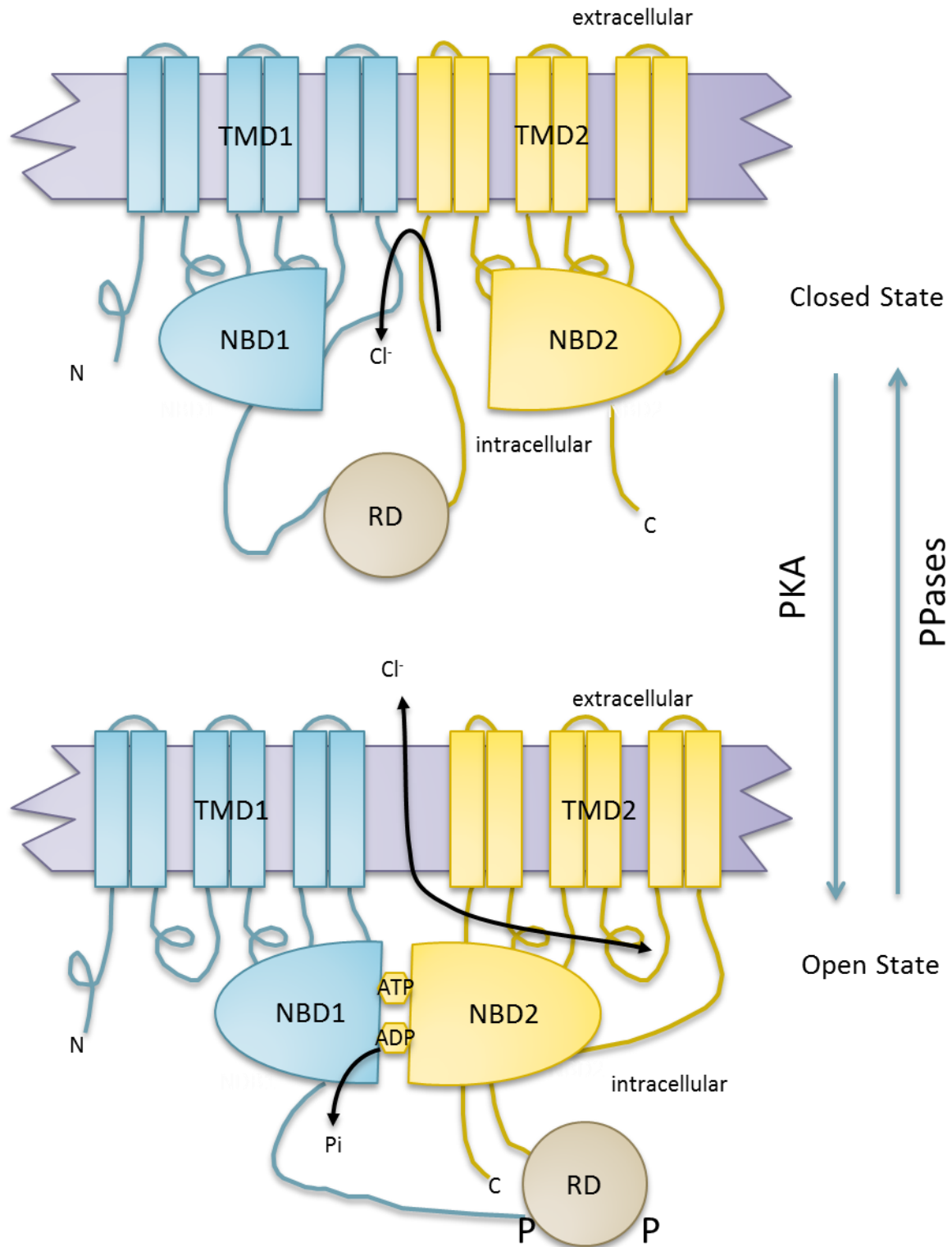


Figure 1.1 – CFTR open and closed states.
Adapted from: (Hwang & Sheppard, 2009)

1.1.6.2 Gating of CFTR is controlled by phosphorylation by protein kinases

In the open state of CFTR, ATP is bound to the NBDs, and the regulatory R domain is phosphorylated by protein kinase A (PKA) in response to elevations in the levels of cAMP (Figure 1.1) (Gadsby & Nairn, 1999; Sheppard & Welsh, 1999). Phosphorylation sites for protein kinase C (PKC) are also present on CFTR, where it is thought that PKC isotypes such as PKC- ϵ are able to prime CFTR to allow for PKA activation (Jia *et al.*, 1997; Liedtke & Cole, 1998). The NBDs form a head-to-tail dimer, with two sites located at the dimer interface responsible for binding ATP (Lewis *et al.*, 2004). One of these sites consists of two Walker motifs on NBD1 and a LSGQQ motif of NBD2 tightly binds ATP. The other site consists of two Walker motifs on NBD2 and a LSGQQ motif of NBD1, where ATP can be rapidly hydrolysed (Lewis *et al.*, 2004; Vergani *et al.*, 2005). The flow of anions through CFTR is thought to be gated by these interactions between ATP and sites 1 and 2, resulting in the dimerisation of NBDs and subsequent changes in TMD conformation (Vergani *et al.*, 2005). An investigation to demonstrate that the regulatory R domain of CFTR controls the gating of CFTR was carried out by Chappe *et al.*, 2005. The nucleotides that encoded the R domain (residues 635 to 836) were replaced with an internal ribosome entry sequence so that the N terminal and C terminal transcripts would be translated on the same mRNA transcript. The resulting translated protein (which was referred to as DeltaR-Split CFTR in the study) was trafficked to the cell membrane and led to constitutively active chloride transport. When co-expressed with the missing R domain, the regulation via PKA is restored and binding of the R domain to other domains of the CFTR protein (Chappe *et al.*, 2005). Further investigations using this system demonstrated that PKC alone enhanced the binding of the R domain with the DeltaR-Split CFTR, and that this was further enhanced by phosphorylation by both PKA and PKC. When all seven PKC consensus sequences that are located on the R domain are mutated, resting conditions are not affected, but binding of the R domain to the DeltaR-Split CFTR by PKA and PKC are both abolished. Resting activity of the DeltaR-Split CFTR with either wild type R domains or the mutated R domains was similar, but when stimulated with cAMP, the ion transport of channels with mutated R domains was greatly reduced. This suggested that the mutated R domains were unresponsive to PKA, and therefore that prior phosphorylation by PKC modulates the PKA-induced domain-domain interactions of CFTR (Seavilleklein *et al.*, 2008). When

the serine and threonine residues at nine PKC consensus sequences on CFTR are replaced by alanines (T582A, T604A, S641A, T682A, S686A, S707A, S790A, T791A and S809A), the response to PKA in excised patches is greatly reduced to 5-10% of that of the wild type (Chappe *et al.*, 2004). This response could not be enhanced by pretreatment by PKC. Stimulation of iodide efflux by chlorophenylthio-cAMP (cpt-cAMP) was delayed in cells that expressed the mutated R domain in a similar fashion to cells expressing wild type CFTR that were treated with chelerythrine, a PKC inhibitor. This suggested that loss of PKC phosphorylation resulted in weak activation by PKA (Chappe *et al.*, 2003). In order to determine which of these nine PKC consensus sequence(s) are necessary for normal regulation of the CFTR channel, further mutational studies were carried out by Chappe *et al.*, 2004. A CFTR mutant that consisted of S707A, S790A, T791A and S809A exhibited similar activation by PKA to that of wild type CFTR. CFTR mutants that consisted of either a triple mutant of T582A, T604A and S641A or a double mutant of T682A and S686A led to a drastically reduced response to PKA. It was determined that the T582, T604, and S686 consensus PKC sequences were essential for responses to PKA (Chappe *et al.*, 2004).

1.1.6.3 Regulation via β_2 adrenergic receptor

β_2 adrenergic receptors are the predominant isotype in the lungs (Carstairs *et al.*, 1985). It has been demonstrated that non-specific beta adrenergic receptor agonists such as isoproterenol activates CFTR mediated chloride transport *in vivo* (Walker *et al.*, 1997). Both CFTR and β_2 adrenergic receptors have PDZ binding motifs located at their C-termini. PDZ binding motifs are able to interact with other proteins, such as cytoskeletal proteins (Brdickova *et al.*, 2001). CFTR is known to co-localise with β_2 adrenergic receptors at the apical membrane. The two interact with one another through a complex of proteins that include ezrin / radixin / moesin-binding phosphoprotein 50 (EBP50). EBP50 is also known as NHERF (Na^+/H^+ exchanger regulatory factor). It is thought that through these interactions, β_2 adrenergic receptors are able to regulate CFTR (Naren *et al.*, 2003). A mutation in the gene for the β_2 receptor such as the Arg16Gly polymorphism is detrimental in cystic fibrosis (Buscher *et al.*, 2002). Specific β_2 adrenergic receptor agonists such as salbutamol and isoproprenaline can activate CFTR (Shamsuddin *et al.*, 2008). There is a

downregulation of β_2 receptors in CF patients (Mak *et al.*, 2002), and this may explain the inefficacy of using beta 2 agonists as a treatment for CF (Mortensen *et al.*, 1993).

1.1.6.4 Regulation via β_1 and β_3 adrenergic receptors

While β_2 adrenergic receptors have been studied quite extensively in airways, less is known about the other adrenergic receptors in the airway – beta 1 and beta 3. Beta 1 receptor protein is seen in CF bronchi, but not in non-CF bronchi (Bossard *et al.*, 2011). Stimulation of the β_3 receptor increases the beat frequency of cilia in both canine and rabbit bronchial epithelial cells (Takeyama *et al.*, 1993; Tamaoki *et al.*, 1993) and mucociliary clearance in rabbit nasal epithelia (Danner *et al.*, 2001). Expression of β_3 receptor protein is higher in CF bronchi compared to non-CF bronchi (Bossard *et al.*, 2011). In a recombinant system where both CFTR and β_3 adrenergic receptors were transfected into A549 cells, it was seen that CFTR was regulated by stimulation of β_3 adrenergic receptors by either non-selective beta agonist isoproterenol in the presence of nadolol (a β_1 and β_2 antagonist), and SR-58611A (a β_3 agonist) or CGP-12177 (partial β_3 agonist) (Leblais *et al.*, 1999). Subsequent investigations with this system found that β_3 adrenergic receptor regulates CFTR via inhibitory G protein subunit $G_{i/o}$, and the PI3K / MAPK pathway (Robay *et al.*, 2005).

1.1.6.5 Regulation via G Protein Coupled Receptors (GPCRs)

G Protein Coupled Receptors (GPCRs) such as purinergic receptors, which include several different types such as P1 receptors (also known as adenosine receptors), and P2Y receptors are thought to be important in the regulation of chloride transport in the airways. CFTR can also be activated via the stimulation of P2Y₂ receptors via Gq/11, PLC and an unknown kinase. This unknown kinase is inhibited by staurosporine, and the activation of CFTR via P2Y₂ stimulation was independent of the following signalling messengers: PKA, PKC, CAMK, P38 MAPK, MEK1/2, tyrosine kinases and c-src (Faria *et al.*, 2009). As shown in Figure 1.2, CFTR activity in normal airways is controlled by the A_{2B} receptor, a subtype of P1 receptor, and that P1 receptor antagonists such as the 5' nucleotidase inhibitor AMPCP abolish chloride ion transport through CFTR. This suggests that adenosine was generated through the hydrolysis of AMP (Huang *et al.*, 2001). Similarly, adenosine deaminase (ADA), which is able to metabolise adenosine, decreases cAMP in resting cells (Lazarowski *et al.*,

2004). This suggests that adenosine is metabolised from ATP in the periciliary liquid layer of the airways, and is then able to activate A_{2B} receptors on the apical surface of resting epithelial cells (Lazarowski & Boucher, 2009).

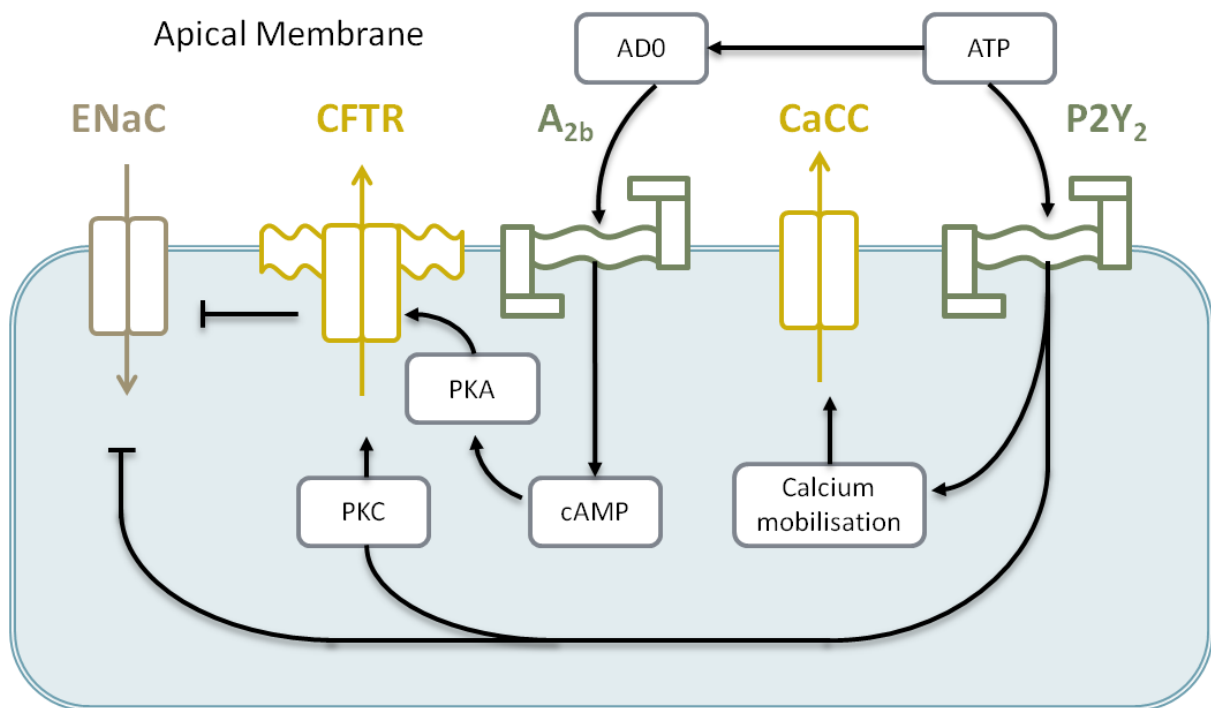


Figure 1.2 – Regulation of CFTR via G Protein Coupled Receptors.

Adapted from: (Lazarowski & Boucher, 2009).

Adenosine, which accumulates in the periciliary liquid layer, can activate A_{2B} receptors that can subsequently lead to elevations in of intracellular cAMP and activation of PKA and CFTR. P2Y₂ receptors are capable of mobilising calcium and activating PKC. PKC is able to enhance PKA mediated phosphorylation and activation of CFTR. The mobilisation of calcium through P2Y₂ receptor activation by ATP is able to activate calcium activated chloride channels on the apical surface of the airways. Under resting conditions, the response from CaCC to stimulation of the P2Y₂ receptor by ATP or UTP is small, but can be increased if there are conditions that include influxes of extracellular calcium or releases of calcium from intracellular stores. P2Y₆ receptors can also activate CaCCs (Morse *et al.*, 2001). While acute stimulation of GPCRs by carbachol increased chloride secretion across T84 monolayers, chronic stimulation produced anti-secretory effects (Toumi *et al.*, 2011).

1.2 Physiology of the Lung

1.2.1 Lung structure

As shown in Figure 1.3, the trachea divides into two bronchi (singular bronchus) as they enter the lungs (Dixon, 1903). Within the lungs themselves, these bronchi become further subdivided to give rise to the bronchioles (Tod, 1917). These branches continue to subdivide, giving rise to the terminal bronchioles that lead to the alveolar sacs. These alveolar sacs are comprised of clusters of alveoli, which are wrapped tightly with blood vessels (Auer & Meltzer, 1911). These alveoli are the centres of gaseous exchange in the lungs. Deoxygenated blood arrives from the heart through the pulmonary artery to the lungs, where oxygen from the inhaled air diffuses in and is exchanged for carbon dioxide in the haemoglobin of red blood cells (West, 1995). The freshly oxygenated blood returns to the heart through the pulmonary veins where it is re-pumped around the body. The two lungs are located in two cavities on either side of the heart, and they are of a similar appearance to one another, but are not identical. Lungs are separated into several lobes. The right lung has three lobes (superior, middle and inferior), whereas the left lung has two (superior and inferior). The lobes themselves are further divided up into firstly segments and then into hexagonal divisions called lobules. The medial right lung border is almost vertical, but the left lung has an indentation known as the cardiac notch, which is where the heart sits. Surrounding each lobe is the pleural cavity, which itself has two pleurae; on the rib cage lies the parietal pleura, and on the surface of the lungs lies the visceral pleura. Between these two pleura is the pleural fluid, which helps lubricate the lungs and keeps the lungs in contact with the rib cage by providing surface tension (West, 1995).

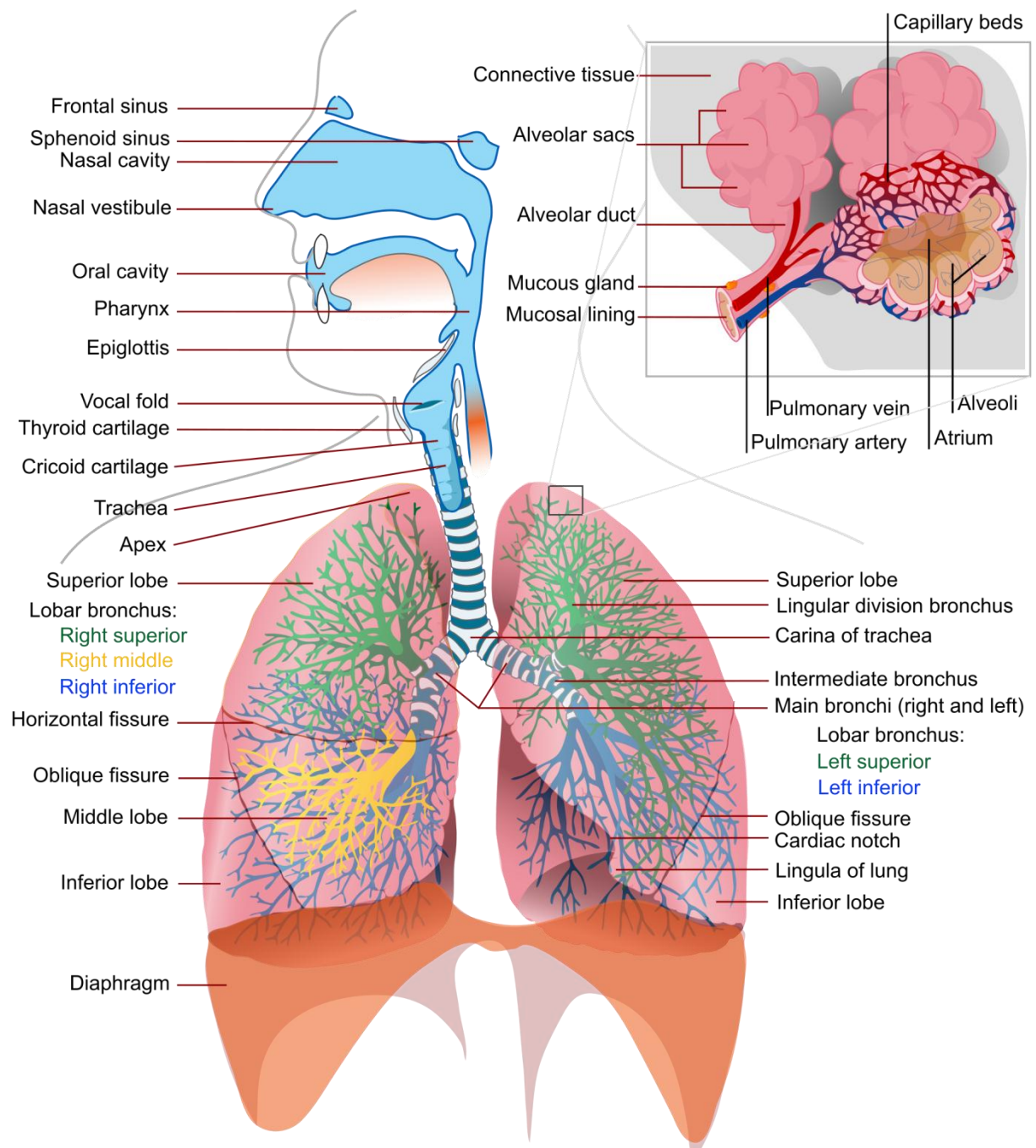


Figure 1.3 – The physiology of the human lungs.
 (Wikimedia Commons, Public Domain Image).

1.2.2 Lung function

The function of breathing is predominantly controlled by the diaphragm, a sheet of internal skeletal muscle, situated at the base of the thorax. When the diaphragm contracts, the bottom of the thoracic cavity of the lung is pulled downward, which results in an increase in volume of the cavity and as a result, a decrease in pressure. This decrease in pressure results in air from outside the lungs at a higher pressure to flow in. The air first enters the body through the oral and nasal cavities, and then passes through the pharynx, larynx and then into the trachea of the lungs, before branching into the bronchi, bronchioles and alveoli. Expiration of air from the body is a passive process which occurs when the diaphragm relaxes. The rib cage is also able to expand and contract to some extent as well, aiding the process (West, 1995).

1.2.3 Underlying tissue of the lung

Mammalian lungs have a soft spongy texture that is honeycombed with epithelium. This structure allows the lungs to have a very high surface area to volume ratio. As shown in Figure 1.4, airway submucosal glands lie beneath the ciliated epithelial cells on the surface, but are connected to that surface via ducts. They are able to secrete mucus when stimulated by acetylcholine or vasoactive intestinal peptide (Ilanowski *et al.*, 2007). Each individual airway gland consists of a primary gland duct, lateral ducts and many secretory tubules (Tos, 1966). The primary gland duct starts from the surface epithelium through the underlying lamina propria and smooth muscle layers into the submucosal space within the submucosal gland. The portion of the primary duct that is closer to the duct opening is lined by columnar ciliated cells that resemble a surface epithelium (Meyrick *et al.*, 1969). Distended duct regions whose diameters are 3 – 4 fold greater than primary ducts can be formed from the submucosal portions of the primary duct (Meyrick *et al.*, 1969; Inglis *et al.*, 1997)

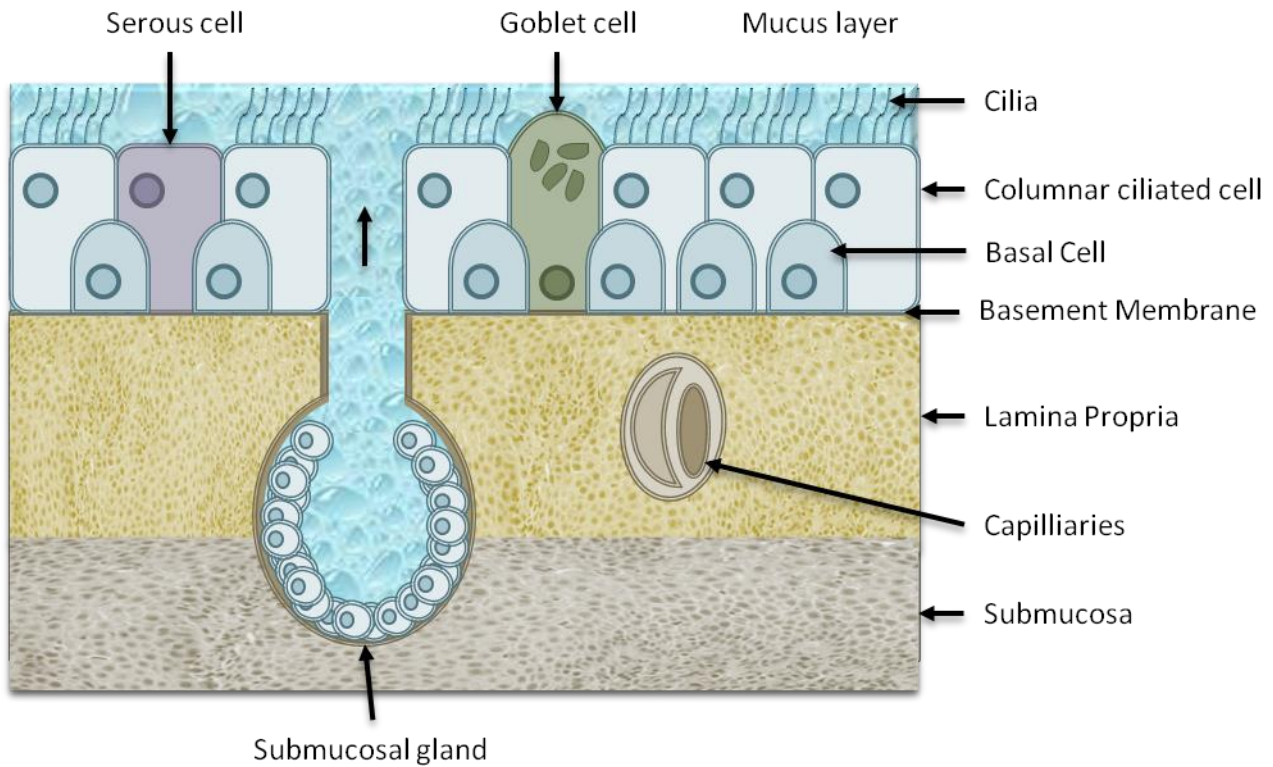


Figure 1.4 – A general overview of the physiology of the tissues on and near the surface of the lung.

The morphology of the distended duct regions has a high degree of variation ranging from straight to convoluted structures (Tos, 1966; Inglis *et al.*, 1997). The primary ducts act as collectors for lateral ducts that divide into many secretory tubules, which are classified serous or mucous according to which cell type they are mostly made up from (Tos, 1966; Meyrick *et al.*, 1969). The mucous tubules may divide several more times into other mucous tubules, but they always end in serous tubules. Neuronal control of mucus secretion is facilitated by electrical stimulation of the superior laryngeal nerves (Johnson, 1935). Secretion of the submucosal glands is in fact predominantly controlled by the parasympathetic nervous system, but also by the local release of stimulatory signals from nociceptive sensory nerves. These nociceptive sensory nerves consist of C- and A δ -fibre axons. The A δ -fibre axons are myelinated and so the action potential is fast-moving, while C- axons are unmyelinated so the action potential is transmitted much more slowly (Barnes, 2001; Tai & Baraniuk, 2002; Widdicombe, 2003; Ballard & Inglis, 2004; Tavee & Zhou, 2009).

1.2.4 Calu-3 cells as a model for lung ion transport

Calu-3 cells are used as a model for serous cells in the respiratory airways of humans, express high levels of CFTR, and respond well to agonists of cAMP and Ca^{2+} (Finkbeiner *et al.*, 1993; Shen *et al.*, 1994).

1.2.4.1 Channels present in Calu-3

The major ion channels and transporters found in Calu-3 cells are shown in Figure 1.5. When Calu-3 cells are stimulated by a cAMP agonist such as forskolin, it has been demonstrated that predominantly HCO_3^- ions are secreted rather than purely chloride ions, and this mechanism has been shown to be Na^+ dependent and Cl^- independent (Devor *et al.*, 1999). This secretion of HCO_3^- ions can be reduced by stimulating calcium activated potassium channels with an agonist such as 1-ethyl-2 benzimidazolinone (1-EBIO). On the other hand, it is seen that if Calu-3 cells experience elevations in Ca^{2+} , or are stimulated with 1-EBIO, only chloride secretion occurs (Devor *et al.*, 1999). The model of Calu-3 secretion is complex. A $\text{Na}^+ \text{-HCO}_3^-$ (NBC) cotransporter on the basolateral membrane mediates the entry of HCO_3^- ions into the cell (Devor *et al.*, 1999) HCO_3^- ions are secreted by Calu-3 cells when there is an elevation of $[\text{Ca}^{2+}]_i$ or if they have been stimulated by 1-EBIO (a K^+ channel activator). This is despite the fact that this causes a decrease in driving force on the $\text{Na}^+ \text{-HCO}_3^-$ (NBC) cotransporter on the basolateral membrane. The enzyme carbonic anhydrase can interconvert CO_2 and H_2O to HCO_3^- and H^+ , or vice versa. The secretion of HCO_3^- ions by 1-EBIO can be accumulated above their electrochemical equilibrium, which is normally maintained by their catalytic breakdown into CO_2 and H_2O by carbonic anhydrase. The potential alkalinisation of this effect is partially masked by a similar increase in the secretion of H^+ , which is likely due to $\text{H}^+ \text{-K}^+$ -ATPase on the apical membrane since this process is sensitive to apical treatments of ouabain (Krouse *et al.*, 2004).

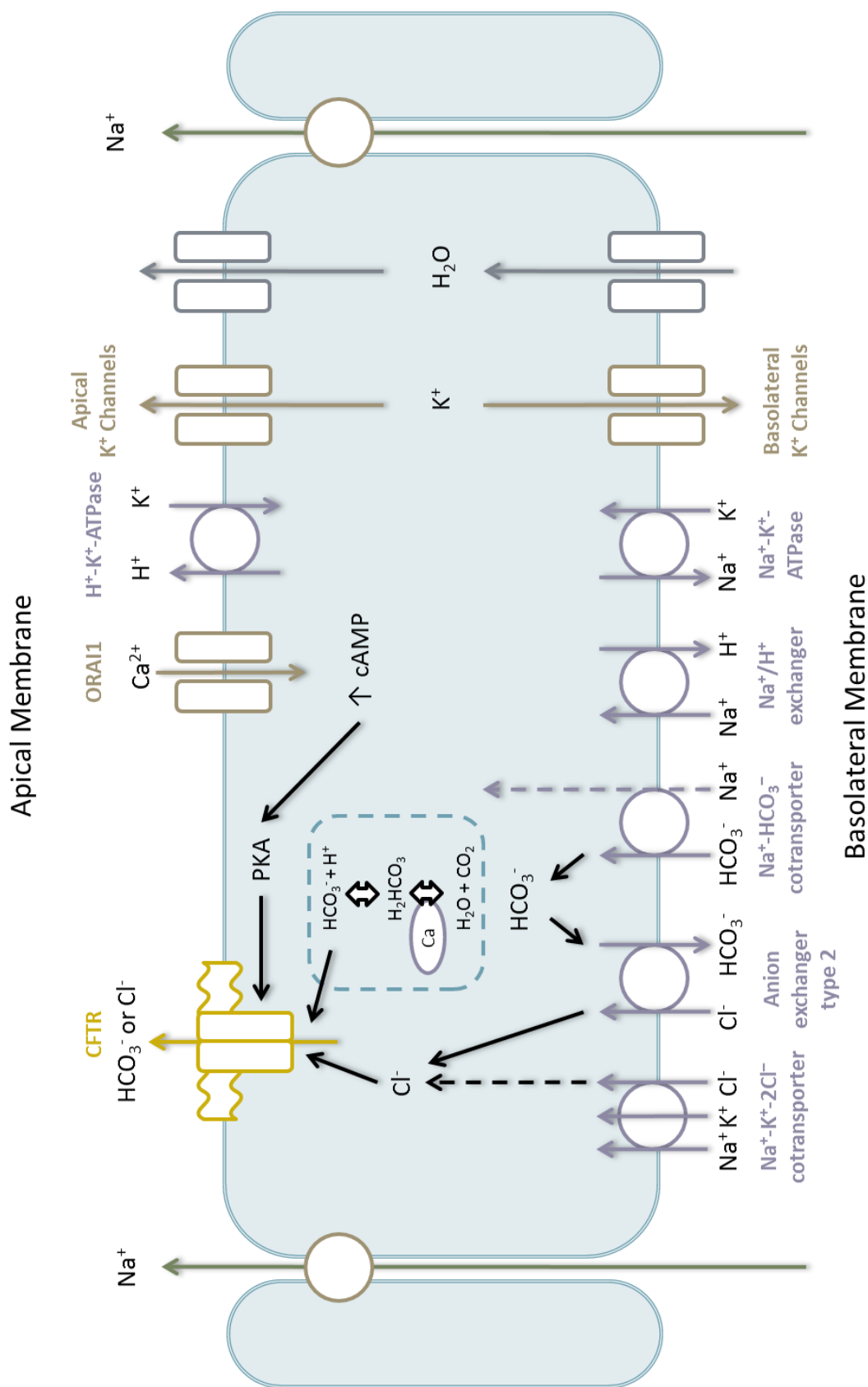


Figure 1.5 – Overview of ion transport in Calu-3 cells.

Compiled and adapted from (Devor *et al.*, 1999; Krouse *et al.*, 2004; Huang *et al.*, 2012; Shan *et al.*, 2012)

There is growing evidence that these HCO_3^- and Cl^- secretions are in fact conducted through the same channel, which is CFTR (Poulsen *et al.*, 1994; Devor *et al.*, 1999; Choi *et al.*, 2001; Krouse *et al.*, 2004). Since forskolin treatment results in HCO_3^- rather than Cl^- secretion, it means that the increase in the secretion of HCO_3^- by forskolin is likely due to activation by cAMP and PKA, which are also activators of CFTR (Devor *et al.*, 1999). Using patch clamp methods, CFTR has been shown to be activated by forskolin, and that HCO_3^- ions can be conducted but at a lower conductance compared to Cl^- ions (Gray *et al.*, 1990; Haws *et al.*, 1994; Poulsen *et al.*, 1994; Linsdell *et al.*, 1997). Since it was found that CF airway epithelia do not exhibit cAMP induced HCO_3^- secretion, this demonstrates that CFTR is responsible for this conductance (Smith & Welsh, 1992)

More recently it has been demonstrated that fluid secretion in Calu-3 cells is mostly driven by Cl^- secretion (Shan *et al.*, 2012). Anion exchange via anion exchanger type 2 (AE2) results in 50-70% of the basolateral Cl^- loading, which is increased upon forskolin stimulation (Figure 1.5) (Huang *et al.*, 2012). This contrasts with earlier work by Devor *et al.* (1999) where the Na-K-2Cl cotransporter was thought to be the mediator of Cl^- entry (Shan *et al.*, 2012). However, studies carried out by Garnett *et al.* 2011 proposed that forskolin stimulation leads to inhibition of basolateral ion exchange (Garnett *et al.*, 2011). Further studies by Garnett *et al.* (2012) demonstrated that the anion exchanger in Calu-3 cells can be regulated by protein phosphatase 1 (PP1) and CFTR (Garnett *et al.*, 2012). In addition, adenylate cyclase can be constitutively activated by Ca^{2+} entry through Orai1, a store-operated Ca^{2+} entry channel (Shan *et al.*, 2012).

1.3 Cystic Fibrosis (CF)

Cystic fibrosis (CF), which is also less commonly known as mucoviscidosis, is an autosomal genetic disease that is characterised by abnormal sodium and chloride transport across epithelia, causing thickened secretions. The name cystic fibrosis is derived from characteristics of the disease, which are scarring (fibrosis) and cyst formation in the pancreas. The disease affects a variety of epithelial tissues, but patients frequently suffer from respiratory failure due to airway inflammation and subsequent chronic bacterial infection (Pilewski & Frizzell, 1999; Sheppard & Welsh, 1999). Cystic fibrosis is also known to affect the function of the pancreas (Naruse *et al.*, 2002) and reproductive system (Chillon *et al.*, 1995). Symptoms of the disease include difficulty breathing that is the result of repeated infections, chronic rhinosinusitis (Davidson *et al.*, 1995), poor growth (Corey *et al.*, 1988), diarrhoea (Hochman *et al.*, 1976), and infertility (Kaplan *et al.*, 1968).

Cystic fibrosis has autosomal recessive inheritance, requiring that both parents have a faulty gene for CFTR. Inheriting one working copy of the CFTR gene prevents the disease. Among Caucasians, 1 in 25 people carry one allele for CF and the disease affects 1 in 2500 live births (Ratjen & Doring, 2003). Mutations in the CFTR channel are known to be responsible for cystic fibrosis (CF) (The Cystic Fibrosis Genetic Analysis Consortium, 1994). The more common cause of CF in patients is the inheritance of two copies of the mutation $\Delta F 508$ in the CFTR channel, which accounts for approximately 70% of cases in Western Europe (Puechal *et al.*, 1999). While the channel can still function, a significantly lower proportion of the mutated CFTR is transported to the surface of the cell since they are marked for destruction at the proteasome, resulting in less CFTR at the cell surface (Cheng *et al.*, 1990; Ward *et al.*, 1995). Other less common CF causing mutations include G542X, G551D, N1303K and W1282X (Araujo *et al.*, 2005). The CFTR mutation G551D does not have an effect on protein processing, but severely reduces the open probability of the CFTR channel (Li *et al.*, 1996; Bompadre *et al.*, 2007).

1.3.1 Cystic Fibrosis in the lung

Airway mucus is composed of water, salts, mucins, anti-microbials, anti-proteases and anti-oxidants (Krouse *et al.*, 2004). The lack of functional CFTR at the cell

surface of serous cells results in mucus that is abnormally thick and viscous, plugging up the submucosal glands and the small airways of the lung. In human respiratory airways, CFTR is predominantly expressed in serous cells of submucosal glands and ciliated cells of the surface epithelium and gland ducts (Engelhardt *et al.*, 1992; Kreda *et al.*, 2005). It is thought that the secretion of Cl^- and HCO_3^- drives water movement across the serous cells (Krouse *et al.*, 2004), eventually giving rise to the periciliary liquid layer; a film of fluid that enables the mucus secreted by goblet cells to be cleared away by ciliated lung epithelial cells. Serous cells are also a source of antimicrobial enzymes which contribute to the maintenance of the aseptic environment of the lungs.

1.3.1.1 High-salt hypothesis

Since many of these enzymes rely on a particular pH in order to function optimally, it has previously been suggested that the altered salt concentration that is commonly seen in the lungs of patients with cystic fibrosis may exacerbate the risk of infection of the airways. It has also been suggested that the pH of the periciliary layer is abnormally low in cystic fibrosis compared to normal airways, which could also inhibit bacterial clearance and natural antimicrobial defences in the lungs (Verkman, 2001). In simple terms, the high-salt hypothesis postulates that cystic fibrosis results in having an abnormally high salt concentration, which in turn inhibits the actions of endogenous antimicrobials that include defensins (Smith *et al.*, 1996). However, more recent reports show that the low salt concentration that is found in normal airways would require either a water-impermeable airway epithelium, which was found not to be the case (Farinas *et al.*, 1997; Matsui *et al.*, 2000), or the presence of non-salt osmolytes, or maintenance of osmotic imbalance through the action of a surface phenomenon of some kind (Verkman, 2001).

1.3.1.2 Low-volume hypothesis

In simple terms, the low-volume hypothesis as depicted in Figure 1.6 postulates that hyperactive epithelial sodium channels (ENaC) that is seen in cystic fibrosis results in increased salt absorption and a decrease in the volume of the periciliary liquid layer. This hyperactivity of ENaC is due to a lack of CFTR inhibition. Water flows transcellularly, which decreases the volume of the periciliary liquid (Wine, 1999). This

dehydrated periciliary liquid layer becomes viscous, which is infection prone (Matsui *et al.*, 1998).

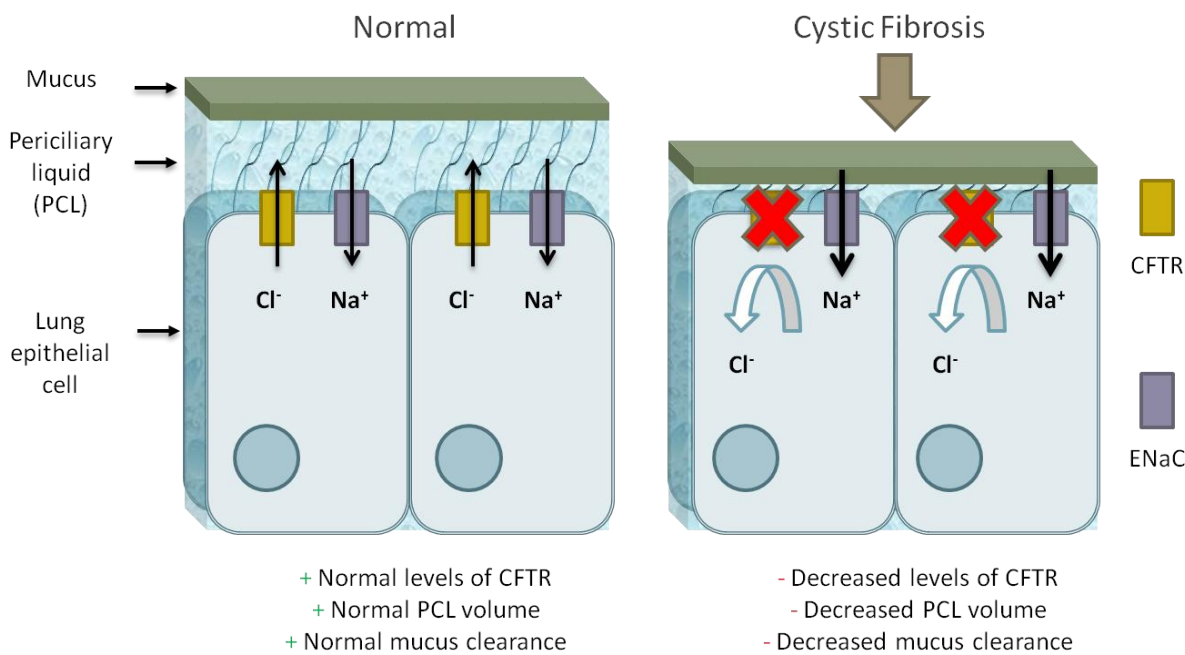


Figure 1.6 – Schematic depicting the low volume hypothesis of cystic fibrosis.

The effect of the lack of necessary CFTR on the apical epithelial surface leads to sodium hyperabsorption, dehydration of the airways and impaired mucus clearance.

In order to test this low volume hypothesis, initial experiments carried out by Matsui *et al.*, 1998 involved setting up airway cultures with PBS on the apical surface and then monitoring the osmolarity and airway surface liquid (ASL) depth. It was seen that the depth of the ASL decreased from an initial 30 μm depth to 10 μm depth after 24 hours, and that there was no increase in chloride concentration as a result. A comparison of normal and CF cultures under confocal and electron microscopy showed that in CF cultures the mucus layer had collapsed the cilia, which prevented transport (Matsui *et al.*, 1998).

1.3.2 Cystic fibrosis in the pancreas

The pancreas is a gland organ that is part of the vertebrate digestive system. It has an exocrine role of secreting enzymes that aid the digestion of food, and an endocrine role of secretion of the hormone insulin that regulates the levels of glucose in the blood. The CFTR mutation that leads to Cystic fibrosis affects these activities by making these secretions thick by reducing bicarbonate and fluid secretion. This leads to blockages in pancreatic ducts caused by the precipitation of proteins in the duct

lumen, and subsequently prevents pancreatic enzymes from being secreted from the pancreatic acini region of the pancreas (Marsey & Winpenny, 2009). This ultimately results in poor digestion of food and reduced nutrient uptake. Obstruction by thickened secretions can result in inflammation, scarring of the pancreas, cyst formation and the destruction of the Islets of Langerhans responsible for insulin secretion, which can lead to high blood sugar and insulin-dependent diabetes.

1.3.3 Cystic fibrosis and the reproductive system

1.3.3.1 Congenital absence of the vas deferens (CAVD)

There are two conditions relating to CAVD, which include congenital unilateral absence of the vas deferens (CUAVD) and the more severe congenital bilateral absence of the vas deferens (CBAVD). CBAVD can result from CF and results in infertility in 2-6% of men. It has been suggested that there was a required amount of functional CFTR protein for the normal embryonic development of the vas deferens (Radpour *et al.*, 2008). Low level expression of CFTR is detected in the epithelium of the human epididymis through 10 to 33 weeks gestation. This suggests that CFTR is required for the correct development of reproductive tissues (Tizzano *et al.*, 1993). However, the current consensus viewpoint is that CBAVD in CF males is that the failure of CFTR to drive salt and water secretion to lubricate ducts leads to the stasis of protein rich cargoes, which results in duct obstruction and subsequent duct destruction (Forstner *et al.*, 1987).

1.3.3.2 Congenital absence of the uterus and vagina (CAUV)

Women with CF are less fertile than healthy women, believed to be caused by thickened cervical mucus (Oppenheimer *et al.*, 1970). The defective CFTR protein expressed in the cervix in CF women does not produce the typical changes in mucus during the menstrual cycle (Johannesson *et al.*, 1998). It has been suggested that CFTR may play a role in the acidification of synaptic vesicles, and thus regulate sexual maturation and fertility (Johannesson *et al.*, 1997). Mutations in CFTR have been associated with CAUV (Timmreck *et al.*, 2003). It is thought that since the development of the müllerian ducts depends on and follows the development of the wolffian ducts, that CFTR may be important for the normal development of both duct

systems (Radpour *et al.*, 2008). However, CF women have been known to become pregnant (Davis, 2006).

1.3.4 Current treatments available for cystic fibrosis

Currently, there are no cures for cystic fibrosis, but there are several treatments available to manage the disease symptoms and to prolong life expectancy and quality of life. These treatments target the primary organs that are affected, which include the lungs, gastrointestinal tract and the reproductive organs. Antibiotics are administered for months at a time to prevent the colonisation of the lungs by harmful bacteria such as *Pseudomonas aeruginosa*. Depending on the treatment, this would require hospitalisation with the antibiotics administered intravenously if pneumonia is suspected. Antibiotics such as aztreonam, colistin and tobramycin can be inhaled to ward off infection (Pai & Nahata, 2001; Westerman *et al.*, 2004; McCoy *et al.*, 2008). Oral antibiotics such as ciprofloxacin or azithromycin are also given (Hansen *et al.*, 2005). Chest physiotherapy (CPT) that involves the percussion of a patient's chest to dislodge mucus can be conducted several times a day. Several devices, which include the ThAIRapy Vest and intrapulmonary percussive ventilator (IPV), can recreate this treatment. More sophisticated devices include Biphasic Cuirass Ventilation, which is portable and designed for home use (van der Schans *et al.*, 2000). DNase enzyme therapy, which uses recombinant human deoxyribonuclease such as Dornase in an aerosol, can break down DNA in the sputum, and thus decrease the viscosity of the mucus (Lieberman, 1968). Hypertonic saline is another aerosol that can increase mucociliary clearance (Elkins *et al.*, 2006).

1.3.5 Treatments currently in development for cystic fibrosis

1.3.5.1 Gene therapy

Gene therapy through the use of vectors such as the viral vectors adenovirus, adeno-associated virus or retro virus, or non-viral such as liposomes, aims to introduce wild-type CFTR into the airway. Both viral and non-viral methods have limitations; viral vectors can produce an immune response, whereas the message delivered by liposomes does not integrate into the genome very well, resulting in little protein being expressed.

1.3.5.2 CFTR correctors and potentiators

Different approaches to increasing CFTR function are currently being researched, which include CFTR correctors and CFTR potentiators. CFTR correctors are compounds that attempt to restore the expression of the $\Delta F508$ CFTR to the apical membrane surface, while CFTR potentiators are compounds that attempt to rescue the gating defect. Some examples of CFTR correctors currently identified and undergoing research include RDR1, which is a pharmacological chaperone that binds to NBD1 of the $\Delta F508$ CFTR that can partially rescue its function in cell lines and mouse models (Sampson *et al.*, 2011).

VX-809, is a CFTR corrector, functions by improving the processing of $\Delta F508$ CFTR in the endoplasmic reticulum, preventing the usual ubiquitination and destruction of CFTR. In cultured HBE from patients with $\Delta F508$ CFTR mutations, chloride secretion was improved to 14% of HBE derived from normal HBEs. It was concluded that VX-809 was more effective than previously identified correctors (Van Goor *et al.*, 2011). Clinical trials of VX-809 have been performed to determine its safety and its efficacy as a treatment. It was seen that VX-809 did significantly reduce elevated sweat chloride values in a dose-dependent manner in the 100 and 200 mg dosage groups, but no significant effect was seen in nasal or lung function (Clancy *et al.*, 2012). Combination treatment of VX-809 and CFTR potentiator VX-770 (also known as Kalydeco, or Ivacaftor) is currently in stage 2 of clinical trials, with initial results showing an 8.5% improvement in lung function in patients with two copies of the $\Delta F508$ CFTR mutation (<http://investors.vrtx.com/releasedetail.cfm?ReleaseID=677520>).

VX-770 has been approved for treatment for children aged 6 and under with the G551D mutation (<http://investors.vrtx.com/releasedetail.cfm?ReleaseID=644257>). The drug was discovered using high throughput techniques of 228,000 compounds using cell-based fluorescence membrane potential assays to determine their effect on CFTR (Van Goor *et al.*, 2009). The compound has been demonstrated to increase chloride secretion in cultured human bronchial epithelial cells (HBE) from patients with the $\Delta F508$ and G551D mutations by 10 fold, to approximately half the normal level of secretion shown in HBE isolated from healthy controls. VX-770 also reduced

sodium absorption, reduced airway dehydration and increased cilia beat frequency. It was seen that the efficacy of VX-770 depended on existing cAMP/PKA signalling (Van Goor *et al.*, 2009). Clinical trials with this compound with patients with at least one G551D mutation to evaluate its safety for use as a treatment for CF showed that there were improvements in lung function and promising results for future trials of the drug (Accurso *et al.*, 2010).

10% of CF causing mutations are the result of premature stop codons. Oral drug ataluren (PTC124) allows ribosomes to read through premature stop codons in order to produce functional protein (Hamed, 2006). In clinical trials, it was seen that ataluren increased nasal chloride transport response and increased full length CFTR production in nasal epithelial cells. 7 of the 9 patient groups of nonsense mutations exhibited improvements with few adverse events (Sermet-Gaudelus *et al.*, 2010). In another trial conducted over a period of weeks with low dose and high dose groups, it was seen that ataluren improved total chloride transport and pulmonary function with few adverse effects (Wilschanski *et al.*, 2011).

1.3.5.3 Alternative ion channel therapy

Other approaches to treating cystic fibrosis include various ways of stimulating other ion channels instead of focusing on CFTR. Such therapies include using activators of calcium activated chloride channels including ANO1 to increase chloride transport, and inhibitors of epithelial sodium channels (ENaC) to reduce sodium absorption (Becq *et al.*, 2011). The ENaC blocker amiloride has long been known to increase the periciliary volume and improve mucociliary clearance in the lung of CF patients (Knowles *et al.*, 1990), however, the drug lacks potency and is rapidly absorbed by the lung. A modification of the drug such as benzamil increase the potency, but also increases resorption of the drug by the lung further (Rodgers & Knox, 1999). Not yet entering clinical trials, the lead compound 552-02 is an ENaC blocker that is two orders of magnitude more potent than amiloride and lasts much longer. Work carried out using sheep found that the compound increased mucociliary clearance persistently (Hirsh *et al.*, 2008). GS 9411 is another antagonist of sodium channels (Jones & Helm, 2009).

Drugs such as Lancovutide (also known as Moli1901 or Duramycin) and denufosol (also known as INS37217) modulate the alternative chloride channels known as CaCCs are at the stage of clinical trials and are potential treatments for cystic fibrosis (Jones & Helm, 2009). UTP or ATP nucleotides can also activate P2Y₂ receptors and lead to an activation of CaCCs, but are not suitable for therapeutic use for CF as they are also bronchoconstrictors in some instances. However, analogues can be used for a similar effect without the risk of bronchoconstriction (Cuthbert, 2011b). One such analogue is denufosol, which can activate P2Y₂ receptors without being broken down by ectonucleotidases due to alterations of its molecular structure (Yerxa *et al.*, 2002). P2Y₂ receptor activation and the activation of CaCCs bypass the defect in CFTR. In recent clinical trials, denufosol improves lung function in cystic fibrosis patients with normal to mildly impaired lung function compared to placebo controls (Accurso *et al.*, 2011). Lancovutide is in early phase trials that also activates CaCCs (Pettit & Johnson, 2011). Lancovutide stimulates Cl⁻ efflux from CF bronchial epithelial cells (CFBE) at 1 μ M, but inhibits Cl⁻ efflux at high concentrations (100 - 250 μ M) (Oliynyk *et al.*, 2010). Another potential target for alternative chloride channel therapy is chloride channel type 2 (CIC-2) (Thiemann *et al.*, 1992). The drug lubiprostone has been suggested to be a CIC-2 opener and can cause chloride transport in a non-PKA dependent manner in T84 monolayers (Cuppoletti *et al.*, 2004a). However, later studies showed that lubiprostone targets the prostanoid EP4 receptor, which is coupled to Gs, which leads to generation of cAMP and activation of CFTR rather than CIC-2 (Bijvelds *et al.*, 2009; Ao *et al.*, 2011; Cuthbert, 2011a).

Activation of potassium channels has been associated with increasing chloride driving force in the airway (Bernard *et al.*, 2003; Szkotak *et al.*, 2004) and the gut (Devor *et al.*, 1996; Greger, 2000; Matos *et al.*, 2007; Roth *et al.*, 2011) and as such could be candidates for alternative ion channel therapy. The human bronchial cell line 16HBE14o- was used to investigate the effect of calcium activated potassium channels on driving force for Ca²⁺ dependent chloride secretion. Ionomycin treatment led to a transient peak followed by a plateau phase, both of which could be eliminated by either niflumic acid, glibenclamide or 5-nitro-2-(3-phenylpropylamino)benzoic acid (NPPB), while DIDS blocked the peak phase alone. ⁸⁶Rb effluxes through both apical and basolateral membranes were stimulated calcium, and could be blocked by

calcium activated potassium channel blockers charybdotoxin, clotrimazole and tetrapentylammonium (TPA). Stimulation with 1-EBIO increased ^{86}Rb effluxes that could be reduced with calcium activated potassium channel blockers. RT-PCR identified the expression of $\text{K}_{\text{Ca}}2.1$ (also known as SK1, with the gene name KCNN1) and KCNN4 (also known as SK4, IK1 or $\text{K}_{\text{Ca}}3.1$). Expression of KCNQ1 was also found but treatment with chromanol 293B and clofilium did not have an effect on cAMP-dependent I_{SC} . It was therefore suggested that there are two separate components of calcium dependent chloride response, and that basolateral KCNN4 plays a major role in calcium dependent chloride secretion in 16HBE14o- cells (Bernard *et al.*, 2003).

Studies carried out by Matos *et al.*, 2007 using colonic crypts have shown that basolateral potassium channels have an important role in providing the driving force for luminal exit of chloride (Matos *et al.*, 2007). To investigate the role of potassium channels in apical chloride secretion in the distal colon, KCNMA1 and KCNN4 knockout mice and the KCNQ1 inhibitor chromanol 293B were used in an Ussing chamber set up. Responses to basolateral forskolin and carbachol were measured, and it was found that knockout mice for $\text{K}_{\text{Ca}}1.1$ had identical responses to wild-type mice, indicating that $\text{K}_{\text{Ca}}1.1$ was not important in governing apical chloride secretion. However, carbachol induced ΔI_{SC} was significantly reduced in KCNN4 knockout mice, although not completely eliminated. This indicated that KCNN4 plays a role in governing apical chloride exit, but not completely. Additional treatment with chromanol 293B eliminated the remaining carbachol response, indicating that a combination of KCNN4 and KCNQ1 are important for governing apical chloride exit in the distal colon (Matos *et al.*, 2007). Moreover, in previous studies in the mouse colon and T84 cells, 1-EBIO potentiates Cl^- secretion by activation of basolateral Ca^{2+} activated potassium channel KCNN4 and apical CFTR (Devor *et al.*, 1996). Recent studies using rectal biopsies from CF patients showed that 1-EBIO similarly potentiates Cl^- secretion in CF tissues by activation of basolateral KCNN4 channels resulting in increased electrical driving force for luminal chloride exit (Roth *et al.*, 2011). The study suggested that activators of KCNN4 could be used in conjunction with CFTR correctors and potentiators to maximise their effectiveness (Roth *et al.*, 2011). 4-chloro-benzo[*F*]isoquinoline (CBIQ) is able to activate KCNN4 and CFTR in

the Calu-3 cell line (Szkotak *et al.*, 2004). When CFTR is stimulated in the colon by either an increase in cAMP or cGMP-dependent phosphorylation, it also leads to coactivation of basolateral KCNQ1 channels and inhibition of ENaC on the apical membrane. In intact enterocytes, Ca^{2+} activates basolateral KCNN4 channels and apical potassium channels, but not apical chloride channels. The activation of these potassium channels nonetheless increase driving force for apical chloride exit (Greger, 2000).

1.4 Matrix Metalloproteinases: A potential pharmacological target for treating Cystic Fibrosis?

1.4.1 What are matrix metalloproteinases (MMPs)?

Matrix metalloproteinases (MMPs) are zinc endopeptidases that are involved in the remodeling and degradation of the extracellular matrix (ECM). Listed in Table 1.3, there are in total 23 different Matrix Metalloproteinases found in humans (Imai & Okada, 2008). Secreted MMPs usually consist of three major domains, which include the propeptide, catalytic and hemopexin-like domains. Membrane-type Matrix Metalloproteinases (MT-MMPs) have a transmembrane C-terminal and cytoplasmic domains (Massova *et al.*, 1998). The hemopexin-like domain is weakly homologous to the heme-binding serum protein hemopexin (Springman *et al.*, 1990). Between the catalytic domain and the hemopexin-like domain is a hinge region of about 16 amino acids (Chung *et al.*, 2000). MMPs are typically secreted from cells as proenzymes with a molecular weight of approximately 55-60 kDa. The proenzyme has a signal peptide on the N-terminal that enables it to translocate to the endoplasmic reticulum, which is subsequently cleaved off. The proenzymes are then packaged into vesicles for transport to the extracellular space (Dzwonek *et al.*, 2004). A cysteine residue in the propeptide domain of the proenzyme (specifically, Cys73) is ligated to the Zn^{2+} ion within the active site, which is referred to as a 'cysteine switch'. The collagenase can become active when the bond between the cysteine residue and the Zn^{2+} ion is disrupted by the propeptide domain being cleaved off (Springman *et al.*, 1990). The important HEXXH motif found within the MMP catalytic domain binds the Zn^{2+} ion required for collagenase activity. When the initial cleavage occurs in the collagen triple helix, the structure then unwinds and becomes susceptible to degradation by gelatinases MMP-2 and MMP-9. The C-terminal hemopexin-like domain is responsible for binding substrates (Xu *et al.*, 2007).

Table 1.3 – Matrix metalloproteinases, their known substrates and tissue expression in humans.

Compiled from: (Nakahara *et al.*, 1997; Murphy *et al.*, 2002; Xu *et al.*, 2002; Palosaari *et al.*, 2003; Kassim *et al.*, 2007; Pirila *et al.*, 2007; Illman *et al.*, 2008; Miller *et al.*, 2008)

Enzyme	Known substrates	Expression
Collagenases		
MMP-1 (collagenase-1)	Collagens I, II, III, VII, VIII and X, gelatin, aggrecan, versican, proteoglycan link protein, casein, α 1-proteinase inhibitor, α 2-M, pregnancy zone protein, ovostatin, nidogen, MBP, proTNF, L-selectin, proMMP-2, proMMP-9	Gingival fibroblasts
MMP-8 (collagenase-2)	Collagens I, II, III, V, VII, VIII and X, gelatin, aggrecan, α 1-proteinase (collagenase-2) inhibitor, α 2-antiplasmin, fibronectin	Neutrophils
MMP-13 (collagenase-3)	Collagens I, II, III and IV, gelatin, plasminogen activator inhibitor 2, aggrecan, perlecan, tenascin	Chondrocytes, synovial membrane, synovial stroma, synovial fibroblasts, gingival fibroblasts, plasma cells
Gelatinases		
MMP-2 (Gelatinase A)	Collagens I, IV, V, VII, X, XI and XIV, gelatin, elastin, fibronectin, aggrecan, versican, proteoglycan link protein, MBP, proTNF, α 1-proteinase inhibitor, proMMP-9, proMMP-13	Gingival fibroblasts, osteoblasts, odontoblasts, human airway epithelial cells
MMP-9 (Gelatinase B)	Collagens IV, V, VII, X and XIV, gelatin, elastin, aggrecan, versican, proteoglycan link protein, fibronectin, nidogen, α 1-proteinase inhibitor, MBP, proTNF	Macrophages, polymorphonuclear leukocytes, rheumatoid arthritis synovium, osteoclasts, odontoblasts, human airway epithelial cells
Stromelysins		
MMP-3 (Stromelysin-1)	Collagens III, IV, IX and X, gelatin, aggrecan, versican, perlecan, nidogen, proteoglycan link protein, fibronectin, laminin, elastin, casein, fibrinogen, antithrombin-III, α 2M, ovostatin, α 1-proteinase inhibitor, MBP, proTNF, proMMP-1, proMMP-7, proMMP-8, proMMP-9, proMMP-13	Rheumatoid synovial fibroblasts, skin fibroblasts
MMP-10 (Stromelysin-2)	Collagens III, IV and V, gelatin, casein, aggrecan, elastin, proteoglycan link protein, fibronectin, proMMP-1, proMMP-8	Rheumatoid synovial fibroblasts, keratinocytes, T-lymphocytes, chondrocytes, osteoblasts, osteoclasts, human airway epithelial cells
MMP-11 (Stromelysin-3)	α 1-proteinase inhibitor	Breast carcinoma cells

Enzyme	Known substrates	Expression
<i>Matrilysins</i>		
MMP-7 (Matrilysin-1)	Collagens IV and X, gelatin, aggrecan, proteoglycan link protein, fibronectin, laminin, entactin, elastin, casein, transferrin, MBP, α 1-proteinase inhibitor, proTNF, proMMP-1, proMMP-2, proMMP-9	Osteoarthritic cartilage, human airway epithelial cells
MMP-26 (Matrilysin-2)	Collagen IV, fibronectin, fibrinogen, gelatin, α 1-proteinase inhibitor, proMMP-9	Mucosal keratinocytes
<i>MT-MMPs</i>		
MMP-14 (MT1-MMP)	Collagens I, II and III, gelatin, casein, elastin, fibronectin, laminin B chain, vitronectin, aggrecan, dermatan sulfate proteoglycan, MMP-2, MMP-13, proTNF	Osteoblasts, osteoclasts, odontoblasts, ameloblasts, human airway epithelial cells
MMP-15 (MT2-MMP)	proMMP-2, gelatin, fibronectin, tenascin, nidogen, laminin	
MMP-16 (MT3-MMP)	proMMP-2	
MMP-17 (MT4-MMP)		Leukocytes
MMP-24 (MT5-MMP)	proMMP-2, proMMP-9, gelatin	
MMP-25 (MT6-MMP)	Collagen IV, gelatin, fibronectin, fibrin	Leukocytes, neutrophils
<i>Others</i>		
MMP-12 (metalloelastase)	Collagen IV, gelatin, elastin, α 1-proteinase inhibitor, fibronectin, vitronectin, laminin, proTNF, MBP	Alveolar macrophages
MMP-19	Collagen IV, gelatin, laminin, nidogen, tenascin, fibronectin, aggrecan, COMP	Blood mononuclear cells, lymphocytes, blood vessels, breast tissue, lung fibroblasts, myeloid cell surface
MMP-20 (enamelysin)	Amelogenin	Odontoblasts
MMP-23 (CA-MMP)		
MMP-28 (epilysin)	Casein	Keratinocytes

1.4.2 Subfamilies of matrix metalloproteinases

Matrix metalloproteinases have been grouped into several subfamilies based on their proteolytic activities and structure (Figure 1.7). These subfamilies include matrilysins (Murphy *et al.*, 2002), collagenases (Mort & Billington, 2001), stromelysins (Visse & Nagase, 2003), gelatinases (Murphy *et al.*, 2002; Dufour *et al.*, 2008) and membrane-type MMPs (MT-MMPs) (Nakahara *et al.*, 1997; Hotary *et al.*, 2000; Sugrue *et al.*, 2001)

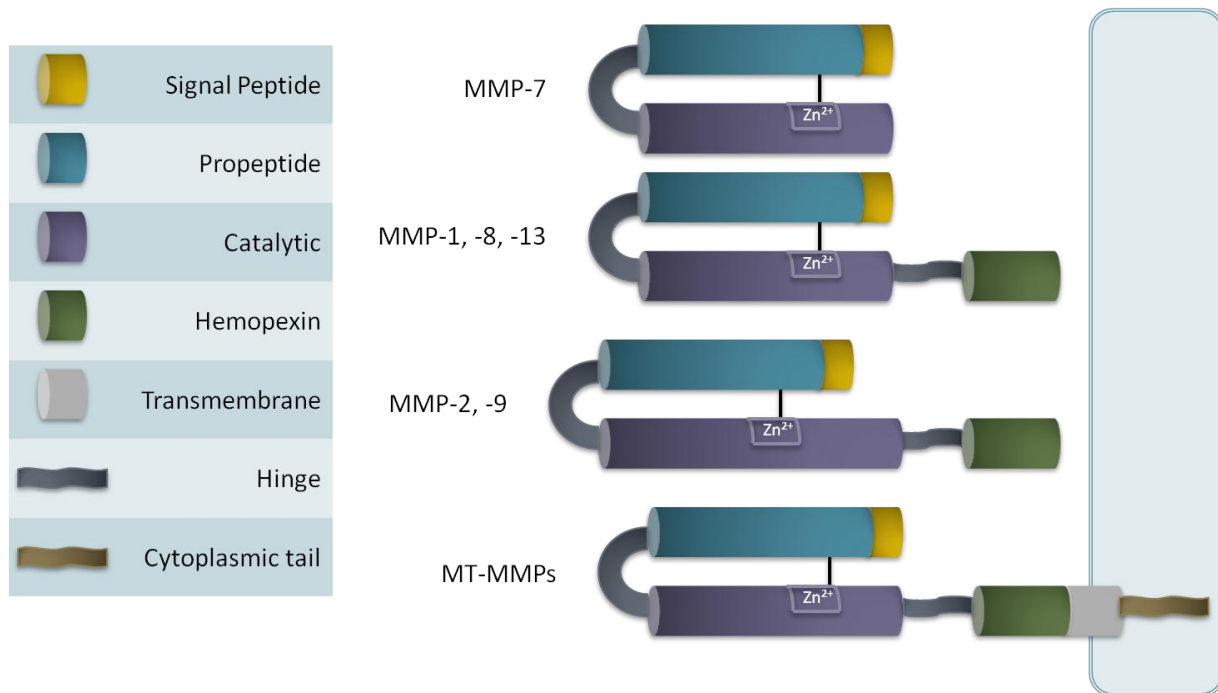


Figure 1.7 – The domain structure of the matrix metalloproteinases.

The propeptide domain contains a Cys⁷³ residue often referred to as a 'cysteine switch'. The catalytic domain contains a HEXXH motif that binds to the Zn²⁺ ion. Matrilysins, such as MMP-7 and MMP-26, are relatively simple MMPs, comprising only the propeptide and catalytic domains. Collagenases and stromelysins are more complex and consist of proptide, catalytic and hemopexin-like domains, and a hinge region. Only the gelatinases, MMP-2 and MMP-9, have a Collagen Binding Domain (CBD) that contains three fibronectin type II molecules. Membrane-type MMPs (MMP-14, -15, -16, -17, -24, and -25) all have a C-terminal cytoplasmic tail, with the exception of MMP-17 and MMP-25. Based on schematics by: (Mort & Billington, 2001; Noel *et al.*, 2012)

1.4.2.1 *Matrilysins*

Matrilysins, such as MMP-7 and MMP-26, are relatively simple MMPs, comprising only the propeptide and catalytic domains. Despite the fact that matrilysins lack the hemopexin-like domain and a transmembrane region (Figure 1.7), they are able to degrade a range of substrates, including aggrecan, casein, collagen IV, elastin, entactin, fibronectin, gelatin and laminin (Murphy *et al.*, 2002).

1.4.2.2 *Collagenases and Stromelysins*

Collagenases and stromelysins are more complex and consist of propeptide, catalytic and hemopexin-like domains, and a hinge region (Figure 1.7). The MMPs that can break down triple-helical fibrillar collagen are MMP-1, MMP-8 and MMP-13. These MMPs are able to cleave collagen at a single locus, producing two fragments 75% and 25% of the size of the original molecule (Mort & Billington, 2001). Stromelysins (MMP-3, MMP-10 and MMP-11), unlike collagenases, cannot degrade fibrillar collagen. However, stromelysins can degrade a wide variety of other ECM components, such as fibronectin, gelatin and laminin (Murphy *et al.*, 2002). MMP-3 is also responsible for activating other MMPs, such as MMP-1 (Visse & Nagase, 2003).

1.4.2.3 *Gelatinases*

The gelatinases, consisting of MMP-2 and MMP-9, are responsible for the degradation of ECM components such as fibrillar collagen (alongside the collagenases), basement membrane components and fibronectin (Murphy *et al.*, 2002). Only the gelatinases, MMP-2 and MMP-9, have a Collagen Binding Domain (CBD) that contains three fibronectin type II molecules (Figure 1.7). These domains are specifically required for the cleavage of collagen and elastin, with a deletion of the CBD resulting in a ~90% reduction in the degradation of gelatin (Xu *et al.*, 2007). MMP-9 is also thought to be responsible for increased cell migration, possibly through the formation of a homodimer between hemopexin domains (Dufour *et al.*, 2008).

1.4.2.4 *Membrane-type Matrix Metalloproteinases (MT-MMPs)*

Membrane-type MMPs (MMP-14, -15, -16, -17, -24, and -25) all have a C-terminal cytoplasmic tail, with the exception of MMP-17 and MMP-25 (Figure 1.7). MT-MMPs are also able to break down collagen – particularly collagen I, aiding cell invasion and

morphogenesis (Hotary *et al.*, 2000). Other extracellular components such as fibronectin, gelatin, laminin, and proteoglycan can also be broken down by MT-MMPs (Nakahara *et al.*, 1997). MT-MMPs can also trigger signal transduction cascades (Li *et al.*, 2008). A furin-type proprotein convertase aids in the activation of the MT-MMPs. The furin recognition site consists of the consensus sequence of amino acids Arg-Arg-Lys-Arg (RRKR) (Sugrue *et al.*, 2001).

1.4.3 General regulation of matrix metalloproteinases

1.4.3.1 Tissue Inhibitors of Metalloproteinases (TIMPs)

MMPs can be regulated either by natural inhibitors (such as TIMPs) or through the use of synthetic inhibitors. The activity of MMPs is regulated in the tissue naturally by Tissue Inhibitors of Metalloproteinases (TIMPs). There are 4 classes of TIMPs that have been studied so far, which include TIMP-1, TIMP-2, TIMP-3 and TIMP-4. These classes of TIMPs have differing binding affinities to MMPs, and can inhibit the activity of MMPs (Fielitz *et al.*, 2004). TIMPs themselves also have to be regulated so that MMPs can still perform their normal ECM remodelling, so a balance between the two is necessary (Brew *et al.*, 2000). Table 1.4 is a summary table showing specific data regarding TIMPs.

Table 1.4 – TIMP summary table.

Based on information gathered by: (Palosaari *et al.*, 2003)

TIMP	Amino Acid Length	Mass (kDa)	Examples of where they are expressed
TIMP-1	184	28.5	Osteoblasts
TIMP-2	194	21.0	Osteoblasts, Chondrocytes
TIMP-3	188	24.0	Chondrocytes
TIMP-4	195	22.0	Chondrocytes

TIMPs consist of two domains; an N-terminal domain consisting of 125 amino acids, and a C-terminal domain consisting of 65 amino acids. Additionally, the two domains are each stabilized by three disulphide bonds formed between cysteine residues (Brew *et al.*, 2000). TIMPs can regulate MMP activity by binding directly to the catalytic site to form a TIMP/MMP complex (Iyer *et al.*, 2007).

1.4.3.2 Subfamilies of TIMPs

There are various differences between the TIMPs with regards to which type of MMPs and other proteins they regulate. TIMP-1, which interacts with the hemopexin domain, was found to inhibit MMP-9's cell migratory function (Dufour *et al.*, 2008). A complex is formed with TIMP-2 and a homodimer of MT1-MMP. This complex can then activate MMP-2 (Ingvarsen *et al.*, 2008). TIMP-2 and TIMP-3 have been found to be more effective inhibitors of MT-MMPs compared with TIMP-1 (Brew *et al.*, 2000). TIMP-3 is also able to inhibit members of the A disintegrin and metalloproteinase (ADAM) and A disintegrin and metalloproteinase with Thrombospondin Motifs (ADAMTS) families, such as ADAM-10, ADAM-12, ADAMTS-4 and ADAMTS-5 (Visse & Nagase, 2003). TIMP-3 has been found to be an effective inhibitor of TNF- α converting enzyme (known as TACE or ADAM-17) (Amour *et al.*, 1998). In response to vascular injury, the levels of TIMP-4 mRNA increases. This suggests that TIMP-4 has a protective role against cardiomyopathy and tumour progression. Active TIMP-4 is able to strongly inhibit MMP-2, MMP-9 and MT1-MMP (Donnini *et al.*, 2008).

1.4.3.3 Synthetic inhibitors

Various chemical inhibitors of matrix metalloproteinases exist that are commonly used, including 1,10-phenanthroline, ilomastat (GM-6001), batimastat (BB-94) and marimastat (BB-2516). Ilomastat, a broad spectrum inhibitor of metalloproteinases, works by binding directly to the Zn^{2+} ion of the catalytic site of the MMP in a bidentate fashion, thus impeding its catalytic activity (Galardy *et al.*, 1994). Batimastat has a hydroxamic acid group and a peptide backbone that can bind to MMPs. The hydroxamic acid group binds to the zinc atom of the catalytic domain, and thus inactivates the enzyme (Davies *et al.*, 1993). 1,10-Phenanthroline inhibits MMPs by acting as a divalent zinc chelator (Santos *et al.*, 2004). However, N-heterocyclic polyaromatic hydrocarbons such as 1,10-Phenanthroline are known to be toxic to organisms (Kobeticova *et al.*, 2008). Marimastat is a synthetic inhibitor modified from Batimastat by British Biotech, and like batimastat, is of the hydroxamate class of MMP inhibitors and works by the same method (Failes & Hambley, 2007).

1.4.4 MMP Regulation in Airway Epithelial cells

Of particular interest are the signalling pathways that lead to MMP expression and how the signalling events are regulated in airway epithelial cells. The major sources of MMPs in the airways are neutrophils, epithelial cells and macrophages (Sagel *et al.*, 2005). Nitric oxide (NO) is produced by airway epithelial cells through the expression of inducible nitric oxide synthase (NOS2). Nitric oxide is responsible for epithelial repair and host defence. At low concentrations, NO induces the activation of MMP-9. MMP-9 has a role in epithelial repair, so the mediation of repair by NO is through the induction of MMP-9. NO is thought to increase the expression of MMP-9 at the gene transcription level through the cGMP-dependent signalling cascade. NO can inhibit MMP-9 at higher concentrations (Bove *et al.*, 2007). In a study by Jurasz *et al.*, 2001, nitric oxide has been linked with MMP-2 and tumor cell-induced platelet aggregation (TCIPA). Two cell lines, A549 (adenocarcinomic human alveolar basal epithelial cells) and Human HT-1080 (human sarcoma cell line) were shown to induce TCIPA. This in turn led to the platelets releasing MMP-2. Inhibitors of MMPs, including phenanthroline and anti-MMP-2 antibodies led to a decrease in platelet aggregation, while NO donors (such as S-nitroso-*n*-acetylpenicillamine and S-nitrosoglutathione) were able to inhibit TCIPA and MMP-2 release. It was suggested that NO inhibits TCIPA partly due to its inhibition of MMP-2 (Jurasz *et al.*, 2001). A further study by Lechapt-Zalcman *et al.*, 2006 demonstrated that TGF- β_1 significantly upregulated MMP-2 in an in vitro model using human nasal epithelial cells (HNEC) to represent airway epithelial cells. MMP-2 RNA expression levels increased with HNEC cells treated with TGF- β_1 compared to controls. TGF- β_1 treatment significantly increased the rate that wounds closed compared to controls, therefore TGF- β_1 upregulated MMP-2, which in turn facilitated the wound repair (Lechapt-Zalcman *et al.*, 2006). As depicted in Figure 1.8, collagen I and thrombin have been shown to increase MMP-2 activity in airway smooth muscle cells, despite actually decreasing the levels of MMP-2 mRNA. However, collagen I and thrombin together increased MMP-14 expression, which then activated MMP-2. Collagen I decreased TIMP-2 activity, which reduced MMP-2 inhibition (Henderson *et al.*, 2007). Moreover, in a study by Lin *et al.*, 2008, the p42/p44 MAPK pathway was implicated using MEK 1/2 inhibitor, which was found to reduce MMP-9 expression. Cells transfected with siRNA for MEK1 and double negative mutants for ERK2 reduced TNF- α induced MMP-9

expression. JNK and NF- κ B inhibitors SP600125 and, helenalin, respectively reduced TNF- α induced MMP-9 expression (Lin *et al.*, 2008).

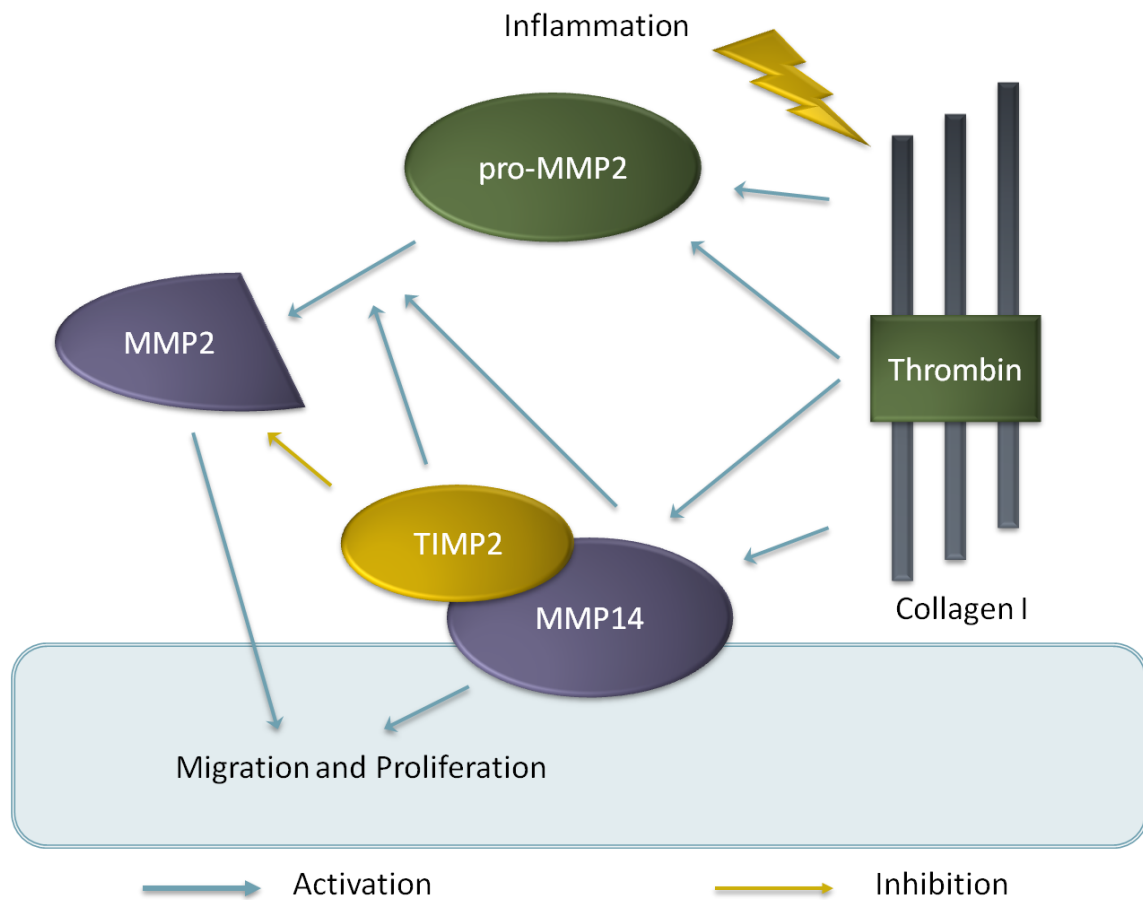


Figure 1.8 – The interactions leading to the expression of MMP-2 as a result of Collagen I and Thrombin.
Based on an illustration by: (Henderson *et al.*, 2007).

PPAR γ , a nuclear receptor, inhibits MMP-9 at the transcriptional level in two different bronchial epithelial cell lines. PPAR γ is expressed in the normal human bronchial epithelial cell lines NL20 and BEAS. PPAR γ can be activated naturally with prostaglandin D₂, or with synthetic compounds including thiazolidinediones (TZDs), pioglitazone or rosiglitazone (Hetzl *et al.*, 2003). PPAR γ upregulates Glut4 and lipoprotein lipase, which limits the expression of proinflammatory cytokines. PPAR γ regulates DNA expression by binding to PPAR response elements (PPREs) on the promoter region of a particular gene. NF- κ B, known to regulate TNF- α induced MMP-9 expression, is inhibited by TZD treatment. Therefore, an upregulation of PPAR γ is causing the reduction in MMP-9 expression through the NF- κ B pathway. There may

be an interaction between PPAR γ and NF- κ B. Treatment with TZDs had no effect on TIMP-1 or MMP-2 production (Hetzel *et al.*, 2003).

1.4.5 Role of MMPs under specific disease conditions

1.4.5.1 Cystic Fibrosis

It has been found that the levels of MMP-8 and MMP-9 are significantly elevated in the bronchoalveolar lavage (BAL) fluid of individuals afflicted with cystic fibrosis (Ratjen *et al.*, 2002; Manoury *et al.*, 2007; Gaggar *et al.*, 2011). Overexpression of MMPs can lead to excessive degradation of surrounding tissues. In a study by Ratjen *et al.*, 2002, it was seen that there was a greater than 300-fold increase in the level of MMP-8 and a 116-fold increase in the level of MMP-9 in the BAL fluid of CF children compared to healthy controls. However, the levels of TIMP-1, which normally inhibit MMPs by binding with a 1:1 molar ratio, were only elevated by 6-fold, resulting in very high MMP/TIMP ratios. The overexpression of MMP-8 and MMP-9 was attributed mostly to neutrophils (Ratjen *et al.*, 2002). In a further study by Sagel *et al.*, 2005, it was seen that the levels of MMP-9 found in the BAL fluid were inversely proportional to the forced expiration volume in one second (FEV₁) of CF children, and that CF children had a significantly higher neutrophil count in the BAL fluid, as well as increased IL-8 (a neutrophil attractant) and neutrophil elastase. MMP-9 is capable of inactivating alpha₁-proteinase inhibitor, which is responsible for inhibiting neutrophil elastase. Neutrophil elastase can also inhibit TIMPs. Therefore, in CF children, there was an elevated neutrophil count and increased levels of IL-8 and neutrophil elastase, which in turn increased MMP-9 expression and increased MMP-9/TIMP-1 ratio. Therefore, there was a decrease in alpha₁-proteinase inhibitor, resulting in further increases in neutrophil elastase activity, leading to decreased TIMP activity and increased proteolytic activity (via MMP-9 and neutrophil elastase) resulting in decreased FEV₁ and therefore decreased lung function (Sagel *et al.*, 2005). Moreover, NO is decreased in the upper airway of CF patients compared to controls and either no different or decreased in the lower airway. There is a decreased expression of iNOS in the airway epithelial cells of CF patients compared with controls. A result of decreased level of iNOS expression is less protection against bacterial, fungal and viral infections. A decreased level of iNOS in CF patients is the

cause of the decreased levels of NO in the airway epithelium (Grasemann & Ratjen, 1999).

1.4.5.2 *Asthma*

Asthma is a condition that involves lung inflammation and shortness of breath due to constriction of the airways. It is seen that the levels of MMP-1, -2, -3, -8 and -9 are elevated in the BAL fluid of individuals with asthma, with the expression of MMP-9 being particularly high in cases of severe asthma (Greenlee *et al.*, 2007). The ratio of MMP-9/TIMP-1 has been found to be elevated in the sputa of individuals afflicted with asthma. In a study carried out by Tanaka *et al.*, 2000 the levels of MMP-9 and TIMP-1 were measured using ELISA and zymography. The bands found during the zymographic analysis and anti-MMP-9 included a band representing the MMP-9/TIMP-1 complex as well as MMP-9. From the zymographic analysis, it showed that the initial high levels of MMP on day one were reduced following methylprednisolone infusion therapy, along with an increase in TIMP-1. This resulted in a much lower MMP-9/TIMP-1 ratio. The peak expiratory flow (PEF) following the therapy of individuals with asthma was also measured, showing an increase over the course of a week (Tanaka *et al.*, 2000). MMP-9 can be produced in a variety of cells within the airway, including macrophages, eosinophils and neutrophils. A high level of MMP-9 is also correlated with eosinophil and neutrophil counts. MMP-9 is partly responsible for the clearing of eosinophils from the airway. High MMP-9 expression in the airway is associated with a high neutrophil count, and is inversely correlated with FEV₁. This suggests that MMP-9 is linked with neutrophil influx and interference with gas exchange with the lung (Greenlee *et al.*, 2007).

1.4.5.3 *Chronic Obstructive Pulmonary Disease*

Chronic obstructive pulmonary disease (COPD), which involves the destruction of alveoli and capillaries of the lung, is characterized by the elevation in levels of various cytokines, such as IL-6, IL-8, IL-1 β , and TNF- α . IL-1 β and TNF- α induce the release of MMP-9 from macrophages. TNF- α also activates NF- κ B, a transcription factor that activates the IL-8 gene, which is a neutrophil attractant. IL-1 β induces the release of neutrophils from the bone marrow. The cytokine expression profile is different in COPD than that of asthma, despite having some overlap between the two. The

cytokines expressed in asthma tend to be from CD4+ T-cells and eosinophils such as IL-4, IL-5 and IL-13, rather than CD8+ T-cells, which produce IL-1 and TNF- α (Chung, 2001). Along with MMP-9, other proteases are also found to be elevated in COPD, including neutrophil elastase, MMP-2, MMP-8, MMP-9 and MMP-12. These various proteases are predominantly secreted from neutrophils and alveolar macrophages. Moreover, some of the fragments that are generated by proteases have chemotactic properties. For instance, within elastin (a component of the ECM), there is a repeating hexamer sequence Val-Gly-Val-Ala-Pro-Gly that is thought to be a chemoattractant for monocytes. In addition, fragments of collagen, such as *N*-Acetyl-Pro-Gly-Pro, have been found to be a chemoattractant for neutrophils. These fragments are produced during lung inflammation as seen in COPD (O'Reilly *et al.*, 2008).

1.4.5.4 Pancreatitis

Levels of MMP-9 are elevated in individuals with pancreatitis. The levels of the cytokines such as IL-1 and TNF- α may be biological indicators of the severity of pancreatitis. The levels of IL-1, TNF- α and MMP-9 are higher with individuals with severe acute pancreatitis (SAP) than those with mild acute pancreatitis, with healthy controls having the lowest levels. Both known to induce the expression of MMP-9, IL-1 and TNF- α , may be responsible for the pathology of the disease through excessive degradation of the ECM (Chen *et al.*, 2006). In another study, the effect of pancreatic trypsin on the activation of proMMP-2 was investigated. It was found that the activation of proMMP-2 via trypsin was highly dependent on a number of different external factors. Through the use of fluorometric assays and zymography, it was seen that the activation of proMMP-2 in the presence of bovine pancreatic trypsin was highly dependent on temperature. It was seen that at 21°C that the activation time was significantly reduced, although there was also a large increase in the degradation of proMMP-2. Without the addition of Ca^{2+} and Brij-35, no activation of proMMP-2 took place. The activation of MMP-2 is also implicated in pancreatitis, and the fact that pancreatic trypsin can activate MMP-2 shows that there is a link between pancreatitis and MMP activation (Lindstad *et al.*, 2005).

1.4.6 Known interactions of MMPs with ion channels

MMPs have been linked to several different types of ion channels.

1.4.6.1 *Cystic fibrosis transmembrane conductance regulator (CFTR)*

Cystic fibrosis transmembrane conductance regulator (CFTR) chloride ion channels are expressed in submucosal gland cells and are thought to be involved in mucus secretion. Studies into the role of MMPs on CFTR were conducted by Duszyk *et al.*, 1999. Two cell lines were used, Calu-3 and A549. The A549 cell line is a useful comparison since it does not express CFTR unlike Calu-3 cells (Duszyk *et al.*, 1999). Western blots and zymographic studies showed that the levels of MMP-2 were knocked down when 1,10-phenanthroline or anti-MMP-2 polyclonal antibodies were used (Duszyk *et al.*, 1999). 1,10-phenanthroline had no significant effect on the short circuit current (I_{SC}) with the A549 cell line, while the I_{SC} in Calu-3 cells was shown to be increased in a concentration dependent manner. Anti-MMP-2 had the same effect of increasing I_{SC} . Recombinant MMP-2 reduced I_{SC} . Since the whole cell current in A549 cells (which do not express CFTR) was not similarly affected, MMP-2 somehow specifically affects CFTR chloride channels and reduces whole cell current by an unknown mechanism (Duszyk *et al.*, 1999). A further study was conducted using the colonic epithelial cells from mouse models, including the CF mice CF null ($Cftr^{tm1Cam}$) and CF $\Delta F508$ ($Cftr^{tm2Cam}$), and various isoforms of phenanthroline were used to study their effectiveness at increasing I_{SC} . It was found that 1,10-phenanthroline was unable to increase the I_{SC} in the null and $\Delta F508$ CF mice, due to the lack of CFTR at the surface (Duszyk *et al.*, 2001).

1.4.6.2 *Chloride channel, Calcium activated (CLCA)*

Chloride channel, Calcium activated (CLCA) is a gene family that translates to secreted proteins thought to be mediators of chloride conductance (Gibson *et al.*, 2005; Mundhenk *et al.*, 2006), by lowering the energy barriers for ion translocation through the pore of endogenous CaCCs (Hamann *et al.*, 2009). CLCA are known to be metal-dependent hydrolases. Hydrolases, which also bind a Zinc ion to facilitate their catalytic activity, have a similar activity to that of Matrix Metalloproteinases. CLCA shares notable homologies to MMPs, including the conserved HEXXH motif that is responsible for binding the zinc ion (Pawlowski *et al.*, 2006).

1.4.6.3 Calcium activated chloride channels (CaCC)

Studies by Jeulin et al., 2008 have shown that EGF can activate CaCCs, which can be inhibited by tyrphostin (AG1478), an EGFR inhibitor. Further shown was that the activation of CaCC via EGF signalling was mediated through src kinase ($p60^{c-src}$), and exposure to pollutants elicited the activation of CaCC via activation of EGFR through proinflammatory cytokines (Jeulin et al., 2008).

1.4.6.4 CIC Proteins

Chloride channels, including CIC-7, interplay with Cathepsin K and MMPs during the degradation of bone. Cathepsin K is a protease involved in bone resorption. Osteoclasts that are deficient in CIC-7 through a knockout were found to have a reduced ability to degrade bone. An inhibitor of CIC-7 called NS5818 also reduced the ability of osteoclasts to degrade bone.

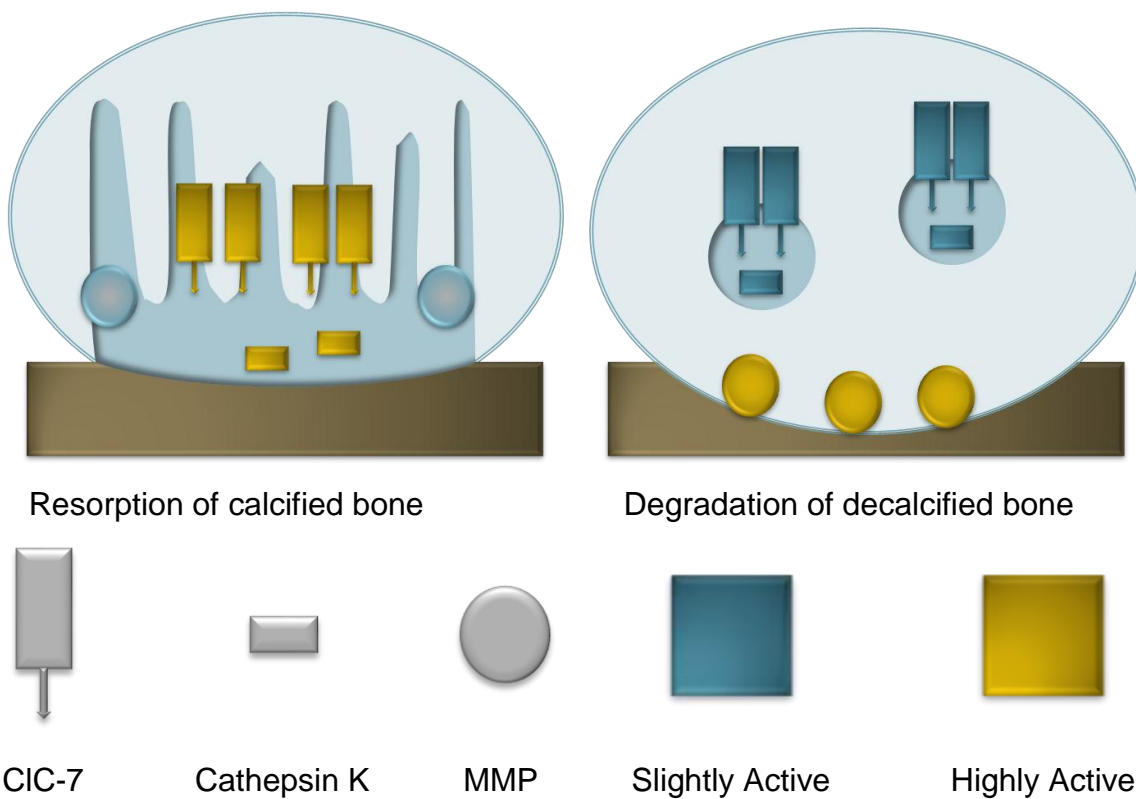


Figure 1.9 – The interplay between CIC-7, Cathepsin K and MMPs during the resorption of calcified bone and degradation of decalcified bone.

Blue represents slightly active, while yellow represents highly active. Image adapted from: (Henriksen et al., 2006)

As depicted in Figure 1.9 above, CIC-7 is highly active during the resorption of calcified bone, along with cathepsin K, with MMPs largely inactive. However, during

the degradation of decalcified bone, the CIC-7 and cathepsin K are mainly packed into vesicles and remain mostly inactive. MMPs are then highly active in the degradation of decalcified bone (Henriksen *et al.*, 2006).

1.4.6.5 Potassium ion channels

In spontaneously hypertensive rat (SHR) models, it was found that MMP-9 mRNA expression in the kidney was reduced compared to control rats, whereas the mRNA expression of TIMP-1, collagen IV and TGF- β 1 was much higher. Long-term treatment with ATP-sensitive potassium channel opener iptakalim increased the mRNA expression of MMP-9 and decreased the mRNA expression of TIMP-1, collagen IV and TGF- β 1. In arteries, iptakalim reduces fibronectin and collagen IV overexpression in the SHR model (Xue *et al.*, 2005). It is thought that iptakalim regulates the activity of MMP-9 through its down regulation of TGF- β 1. It is possible that there is in fact a link between potassium channels, TGF- β 1 and MMP-9 (Xue *et al.*, 2005). By using CF and non-CF bronchial monolayers, it has been seen that EGF/EGFR signalling is reduced in CF. As EGF signalling is coupled to potassium channels, it is also seen that there is a 40 - 70% reduction in potassium currents and a reduced expression of KvLQT1, ATP-sensitive potassium and calcium activated potassium channels. The reduction in potassium current and EGF signalling is a likely contributor to slowing down bronchial repair in CF (Trinh *et al.*, 2008). Another ligand of EGFR, heparin-binding EGF-like growth factor, has been shown to mediate oxyhaemoglobin-induced expression of voltage-dependent potassium channels in rabbit cerebral artery myocytes. Oxyhaemoglobin can induce the activation of MMPs, which is able to cleave a heparin-binding EGF-like growth factor (HB-EGF) precursor protein from the cell surface leading to the activation of the EGFR receptor. The activation of the EGFR receptor leads to the endocytosis of the voltage-dependent potassium channels (Koide *et al.*, 2007).

1.5 Epidermal Growth Factor: Inducer of Matrix Metalloproteinases

Epidermal growth factor (EGF) is a growth factor that plays an important role in the regulation of cell growth, proliferation, and differentiation by binding EGFR, a receptor tyrosine kinase of the ErbB family, on the cell surface (Iamaroon *et al.*, 1996). This leads to the initiation of several signalling pathways such as MAPK, Akt and JNK (Oda *et al.*, 2005). TGF- α , another possible ligand of EGFR, has been shown to induce a motile fibroblast-like phenotype in the rat Nara Bladder Tumour II (NBTII) carcinoma cell line through the expression of a 95 kDa gelatinase with extracellular matrix-degrading potential (Gavrilovic *et al.*, 1990).

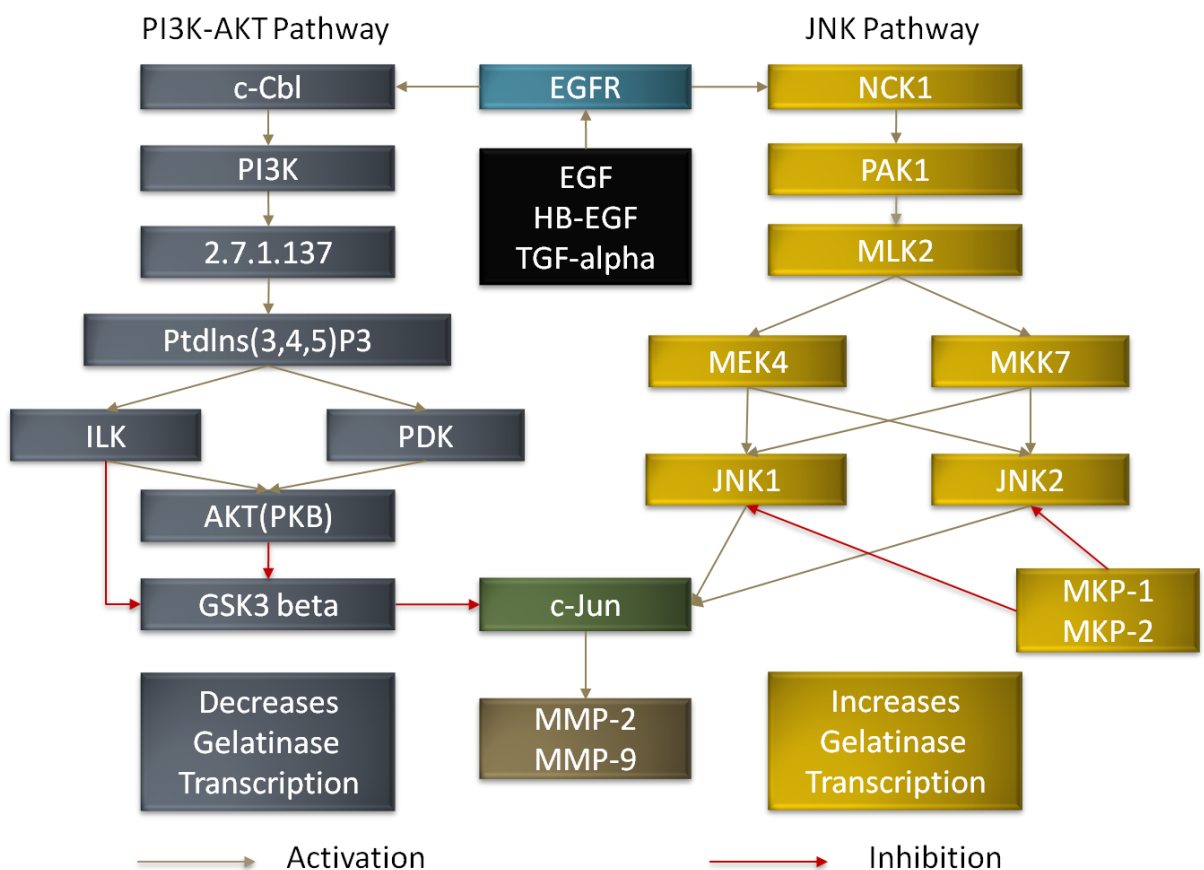


Figure 1.10 – Schematic depicting MMP-9 induction via EGF, HB-EGF and TGF- α .

MMP-9 can also be induced by a number of proinflammatory cytokines, including TNF- α and IL-1 β .

TNF- α also induces the expression of MMP-9 in A549 cells, a carcinomic human alveolar basal epithelial cell line, through several signalling cascades including the p42/p44 MAPK and JNK pathways. Brown lines represent an downstream activation, while red lines represent inhibition. Based on information from: (Atkinson & Senior, 2003; Poitras *et al.*, 2003; Lin *et al.*, 2008).

Later work implicated the signalling pathway shown in Figure 1.10 showing how TGF- α may induce metalloproteinases. The induced expression of MMP-9 with TNF- α has been shown to be statistically significant in a time and concentration dependent

manner using zymography in A549 cells cultured in serum-free media at 37 °C. The p42/p44 MAPK pathway was found to be involved through the use of an inhibitor of MEK 1/2 (an upstream component of the pathway) called U0126. The inhibitor was found to reduce the expression of MMP-9 in a concentration-dependent manner. This result was confirmed using cells transfected with siRNA for MEK1 and double negative mutants for ERK2, showing a reduction in TNF- α induced MMP-9 expression. To investigate if JNK regulated MMP-9 expression in A549 cells, an inhibitor for JNK (SP600125) has been used, causing a reduction in TNF- α induced MMP-9 expression. To show that NF- κ B was involved in the TNF- α induced expression of MMP-9, an inhibitor of NF- κ B (helenalin) has been used, resulting in a decrease in expression in a concentration-dependent manner (Lin *et al.*, 2008). Phosphatidylinositol 3-Kinase (PI3K) as shown in the signalling pathway above (Figure 1.10) is also known to be involved in the biosynthesis and activity of CFTR, which links EGF, EGFR and gelatinase expression to CFTR regulation. The mechanism with which PI3K regulates CFTR is through heterologous desensitisation and regulation of the β_2 -adrenergic receptors (Roux *et al.*, 2010). Transforming growth factor β_1 inhibits the β_2 -adrenergic receptor agonist-stimulated alveolar epithelial transport though PI3K, so PI3K inhibition can aid alveolar fluid clearance (Roux *et al.*, 2010). In a study by Uribe *et al.*, 2002, interferon- γ has been shown to increase tyrosine kinase phosphorylation via the release of TGF- α , which inhibits calcium-activated chloride secretion. It was also demonstrated that another ligand of EGFR – EGF, is able to inhibit calcium activated chloride secretion (Uribe *et al.*, 2002). The regulation of other metalloproteinases and lung inflammation induced by IL-8 has been shown to be partly mediated through EGFR. Neutrophil elastase was found to induce the metalloproteinase meprin alpha, which in turn is able to release soluble TGF- α . TGF- α activates EGFR resulting in the production of the proinflammatory cytokine IL-8, leading to lung inflammation. Neutrophil elastase can also bring about IL-8 induction through the TLR4-MAL/MyD88-IRAK-NF κ B pathway (Figure 1.11) (Bergin *et al.*, 2008)

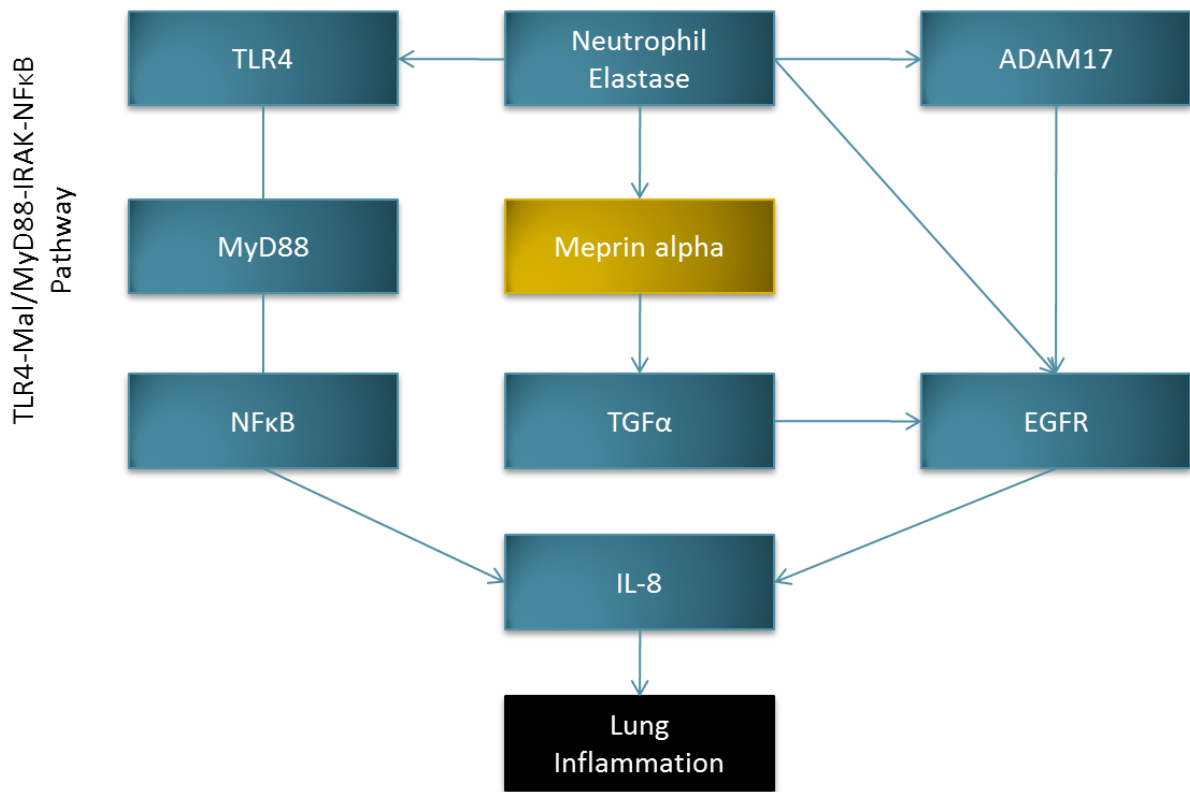


Figure 1.11 – The effect of neutrophil elastase on lung inflammation.

Schematic showing the effect of neutrophil elastase on IL-8 induced lung inflammation, which is mediated through metalloproteinase meprin alpha, and EGFR and its ligand TGF- α . Based on information from: (Bergin *et al.*, 2008)

1.5.1 EGF and EGFR in lung disease

EGF, as well as other growth factors such as PDGF, endothelin, basic fibroblast growth factor (FGF2), Transforming growth factor beta (TGF- β), and cytokines such as TGF- α are secreted by damaged lung epithelial tissues indicating that EGF is present in the lung and involved in the repair of lung tissue (Mercer *et al.*, 2006). The EGF receptor is expressed by bronchial epithelial cells, and regulates not only tissue repair, but also mucin production (Shute *et al.*, 2003). EGFR dependent mucin production is facilitated by fibrinogen binding to Intercellular Adhesion Molecule 1 (ICAM-1) (Kim & Nadel, 2009). Tissue damage occurring in CF can be worsened by poor EGF signalling. In the lung, EGFR signalling and potassium channel activity facilitate cell proliferation and migration. The inhibition of potassium channels by clofibrate and glibenclamide reduced wound repair in NuLi (normal lung) and CuFi (cystic fibrosis) cells (Trinh *et al.*, 2008). The presence of EGF in the sputum of CF patients increases during therapy (Colombo *et al.*, 2011) and EGFR is upregulated in the airways of asthma and COPD patients (Lai & Rogers, 2010). Levels of EGF are

also elevated in patients that have suffered from an acute asthma attack (Enomoto *et al.*, 2009). TNF- α also facilitates wound repair in NuLi and CuFi cells, which can be prevented by matrix metalloproteinase inhibitor GM6001 and EGFR inhibitor AG1478, suggesting that the wound healing process is mediated through transactivation of the EGF receptor and stimulation of the K_v LQT1 and K_{ATP} potassium channels (Maille *et al.*, 2011b). Similarly, EGF is also important in modulating K_v LQT1 and K_{ATP} potassium channels in the lung in alveolar epithelial cells to promote repair, which can be inhibited by tyrosine kinase and potassium channel inhibitors (Trinh *et al.*, 2007).

1.5.2 EGF and potassium ion transport in other tissues

As described in Figure 1.12, EGF plays an important role in intestinal chloride ion transport (McCole & Barrett, 2009) and that there is a link between MMP activity and potassium ion channel regulation that involves Heparin binding EGF (HB-EGF) shedding by MMP cleavage in rabbit cerebral artery myocytes (Koide *et al.*, 2007). Activation of EGFR in the gut leads to an inhibition of basolateral potassium channels via a signalling mechanism consisting of phosphatidylinositol 3-kinase (PI3K) and protein kinase C- ϵ (PKC- ϵ). This signalling mechanism is favoured over an EGFR – ERK signaling pathway also present, which has an inhibitory effect on apical chloride secretion (Chow *et al.*, 2000).

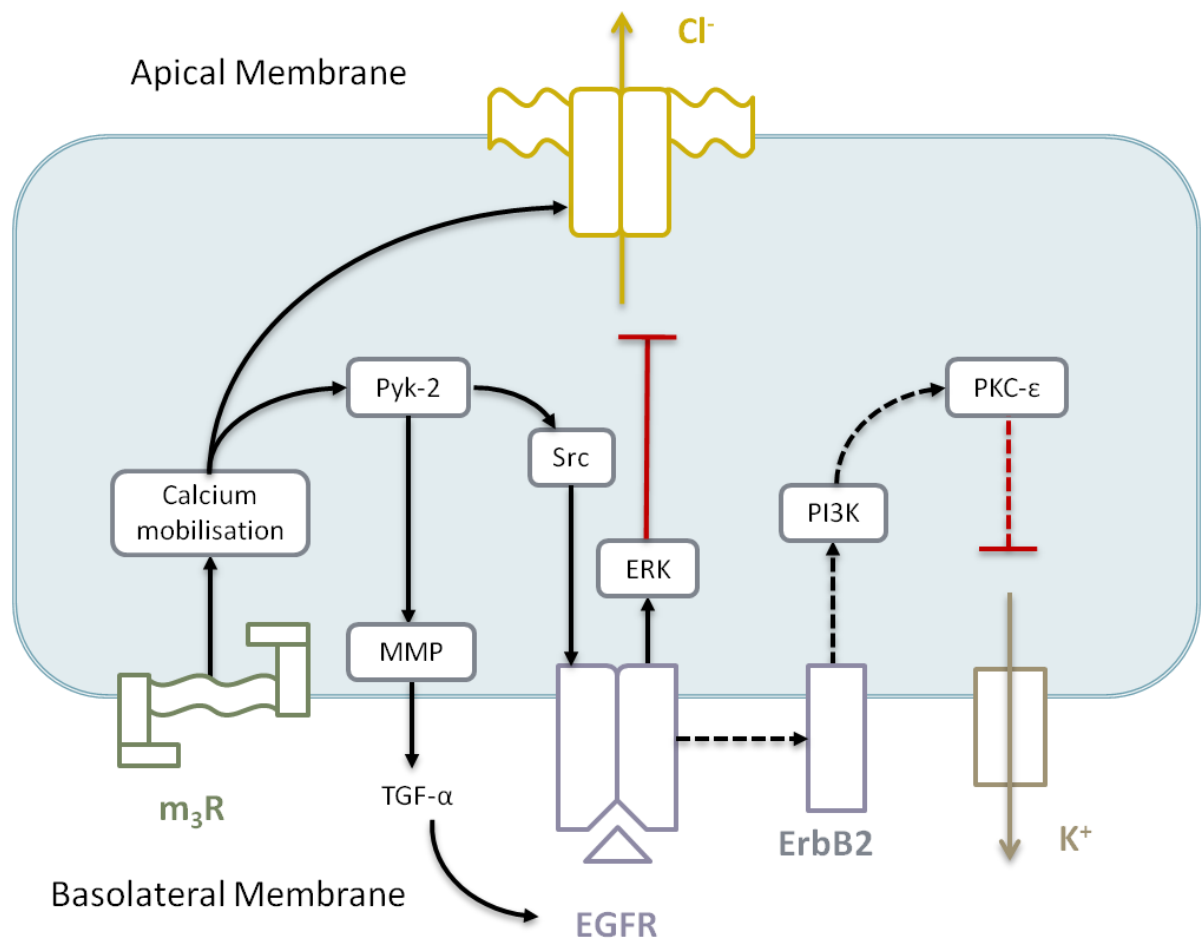


Figure 1.12 – The role of EGF on chloride secretion in the gut.

Dashed lines represent direct effects of EGFR signalling, whereas the solid lines represent transactivation processes. Based on a schematic by: (McCole & Barrett, 2009).

Moreover, the voltage-gated potassium channel KCNA2 is regulated by tyrosine kinases such as EGFR. The channel undergoes endocytosis when tyrosine kinases are active (Nesti *et al.*, 2004). Activation of EGFR leads to a sustained increase in KCNN4 conductance in vascular smooth muscle cells extracted from rat basilar arteries. This effect was seen using several different ligands of EGFR such as EGF, TGF- α and HB-EGF, which could be blocked by tyrosine kinase inhibitor, AG1478, or iberiotoxin, a KCNN4 specific inhibitor (Ivanov *et al.*, 2006). In the skin, wound healing is promoted by EGF by activating protein kinase C, protein tyrosine kinase and ERK MAPK, and as a result regulates potassium channels. Potassium channel activity has been associated with wound healing (Kang *et al.*, 2008). In bladder urothelial cells cultured from patients with interstitial cystitis, EGF and HB-EGF modulates inward potassium currents through regulation of $K_{ir}2.1$ (Sun *et al.*, 2007). The activation of

EGFR by EGF is known to modulate the KCNA3 channel in HEK293 cells (Bowlby *et al.*, 1997).

1.5.3 Potassium channels in the lung

Early work carried out using the Calu-3 cell line identified the expression of KCNN4 and KCNQ1 which could be characterized by using potassium channel inhibitors clofilium and clotrimazole (Cowley & Linsdell, 2002). Blockers for potassium channels such as KCNN4 and KCNA3 are potential treatments for conditions such as asthma and that they are important in regulating levels of intracellular calcium and regulate chloride secretion (Bradding & Wulff, 2009). The submucosal gland cell line Calu-3 are known to regulate their volume in response to changes in osmolarity. Voltage gated potassium channels including $K_v4.1$ and / or $K_v4.3$ allow the cell to decrease cell volume following an initial cell swelling, and that calcium activated potassium channels $K_{Ca}1.1$ and KCNN4 are also involved in cell volume recovery (Harron *et al.*, 2009). Calu-3 cells are also known to express mRNA and protein for KCNQ1, KCNQ3, KCNQ4 and KCNQ5. These channels are responsible for chromanol 293B and XE991 sensitive basal anion currents (Moser *et al.*, 2008). Apically localized two pore domain potassium channels are also thought to play an important role in transepithelial anion secretion in Calu-3 cells (Davis & Cowley, 2006). Blockers of two pore domain potassium channels inhibit both sodium absorption and anion secretion in polarized, normal human bronchial epithelial cells at lower concentrations when applied to the basolateral membrane compared to the apical membrane (Zhao *et al.*, 2011). Since EGF has previously been linked to regulating potassium channels in epithelial tissues, it is clear that a detailed look at the effects of EGF on ion transport in the lung could be a beneficial avenue for alternative ion channel therapy in cystic fibrosis.

1.6 Purpose of Study, Hypothesis and Aims

While the role of EGF in the gut has been investigated in some depth, very little is currently known about the role of EGF in the lung with regards to ion transport. In particular, the role of EGF in regulating ion transport in Calu-3 cells has not been previously investigated. Although some work with Calu-3 cells has been conducted on potassium channels with regards to KCNN4 (Devor *et al.*, 1999; Palmer *et al.*, 2006) and KCNQ1 (Palmer *et al.*, 2006), the expression of some potassium channels such as KCNA2 and KCNA3 in Calu-3 cells is still currently not known.

Thus in order to address these gaps in the current knowledge, the purpose of this work was to discover the mechanism with which epidermal growth factor (EGF) can regulate ion transport in the airways. The experimental methodology in this study principally employed the use of the submucosal Calu-3 cell line as a model of chloride transport in the human lung. This new knowledge would allow for the discovery of potential therapeutic targets for which drugs could be developed in order to improve the lives of those living with diseases such as CF.

We initially hypothesised that MMPs directly or indirectly interact with CFTR leading to decreased Cl^- channel function observed in the literature (Duszyk *et al.*, 1999). From studies previously carried out in the gut (McCole & Barrett, 2009), we further hypothesised that EGF had an effect on chloride transport in the airways. The effect was either facilitated via a direct signalling pathway or through a transactivation process involving sheddases as described previously (Liebmann, 2011).

Therefore to test these hypotheses, the principle aims of this study included:

- Characterising the functional response of Calu-3 monolayers to forskolin and UTP stimulation and demonstrating the gene and protein expression of chloride channels and candidates;
- Investigating gelatinase activity in the Calu-3 cell line in response to the stimulants phorbol-12-myristate-13-acetate (PMA) and EGF using gelatin zymography and investigating the link between MMPs and CFTR in the airways using short circuit current;
- Investigating the link between the EGF signalling pathway and the regulation of potassium channels in the airway, with possible implications for chloride transport;
- Investigating the link between the EGF signalling pathway on stimulated chloride transport;
- Examining the gene expression of potential regulators of chloride transport including beta receptors and potassium channels in airway epithelial cell lines, particularly Calu-3. Subsequently, investigating if EGFR transactivation occurs upon stimulating the β_2 adrenergic receptor.

Chapter 2 Materials and Methods

2.1 Cell culture

The Calu-3 cell line was obtained from the American Type Culture Collection (ATCC, Rockville, MD). The A549 cell line was kindly donated by Darren Sexton (University of East Anglia), and the CFPAC cell line was kindly provided by John Winpenny (University of East Anglia). The initial vials of Calu-3 (ATCC, HTB-55, passage 19), A549 (ATCC, CCL-185) and CFPAC cells (ATCC, CRL-1918) were frozen in a dewar of liquid nitrogen until required. Calu-3 cells were used between passage 19 and 60 for all investigations.

2.1.1 Preparation of culture media

The culture media for Calu-3 cells was based on previous studies (Winton *et al.*, 1998a; Liang *et al.*, 2009). This media was Minimum Essential Medium (41090, Invitrogen), which contained Earle's Salts, non essential amino acids, GlutaMAX™ and low glucose (1.0 g/L), supplemented with 10% fetal calf serum (Invitrogen) and 1% penicillin/streptomycin (Invitrogen). For A549 cells, the culture media, based on previous studies (Pelletier *et al.*, 2002), was RPMI 1640 (21875, Invitrogen), which contained L-glutamine, supplemented with 10% fetal calf serum (Invitrogen) and 1% penicillin/streptomycin (Invitrogen). For CFPAC cells, the culture media was Iscove's Modified Dulbecco's Medium (Sigma), supplemented with 20 mM L-glutamine (Invitrogen), 10% fetal calf serum (Invitrogen) and 1% penicillin/streptomycin (Invitrogen). The fetal calf serum and penicillin/streptomycin was aliquoted and then frozen until required. The complete culture media was aliquoted into 50 ml tubes and refrigerated until required.

2.1.2 Initial seeding and maintenance

The Calu-3 cells were thawed quickly in a 37 °C water bath until completely defrosted. An aliquot from the prepared culture media was placed in a water bath at 37 °C for 30 minutes. Inside a sterile class II airflow hood, the Calu-3 cells were pipetted into a T25 tissue culture flask (NUNC) initially along with 4 ml of the warmed prepared culture media to give 5 ml in total. The culture flask was then transferred into a humidified incubator that was maintained at 37 °C and with 95% O₂ and 5%

CO₂. For cell viability and growth assays, cells were grown on 12 or 24 well plates (NUNC) as appropriate and the cell suspension obtained through incubation with 0.25% trypsin/EDTA (Invitrogen). For Western blotting and gelatin zymography studies, cells were also grown on 24 well plates until confluent, washed with PBS and fed with serum free media. The conditioned media was collected over a period of days. The tissue culture media is replaced in a sterile airflow hood every two days.

2.1.3 Trypsinization and splitting procedure

After the Calu-3 cells became 80% confluent within the culture flask, the trypsinisation and splitting procedure was necessary. Firstly, Trypsin/EDTA (Invitrogen) was pipetted out into 5 and 10 ml aliquots and then frozen until required. An aliquot of culture media, PBS and an aliquot of trypsin/EDTA was put into a water bath at 37 °C for 30 minutes. A hood was prepared with a rack for the warmed media and 0.25% trypsin/EDTA, the warmed PBS, the tissue culture flask(s) of cells, additional flasks, a container of 1:10 trigene, 5 ml and 10 ml pipettes and a pipetting gun. The tissue culturing flask containing the cells was washed with 5 ml (T25) or 10 ml (T75) of PBS three times and the liquid was poured off into the container of 1:10 trigene. Then, 2.5 ml (T25) or 5 ml (T75) of 0.25% trypsin/EDTA was added to the tissue culturing flask of Calu-3 cells, and the flask was then placed inside an incubator at 37 °C for approximately 10 minutes. The cells were gently agitated during this time to free them from the plastic. Then, the cell suspension was pipetted into a 15 ml centrifuge tube, spun at 800 rpm for two minutes, and was resuspended into 10 ml of culture media, before being pipetted into a fresh flask. The new flask was then placed into the incubator at 37 °C and at 95% O₂ and 5% CO₂. The split ratio commonly used for this process was 1:3.

2.1.4 Freezing down procedure

Following a splitting procedure, the remaining cells not allocated to reseeding a new culture flask following the split were centrifuged at 1000 rpm for 4 minutes. The supernatant that is formed was removed, leaving behind a pellet of cells. The cells were then resuspended by pipetting up and down about 20 times in freezing media, consisting of 95% culture media with 5% DMSO added to prevent crystal formation. The cell suspension was then pipetted into 5 cryovials with 1 ml in each, and then

stored into a container of 250 ml isopropanol at -80 °C to slowly freeze them. The cryovials were then frozen within a dewar of liquid nitrogen until required.

2.2 Reverse Transcriptase Polymerase Chain Reaction (RT-PCR)

2.2.1 RNA extraction

Cells were grown to confluence in a T25 flask (NUNC). A cell scraper was used to harvest cells and the resulting suspension was spun in a 15ml conical tube at 800 rpm for 5 minutes. The supernatant was removed and the cells were resuspended in 1% PBS and were transferred into 1.5 ml Eppendorf tubes. The tubes were pulsed at 13,000 rpm and the supernatant was removed. 800 μ l of Trizol reagent and 200 μ l of chloroform was added to each tube in a fume hood. The tubes were briefly vortexed and spun at 4 °C at 13,000 rpm for 15 minutes. The supernatant was removed and pipetted into a fresh 1.5 ml Eppendorf with an equivalent volume of 100% isopropanol. The tubes were incubated at room temperature for 10 minutes. The RNA was pelleted by centrifuging at 4 °C at 13,000 rpm for 15 minutes. The supernatant was removed and 1 ml of 70% ethanol made with nuclease free water was added, and then the tube is gently mixed. The tubes were centrifuged at 4 °C at 13,000 rpm for 15 minutes and the supernatant was removed and discarded. The RNA pellet was air dried for approximately 10 minutes, and then was resuspended in approximately 20 μ l of nuclease free water. The resulting RNA samples were then tested for purity and concentration by using a nanodrop spectrophotometer (Thermo Scientific). 1 μ l of RNA was analysed to give the RNA purity, and the concentration in ng/ μ l. $A_{260/280}$ values refer to contamination by proteins. Ideal values for this measure are around 2.0. $A_{260/230}$ values indicate the degree of contamination by phenolate ions, thiocyanates, and other organic compounds, with around 2.0 being a pure RNA sample.

Each RT-PCR figure shows gene expression from one RNA sample and from one passage of cells. Replicates used RNA samples harvested from cells at a different passage number. The RNA samples used for RT-PCR in Figure 3.7, Figure 3.8 and their replicates had $A_{260/280}$ values of between 1.17 to 2.07, $A_{260/230}$ values of between 1.08 to 2.19 and concentrations between 502.3 and 5016.0 ng/ μ l. The RNA samples used in Figure 6.3, Figure 6.4 and their replicates had $A_{260/280}$ values of between 1.67

to 1.90, $A_{260/230}$ values of between 0.29 to 1.05 and concentrations between 112.0 and 479.0 ng/ μ l. RNA samples used in Figure 5.5, Figure 7.10 and their replicates had $A_{260/280}$ values of between 1.87 to 2.02, $A_{260/230}$ values of between 1.03 to 1.89 and concentrations between 416.2 and 3066.2 ng/ μ l.

2.2.2 Preparation of samples for reverse transcription

The samples were diluted 1:10. 0.5 ml Eppendorf tubes were labelled, and two 1.5 ml Eppendorfs were used to create a mastermix – one contained the RNA of interest, and the other without (for use as a negative control). The mastermix was created using a QIAGEN One Step PCR kit, which contained 5 x Buffer, deoxynucleotide triphosphates (dNTPs), Enzyme Mix and nuclease free water. 1.5 μ l of each primer (sense and anti-sense) was added to each tube accordingly.

Table 2.1 – Concentration of PCR reaction mix components

Component	Volume (μ l)	Final Concentration
RNAse-free water	Variable	-
5x RT-PCR buffer	5	1X
dNTP mix	1	400 μ M per dNTP
Primer A	1.5	0.6 μ M
Primer B	1.5	0.6 μ M
RT-PCR Enzyme mix	1	-
Template RNA	Variable	2 μ g per reaction

A summary of how the samples were prepared is described in Table 2.1. An Applied Biosystems 96-well thermal cycler was used to carry out the RT-PCR reactions. RT was performed at 50 °C for 30 mins and Taq polymerase activated 95 °C for 15 mins. The product was subject to 40 rounds of three step cycling, consisting of denaturation (94 °C for 1 min), annealing (52 °C for 1 min) and extension (72 °C for 1 min 30 s). The final elongation step was performed at 72 °C for 10 mins. The products were stored at 4 °C, until required. β -actin was used as a positive control and each sample had a corresponding negative control consisting of the PCR reaction without the addition of the template RNA, indicated as (-).

This primer sequences used are listed in Table 2.2 and Table 2.3. The β -actin, bestrophin and anoctamin primers were a kind gift from Laura Marsey (University of

East Anglia). The primer sequences for the beta adrenergic receptors were taken from Bossard *et al.* (2011); KCNA2 and KCNA3 were taken from Mackenzie *et al.* (2003); CFTR and KCNN4 were taken from Cowley & Linsdell (2002) and KCNQ1 was taken from Currid *et al.* (2004)

Table 2.2 – Chloride channel primer information and sequences.

Gene Name	Accession Number	Primer Sequences – Sense	Primer Sequences - Antisense	Length (bp)
ACTB	NM_001101.3	272-GCATCCTCACCCCTGAAGTAC-291	728-TTCTCCTTAATGTCACGCAC-709	456
BEST1	NM_004183.3	1952-CTGTATCAGAGGCCAGGCTA-1971	2263-GTTGGTGAATTGTCACAAAG-2244	311
BEST2	NM_017682.2	509-AGTTGAAACCTGAACTCATCCT-533	929-AGAAAGTTGGTCAAAAGTCATCAT-905	420
BEST3	NM_032735.2	1476-ACAAGTCCATGTCCTTAC-1500	1991-TTTAGAAAGGTATCACAGGTCT-1967	515
BEST4	NM_153274.2	1007-TTTGAGACAAATCAGCTCATAGACC-1031	1616-TCTTCTCTTTCAAGTTCTGTCCTCA-1592	609
ANO1	NM_018043.5	2122-TGATCTCAAGGCTTTCCTG-2141	2397-GCTGCTTCAGTTAGGTAG-2378	275
ANO2	NM_020373.2	2285-CTCCGGAGTACATGAAATG-2304	2493-CTTGCCAATTCCAGAGAGAA-2474	208
ANO3	NM_031418.2	2208-TGATAGACCTCTGCCCTCAG-2227	2361-TTTTCCACTGAGGTATGGA-2342	153
ANO4	NM_178826.3	2935-TGATAGACCTCTGCCCTCAG-2954	3156-AAAACACGAGGTGGCTCAAAG-3137	221
ANO5	NM_213599.2	1494-TGGGTCAACCTTATTGTTGGA-1513	1831-TTGACCTGCTTTAGGGATGCA-1812	337
ANO6	NM_001025356.2	1459-GTTTTGGAACCCCTGGCTTT-1478	1659-GAATGGTTCTTCTCTGA-1640	180
ANO7	NM_001001891.3	1862-TTCACCCCTCAAGGTTCAT-1881	2082-ACCTCCCTGCATGTTGTTGAT-2063	220
ANO8	NM_020959.2	1257-GTGCCTCGTCTGTTCT-1276	1518-GAGGCTCAGGTACGAGTTGA-1499	261
ANO9	NM_001012302.2	703-GACGGGCCCTAGTCCTTC-722	877-ATTGGTCAAAAGGGTGGTGA-858	174
ANO10	NM_018075.3	694-GACAGTGAAGCCCTGAAGAA-713	915-CGAGGCAAAGATCACGTACT-896	221
CFTR	NM_000492.3	471-CAAGGAGGAACGCTCTATCG-490	796-ACGGAGGAACAACTCCCCAG-777	326

Table 2.3 – Primer information – beta adrenergic receptors and potassium channels

Gene Name	Accession Number	Primer Sequences - Sense	Primer Sequences - Antisense	Length (bp)
ADRB1	NM_000684.2	350-GCTGCAGACGCTCACCA-366	562-GCGAGGTAGGGTCCAG-546	212
ADRB2	NM_000024.5	404-CACAGCCATTGCCAAGTTCG-423	691-CGGCCTATTCTGGTCAGC-671	287
ADRB3	NM_000025.2	604-ACCTGGCTGTGACCAAC-620	726-ACTGGCTCATGATGGCGC-708	122
KCNQ1	NM_000218.2	1110-CTTTGCCATCTTCTTTG-1128	1521-AGTGTGGCTCTCCTTAC-1540	411
KCNA2	NM_004974.3	702-AGACCCAGGAGTGTGAGA-721	1239-GGAATAGGTGTGAAAGGTCA-1220	538
KCNA3	NM_002232.3	1732-GAAGTTGCCAGCACCTCTCCTTC-1756	2000-GGCACGGTCCACACAAATACTGAGC-1977	269
KCNN4	NM_002250.2	909-CGGCGTCCTGCTCAACG-925	1242-CACCAGGGCTGTGCAG-1224	337

2.2.3 Preparing the ethidium bromide gel

The gel equipment was assembled and the electrophoresis chamber filled with 1 X Tris-Borate-EDTA (TBE), made with 17.02 g of TBE buffer (Sigma) in 1 l of distilled water. 40 g of agarose (Sigma) was added to 400 ml of TBE to produce a 1% gel solution, and was heated in a microwave for 3.5 minutes until boiling, with gentle mixing mid way through. The gel mix was cooled and 8 μ l of ethidium bromide solution was then added. The solution was poured slowly into an enclosed frame, and the combs were inserted into the frame. The gel was left to set for approximately 15 minutes. The samples were retrieved from the PCR machine and 5 μ l of loading buffer was added to each. The samples were loaded with Hyperladder I (BIO-RAD) at each end with a space of one gap. The gel was then run at 150 V for 1 hour.

2.2.4 Imaging the gels and densitometry

After the gel had run, they were removed from the apparatus and the products visualized digitally using a Bio-Doc-It System (UVP). A digital image was saved onto floppy disk and transferred to a PC. The digital image was converted to bitmap and opened using ImageJ software. The bands were selected and the area, mean grey value and optical density values were recorded. The values for the tester samples were normalised to the β -actin control, and then the mean fold change in RNA expression was calculated using a spreadsheet in Microsoft Excel. The full process is described below:

$$\frac{\text{Mean Stimulated Sample Optical Density} / \beta\text{-actin optical density}}{\text{Mean Unstimulated Sample Optical Density} / \beta\text{-actin optical density}}$$

The data were then graphed using Graphpad Prism 5.0 software.

2.2.5 Band extraction and sequencing

QIAquick Gel Extraction Kits were used to extract and purify DNA of 70 bp to 10 kb from standard or low-melt agarose gels in Tris-acetate-EDTA (TAE) or TBE buffer.

2.2.6 Obtaining and solubilising the gel slice

The DNA fragment was excised from the agarose gel with a clean, sharp razor blade, ensuring that the size of the gel slice was minimised by removing excess agarose. The gel slice was weighed in a 1.5 ml microcentrifuge tube. 3 volumes of Buffer QG

were added to 1 volume of gel (100 mg approximates to 100 μ l). The maximum amount of gel slice per QIAquick column is 400 mg, so for gel slices greater than 400 mg, more than one QIAquick column was used. The tubes containing the gel slides and buffer QG were incubated on a heat block at 50 °C for 10 minutes (or until the gel slice had completely dissolved). To help dissolve gel, the tube was mixed by vortexing every 2–3 minutes during the incubation, making sure that the agarose had solubilised completely. After the gel slice had dissolved completely, the colour of the mixture was checked to determine that it was yellow. If the colour of the mixture was orange or violet, 10 μ l of 3 M sodium acetate, pH 5.0 was added, and mixed. The colour of the mixture should turn to yellow. The adsorption of DNA to the QIAquick membrane is efficient only at pH \leq 7.5. The Buffer QG contains a pH indicator which is yellow at pH \leq 7.5 and orange or violet at higher pH, indicating the optimal pH for DNA binding. 1 gel volume of isopropanol was added to the sample and mixed. For example, if the agarose gel slice was 10 mg, 100 μ l isopropanol was added. This step increases the yield of DNA fragments less than 500 bp and greater than 4kb. For DNA fragments between 500 bp and 4 kb, addition of isopropanol has no effect on yield.

2.2.7 Loading sample into spin columns

Ethanol (96–100%) was added to the stock Buffer PE as directed. QIAquick spin columns (one for each slice) were placed in the 2 ml collection tubes. The samples were applied to the QIAquick column to bind DNA, and were centrifuged for 1 minute. The maximum volume of the column reservoir was 800 μ l. For sample volumes of more than 800 μ l, the remaining sample was loaded and spun again. The flow-through was discarded, and the QIAquick column was placed back in the same collection tube. 0.5 ml of Buffer QG was added to each QIAquick column and centrifuged for 1 minute to remove all traces of agarose. To wash, 0.75 ml of Buffer PE was added to each QIAquick column before they were centrifuged for 1 minute. The flow-through was discarded and the QIAquick columns were centrifuged for an additional 1 minute at 17,900 \times g (13,000 rpm). Finally, the QIAquick columns were placed into a clean 1.5 ml microcentrifuge tube.

2.2.8 Elution of DNA

To elute DNA, 50 µl of Buffer EB (10 mM Tris-HCl, pH 8.5) or water (pH 7.0–8.5) was added to the centre of the QIAquick membranes and the columns were centrifuged for 1 minute. Alternatively, for increased DNA concentration, 30 µl elution buffer was added to the centre of the QIAquick membrane, the column left stand for 1 min, and then was centrifuged for 1 minute. Elution efficiency is dependent on pH. The maximum elution efficiency is achieved between pH 7.0 and 8.5, so the pH value was checked to be within this range, and the DNA stored at –20 °C as DNA may degrade in the absence of a buffering agent. The resulting extracted DNA was sequenced by the John Innes Genome Laboratory (Norwich Research Park, Norwich, UK).

2.3 Western Blotting

2.3.1 Preparation of solutions

The following solutions were prepared in order to carry out the Western blotting experiments:

Table 2.4 – Solutions required for Western blotting.

Solution	Constituent	Concentration
10x SDS Running Buffer (1 litre)	Tris Glycine SDS	0.25 M 0.5 M 3%
10x Transfer Buffer (1 litre)	Tris Glycine SDS	480 mM 390 mM 3%
6x Protein loading dye (10 ml)	Tris Glycerol Bromophenol blue β-mercaptoethanol	6 mM 20% 0.005% 5%
10x Tris-buffered saline with Tween (TBST) (1 litre)	Tris NaCl Tween	0.25 M 1.5 M 0.5%
Coomassie Blue membrane stain (1 litre)	Coomassie brilliant blue MeOH Acetic acid H ₂ O	0.25% 45% 10% 45%

2.3.2 Protein extraction and quantification

2.3.2.1 RIPA buffer extraction

The cells were grown until confluent in T75 tissue culturing flasks and then were trypsinised to obtain the cell suspension, which was then pelleted by centrifuge at 1,000 rpm for 5 minutes. The supernatant was removed and PBS was added. The cells were resuspended, transferred into an Eppendorf tube and pelleted by centrifuge at 1,000 rpm for 5 minutes. 1 ml of cold RIPA buffer was added and the pellet was agitated on ice for 15 minutes. The cells were then centrifuged at the maximum speed at 4 °C for 15 minutes. The supernatant was removed and

transferred to a fresh Eppendorf tube, then labelled and frozen, and the pellet was discarded. The protein was quantified using a BCA Protein Assay Kit (Pierce).

2.3.2.2 Hot SDS buffer extraction

Cells were grown to 100% confluence in tissue culture flasks and then trypsinised to obtain the cell suspension, which was then pelleted by centrifuge at 1,000 rpm for 5 minutes. The supernatant was removed and 150 μ l of lysis buffer (1% SDS, 10 mM Tris-HCl pH 6.8, double-distilled water (ddH₂O)) was added. Each sample was then boiled at 100 °C for 5 minutes and then sonicated for one minute in short 10 second bursts, whilst being kept on ice between bursts. Protein was quantified as before.

2.3.2.3 NP-40 buffer extraction

Cells were grown to 100% confluence in tissue culture flasks. Typically two T75 flasks were used per extraction. The flasks were rinsed with ice cold PBS two to three times. The cells were scraped to one edge of the T75 flask, and 1ml of NP-40 buffer was added. The cell suspension was transferred to 1.5 ml Eppendorf tubes and then spun for 5 minutes at 13,000 rpm. The supernatant was removed and discarded, leaving behind a pellet. The pellet was then frozen with liquid nitrogen and ground up using a mortar and pestle, and 80 μ l of NP-40 was added. The resulting powder was transferred to a 0.5 ml Eppendorf tube and was kept on ice for five minutes. The tubes were spun for 10 minutes at 13,000 rpm at 4 °C. The supernatant was removed and retained for cytosolic proteins, and the pellet was processed further. The pellet was rinsed in ice cold 1% PBS. 20 μ l of NP-40 was added to the pellet. The cells were homogenised, and then left on ice for 5 minutes, and then spun for 10 minutes at 13,000 rpm at 4 °C. The supernatant was removed and retained for membrane proteins while the pellet was discarded. Protein was quantified as before.

2.3.3 Protein separation

The samples were prepared on ice so that 30 μ g of protein was allocated to each lane on the gel. An additional sample was prepared to compensate for any sample lost during boiling. The BIO-RAD assay spreadsheet provided a volume for each 10 μ g of sample, so this was multiplied by three to give a value for 30 μ g. For protein samples loaded into more than one well, the value was multiplied by the amount of wells used. For every 30 μ g of sample, 5 μ l of protein loading dye was used. Before

the samples were loaded, they were boiled for three minutes and then allowed to cool. Then the samples were lightly spun to allow the protein to settle on the bottom of the tube. The gel apparatus was then set up as for gelatin zymography (see Section 2.5), and the samples were loaded along with a marker, making sure to label the gel so that the orientation could easily be determined. The gels were then run at 80 mV until the samples have passed through the stacking (upper) gel and had entered the separation (lower) gel. The voltage was then increased to 100 mV, and was left for approximately 2.5 hours to run. After the samples had run, the running buffer was poured out and the gel apparatus was dismantled.

2.3.4 Protein Transfer

The PVDF membrane was soaked in methanol before use. From the 10x transfer buffer stock solution, the transfer buffer was made up with 100ml of buffer, 200ml methanol and 700ml distilled H₂O. The papers, sponge and membrane were then soaked in the transfer buffer.

2.3.4.1 Wet transfer technique

For determining the expression of MMP-2 in Calu-3 cells, the gel cassette was set up in the following order: Black side of the cassette, sponge, paper, gel, membrane, paper, sponge. The gel was removed gently with a spatula. The cassette was then placed into the tank, with the black side of the cassette facing the black side of the holder, along with an ice pack and approximately 750 ml of transfer buffer. The blot was then run at 200 mA for 1 hour in a cold room.

2.3.4.2 Semi-dry technique

For subsequent investigations, the semi-dry technique was used in place of wet transfer. The PVDF membrane was cut to a size slightly larger than the gel and was then soaked in 100% methanol, then washed in TBST. Two sheets of filter paper (Whatman) were cut to a size slightly larger than the membrane and soaked in transfer buffer. One of the soaked sheets of filter paper was placed into a trans-blot SD assembly (BIO-RAD), which consisted of a flat anode bed with integrated electrode assembly. The membrane was then carefully placed on top of the filter paper, ensuring all the time that it was kept wet with transfer buffer. The gel was removed from the gel apparatus and placed on top of the membrane. The other sheet

of filter paper was placed on top of the gel to form a sandwich, with any potential air bubbles removed by using a roller. The cathode was placed onto the apparatus and a constant current of 200 mA applied for 45 minutes at room temperature.

2.3.5 Antibody treatment

The cassette was disassembled and the membrane was then blocked in a square dish protein side up in 5% Milk/TBST for 1 hour. The primary antibody was prepared in a square dish in 10 ml of 5% Milk/TBST with the membrane, which was incubated on a shaker in a cold room overnight. The antibody can be reused if frozen. Listed below in Table 2.5 are the antibodies used for Western blotting.

Table 2.5 – Antibodies used for Western blotting.

Antibody type	Raised in	Reactivity	Concentrations used	Company
MMP	rabbit	anti-human	1:1000	Millipore
CFTR	mouse	anti-human	1:500	R & D Systems
β-actin	rabbit	anti-human	1:1000	Invitrogen
BEST1	mouse	anti-human	1:500	Novus Biologicals

Specific target sequences for the antibodies are unknown, although the R & D Systems CFTR antibody targets the R domain. Secondary antibodies used included horse radish peroxidise (HRP) labelled goat anti-human from Millipore, and green (480 nm) and red (600 nm) fluorescently labelled goat Alexa Fluor with reactivities of anti-mouse and anti-rabbit, respectively, from Invitrogen. HRP antibodies were used at 1:1000 dilutions, and Alexa Fluors at 1:2000 dilution. The membrane was then washed in TBST and 1% PBS. The secondary antibody was prepared in a square dish in 10 ml of 5% Milk/TBST with the membrane, which was incubated at room temperature for 2 hours. The membrane was then washed 5 times for 10 minutes in TBST and once in 1% PBS.

2.3.6 Signal detection

If HRP conjugated secondary antibodies were used, an equal part of the developing solution (SuperSignal West Pico Kit, 5 ml total per membrane) was added and the membrane was left for 5 minutes. The membrane was slightly dried and then loaded into an X-ray cassette inside a plastic bag or document wallet protein side up, avoiding air bubbles. The membrane was secured using tape. The film was opened in

a dark room, and one corner of the film was cut off. The membrane was then placed in the cassette, which was then closed and then left to expose for approximately 1 minute. The membrane was removed from the cassette making sure not to smear the membrane, and placed into the xograph. The membrane was not removed until it was lined up with the film and the marker had been added with permanent marker pen. In the case of use of Alexa Fluor secondary antibodies, membranes were imaged using an Odyssey infrared imager, and the band densities were determined using the ImageJ software.

2.4 Flow Cytometry

2.4.1 Cell counting

The hemacytometer and coverslip were first cleaned thoroughly with 70% ethanol, so that they were sterile and ready for use. Any excess ethanol was wiped off with blue roll. The coverslip was then placed in the centre of the haemacytometer. The cell suspension may be diluted several times (1:2, 1:10 and 1:100 dilutions) so that the concentration of cells was low enough to be suitable for counting. Of this cell suspension, approximately 9 μ l was pipetted onto one of the two available counting chambers of the haemacytometer, ensuring that no bubbles were introduced and that the chamber was not overfilled. The cell suspension was left to settle for 10 seconds. The cells were counted in each of the labelled areas (A, B, C and D). Cells touching the top and left borders were counted, but cells touching the bottom and right borders were not counted. The total cell count in areas A, B, C and D was calculated. The total cell count needs to be between 100 and 400, otherwise a different dilution factor must be used to ensure accuracy of counting. To calculate the concentration of cells per ml, the following equation was used:

$$\text{Cells/ml} = n \times 10^4 \times d$$

Where: n is the **average** number of cells in the squares of the hemacytometer.
d is the dilution factor used.

Once the concentration of cells was known, the total amount of cells in a given volume of cell suspension can then be determined by multiplying the concentration by the volume of cell suspension.

2.4.2 Cell viability with propidium iodide

To assess cell viability, a flow cytometry based approach using propidium iodide dye was used. 5 µl of propidium iodide was added to 195 µl of cell suspension. The sample was then run through a flow cytometer where the percentage of viable cells could be determined. Two controls were set up using initial cell suspension samples (as positive controls) and cell suspensions treated with Triton X-100 (negative controls). The resulting cell suspensions were run under the flow cytometer for analysis.

2.4.3 Cell growth and serum starvation

After the Calu-3 cells were trypsinised at approximately 60-80% confluence, within an airflow hood, culture media was added to make the volume up to 10 ml to inactivate the trypsin. The amount of cells per ml was known from counting the cells with the haemacytometer. The concentration of cells was used in order to determine the volume of cell suspension required to obtain a set number of cells. 5 mM of carboxyfluorescein diacetate succinimidyl ester (CFSE) stock solution was prepared by adding 18µl of DMSO to the 50 µg of lyophilized CFSE powder. The volume of cell suspension required to obtain 1 million cells per ml was determined by cell counting. The cell suspension was centrifuged at 800 rpm for 2 minutes, pelleted, and was then resuspended in the appropriate amount of 1% PBS to achieve a final concentration of 1 million cells per ml. 2 µl of 5mM CFSE stock solution was required for every ml of cell suspension, giving a 10 mM final solution. After the dye was added, the cell suspension was incubated at 37 °C for 10 minutes. 5 volumes of ice-cold media were added to quench the staining, and the solution was further incubated for 5 minutes on ice. The cells were then centrifuged at 800 rpm for 2 minutes, and then pelleted, and resuspended in fresh media twice. In one of the 12-well plates, the volume required for the specific cell counts (10,000, 20,000, 30,000 and 50,000) were pipetted using P200/P1000 pipettes into a 12-well plate, along with 500 µl of media with 10% fetal calf serum. In the other 12-well plate, the volume required for 20,000 cells was added to media made up with specific amounts of fetal calf serum (0%, 1%, 2% and 10%) were pipetted using P200/P1000 pipettes into a 12-well plate. Each time, the cells were pipetted up and down to maintain a single cell suspension. The seeded 12-well plates were then labelled, covered and placed into an incubator at 37 °C with 5%

CO₂. Once the cells on the 12-well plates were confluent, each well was trysinated, and propidium iodide was added (to determine cell viability). The cells are then analysed by a Flow Cytometer and the readings were recorded.

2.5 Gelatin Zymography

Conditioned media samples from A549 or Calu-3 cells were loaded into 7% polyacrylamide gels containing 2 mg/ml gelatin were subjected to electrophoresis under non-reducing conditions. Firstly, the gel apparatus was cleaned thoroughly with 70% ethanol, particularly the glass plates. The gel apparatus was then set up, making sure to check for leaks using distilled water. Ammonium persulfate (APS) (Sigma) was dissolved in PBS, while the gelatin (Sigma) was warmed up and dissolved in distilled water. The APS and TEMED (BIO-RAD) were added last as these cause the gel to set. The running gel mixture was mixed well and then pipetted between glass plates to within 2 cm of the top. The mixture was levelled off with isopropanol and left to set for approximately 20 minutes. When the gel was set, the water was poured off and the gel dried as much as possible. The comb was placed between the plates and pushed down about half way. Again, the APS and TEMED was added last as these cause the gel to set. The mixture was immediately used to fill between the glass plates, and then the comb was gently pushed down, making sure to avoid the formation of bubbles. The gel was then left to set for approximately 5 minutes.

2.5.1 Preparation of solutions

The following solutions must be prepared in order to carry out the gelatin zymography experiments and are shown in Table 2.6.

Table 2.6 – Table of solutions required for gelatin zymography.

Solution	Constituent	Final Concentration
Lower gel buffer	Tris (pH 6.8) SDS Distilled water (dH ₂ O)	0.5 M 0.4% -
Upper gel buffer	Tris (pH 6.8) SDS dH ₂ O	0.5 M 0.4% -
7% lower/running gel mixture	Acrylamide dH ₂ O Gelatin Lower Gel Buffer APS TEMED	40% - 2 mg/ml - 10% 2%
5% upper/stacking gel mixture	Acrylamide dH ₂ O Upper Gel Buffer APS TEMED	40% - 4x 10% 2%
Tris Assay Buffer	Tris CaCl ₂ dH ₂ O	50 mM 5 mM -
Coomassie blue solution	Coomassie Blue Acetic Acid Ethanol dH ₂ O	0.2% 7.5% 50% 42.3%
Non-reducing buffer	Tris (pH 6.8) SDS Bromophenol Blue Glycerol	1 M 10% 3% 40%

2.5.2 Preparing samples

20 μ l of the sample was added to 5 μ l 5x non-reducing buffer and kept on ice. The standard molecular weight marker used was Precision Plus Protein Standards All Blue (BIO-RAD). The gel was checked to make sure it had set and the comb was removed carefully to avoid the formation of bubbles. The gel was unclipped from apparatus and moved to the tank. The 10x Running Buffer was diluted to 1x with distilled water. 750 ml of this 1x running buffer was poured into the tank, in between and around the gel(s). The tank was not filled to the top until it had been moved to the power pack in order to prevent spillages. 12 μ l of samples and marker were loaded into each well using a syringe or microtips, making note if any wells were loaded with more or less sample. Two lane gaps were left between the marker and samples as the β -mercaptoethanol (Sigma) can leak across into other lanes, which might affect the stability of the protein in the samples.

2.5.3 Running the samples

The tank was connected to the power pack in a cold-room and was run for approximately 15 minutes at 30 mA for the two gels to stack and then a further hour at 40 mA for the two gels to run. The tank was checked for leaks and then the power pack was turned off when the coloured bands of the marker reach the bottom of the gel. The running buffer was poured off and the apparatus was taken apart. The gel was removed carefully and placed into 2.5% Triton (Sigma), where it was left to wash for 15 minutes. The 2.5% Triton was poured off and fresh 2.5% Triton was poured on to wash the gel again for 15 minutes. The 2.5% Triton was poured off and Tris Assay Buffer (TAB) was poured on and the gel was incubated overnight in a dry 37°C incubator, on a rocking table if possible.

2.5.4 Staining the gel

The following day, the TAB was poured off, and Coomassie Blue (Sigma) poured on, and the gel rocked for 15-20 minutes. The Coomassie Blue was poured off and then de-stain (30% MeOH, 1% acetic acid, Sigma) was poured on. The gels were then rocked until the upper gel was clear (which served as a good indication of how clear the gel get when there is no gelatin in the gel). The gel can be stored for weeks before imaging and analysing using an Odyssey Scanner in a Glycerol/Methanol mix.

Inhibition studies were conducted by adding 1 μ M GM-6001 to the Triton-X100 and TAB buffer.

2.6 Short Circuit Current

2.6.1 Tissue culturing

Cells were seeded at approximately 50,000 cells onto Costar® Transwell™ Permeable Supports of pore size 0.4 μ m and 1.12 cm^2 area (Fisher UK). 1ml of media was added to the basolateral side of the well, with 500 μ l added to the apical side. Transepithelial resistance was measured using an epithelial voltohmmeter (EVOM) (World Precision Instruments) until a confluent monolayer was formed, with an approximate resistance of 800 Ωcm^2 for Calu-3, and 200 Ωcm^2 for A549 cells. The apical fluid was then removed forming an air-liquid interface, and the cells allowed to further differentiate for typically seven days before use.

2.6.2 Preparation of Ussing chamber

Shown in Figure 2.1 is a schematic of the Ussing chamber used. Both sides of the epithelium were bathed in 5ml of Krebs-Henseleit solution that was continuously circulated through the half chambers, maintained at 37°C and continuously bubbled with 95% O₂ / 5% CO₂. The composition of the Krebs-Henseleit bath solution used was similar to that used by Cuthbert (Cuthbert, 2001) and had the following composition (in mM): NaCl 118, KCl 4.7, CaCl₂ 2.5, MgCl₂ 1.2, NaHCO₃ 25, KH₂PO₄ 1.2 and glucose 11.1 (pH 7.4). The permeable supports were left for 30 mins to equilibrate before experiments were started. In some experiments that investigated the apical membrane in isolation, the basolateral side of the monolayer was permeabilised by the addition of nystatin (0.36 mg ml⁻¹) for 15 minutes to the basolateral chamber (Anderson & Welsh, 1991). A chloride gradient from basal to apical was set up by replacing the Krebs-Henseleit solution in the apical chamber with Krebs-Gluconate of the following composition (in mM): NaCl 38, Na Gluconate 80.0, KCl 4.7, CaCl₂ 4.0, MgCl₂ 1.2, NaHCO₃ 25, KH₂PO₄ 1.2 and glucose 11.1 (pH 7.4). The CaCl₂ concentration was increased to allow for the chelating effect of the gluconate.

Table 2.7 – Summary of compounds used and their appropriate chambers.

Compound	Vehicle	Stock Concentration (mM)	Final Concentration (µM)	Action	Appropriate Chamber
AG1478	DMSO	5	5	EGFR inhibitor ENaC inhibitor General K ⁺ channel inhibitor Na-K-Cl cotransporter inhibitor CFTR inhibitor (intracellular) Specific β ₃ adrenergic receptor agonist Ca ²⁺ activated K ⁺ channel inhibitor General PKC inhibitor Specific KCNQ1 inhibitor General Cl ⁻ channel inhibitor Adenylate cyclase agonist CFTR inhibitor (extracellular) General MMP inhibitor Control for GM-6001 Specific KCNN4 inhibitor β ₂ adrenergic receptor antagonist β ₃ adrenergic receptor antagonist Adenylate cyclase inhibitor CaCC inhibitor Selective PKC inhibitor β ₂ adrenergic receptor agonist PKC and PKA inhibitor ERK inhibitor CaCC agonist PI3K inhibitor	Basolateral Apical Basolateral Basolateral Basolateral Basolateral, apical Basolateral Basolateral Basolateral Apical Basolateral, apical Apical Apical Apical Apical Apical Basolateral Basolateral Basolateral Basolateral Basolateral Basolateral Basolateral, apical Basolateral Basolateral Basolateral Apical Basolateral
Amiloride	DMSO	10	10		
Barium Chloride	ddH ₂ O	5000	5000		
Bumetanide	Ethanol	100	100		
CFTR _{inh} 172	DMSO	10	10		
CGP-12177	DMSO	1	0.1 – 10		
Charybotoxin	ddH ₂ O	0.1	0.1		
Chelerythrine chloride	DMSO	10	10		
Chromanol 293B	DMSO	10	10		
DIDS	DMSO	200	200		
Forskolin	Ethanol	10	10		Basolateral, apical
GlyH-101	DMSO	50	50		
GM-6001	DMSO	1	1		
GM-6001 control	DMSO	1	1		
Iberiotoxin	ddH ₂ O	0.01	0.01		
ICI-118551	DMSO	10	10		
L-748,377	DMSO	10	10		
MDL-12330A	DMSO	20	20		
Niflumic acid	Ethanol	200	200		
Rottlerin	DMSO	5	5		
Salbutamol	DMSO	1	1		Basolateral, apical
Staurosporine	DMSO	0.1	0.1		
U0126	DMSO	25	10		
UTP	ddH ₂ O	100	100		
Wortmannin	DMSO	50	50		

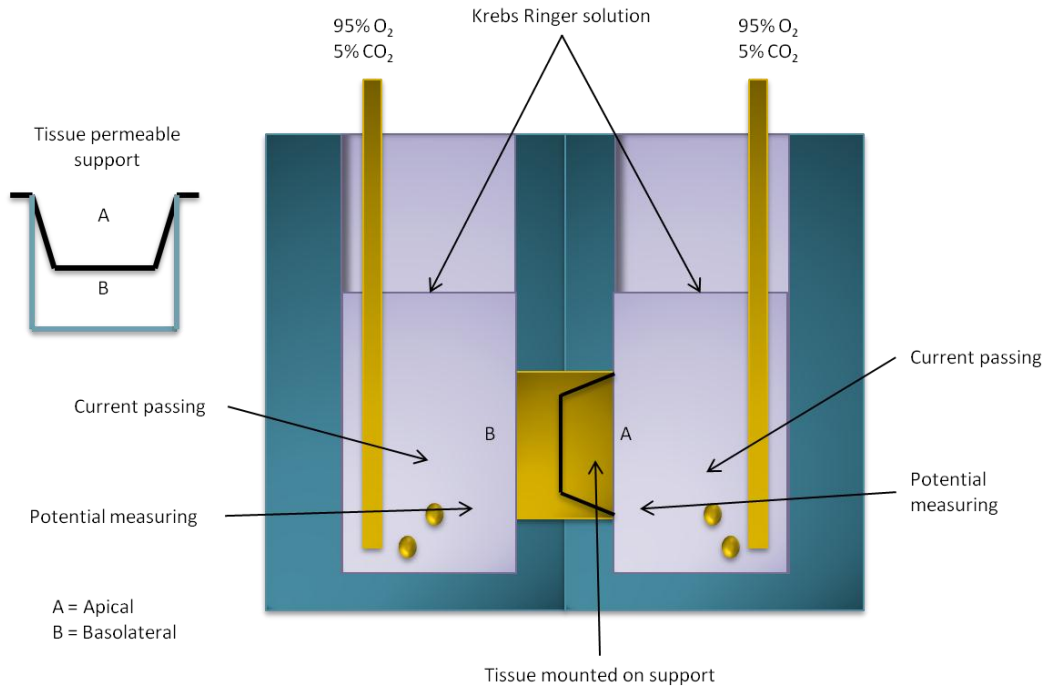


Figure 2.1 – Ussing chamber schematic.

Cells are grown on permeable supports. The Ussing chamber consists of two separate halves containing Krebs solution, with the support placed on an insert between the two. An oxygen/carbon dioxide mix is bubbled through in order to mix and aerate the Krebs solution. The potential measuring electrode measures the membrane potential and the current passing electrode pumps in current in order to reset this residual potential to zero. This current is referred to as the short circuit current (I_{sc}).

The inhibitors listed in Table 2.7 were left on side to thaw and are then centrifuged at 13,000 rpm. The dummy sample was loaded into an Ussing chamber (Physiological Instruments, Figure 2.1) and the 3 M KCl/agar, Ag/AgCl₂ cartridge electrodes (Physiological Instruments) were inserted, with the potential measuring electrodes in the holes closest to the sample, and the current passing electrodes away from the sample. Each chamber was filled with 5 ml Krebs-Henseleit solution and the level was marked with pen.

2.6.3 Compensating for voltage and fluid resistance

As shown in Figure 2.2, compensation for voltage and fluid resistance was required before using the Ussing chamber. The Ussing chamber apparatus was set up as described with an empty chamber slider. The dials were reset to the zero position. Then, the voltage offset is used to compensate for voltage differences between the measuring electrodes. This is performed by selecting voltage in both the meter and mode settings. If the voltage was negative, a positive offset was required and if positive, a negative offset was required. This was selected using the offset button. The dial was then turned until the reading read zero volts.

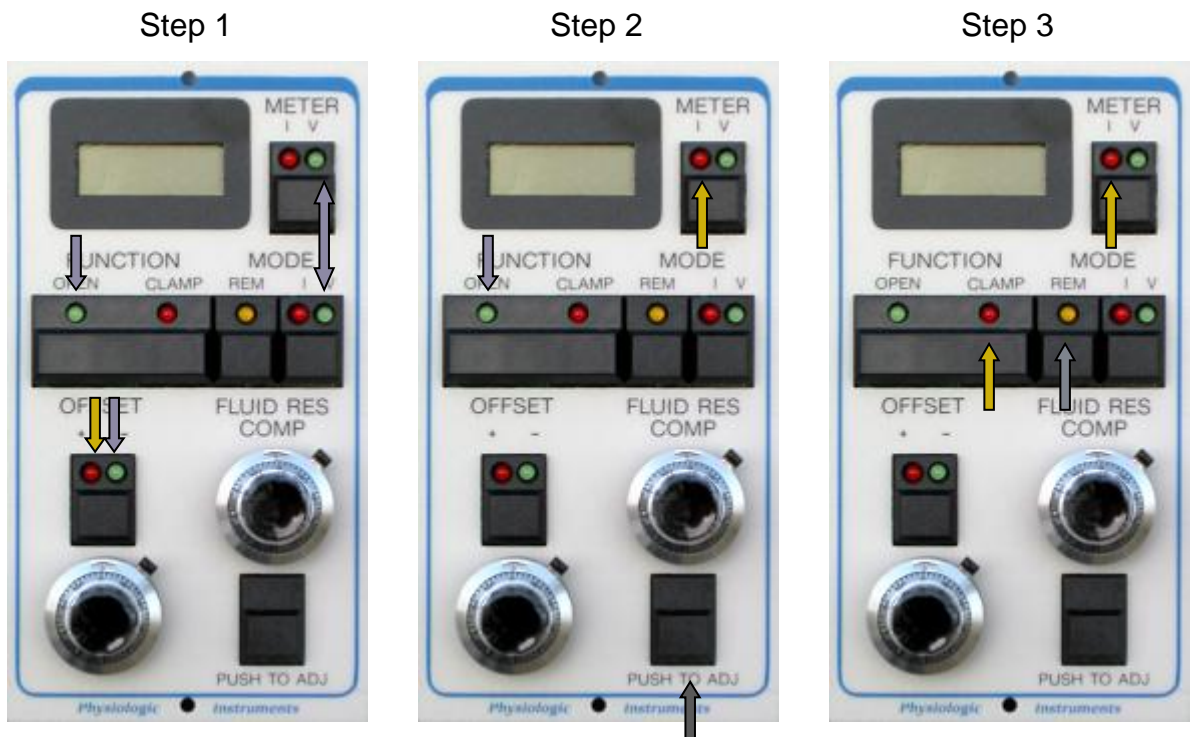


Figure 2.2 – Schematic of how to set the voltage clamp.

Next, the fluid resistance needed to be compensated for. This was performed by switching the meter to read current, and then the “push to adj” was pushed and held. The fluidic resistance compensation dial was then adjusted until the current read zero. Figure 2.3 depicts the Ussing chamber setup used. The permeable support was then loaded into a chamber slider and the Ussing chamber was re set up with the tissue loaded into a chamber slider. A VCC MC6-2 clamp (Physiological Instruments) is enabled when the REM button under mode is depressed, allowing the clamp to be controlled remotely by a computer. When enabled, the VCC MC6-4 clamps the resting transepithelial potential difference to zero.

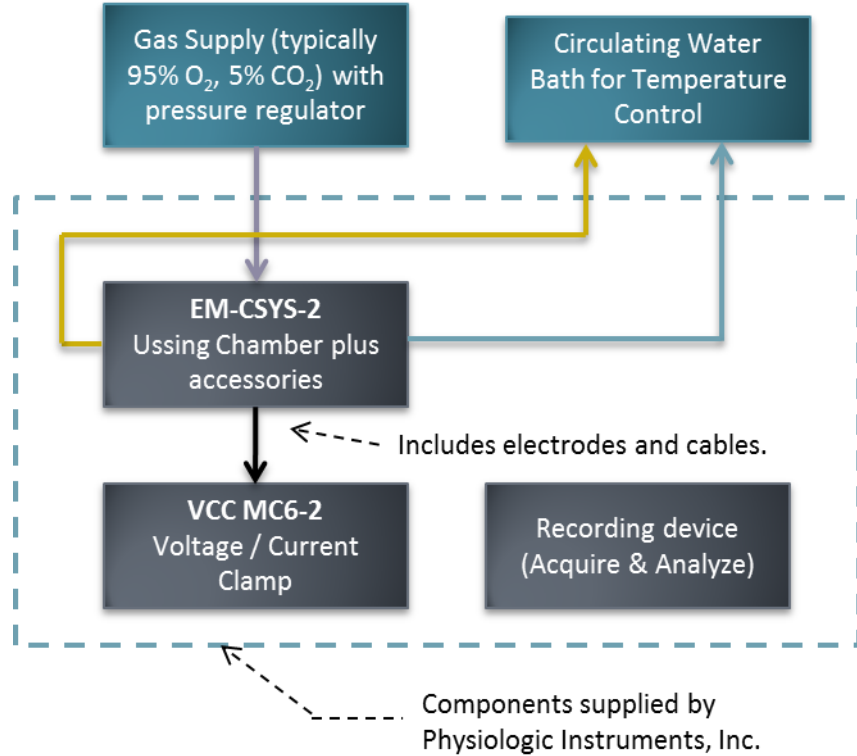


Figure 2.3 – Block diagram of the apparatus used during an Ussing chamber investigation.

As depicted in Figure 2.3, the VCC MC6-2 is the voltage clamp amplifier that has a pulse generator and can interface with a computer via an interface cable and the 25-pin D-sub connector on rear panel of the amplifier. The VCC MC6-2 was directly controlled by a computer using the Acquire and Analyze 2.3 software once the REM button on the amplifier controls was depressed. The DM-MC6 single channel input module was connected to the back of the VCC MC6-4 via modular plugs. The DM-MC6 was connected to the current passing and potential measuring electrodes that were mounted in the EM-CSYS-2 Ussing Chamber System. The voltage clamp amplifier then measured the potential difference across the epithelium generated by ion transport and injected current into the Ussing chamber through the current passing electrodes. This injected current was equal and opposite to the ionic current across the epithelium. Through the Acquire and Analyze 2.3 software user interface, the reference value was taken at the start of each experiment with a blank insert mounted in the Ussing chamber to calibrate the system. The short circuit current was then measured by the voltage clamp amplifier at a period of once per 10 seconds (0.1Hz), converted to digital using a DI-720 analog to digital converter (DataQ Instruments) with a sampling rate of 200kHz. This high sampling prevented aliasing

by exceeding the Nyquist rate. The resulting digital measurements were output to the computer via the Acquire and Analyze 2.3 software with no additional filtering.

2.7 How the data were analysed

A reading for the I_{SC} (short circuit current), R_{TE} (transepithelial resistance) and V_{TE} (transepithelial voltage) was measured over a period of 60 seconds by calculating a mean value from 6 data points. Before each addition of a compound, a reading was taken. These data were exported directly to Microsoft Excel, where calculations to determine the effect of a compound could be carried out as follows. The data to follow have been represented using two different methods. Firstly, they are represented as bar graphs showing the delta change in I_{SC} from the previous compound. For example, if amiloride was placed into the apical chamber first followed by another compound over a range of concentrations, then the first delta short circuit current change value (ΔI_{SC}) would be the I_{SC} of amiloride minus the I_{SC} of the baseline current, and the second set of values would be each I_{SC} value of the compound at various concentrations minus the value for amiloride. If a new compound was introduced later, the delta I_{SC} value would have the previous compound subtracted from it. The second set of graphs show a representative raw trace output that corresponds to the bar graph to the left. I_{SC} is measured at fixed time intervals and plotted on a graph. The time at which a compound is introduced is indicated on the graph. Data, including those looking at the magnitude of responses to compounds and representative raw traces, are transferred from Excel to GraphPad Prism version 5.0 for Windows package for data representation and statistical analysis.

2.8 Experimental Design

When conducting Ussing chamber studies, firstly, it was important to let the tissue equilibrate in the new Ussing chamber environment for at least 30 minutes, allowing the ion transport to stabilise. It was also necessary to block the epithelial sodium channels on the apical membrane with amiloride at the start of each experiment. This was to remove sodium ion transport, so only chloride ion transport was measured. Subsequently, the test compounds were added and their effects on chloride ion transport were measured. Then GlyH-101, a CFTR inhibitor, was typically used to see whether or not the short circuit current (I_{SC}) increase was due to chloride transport

through CFTR. Finally, bumetanide was used at the end of each experiment to block the Na-K-2Cl cotransporter on the basolateral membrane to remove all ion transport across the membrane. Calu-3 cells were selected as they express CFTR highly, and A549 cells were selected as a control as they do not express CFTR (Bossard *et al.*, 2007). When conducting experiments where cells are preincubated with an inhibitor, it was in the bath solution for the complete duration of the experiment.

2.9 Statistical Analysis

Values and error bars were expressed as means \pm standard error of the mean (S.E.M.) and n represented the number of experiments. Individual treatments were compared using a one-way ANOVA with Tukey's post hoc test and significance was taken as $P \leq 0.05$. The level of significance is indicated as: * $P \leq 0.05$, ** $P \leq 0.01$ and *** $P \leq 0.001$. Analysis was performed using GraphPad Prism version 5.00 for Windows package. The one-way ANOVA with Tukey's post hoc test has been successfully used previously in similar investigations (Ducroc *et al.*, 2005; Savitski *et al.*, 2009).

The one-way ANOVA is a common method to compare multiple groups and is favoured over multiple individual t-tests. The test makes several assumptions such as: the samples being independent, variances of populations being equal and that the response variable must be approximately a normal distribution. As long as these assumptions are met, the test is reliable. Due to the nature of our data, these assumptions can be met.

The Tukey's post hoc test was used over potential alternatives such as Bonferroni's and Newman-Keuls due to limitations in number of groups compared and lack of confidence intervals respectively. Tukey's post-hoc test makes two assumptions about the data being analysed, which are that each data set is independent, and that there is equal variation across the observed observations. These assumptions held true with the data sets used in the multiple comparison tests. The formula for the Tukey test is as follows:

$$qs = \frac{YA - YB}{SE}$$

To determine statistical significance, the qs value is calculated by subtracting the larger of the two means (YA) from the smaller of two means (YB) and divided by the standard error of this dataset found during the ANOVA. The calculated qs values are compared to $q_{critical}$, which is obtained from a table of critical values, and is dependent of the total number of means in the test. If the qs value is larger than the value, the two means are said to have a statistically significant difference between them.

Chapter 3 Functional Characterisation and Gene Expression of Cl⁻ Channels in the Calu-3 cell line

3.1 Introduction

CFTR is a phosphorylation dependent chloride ion channel that is generally expressed on the apical surface of lung epithelia (Rosenfeld *et al.*, 1992). While CFTR can either act in an absorptive or secretory role, this is greatly dependent on the particular tissue (Kunzelmann, 2001). In the lungs, CFTR is the main transporter of chloride ions and is generally secretory (Merigo *et al.*, 2007). In the disease condition cystic fibrosis, mutations in this channel lead to less functional CFTR at the cell surface ultimately leading to a dehydration of the lungs and thickened mucus (Matsui *et al.*, 1998). Since Calu-3 cells express high levels of CFTR, and respond well to agonists of cAMP and Ca²⁺ (Finkbeiner *et al.*, 1993; Shen *et al.*, 1994), they were selected for this study. It has been demonstrated that predominantly HCO₃⁻ ions are secreted rather than purely chloride ions when Calu-3 cells are stimulated by a cAMP agonist such as forskolin, and this mechanism has been shown to be Na⁺ dependent and Cl⁻ independent (Devor *et al.*, 1999). More recently, it has been demonstrated that HCO₃⁻ ions are recycled at the basolateral membrane during fluid secretion by Calu-3 cells (Shan *et al.*, 2012).

In order to validate that our Calu-3 model and experimental set up works, the Calu-3 cells needed to be characterised first. The first principle aim was to determine what the transepithelial resistance was for the Calu-3 cells used in this project, in order to determine if the Calu-3 cells are growing and forming monolayers. This is important since only intact monolayers can produce meaningful results in our short circuit current experiments. The transepithelial resistance was also measured after the air-liquid stage. Secondly, in order to confirm the expression of CFTR and calcium activated chloride channel candidates in the Calu-3 cell line, RT-PCR was employed. Of the calcium activated chloride channel candidates, the expression of BEST1-4 and

anoctamins 1-10 were investigated. In addition to gene expression, of interest is to determine whether BEST1 and CFTR proteins are expressed in the Calu-3 cell line. This was important since it would confirm gene expression of chloride channels and candidates to further provide evidence for the presence of these channels in our model cell line alongside the short circuit current investigations.

3.2 Results

3.2.1 Determining transepithelial resistance

First, it was necessary to know when the cells were forming a confluent monolayer on the supports before removing the apical fluid to put them at an air-liquid interface. This was to simulate *in vivo* conditions of the lung epithelium as much as possible. The resistance over a period of days for the Calu-3 cell line was measured by an EVOM epithelial voltohmmeter and recorded. 5 of the 6 wells are seeded from each snapwell plate, with the last well designated a blank. The transepithelial resistance for a seeded well is calculated by subtracting the value for the blank well from the value of each seeded well, and then multiplying the value by the area of the well (in this case, 1.12 cm^2). Figure 3.1 shows the data obtained for the measured transepithelial resistance across Calu-3 monolayers over a period of days.

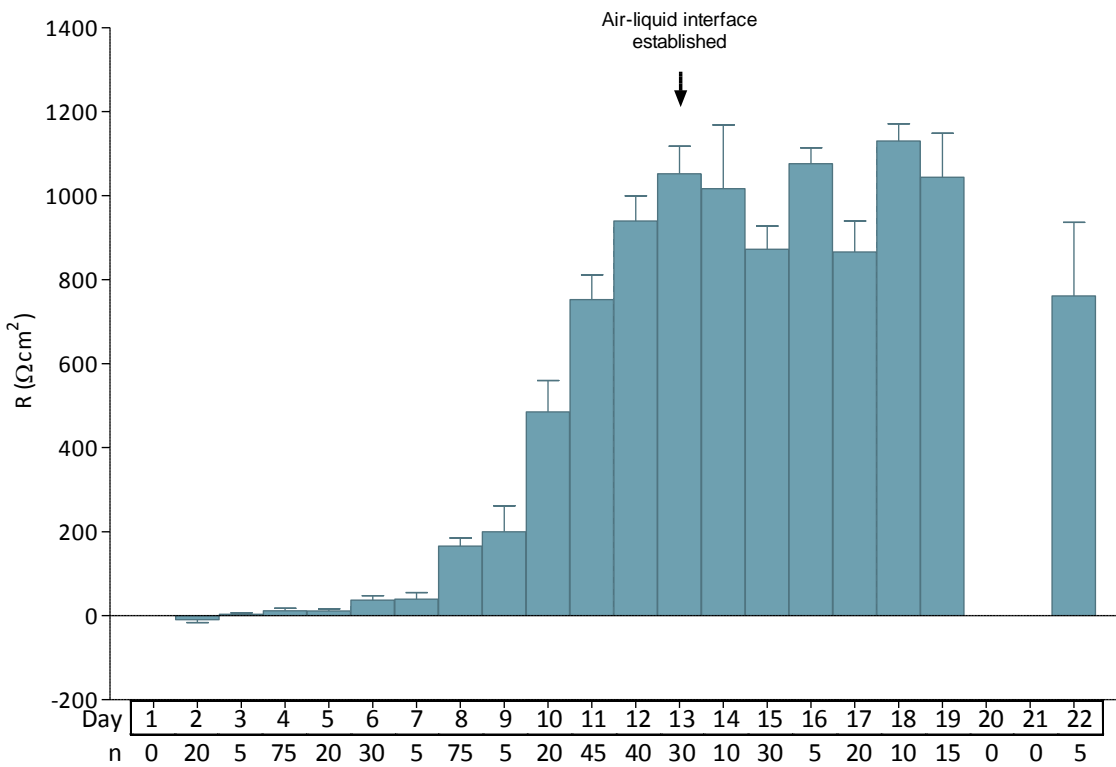


Figure 3.1 – Calu-3 transepithelial resistance readings.

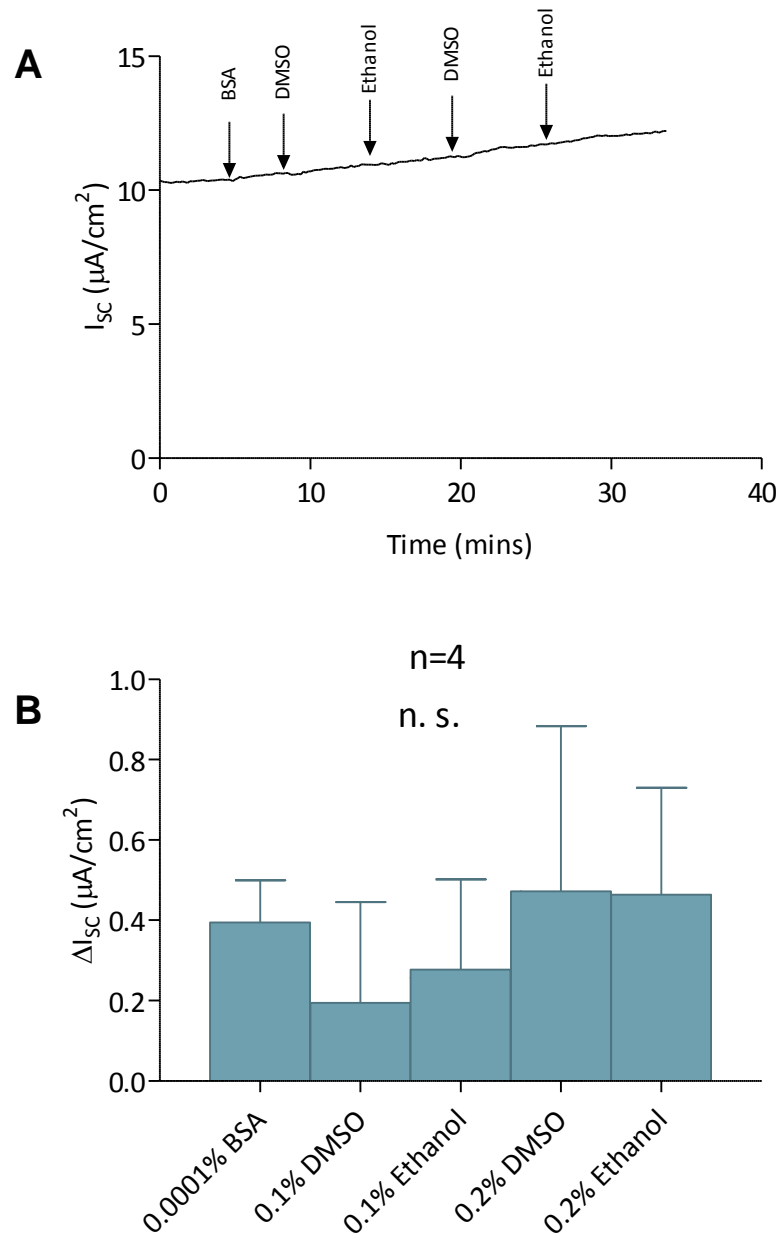
These transepithelial readings were recorded over a period of days as determined using an EVOM - Epithelial Voltohmmeter for the Calu-3 cell line. Air liquid interface (ALI) was established once the RTE had become stabilised. This was generally at day 12 from seeding.

The mean transepithelial resistance as measured from the permeable support plate before their use in the Ussing chamber was $983 \pm 32 \Omega\text{cm}^2$ ($n=135$). After approximately 7 days at air liquid interface, the recorded transepithelial resistance as measured in the Ussing chamber after 30 minutes of equilibration time was $411 \pm 18 \Omega\text{cm}^2$ ($n=98$). The calculated V_T averaged $4.6 \pm 0.3 \text{ mV}$ ($n= 98$).

3.2.2 Calu-3 Vehicle Controls

To test that the vehicles that the compounds are dissolved in are not affecting the short circuit current, equivalent volumes of three different vehicles were added to the appropriate chambers onto Calu-3 monolayers. 0.0001% BSA and 0.1% ethanol are added to the basolateral side to represent epidermal growth factor (EGF), forskolin and bumetanide additions. 0.1% DMSO represents amiloride and GlyH-101 additions. It was seen that vehicle controls produce negligible currents, with the most current

generated by 0.2% DMSO, which was $0.5 \pm 0.4 \mu\text{A cm}^{-2}$ (n=4). Taken together, this suggests that the majority of the currents generated are due to the effect of the compound and not the vehicle.



3.2.3 Forskolin characterisation in Calu-3

It has been previously demonstrated that Calu-3 cells express CFTR (Haws *et al.*, 1994). The adenylate cyclase agonist, forskolin, was used to demonstrate that the Calu-3 cells were functioning normally. Figure 3.3 (A and B) shows an addition of 10 μ M amiloride is applied to the apical side to inhibit epithelial sodium channels (ENaC) that could affect chloride ion transport. Addition of 10 μ M forskolin to the basolateral side increased the short circuit current to a peak value (ΔI_{SC}) of $15.5 \pm 2.1 \mu$ A cm^{-2} ($n=5$, $p<0.001$), which subsequently reduced to a plateau (ΔI_{SC}) of $7.1 \pm 0.4 \mu$ A cm^{-2} ($n=5$). In order to determine if the increase in I_{SC} after forskolin addition was due to an increase in chloride transport through CFTR, the CFTR inhibitor GlyH-101 was employed. Total inhibition of the resting forskolin response is achieved on addition of 50 μ M GlyH-101 to the apical side of Calu-3 cells causing a decrease in current (ΔI_{SC}) of $8.2 \pm 1.5 \mu$ A cm^{-2} ($n=5$, $p<0.01$). 100 μ M bumetanide was added to the basolateral side, causing an additional decrease (ΔI_{SC}) of $7.3 \pm 1.6 \mu$ A cm^{-2} ($n=5$) from the GlyH-101 inhibition. Bumetanide is a Na-K-2Cl cotransporter inhibitor that prevents chloride secretion by blocking the movement of Cl^- into the cell across the basolateral membrane (Amsler & Kinne, 1986).

In order to determine if the response to forskolin was either mostly due to chloride secretion, or whether there was an activation of basolateral potassium channels that could contribute increase driving force for chloride exit from the apical membrane, a subsequent experiment using calcium chelator, 1,2-bis(2-aminophenoxy)ethane-N,N,N',N'-tetraacetic acid (BAPTA-AM), prior to forskolin stimulation was conducted. In Figure 3.3 (C and D), Calu-3 monolayers were preincubated with 10 μ M BAPTA-AM on the basolateral side for 30 minutes and then stimulated with 10 μ M forskolin, also to the basolateral side. Addition of forskolin generated a peak value (ΔI_{SC}) of $7.9 \pm 1.5 \mu$ A cm^{-2} ($n=5$, $p<0.05$), which subsequently reduced to a plateau (ΔI_{SC}) of $5.3 \pm 0.7 \mu$ A cm^{-2} ($n=5$, $p<0.05$). In order to determine if the increase in I_{SC} from forskolin was due to an increase in chloride transport through CFTR, complete inhibition of this response is again achieved on addition of 50 μ M GlyH-101 on the apical side, leading to a decrease (ΔI_{SC}) of $6.0 \pm 1.3 \mu$ A cm^{-2} ($n=5$, $p<0.05$). The remaining short circuit current was removed using 100 μ M bumetanide to the basolateral side, causing a decrease of $11.8 \pm 1.6 \mu$ A cm^{-2} ($n=5$).

Taken together, these results suggest that forskolin stimulation working through CFTR since total inhibition was achieved with GlyH-101. Forskolin stimulation also has a potassium channel dependent component that can be eliminated with preincubation with BAPTA-AM, as well as a chloride component that is similarly not eliminated.

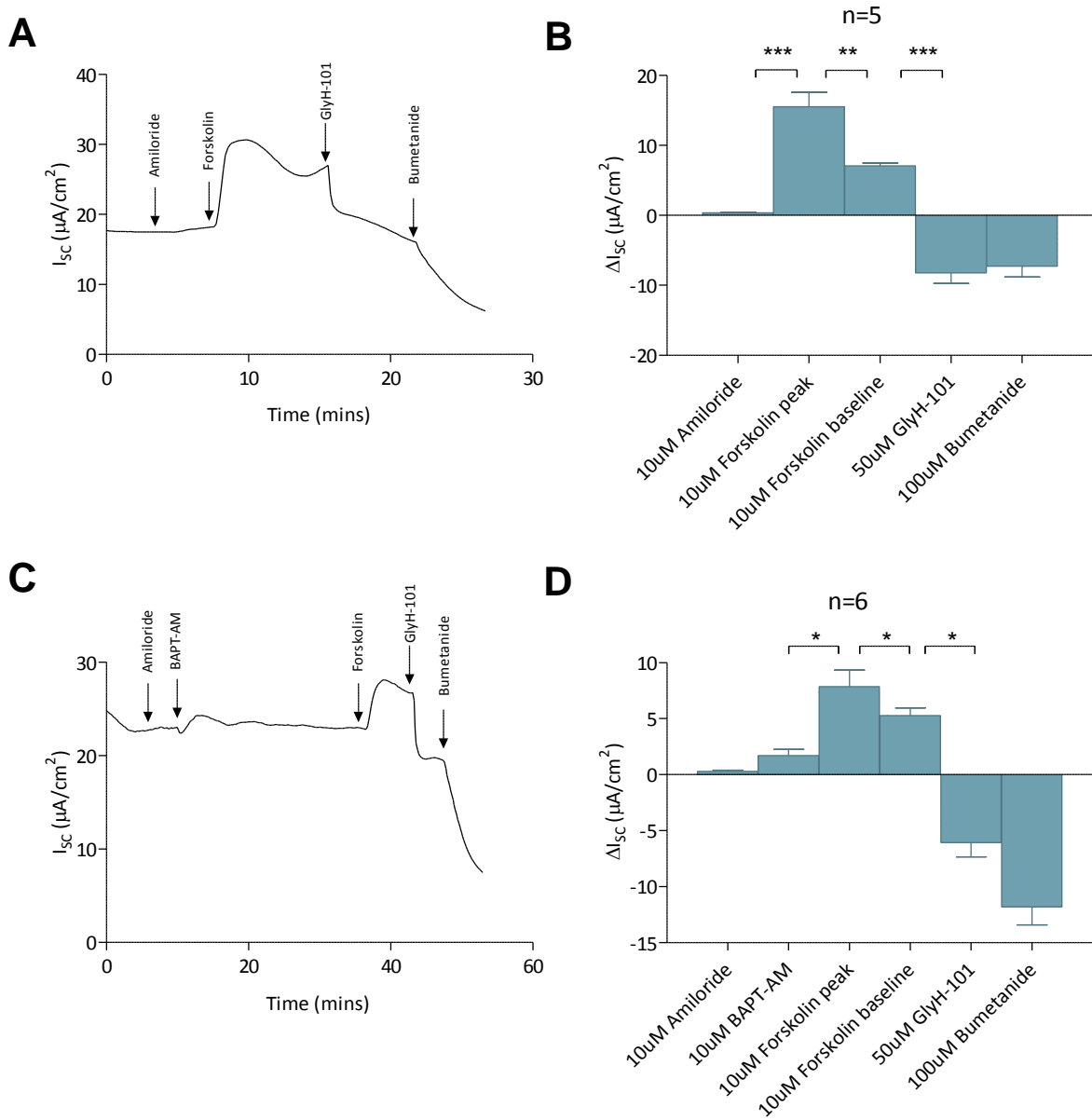


Figure 3.3 – Characterisation of forskolin response across Calu-3 monolayers.

Trace (A) and Bar graph (B) show the change in short circuit current across a Calu-3 epithelium in response to 10 μM forskolin. With Calu-3 epithelia, 10 μM forskolin increases I_{SC} when added acutely to the basolateral side. The increase is inhibited by 50 μM GlyH-101, a CFTR inhibitor. Trace (C) and Bar graph (D) show characterisation of CFTR response with 10 μM BAPTA-AM and 10 μM forskolin for the Calu-3 cell line. Statistical analysis was performed using a one way ANOVA with Tukey's Multiple Comparison test, where $P<0.05$ was deemed statistically significant.

3.2.4 UTP Characterisation in Calu-3

The P2Y agonist, uridine-5'-triphosphate (UTP), was used to characterise calcium activated chloride channels in the Calu-3 cell line as shown in Figure 3.4 (A and B). When stimulated with 100 μ M UTP on the apical side, a sharp, transient peak occurred of $1.0 \pm 0.4 \mu\text{A cm}^{-2}$ (n=6). Immediately after the transient peak, there was a very small, but measurable higher baseline of $0.5 \pm 0.4 \mu\text{A cm}^{-2}$ (n=6). In order to provide additional evidence that the response to UTP was due to stimulation of calcium activated chloride channels, 200 μ M niflumic acid was applied to the apical side to block CaCCs and restimulation with 100 μ M UTP was attempted. The addition of niflumic acid decreased short circuit current sharply by $3.0 \pm 1.5 \mu\text{A cm}^{-2}$ (n=6, p<0.05). No additional increases occurred after restimulation by 100 μ M UTP after the addition of niflumic acid ($0.1 \pm 0.3 \mu\text{A cm}^{-2}$ (n=6)). A subsequent combination of 50 μ M GlyH-101 on the apical side and 100 μ M bumetanide on the basolateral side brought about further decreases of $2.6 \pm 0.9 \mu\text{A cm}^{-2}$ (n=6) and $0.5 \pm 0.3 \mu\text{A cm}^{-2}$ (n=6), respectively.

Similarly, an experiment was conducted looking at UTP response in response to preincubation with calcium chelator BAPTA-AM shown in Figure 3.4 (C and D). Calu-3 monolayers were treated with 10 μ M BAPTA-AM on the apical side for 30 minutes and were then treated with 100 μ M UTP on the apical side. It was seen that there was still a response to UTP in the form of a sharp peak in current at $1.1 \pm 0.1 \mu\text{A cm}^{-2}$ (n=6) with no measurable increase in the subsequent baseline current. The short circuit current was decreased by $7.8 \pm 1.1 \mu\text{A cm}^{-2}$ (n=6) with treatment of 200 μ M niflumic acid on the basolateral side. Attempts to stimulate CFTR with 10 μ M forskolin on the basolateral side resulted in a relatively small peak of $4.7 \pm 0.9 \mu\text{A cm}^{-2}$ (n=6). 50 μ M GlyH-101 was applied to the apical side to eliminate the induced CFTR current by forskolin, causing a decrease of $7.1 \pm 1.0 \mu\text{A cm}^{-2}$ (n=6). The remaining short circuit current was effectively eliminated by addition of 100 μ M bumetanide on the basolateral side, further decreasing the I_{SC} by $3.4 \pm 0.5 \mu\text{A cm}^{-2}$ (n=6).

Taken together, the standard response to UTP is small across Calu-3 monolayers, and is not eliminated by BAPTA-AM, suggesting that the UTP response is not activating calcium activated chloride channels, but more likely, either CFTR itself or basolateral calcium activated potassium channels (subsequently increasing chloride

driving force). Niflumic acid inhibits I_{SC} below baseline levels and thus is blocking more than just CaCC response.

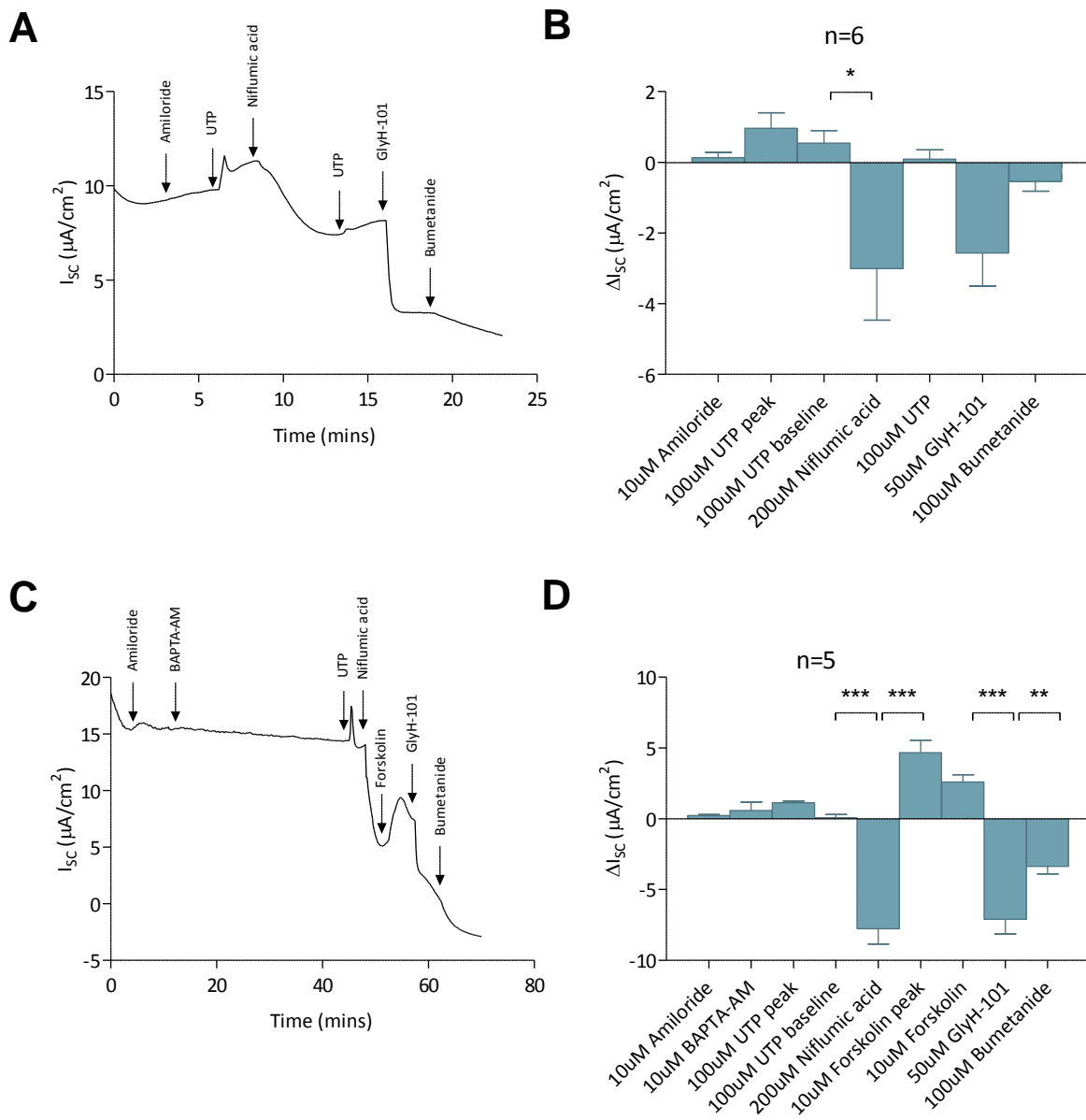


Figure 3.4 – Characterisation of UTP response across Calu-3 monolayers.
 Traces and Bar graph to show Calu-3 characterisation in response to 100 μM UTP (A and B) and 10 μM BAPTA-AM pretreatment with subsequent stimulation with 100 μM UTP (C and D). Statistical analysis was performed using a one way ANOVA with Tukey's Multiple Comparison test, where $P<0.05$ was deemed statistically significant.

To determine if the response to UTP was due to a conductance on the basolateral membrane, the basolateral membrane was permeabilised with 0.36 mg/ml nystatin and a basal to apical chloride current applied (Figure 3.5 A and B).

If the basolateral membrane is permeabilised, the response to UTP is effectively eliminated, with the response to UTP with basolateral membrane permeabilisation is $0.6 \pm 0.3 \mu\text{A cm}^{-2}$ ($n=3$). Subsequent stimulation with forskolin is not effected in this way and continues to produce a large increase to $83.2 \pm 13.1 \mu\text{A cm}^{-2}$ ($n=3$) which is completely inhibited by 50 μM GlyH-101. This result shows that the UTP response is likely to be linked to calcium activated potassium channels on the basolateral membrane.

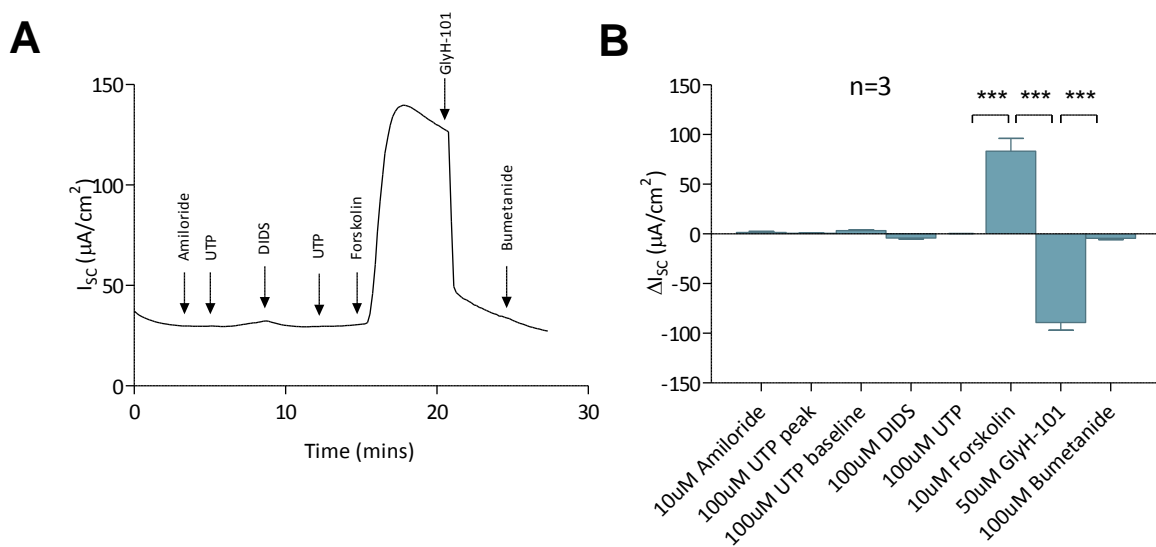


Figure 3.5 – Characterisation of UTP response across permeabilised Calu-3 monolayers.

Trace (A) and Bar graph (B) to show the characterisation of calcium activated chloride channels with 100 μM UTP and basolateral membrane permeabilisation. Statistical analysis was performed using a one way ANOVA with Tukey's Multiple Comparison test, where $P<0.05$ was deemed statistically significant.

3.2.5 Endogenous levels of chloride channel gene and protein expression in three cell lines

In order to determine which chloride channels (CFTR, BESTs, ANOs) were expressed in epithelial cell lines, RT-PCR was carried out on three cell lines – Calu-3, CFPAC and A549 for a minimum of three repeats, with positive bands cut out, extracted and sent for sequencing. The Calu-3 cell line was used since this is our chosen model for submucosal gland cells. A549 cells were selected for comparison since they are a widely used model of type II alveolar epithelial cells. CFPAC was used as a control comparison for the airway cell lines and known to express CaCCs (Marsey & Winpenny, 2009).

3.2.5.1 *CFTR* is expressed in Calu-3 cells

Calu-3 has been demonstrated to express CFTR in numerous studies (Brouillard *et al.*, 2001; Baudouin-Legros *et al.*, 2003) and our data are in agreement as shown in Figure 3.6.

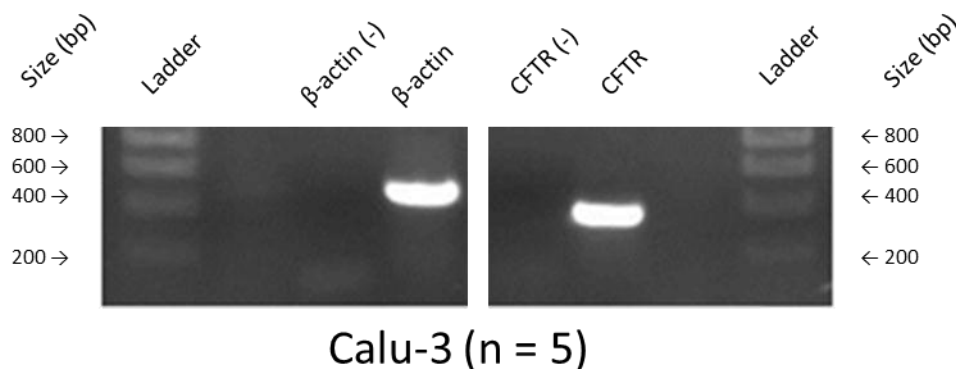


Figure 3.6 – Endogenous levels of CFTR message in the Calu-3 cell line.

A positive band for CFTR was seen at the correct band size of 326 bp, and a further positive band was seen for β-actin at 456 bp. This result was repeated 5 times giving the same outcome. Number of repeats indicated in brackets.

3.2.5.2 *BEST* genes are expressed in the Calu-3 cell line

The results in Figure 3.7 show that gene expression of BEST1 and BEST3 was detected in all cell lines. BEST2 was detected only in A549 cells, while BEST4 was expressed only in CFPAC cells.

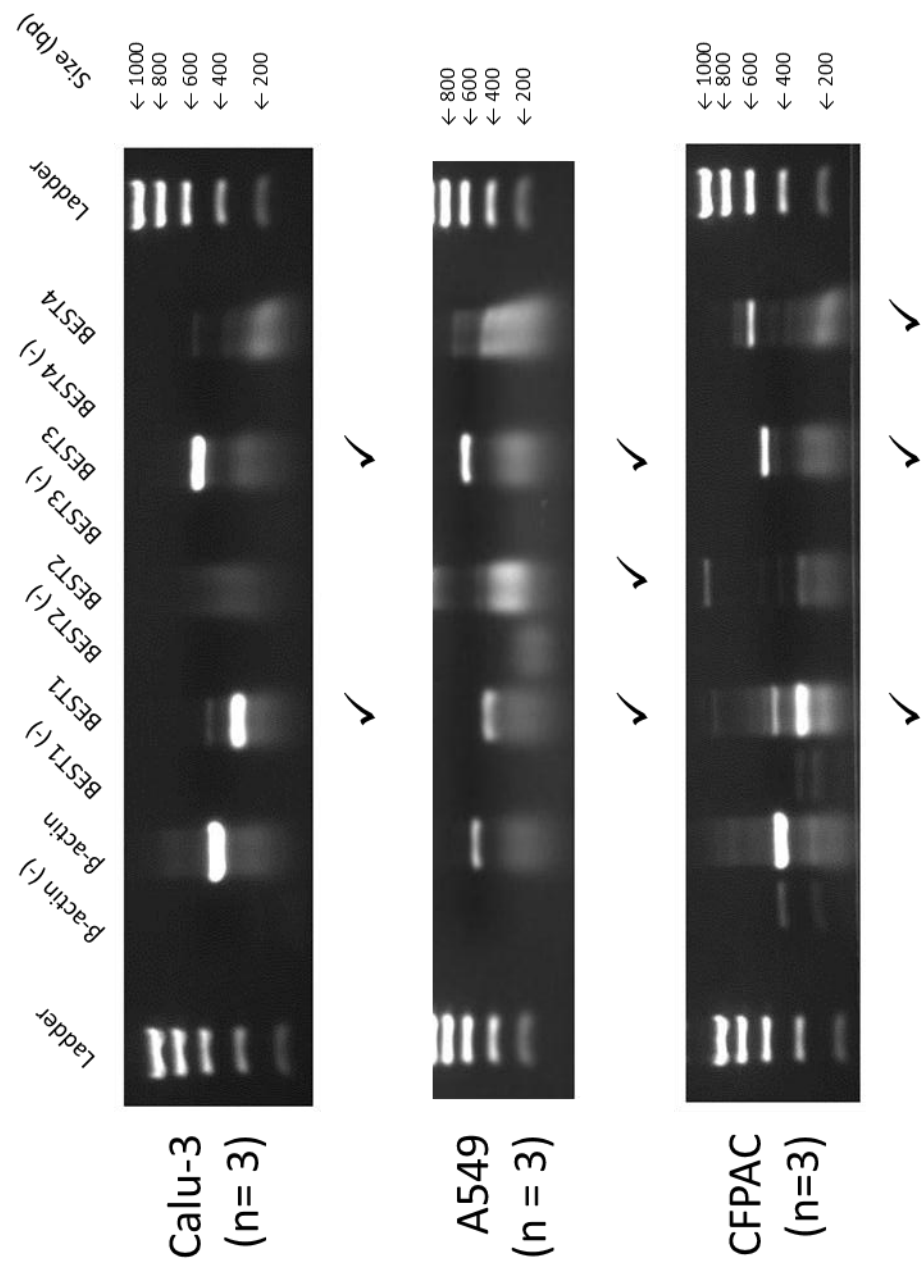


Figure 3.7 – Endogenous levels of bestrophin message in the Calu-3, CFPAC and A549 cell lines.

CFPAC is used as a control comparison. RT-PCR consisted of 3 repeats. Ticks represent bands that have been confirmed by sequencing. Instances where bands appeared in the negative controls were not seen in repeats for that particular gene. Number of repeats indicated in brackets.

3.2.5.3 *Anoctamin genes are expressed in epithelial cell lines*

As shown in Figure 3.8, ANO1 was expressed in Calu-3 and CFPAC cells, but not A549 cells. ANO2 and ANO3 were expressed solely in CFPAC cells. ANO4 and ANO5 were expressed in all three cell lines, while ANO6 was expressed in Calu-3 and CFPAC cell lines only. ANO8 was expressed in all three cell lines, while ANO10 was expressed only in Calu-3 and CFPAC cells. ANO7 and ANO9 were not expressed in any of the tested cell lines. Taken together, these results demonstrate that Calu-3 and CFPAC cell lines express a wide array of calcium activated chloride channel candidates, while A549 cells express a relatively limited range of anoctamin genes.

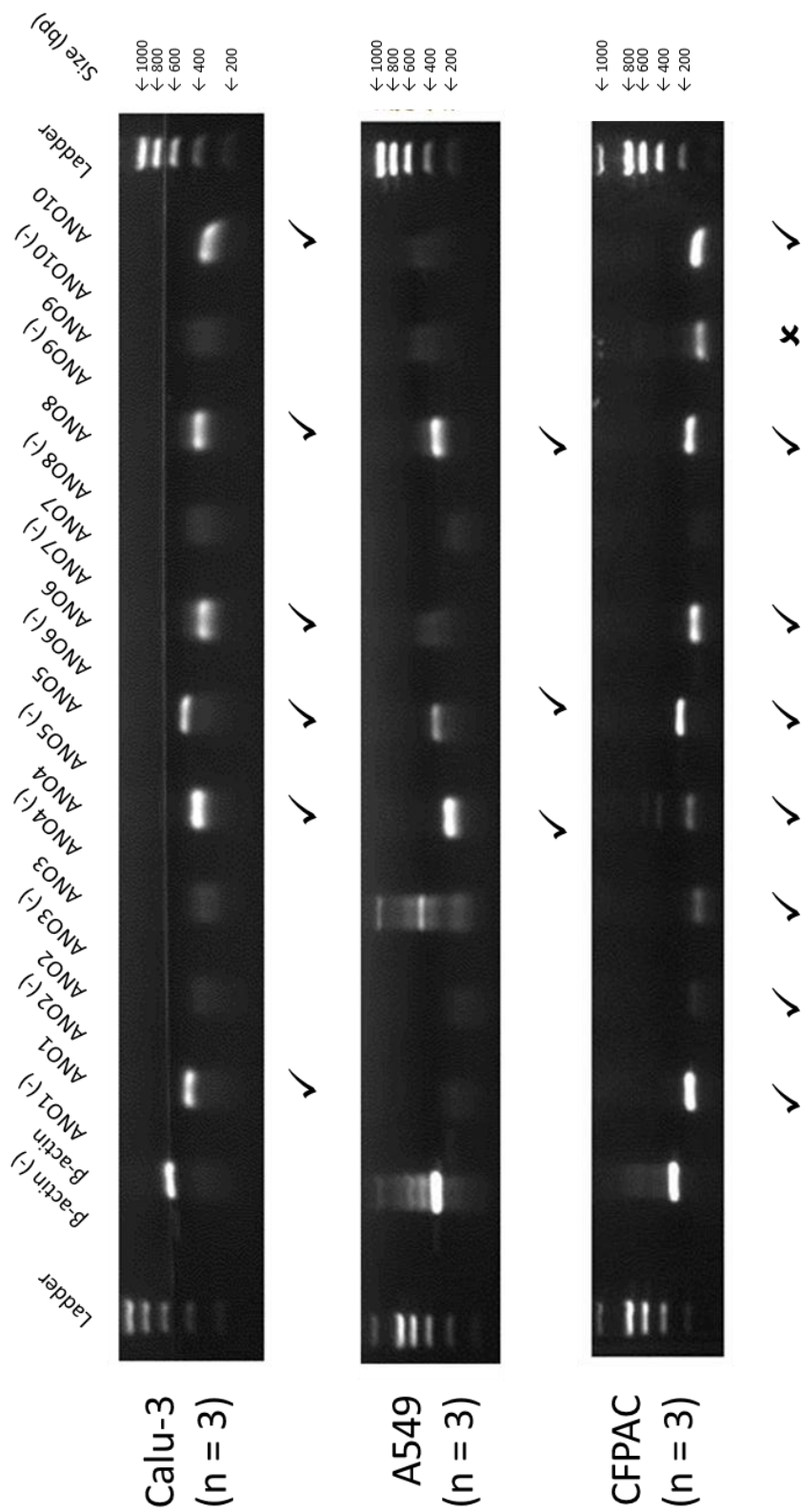


Figure 3.8 – Endogenous levels of expression of anoctamin message in Calu-3, CFPAC and A549 cells.
 CFPAC is used as a control comparison. Ticks represent bands that have been confirmed by sequencing. Crosses represent bands that are not the correct gene tested. Number of repeats indicated in brackets.

3.2.6 CFTR fragments detected in Calu-3 cells

In order to detect the presence of CFTR protein in the Calu-3 cell line, different extraction methods were used in an attempt to increase the yield of CFTR protein as much as possible, which included using RIPA and Hot-SDS techniques. Fluorescent antibodies were used to differentiate between protein of interest and loading control β -actin. Calu-3 cells were grown to confluence in tissue culture flasks before extraction using the Hot-SDS extraction technique as described previously in the Materials and Methods. Gels were loaded with varying amounts of protein to determine the optimal amount required for antibody detection.

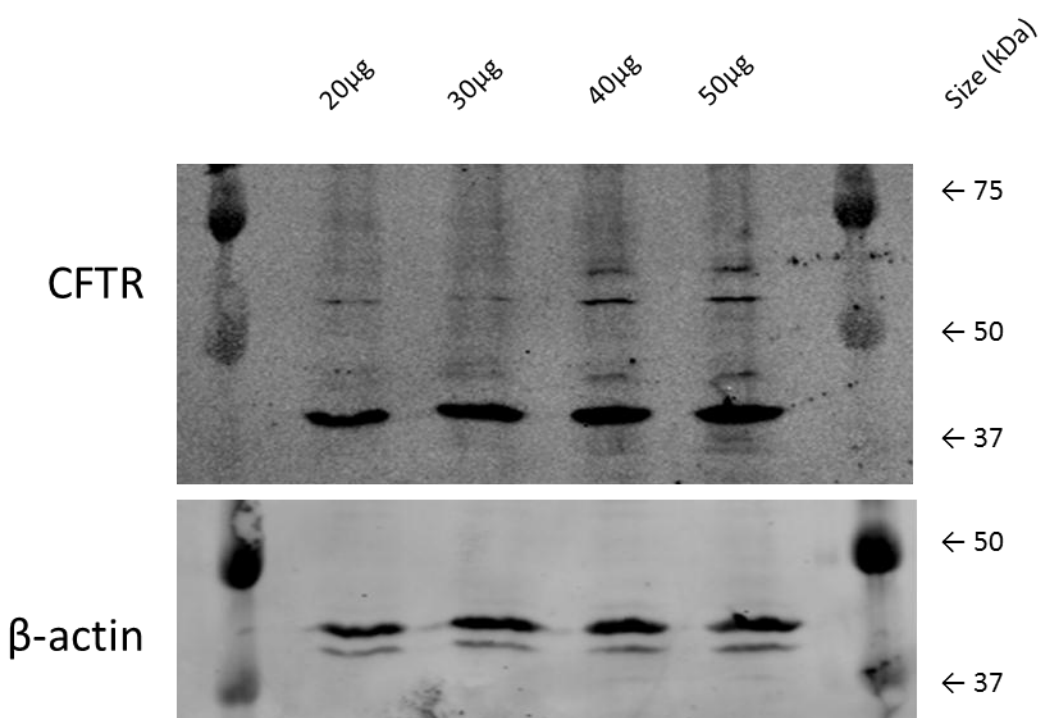


Figure 3.9 – Characterisation of CFTR protein expression in the Calu-3 cell line.

Total protein was extracted using the hot SDS method and 20 – 50 μ g loaded. Western blot shows bands at approximately 45 kDa that correspond to the CFTR R+NBD1 domains. Loading controls are for human β -actin. Representative of two blots.

It is seen that strong bands were detected for CFTR at a molecular weight of approximately 40 kDa. There are also additional bands detected at a higher molecular weight at approximately 55 and 60 kDa when 40 μ g and 50 μ g of protein is loaded. Taken together, this suggests that this particular extraction technique may have led to the breakup of the CFTR protein creating smaller, detectable fragments. The large dark band corresponds to the size of the R domain plus NBD1 domain of CFTR at

~45 kDa (Chang *et al.*, 2009), the R domain of which the primary antibody was raised against.

3.2.6.1 *BEST1 protein is expressed in the Calu-3 cell line*

In order to determine if bestrophin 1 (BEST1) protein was expressed in the Calu-3 cell line, tissue culture flasks were grown to confluence and extracted using the NP-40 technique as described in the Materials and Methods. Each lane was loaded with 20 µg of protein. The first lane was loaded with protein obtained from a lysate of CHO cells transfected with BEST1 as a positive control kindly provided by Kirsty Kirk (Winpenny Lab, University of East Anglia). A subsequent lane was loaded with a protein lysate of unstimulated Calu-3 cells. All the lanes were duplicated as an internal replicate, and the experiment was repeated successfully three times.

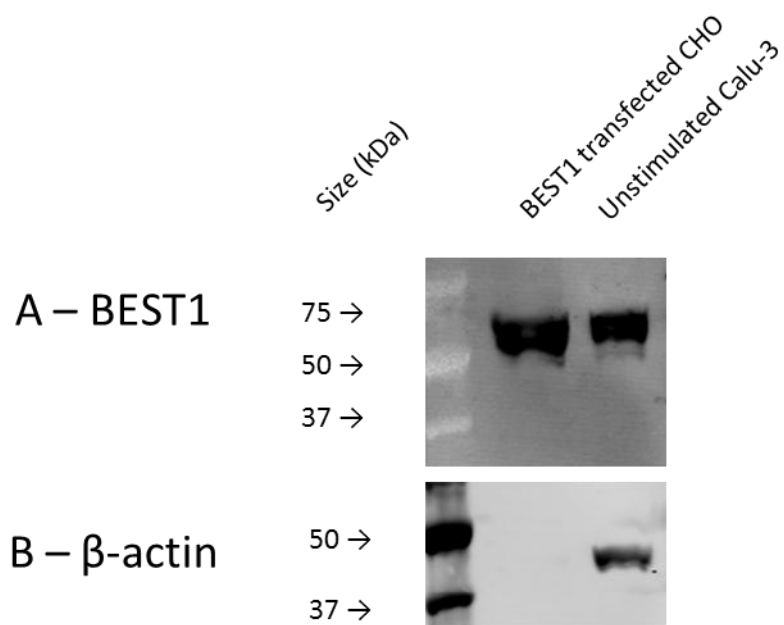


Figure 3.10 – Characterisation of BEST1 protein expression in the Calu-3 cell line.

Total protein was extracted using the NP-40 method. (A) Shows bands at approximately 68 kDa that positively correspond to BEST1 protein. (B) Shows loading controls for human β -actin. CHO cells are derived from Chinese hamster ovary, and thus show no reactivity using antibodies raised against human β -actin. Representative of three blots.

As shown in Figure 3.10, it was seen that BEST1 was well expressed in all samples corresponding to a dark band at 68 kDa (Milenkovic *et al.*, 2009). Taken together, it shows that BEST1 is expressed in Calu-3 cells.

3.3 Discussion

3.3.1 Forskolin responses are biphasic and sustained

Resistance measurements for Calu-3 cells were broadly in line with values found in previous studies that include approximately $100 \Omega\text{cm}^2$ (Shen *et al.*, 1994), $474 \pm 44 \Omega\text{cm}^2$ (Haghi *et al.*, 2010). Stimulators of cyclic adenosine monophosphate (cAMP), which include forskolin, are known to activate the CFTR channel in Calu-3 cells. The CFTR channel is the predominant cAMP-stimulated chloride conductance in Calu-3 cells (Haws *et al.*, 1994). The increase in current due to the basolateral addition of forskolin on Calu-3 monolayers is known to be due to the activation of adenylate cyclase that increases intracellular cAMP, of which CFTR is dependent for activation (Shen *et al.*, 1994; Kelley *et al.*, 1997; Devor *et al.*, 1999). By measuring isotopic fluxes of $^{36}\text{Cl}^-$ and $^{22}\text{Na}^+$ across short-circuited Calu-3 cells, it has been shown that almost none of the basal I_{SC} is Cl^- secretion or Na^+ absorption. In actuality, the major component of basal I_{SC} in Calu-3 cells is HCO_3^- secretion (Liedtke & Cole, 1998). Forskolin has been previously shown to produce small currents in Calu-3 cells, which could be inhibited by addition of basolateral bumetanide, quinidine, barium, or diphenylamine-2-carboxylate (DPC). The forskolin induced currents are unaffected by high apical concentrations of 4,4'-diisothiocyanostilbene-2,2'-disulphonic acid (DIDS) (Moon *et al.*, 1997). Application of GlyH-101 to the apical surface of the Calu-3 membranes abolished increases due to forskolin. GlyH-101 is an inhibitor of CFTR and has been used previously to inhibit forskolin induced hyperpolarisation in mouse nasal epithelia (Muanprasat *et al.*, 2004). Forskolin has also been reported to activate other ion channels besides CFTR in other cell types (such as pulmonary arterial smooth muscle) that include basolateral Ca^{2+} activated potassium channels (Barman *et al.*, 2003). Since the activation of Ca^{2+} activated potassium channels can be induced by elevations in intracellular calcium in the Calu-3 cell line (Cowley & Linsdell, 2002), chelators of calcium would decrease their activity. Our results show that BAPTA-AM preincubation reduced the forskolin response, but does not eliminate it, suggesting that reduced activity of basolateral Ca^{2+} activated potassium channels would decrease driving force for chloride exit.

3.3.2 CFTR regulatory domain fragments detected in Calu-3 cells

Three extraction methods were used on Calu-3 cells in order to try to obtain a full length CFTR protein of 170 kDa with varying degrees of success. The RIPA method and NP-40 extraction techniques were not very successful at providing enough protein to enable detection with the antibody used. The antibody used was Human CFTR R Domain MAb (Clone 13-1), Mouse IgG1 (R & D Systems). The most successful method employed for extraction of CFTR was using the Hot-SDS method, with CFTR fragments being detected. The large dark band corresponded to the size of the R domain plus NBD1 domain of CFTR at ~45 kDa (Chang *et al.*, 2009), the R domain of which the primary antibody was raised against. While this technique yielded by far the most protein, it is likely that the technique was too harsh and split several R domain fragments from CFTR molecules rather than preserving the full length protein including transmembrane domains. Milder NP-40 extraction methods were employed, but were unsuccessful. The CFTR antibody used in this study has been previously used successfully with Calu-3 cells, although the Calu-3 specific data were not shown (Vastiau *et al.*, 2005). CFTR protein has previously been demonstrated to be present in the Calu-3 cell line when it was initially characterised, and this is in agreement with the data in my study (Shen *et al.*, 1994)

3.3.3 UTP responses were transient and dependent on basolateral potassium channels

The data obtained in this study shows that UTP can cause a small transient increase in current that is not statistically significantly higher than the baseline readings. The data obtained in this study strongly suggests that CFTR is the predominant chloride channel in Calu-3, and not CaCCs, which has been shown previously to be the case with existing studies in the airway (Shen *et al.*, 1995; Fischer *et al.*, 2010). CFTR is thought to be the principal chloride secretory pathway in non-CF airways for both cAMP and Ca^{2+} agonists (Namkung *et al.*, 2010).

Moreover, the series of experiments in this investigation sets itself apart from similar work carried out previously (Wang *et al.*, 2008). The authors found that treatment on the apical side of Calu-3 cells with adenosine (10 μM) led to an increase in short circuit current of $21 \mu\text{A cm}^{-2}$. This was concluded to be as a result of activation of cAMP signalling, that activates CFTR on the apical membrane and Ca^{2+} signalling

that activates Ca^{2+} activated potassium channels on the basolateral membrane. They used inhibitors of Ca^{2+} (BAPTA-AM) and PLC (aminoethoxydiphenyl borate) to show statistically significant decreases in the adenosine induced increases in ΔI_{SC} compared to adenosine treatment alone. Clotrimazole was used to inhibit Ca^{2+} activated potassium channels to demonstrate their involvement in the process (Wang *et al.*, 2008).

The opening of Ca^{2+} activated potassium channels hyperpolarises the membrane potential which results in an increase in the electrochemical driving force for anion exit across the apical membrane (Devor *et al.*, 1999). The reduction of I_{SC} below baseline caused by niflumic acid is due to inhibition of CFTR, which is in line with previous studies. The chemical structure of niflumic acid resembles that of diphenylamine-2-carboxylate, which is known to block CFTR. In excised inside out patches of wild type human CFTR, niflumic acid led to a decrease in CFTR current (Scott-Ward *et al.*, 2004). Permeabilisation in this study removes the influence of Ca^{2+} activated potassium channels, and thus an increase in driving force for apical chloride exit due to apical UTP cannot occur.

3.3.4 Bestrophins are expressed in Calu-3, CFPAC and A549

In overexpression studies, bestrophin 1 (BEST1) was found to function as a calcium activated chloride channel (Barro Soria *et al.*, 2009). BEST1 is primarily located in the endoplasmic reticulum, and influences the uptake of calcium ions into calcium stores. It is thought that BEST1 conducts chloride ions as a counter ion to facilitate uptake of calcium ions into calcium stores in the cytosol (Neussert *et al.*, 2010). From the short circuit current data in Calu-3 cells gathered and presented in this chapter, the responses from UTP were very small and not statistically significant (Figure 3.4). It may be the case that CaCCs are either not expressed or have very low levels of expression. So, to address this, our investigation demonstrates bestrophin expression in Calu-3 cells and others (Figure 3.7), which is important since these chloride channel candidates could potentially affect ion transport. Specifically, while my study demonstrates that BEST1 and BEST3 were expressed in Calu-3, it was previously found by Kunzelmann's group that BEST4 is expressed rather than BEST3 (Barro Soria *et al.*, 2009). These differences could be accounted for by different experimental protocols used for extraction and amplification, as well as differences in

the sequence of primers used. Total RNA isolation used by Kunzelmann's group compared to Trizol® extraction method used in this investigation. Kunzelmann's RT-PCR protocol had fewer and shorter cycles; a higher annealing temperature is used (60°C compared to 52°C) and uses a shorter final elongation step (1 minute compared to 10 minutes). Prior work carried out by Marsey & Winpenny that looked at bestrophin expression in CFPAC cells found expression of all four bestrophins (Marsey & Winpenny, 2009), whereas my study confirmed that BEST1, BEST3 and BEST4 were expressed and BEST2 was also expressed in some repeats. The data regarding bestrophin expression in the A549 cell line is currently novel in the field at this time. Bestrophins have been demonstrated to be localised on the endoplasmic reticulum and control intracellular Ca^{2+} signalling rather than being a transmembrane ion channel like CFTR (Barro-Soria *et al.*, 2010). This might explain why expression of bestrophins appeared strong yet the response to UTP was very small.

3.3.5 Anoctamins are expressed in Calu-3, CFPAC and A549

The transmembrane family of anoctamins are found in all eukaryotes, and there are 10 members of the family in total (ANO1 – 10) in vertebrates (Schroeder *et al.*, 2008; Pifferi *et al.*, 2009; Stohr *et al.*, 2009). The anoctamin family appears to have evolved from a series of gene duplication events (Milenkovic *et al.*, 2010). Of these members, ANO1 and ANO2 can produce similar calcium activated chloride currents and so are thought to be a calcium activated chloride channels (Schroeder *et al.*, 2008; Almaca *et al.*, 2009; Pifferi *et al.*, 2009; Stephan *et al.*, 2009; Stohr *et al.*, 2009). Furthermore, it has been shown that ANO6 and ANO7 are also able to produce a calcium activated chloride conductance (Schreiber *et al.*, 2010). When co-expressed with ANO1, both ANO9 and ANO10 were found to suppress the baseline chloride conductance, which suggests that the proteins are able to inhibit the activity of other anoctamin family members (Schreiber *et al.*, 2010). From the short circuit current data in Calu-3 cells gathered and presented in this chapter, the responses from UTP were very small and not statistically significant (Figure 3.4). It may be the case that CaCCs are either not expressed or have very low levels of expression. These responses may not necessarily be due to bestrophins, but rather anoctamins. To address this, our investigation demonstrates expression of an array of genes from the anoctamin family of calcium activated chloride channel candidates in Calu-3 cells and others (Figure

3.8), which is important since these chloride channel candidates could potentially affect ion transport. Epithelial anoctamin expression data compiled by Kunzelmann *et al.*, 2009 is currently the most complete. Kunzelmann's group detected the expression of ANO1 in CFPAC and A549, whereas our study showed expression of ANO1 in Calu-3 and CFPAC but not A549 cells. Kunzelmann's group did not detect ANO2, ANO3 and ANO4 in any of our tested cell lines, whereas our study found expression of ANO2 and ANO3 in CFPAC cells, and ANO4 in all three cell lines. Kunzelmann's group found ANO5 expression in Calu-3 and A549 cell lines and not in CFPAC cells, whereas our study found expression of ANO5 in all three cell lines. Kunzelmann's group found strong expression of ANO6 in all three cell lines, whereas our group found strong expression of ANO6 in Calu-3 and CFPAC cells but not A549. ANO7 expression was not found in any of the cell lines by either Kunzelmann's group or our data. Kunzelmann's ANO8 expression was found to be strong in A549 and Calu-3, and weaker in CFPAC, whereas our data found that expression of ANO8 was strong in all three cell lines. Kunzelmann's group detected some ANO9 expression in all three cell lines, whereas our data showed expression in CFPAC only. Kunzelmann's group did not find ANO10 expression in any of the cell lines, whereas our data found ANO10 expression in CFPAC and Calu-3. In general, there is agreement between our data and Kunzelmann's group, but there are differences, particularly with the CFPAC line. These differences could potentially be accounted for by different experimental protocols used for extraction and amplification (not indicated by the paper), as well as potentially some differences in the sequence of primers used (although the primer sequences for all genes investigated are not indicated in the paper). Despite the fact that many anoctamins are expressed in Calu-3 cells, the response to UTP from functional data from this investigation was not statistically significant, which suggests that these channels are likely to not be expressed as a functional protein. Further work could look into testing whether anoctamin proteins are expressed in the Calu-3 cell line (see Future Work, section 8.4).

Chapter 4 Induction of Metalloproteinases and their Effect on Short Circuit Current

4.1 Introduction

It has been demonstrated previously that broad spectrum MMP inhibitor 1,10-phenanthroline had no significant effect on the short circuit current (I_{SC}) with the A549 cell line, while the I_{SC} in Calu-3 cells was shown to be increased in a concentration dependent manner (Duszyk *et al.*, 1999). Anti-MMP-2 had the same effect of increasing I_{SC} . Recombinant MMP-2 reduced I_{SC} . Since the whole cell current in A549 cells (which do not express CFTR) was not similarly affected, MMP-2 somehow specifically affects CFTR chloride channels and reduces whole cell current by an unknown mechanism (Duszyk *et al.*, 1999). This study remains the only study looking at the relationship between MMPs and the CFTR channel. If MMP-2 can negatively regulate the CFTR channel, use of MMP-2 inhibitors could be used to remove the negative regulation of MMP-2 on CFTR, and thus increase chloride transport. To explore the link between MMP-2 and CFTR could potentially lead to new therapeutic targets to treat cystic fibrosis.

Since MMP-2 was thought to regulate the CFTR channel, it was necessary to first determine the presence of MMP-2 protein in Calu-3 cells and whether the protein is secreted or retained inside the cell. This would be important to demonstrate since if MMP-2 has a negative effect on CFTR activity, we need to demonstrate that the enzyme is in fact present and expressed. The A549 cell line was selected as a control since it does not express CFTR (Mohammad-Panah *et al.*, 1998; Carreiras *et al.*, 1999; Bossard *et al.*, 2007; Xu *et al.*, 2010). Gelatin zymography was used to determine the presence of gelatinases in the conditioned media of unstimulated and stimulated cell samples through their catalytic breakdown of gelatin substrate within a protein gel. When stained with coomassie brilliant blue, the undegraded gelatin in the background will be stained blue, while areas of where gelatin has been degraded by gelatinases will remain clear and unstained. The molecular weight of the gelatinase

can be estimated with a molecular weight marker ran at the same time of the gel. Of particular interest are the MMP-2 and MMP-9 gelatinases, which have molecular weights of 66 and 93 kDa, respectively. A549 cells were used as a comparison since they can be induced to secrete both gelatinases (Lin *et al.*, 2008).

In order to find the optimal seeding density required to achieve confluence in a 12-well plate within a reasonable timeframe for 12-well plates for A549 and Calu-3 cells, cell growth assays using the cell division tracking dye carboxyfluorescein diacetate succinimidyl ester (CFSE) (Hawkins *et al.*, 2007) were performed first to provide a quantitative measure of cell growth. The conditioned media from these cells would later be used for the zymography. In order to perform gelatin zymography successfully, it requires the use of no foetal calf serum. This is because foetal calf serum can mask the digested bands in the resulting gel and produce unreliable results (Jung, 2008). Therefore it was necessary to determine if A549 and Calu-3 cells were able to grow in no serum. Thus, in order to assess the growth rate of A549 and Calu-3 cells under different concentrations of foetal calf serum, serum starvation assays were also performed.

In order to stimulate gelatinase production in the cells, phorbol 12-myristate 13-acetate (PMA), a gelatinase stimulator (Fini *et al.*, 1995) that is known to be toxic to cells in high concentrations (Kuroda *et al.*, 1987), was used. Therefore, to assess the viability of cells in no serum and PMA, a cell viability assay was performed. This was important since the cells producing gelatinases for use with zymography needed to be known to be healthy. The cell viability assay used the propidium iodide dye, which is a vital dye with the ability to intercalate DNA (Restrepo-Hartwig & Ahlquist, 1996) and fluoresce at the 562-588 nm wavelength (red) when excited by 488 nm laser light via flow cytometry (Schneider *et al.*, 2001). Propidium iodide is membrane impermeant, so cannot traverse the cell membranes of healthy viable cells (Ha & Snyder, 1999).

In order to determine if MMPs can affect chloride transport, recombinant MMP-2 was used since it was seen previously by Duszyk *et al.* (1999) that it could reduce the short circuit current. The non-selective MMP inhibitor, GM-6001, was used to see if blocking MMP-2 activity could increase I_{sc} like another MMP inhibitor, 1,10-phenanthroline, as used by Duszyk *et al.* (1999). The GM-6001 control compound,

which is an inactive form of GM-6001 (Ha & Snyder, 1999), was used as the control. This experiment was to clarify if the increases in current from 1,10-phenanthroline were due to the fact it was an MMP inhibitor, or rather an effect of the compound itself on another ion channel or signalling messenger. To complement the result of GM-6001, Anti-MMP-2 antibodies were used to see if blocking MMP-2 increased the I_{sc} , and mixed IgG antibodies were used as the control. EGF was used since it was known that EGF had an effect on potassium channel endocytosis, and that may affect the driving force for chloride ion transport (Koide *et al.*, 2007). EGF is also a potent inducer of gelatinases (Lin *et al.*, 2008). Any effects of EGF will be further tested experimentally using AG1478, barium chloride and basolateral membrane permeabilisation to determine how the response is regulated in terms of EGFR signalling and influence of potassium channels. As before, the A549 cell line was used as a comparison since it does not express CFTR.

4.2 Results

4.2.1 Determining Optimal Cell Growth using Carboxyfluorescein succinimidyl ester (CFSE)

The cell growth assay was performed as described in the protocol with both Calu-3 and A549 cells. The results obtained during the assay follow. The CFSE analysis works as a cell division tracker since the CFSE probe enters the cells and is distributed evenly between the two daughter cells as shown in Figure 4.1 (Gett & Hodgkin, 1998). You would therefore expect that the initial fluorescence to be high. If the cells are viable and are dividing, the fluorescence intensity should decrease and the peak fluorescence should shift. The CFSE probe can be detected by flow cytometry (Weston & Parish, 1990).

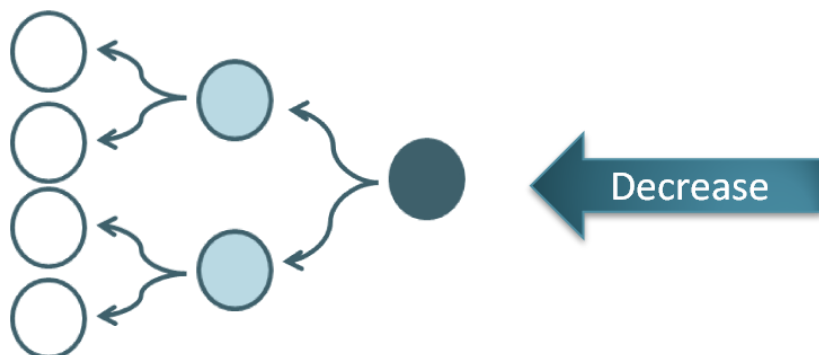


Figure 4.1 – How the CFSE fluorescence intensity decreases with cell growth.

To obtain a quantitative result, the X-Mean values (mean fluorescence intensity), were recorded for each sample (which were performed in triplicate), and then averaged to give a final value. This value was compared to the other data sets using firstly a one-way ANOVA with a Tukey's Multiple Comparison Test to compare each sample to determine any significant difference. X-mean values differ across results due to non-uniform pulsing of the CFSE probe, but within the dataset, it is internally consistent so is analysed accordingly.

A549 cells showed significant decreases in cell growth using high seeding densities compared to low ones (Figure 4.2, A and C). Without serum, A549 cells grew poorly compared to other samples at higher serum concentrations (Figure 4.3, A and C). Calu-3 cells showed decreases in cell growth, but often not significantly (Figure 4.2, B and D) and no significant difference in growth between different serum concentrations (Figure 4.3, B and D). Taken together, these results suggest that the Calu-3 cell line is best seeded at higher densities (50,000 cells in a 12 well plate) to hasten growth and that they have a high tolerance for growing in serum free media required for gelatin zymography. The A549 cell line however is best seeded at a lower density (20,000 cells in a 12 well plate). A549 cell growth rates are more affected by serum free media. However, from an experimental standpoint, the growth rate was still adequate for use with gelatin zymography.

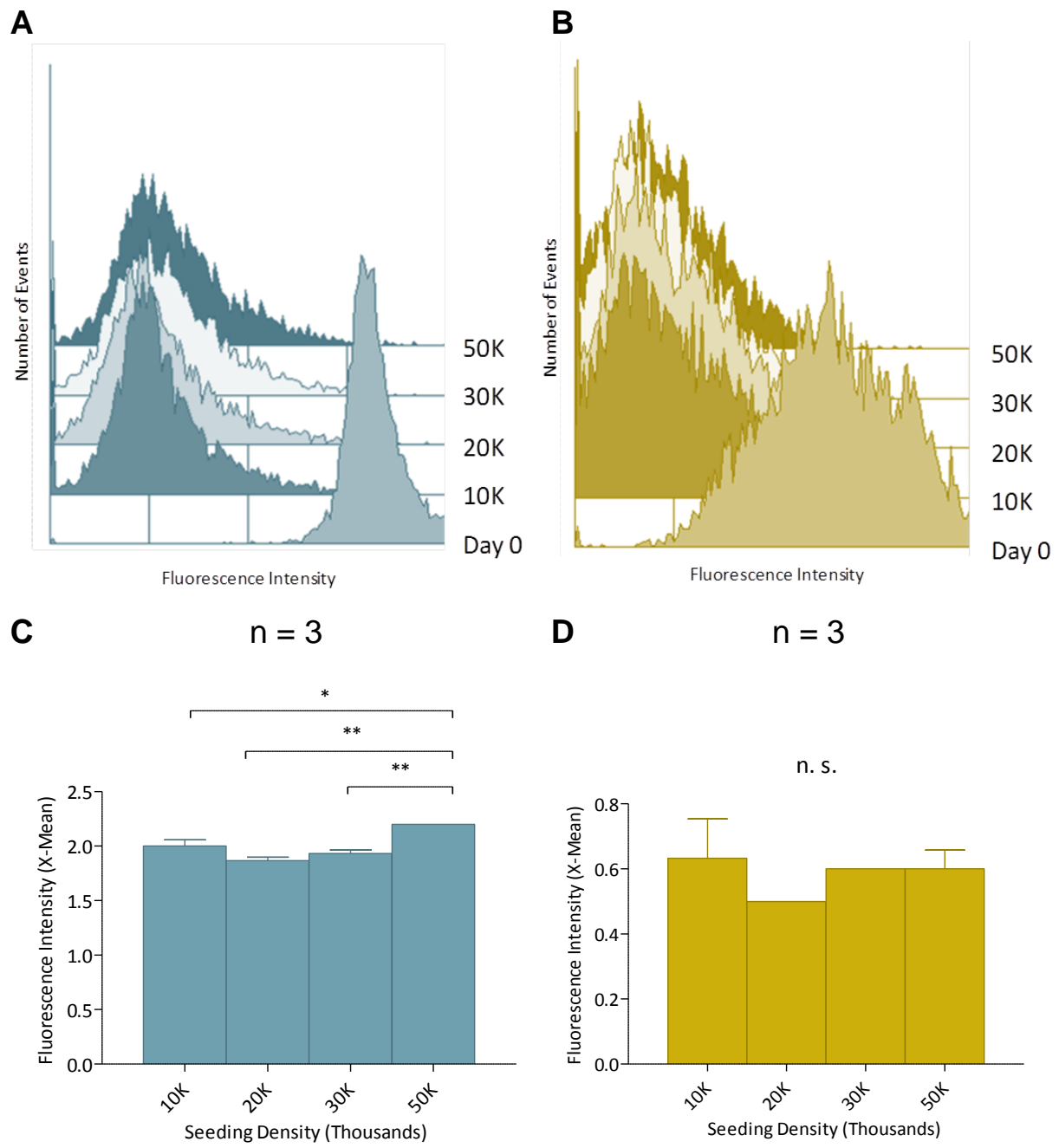


Figure 4.2 – Calu-3 growth is unaffected by seeding density.

Raw histogram output of flow cytometer for the A549 (A) and Calu-3 (B) cell line showing number of events against intensity for discrete seeding densities (10K, 20K, 30K and 50K). Assessment of cell growth by measuring CFSE fluorescence intensity using the A549 cell line (C) and the Calu-3 cell line (D). Greater fluorescent intensities indicate less growth, while smaller fluorescent intensities indicate stronger growth. Statistical analysis was performed using a one way ANOVA with Tukey's Multiple Comparison test, where $P < 0.05$ was deemed statistically significant.

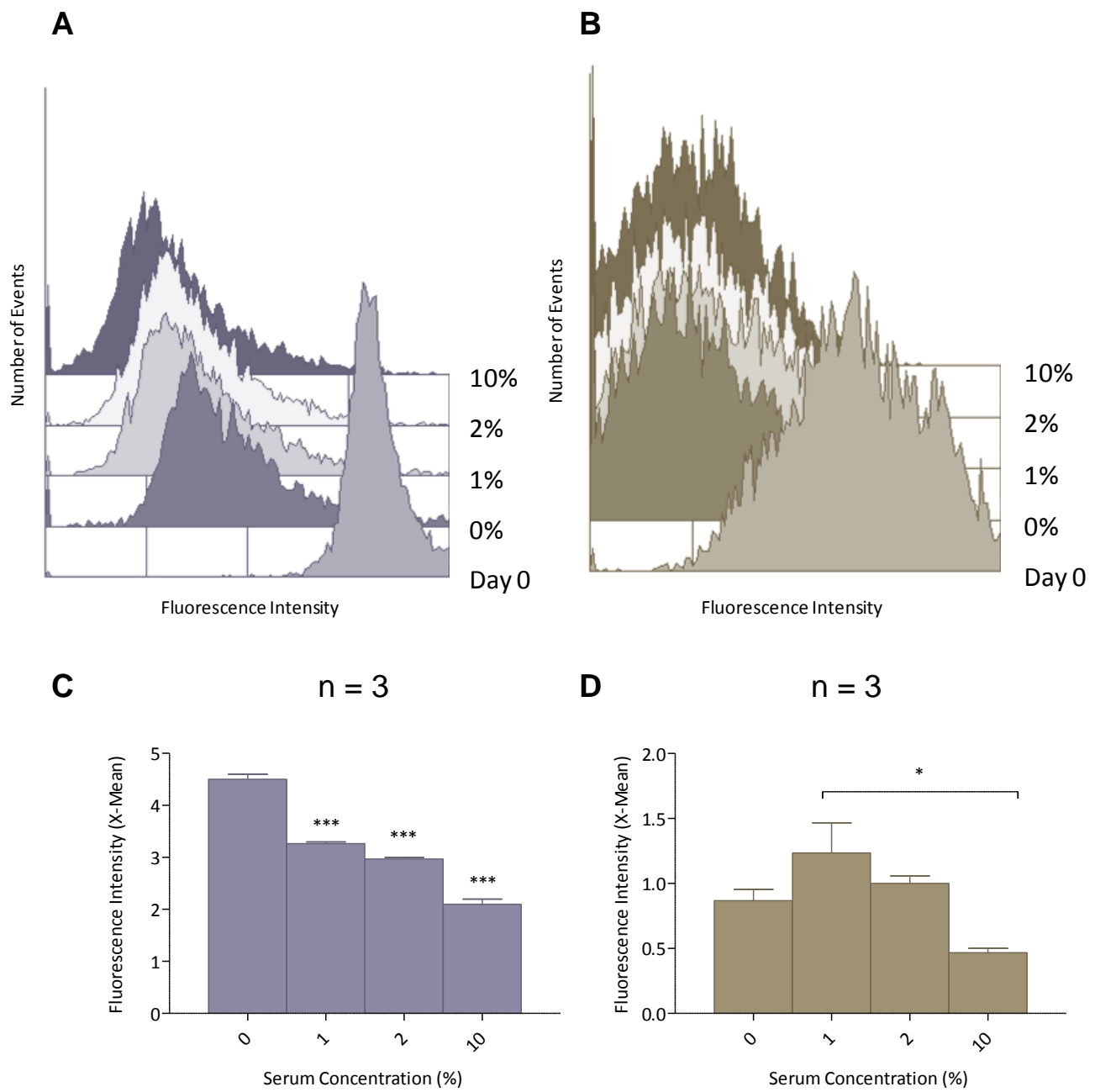


Figure 4.3 – Calu-3 cell growth is largely unaffected by low / no serum media.

Raw histogram output of flow cytometer for the A549 (A) and Calu-3 (B) cell line showing number of events against intensity for discrete serum concentrations (0, 1, 2 and 10%). Assessment of cell growth under serum starvation by measuring CFSE fluorescence intensity using the A549 cell line (C) and the Calu-3 cell line (D). Greater fluorescent intensities indicate less growth, while smaller fluorescent intensities indicate stronger growth. Statistical analysis was performed using a one way ANOVA with Tukey's Multiple Comparison test, where $P < 0.05$ was deemed statistically significant.

4.2.2 Calu-3 cells are viable with PMA incubation

Propidium iodide (PI) is a DNA intercalating agent that can be used to assess cell viability. PI cannot traverse the cell and nuclear membranes of viable cells, but can access the DNA of damaged cells. When PI is bound to nucleic acids, the fluorescence excitation maximum is 535 nm and the emission maximum is 617 nm (Figure 4.4). The region where the majority of the cell population lies is gated to discount debris, marked R1. The gates used are shown in Figure 4.5 and Figure 4.6 (B, C and D). The percentage of PI positive cells that occupy this gate of the total population of cells within the gate indicates the level of cell viability in the cell suspension. The PI positive cells are identified using the M1 gate, giving the percentage of dead cells within R1. The percentage values are analysed statistically using firstly a one-way ANOVA with a Tukey's Multiple Comparison Test to compare each sample to determine any significant difference. The variables tested in these comparisons are viability in response to PMA, a stimulator of MMPs, and viability over a period of 72 hours without stimulation.

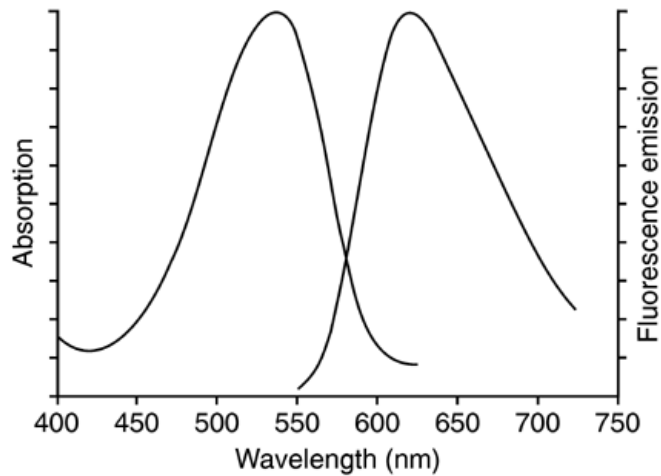
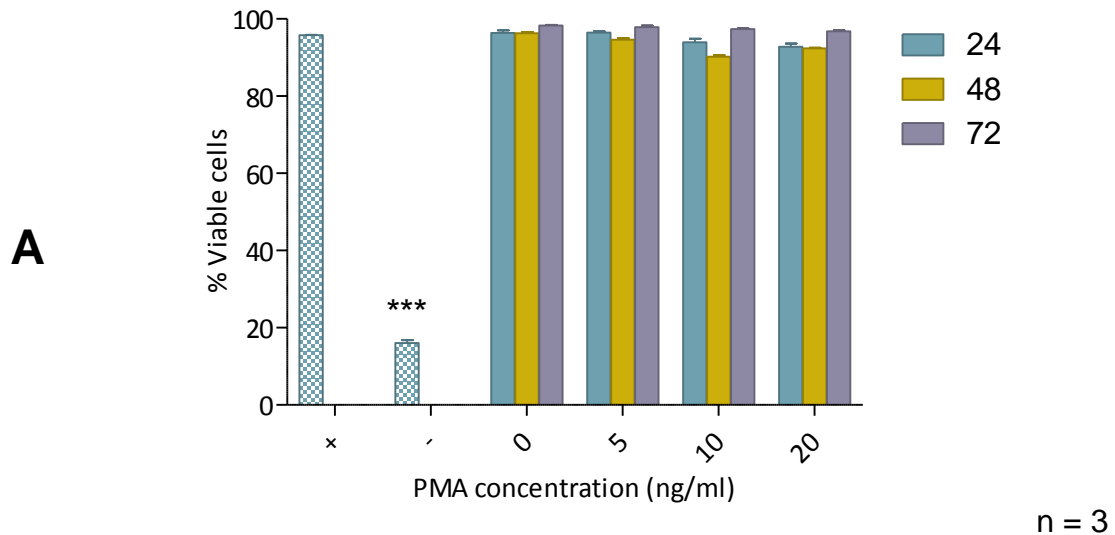
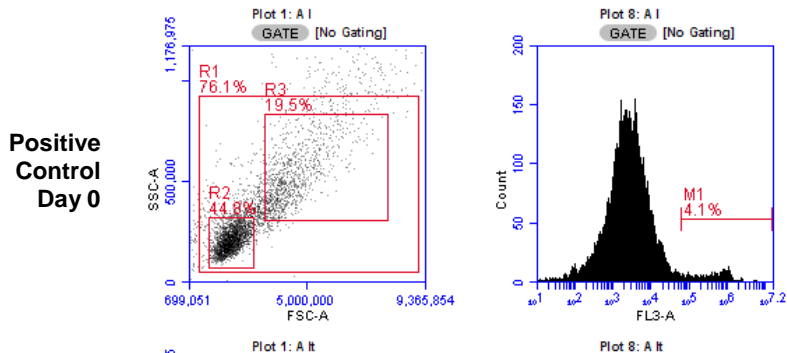


Figure 4.4 – Representation of propidium iodide spectra.

Figure 4.5 shows that varying concentrations of PMA does not significantly change the cell viability of A549 cells, nor does the viability of cells decrease after 24, 48 and 72 hours. Figure 4.6 shows that varying concentrations of PMA does not significantly change the cell viability of Calu-3 cells, nor does the viability of cells decrease after 24 and 72 hours.

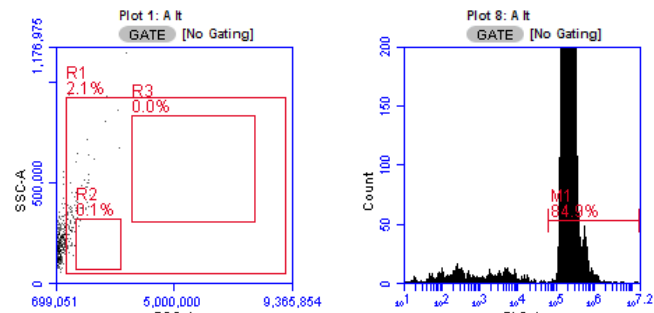


B



C

Negative Control Triton Treated



D

Representative Sample

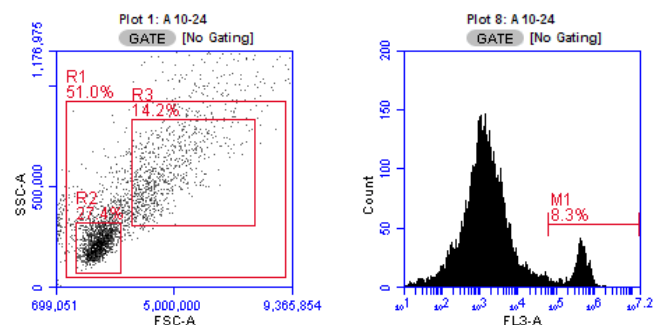


Figure 4.5 – A549 cells are viable in the presence of PMA over a period of time.

A) Percentage cell viability of A549 cells stimulated with PMA after 24, 48 and 72 hours. B) Representative flow cytometer output of Day 0 control. C) Representative flow cytometer output of triton treated negative control. D) Representative flow cytometer output of a tested sample. Statistical analysis was performed using a one way ANOVA with Tukey's Multiple Comparison test, where $P < 0.05$ was deemed statistically significant.

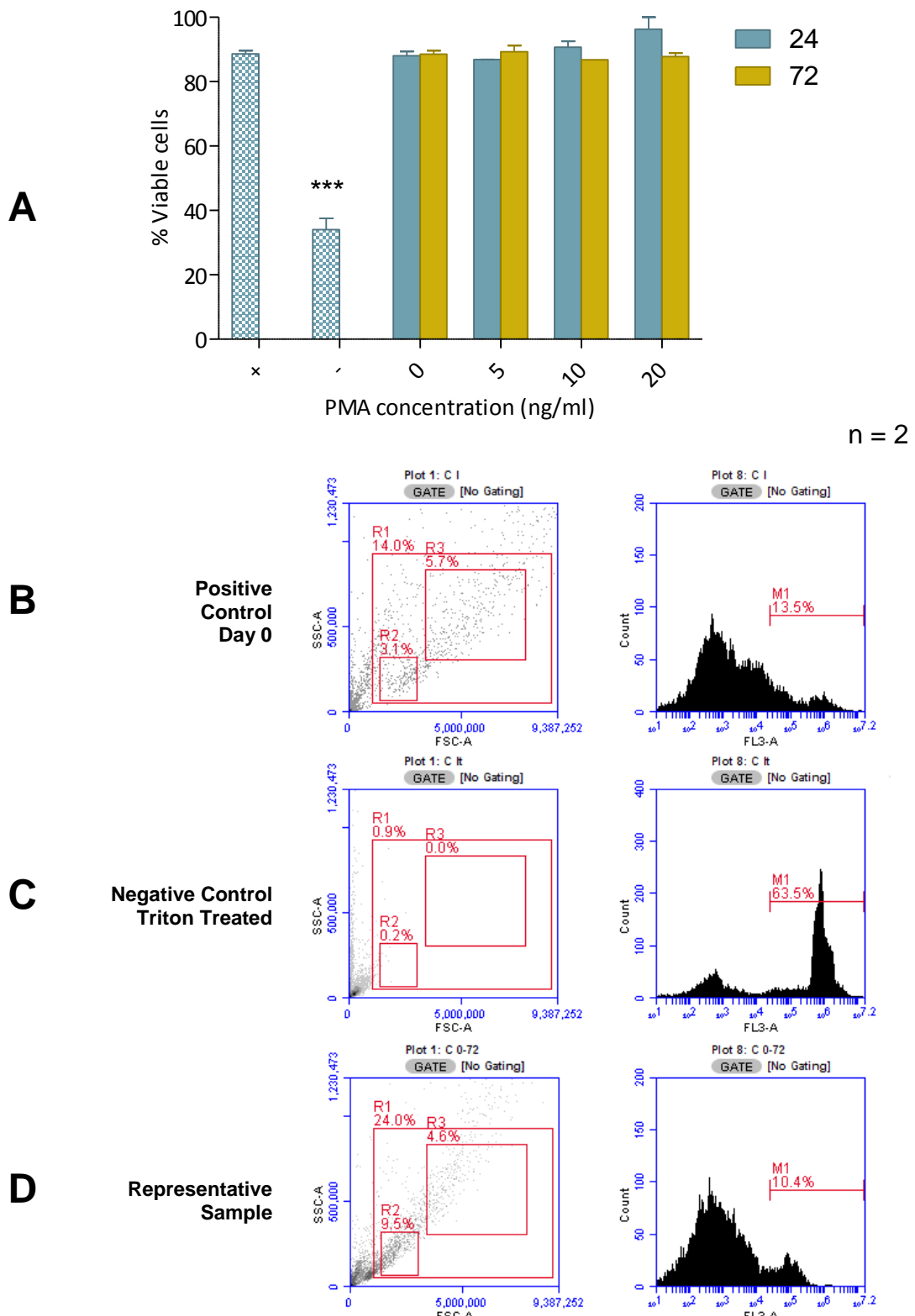


Figure 4.6 – Calu-3 cells are viable in the presence of PMA over a period of time.

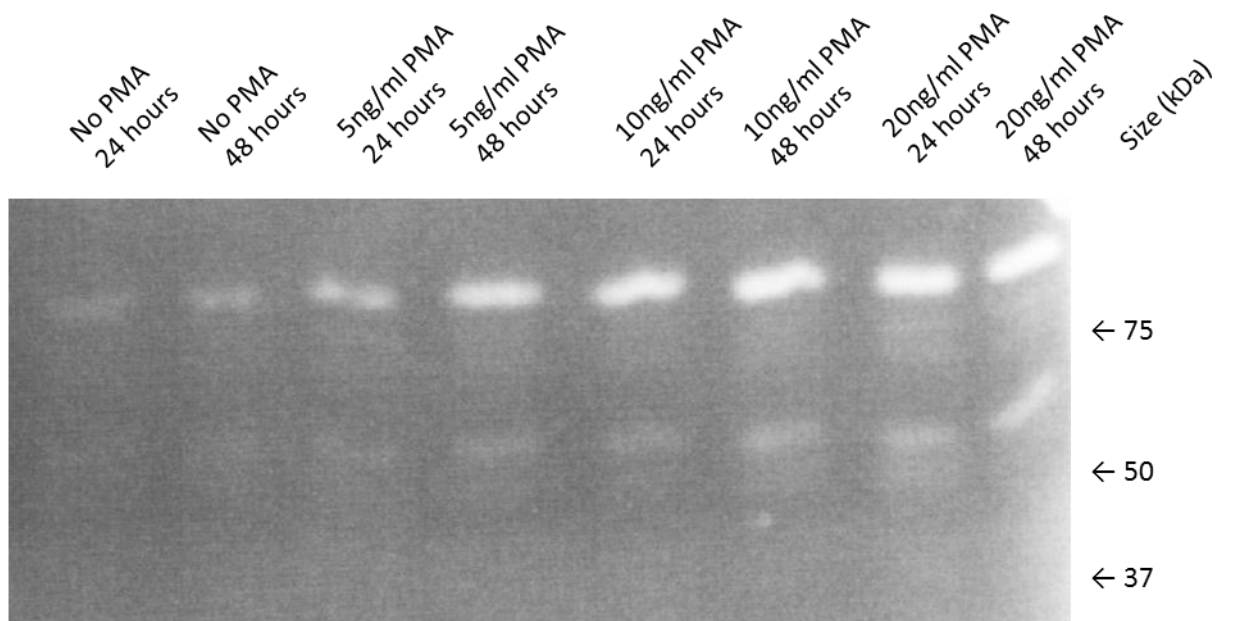
A) Percentage cell viability of Calu-3 cells stimulated with PMA after 24 and 72 hours. B) Representative flow cytometer output of Day 0 control. C) Representative flow cytometer output of triton treated negative control. D) Representative flow cytometer output of a tested sample. Statistical analysis was performed using a one way ANOVA with Tukey's Multiple Comparison test, where P<0.05 was deemed statistically significant.

4.2.3 Detecting gelatinase function with gelatin zymography

The gelatinase activity of unstimulated Calu-3 and A549 cells was evaluated. Then, cells were treated with PMA or EGF, two known stimulators of gelatinases (Fini *et al.*, 1995; Tian *et al.*, 2007). EGF has previously been shown to be involved in the regulation of ion channels (Koide *et al.*, 2007), so its effect on MMP expression with Calu-3 and A549 cell lines was also investigated.

4.2.3.1 PMA incubation for 24 and 48 hours induces gelatinase function

Unstimulated, both the Calu-3 and A549 cell line produce barely detectable levels of gelatinases (Figure 4.7, A and B). PMA is confirmed to produce 66 kDa and 93 kDa gelatinases that correspond to MMP-2 and MMP-9 in A549 and Calu-3 cells (Figure 4.7, A and B). For A549 samples, the ~93 kDa band is produced more than the ~66 kDa band. There is also a stronger band at ~70 kDa. The strongest bands tend to occur at higher concentrations of PMA such as between 10-20 ng/ml (Figure 4.7, A). Calu-3 cells have a tendency to produce more of the ~66 kDa band, which are strongest at 48 hours with 5 ng/ml PMA the majority of the time (Figure 4.7, B). Taken together, this set of data demonstrates that gelatinases can be effectively upregulated by PMA in both the A549 and Calu-3 cell lines. The molecular weights of these gelatinases correspond to MMP-2 (66 kDa), proMMP-2 (72 kDa) and MMP-9 (93 kDa).



A A549 cell line

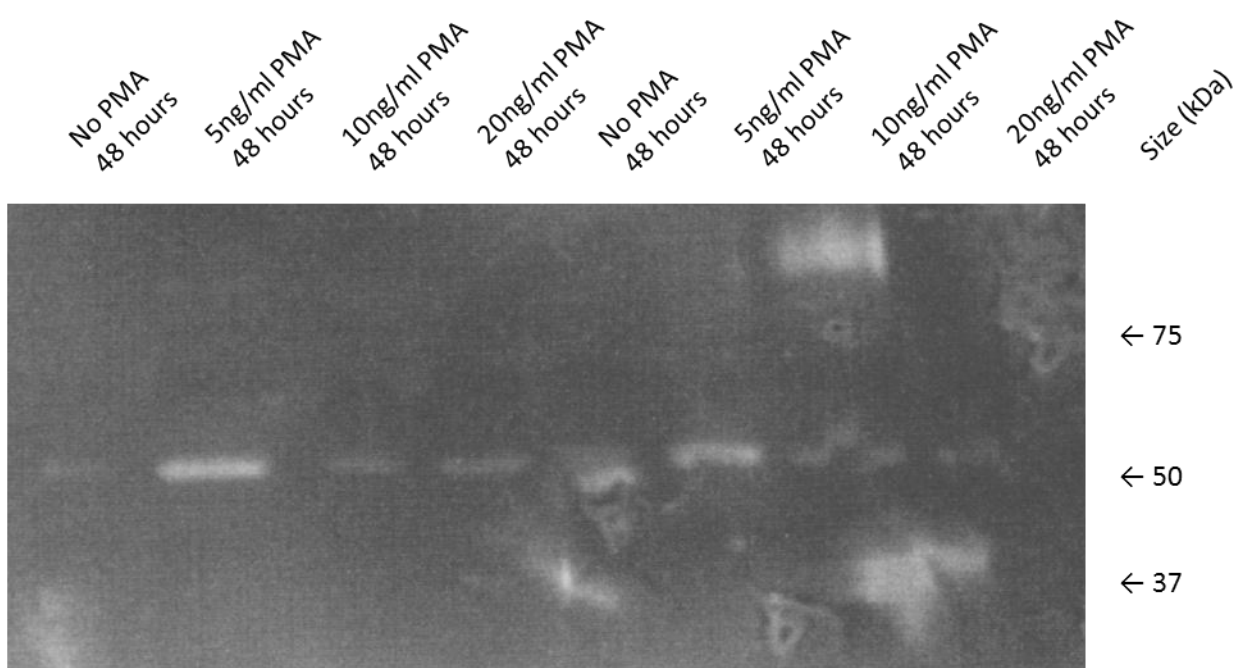


Figure 4.7 – Gelatinase activity is induced by PMA in A549 and Calu-3 cells

4.7 – Gelatinase activity is induced by PMA in A549 and Calu-3 cells.
 Zymogram showing gelatinase activity in stimulated A549 (A) and Calu-3 (B) cell samples. The concentration of the PMA compound used is indicated in ng/ml. The cells were left in conditioned media for either 24 or 48 hours as indicated. This is a positive (raw) image of the zymography gel.

4.2.3.2 PMA and EGF incubation for 24 and 48 hours induces gelatinase function

A549 cells stimulated with both PMA and EGF show at least three strong bands at ~90 kDa and two at ~66 kDa with all tested compounds and concentrations at 24 hours. After 48 hours, the activity of gelatinases stimulated with EGF appears to decrease slightly, whereas the cells that were stimulated with PMA showed stronger activity after 48 hours than at 24 hours (Figure 4.8, A and B).

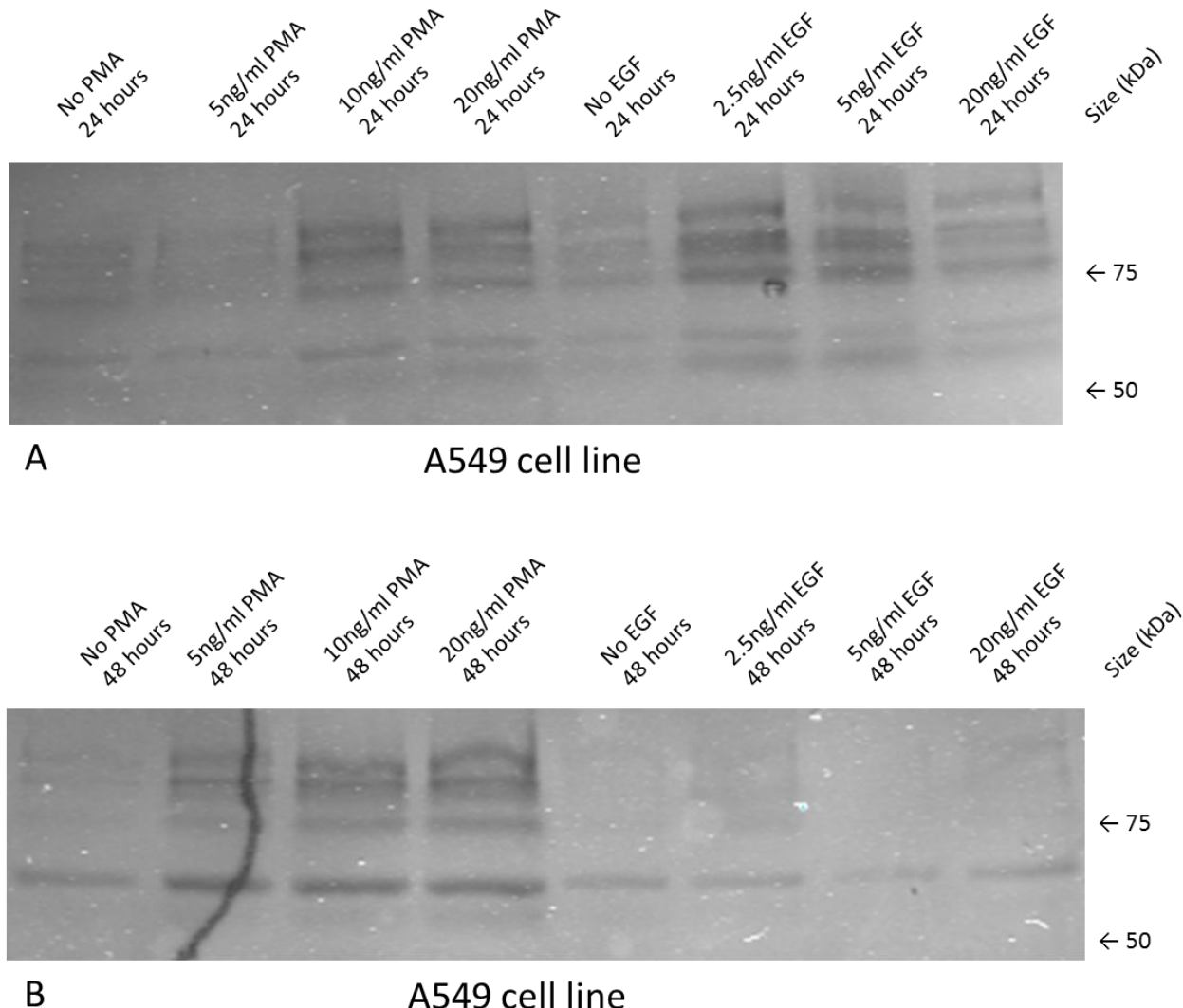


Figure 4.8 – Gelatinase activity is induced by PMA and EGF in A549 cells.

Zymogram showing gelatinase activity in stimulated A549 cell samples after 24 (A) and 48 (B) hours. The concentration of compound (PMA or EGF) used is indicated in ng/ml. The cells were left in conditioned media for either 24 or 48 hours as indicated. This is a negative image of the zymography gel using an Odyssey scanner.

Calu-3 cells stimulated with both PMA and EGF exhibit a very similar response to A549 cells. The zymogram shows at least two strong bands at ~90 kDa and one at ~66 kDa with all tested compounds and concentrations at 24 hours. After 48 hours, the activity of gelatinases stimulated with EGF appears to decrease, whereas with PMA stimulation, the activity of the gelatinases at 24 and 48 hours appears to be the same or a slight decrease (Figure 4.9, A and B).

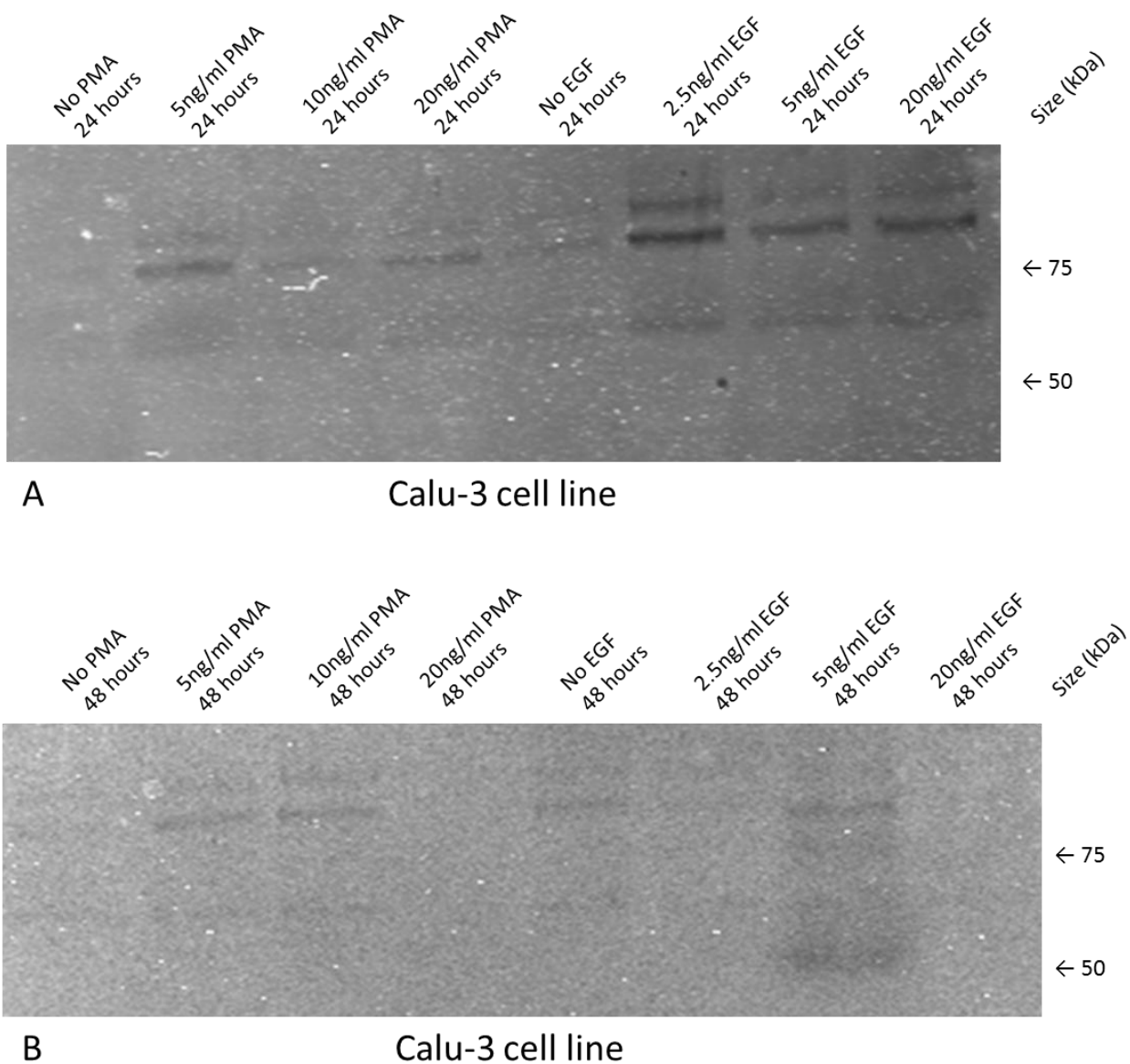


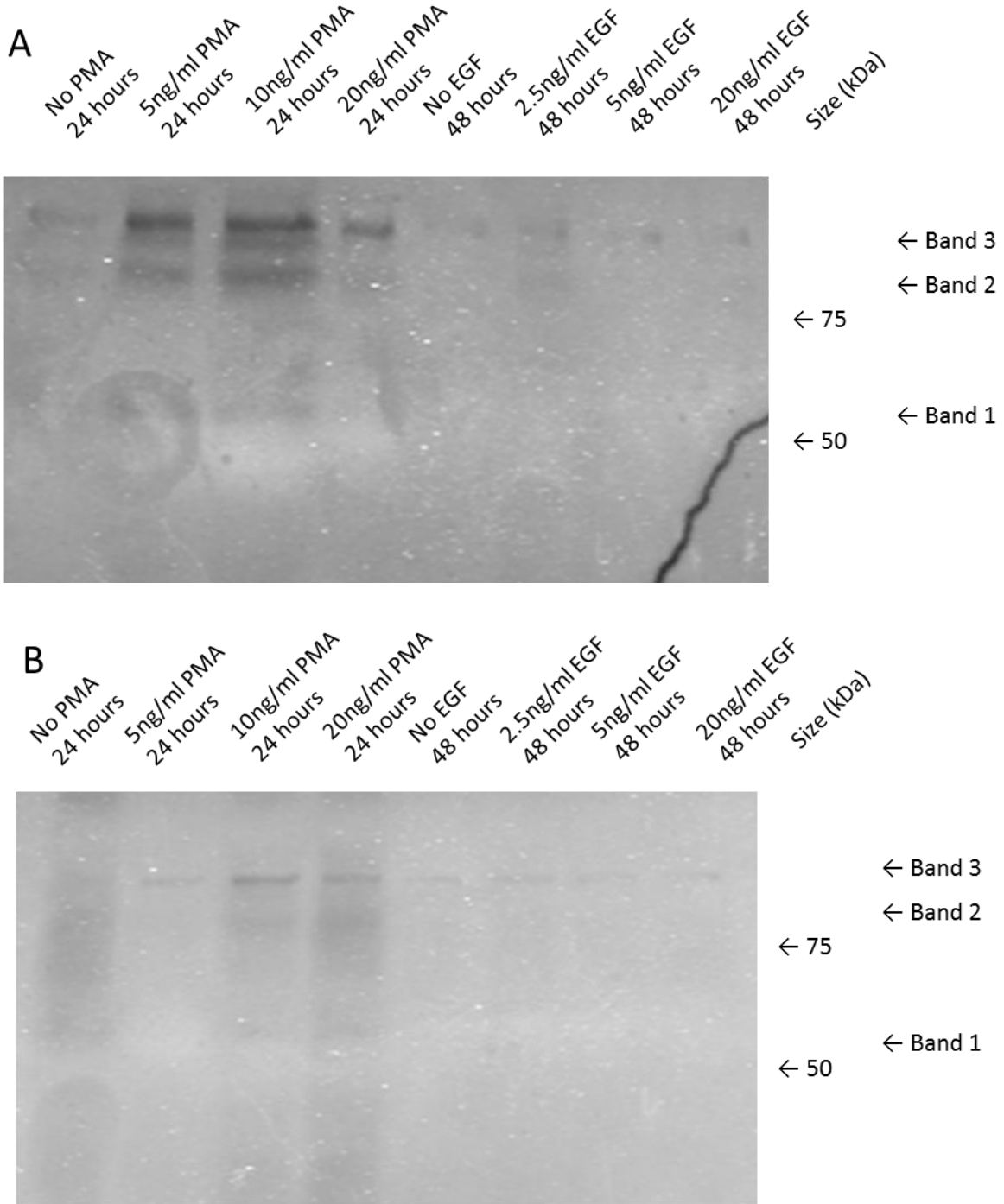
Figure 4.9 – Gelatinase activity is induced by PMA and EGF in Calu-3 cells.

Zymogram showing gelatinase activity in stimulated Calu-3 cell samples after 24 (A) and 48 (B) hours. The concentration of compound (PMA or EGF) used as indicated in ng/ml. The cells were left in conditioned media for either 24 or 48 hours as indicated. This is a negative image of the zymography gel using an Odyssey scanner.

4.2.3.3 PMA and EGF incubation with GM-6001 for 24 and 48 hours reduces gelatinase function

An experiment was performed where conditioned media from A549 cells was collected at both 24 and 48 hours with one set of samples stimulated with varying concentrations of PMA and EGF (0 ng/ml – 20 ng/ml), while the other was incubated with 10 μ M GM-6001 as well as stimulated with PMA / EGF. The A549 cell line was chosen for this experiment since this cell line produced higher gelatinase activity over the series of experiments. These samples were then subjected to gelatin zymography. The zymogram gel with 10 μ M GM-6001 treated samples was treated with 10 μ M GM-6001 in the overnight tris assay buffer (TAB) while the zymogram gel with the untreated set of samples were left untreated. The resulting zymogram gels were imaged as before and subjected to densitometry analysis to determine if gelatinase activity could be effectively knocked down by GM-6001.

When treated with GM-6001 and then subsequently stimulating with PMA / EGF, it is seen that the activity of the gelatinases in A549 cells is reduced somewhat; particularly bands 1 and 2. When subjected to densitometry analysis, it was seen that when 5 ng/ml EGF was used, 10 μ M GM-6001 knocked down the activity of bands 1 and 2 by 50% and 45% respectively. Band 3 was only knocked down by 9% (Figure 4.10 and graphically represented by Figure 4.11). Taken together, this result shows that 10 μ M GM-6001 can effectively inhibit MMP-2, and can inhibit smaller molecular weight variants of MMP-9. Larger molecular weight variants of MMP-9 are less effectively inhibited.



A549 cell line

Figure 4.10 – PMA and EGF induced increases in gelatinase activity are inhibited by GM-6001 in A549 cells.

Parallel zymograms showing (A) gelatinase activity in PMA/EGF stimulated A549 cell samples after 24 and 48 hours. (B) gelatinase activity in the presence of GM-6001 in PMA/EGF stimulated A549 cell samples after 24 and 48 hours. The concentration of compound used (PMA or EGF) is indicated in ng/ml. The cells were left in conditioned media for either 24 or 48 hours as indicated. This is a negative image of the zymography gel using the Odyssey scanner.

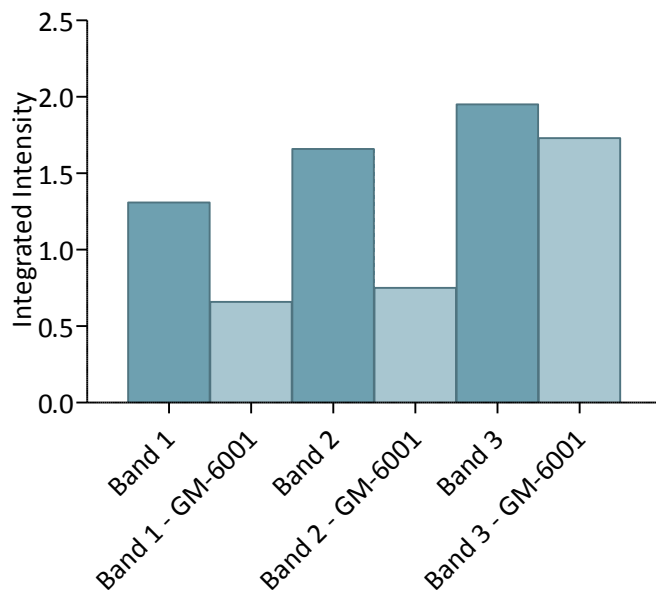


Figure 4.11 – Gelatin Zymography of EGF-treated A549 cells inhibited by GM-6001 after 48 hours.

EGF induced increases in gelatinase activity are inhibited by GM-6001 in A549 cells. A graph to show the knockdown in integrated intensity by GM-6001 during stimulation of A549 cells by 5 ng/ml EGF.

4.2.4 MMP-2 is detected in Calu-3 conditioned media

It is seen from a Western blot (Figure 4.12) that MMP-2 is mainly localised in the conditioned media rather than within the cell. It was also seen that Calu-3 cells produced far more MMP-2 than A549 cells. This result was not unexpected since MMP-2 is known to be a secreted metalloproteinase.

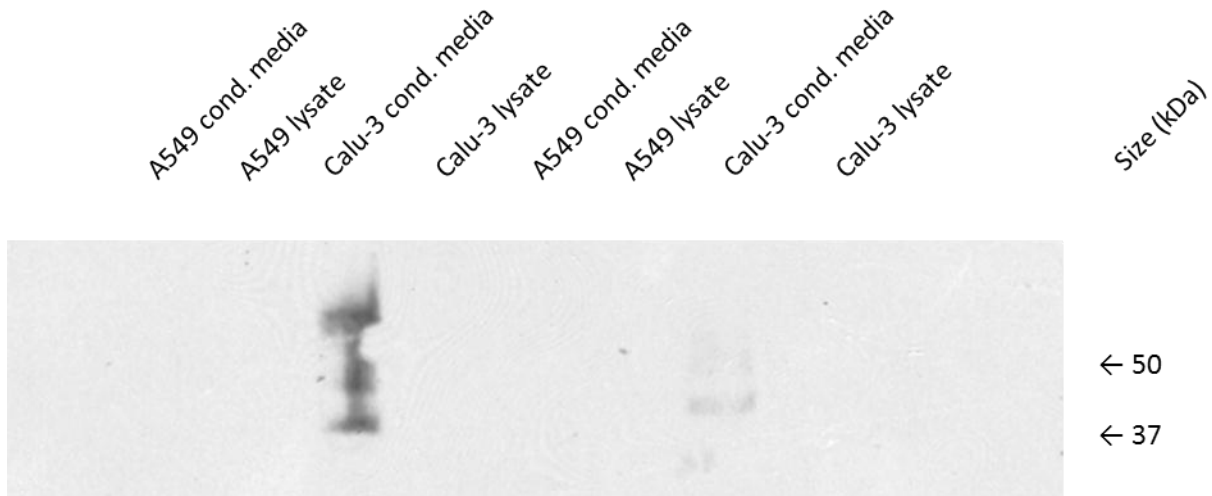


Figure 4.12 – Western Blot depicting the presence of MMP-2 within two cell lines using the RIPA extraction method and conditioned media.

4.2.5 Acute addition of GM-6001 does not affect I_{SC} across Calu-3 monolayers

MMP-2 inhibitor GM6001 was applied apically to intact Calu-3 monolayers to assess if residual MMP activity is affecting ion transport (Figure 4.13, A and B). 1 μ M GM-6001 to the apical side resulted in a negligible increase of $0.5 \pm 0.5 \mu\text{A cm}^{-2}$ (n=3) in short circuit current. Successive additions of GM-6001 that included 2 μ M, 4 μ M and 8 μ M resulted in increases of $1.3 \pm 0.7 \mu\text{A cm}^{-2}$ (n=3), $2.1 \pm 1.0 \mu\text{A cm}^{-2}$ (n=3) and $2.8 \pm 1.0 \mu\text{A cm}^{-2}$ (n=3), respectively, compared to pre-GM-6001 treatment values. Complete inhibition of the response was achieved by applying CFTR blocker 50 μ M GlyH-101 to the apical side, resulting in a decrease of $10.7 \pm 0.6 \mu\text{A cm}^{-2}$ (n=3, p<0.001). Further inhibition of short circuit current was a result of basolateral treatment of 100 μ M bumetanide, resulting in a decrease of $2.1 \pm 0.4 \mu\text{A cm}^{-2}$ (n=3, p<0.001).

A similar experiment with intact Calu-3 monolayers was conducted by substituting GM-6001 with the modified GM-6001 control compound, which is designed not to have an effect on MMP activity (Figure 4.13, C and D). Apical addition of 1 μ M GM-6001 control resulted in a decrease in I_{SC} of $0.1 \mu\text{A cm}^{-2}$ (n=1). Successive additions of GM-6001 control to the apical side that included 2 μ M, 4 μ M and 8 μ M resulted in increases of $0.2 \mu\text{A cm}^{-2}$ (n=1), $0.9 \mu\text{A cm}^{-2}$ (n=1) and $2.2 \mu\text{A cm}^{-2}$ (n=1) respectively compared to pre-GM-6001 treatment values. Complete inhibition of the response was achieved using 50 μ M GlyH-101 to the apical side, resulting in a decrease of $11.5 \mu\text{A cm}^{-2}$ (n=1). Further inhibition of short circuit current was a result of basolateral treatment of 100 μ M bumetanide, resulting in a decrease of $3.6 \mu\text{A cm}^{-2}$ (n=1).

Taken together, the results suggest that GM-6001 appears to increase short circuit current in Calu-3 monolayers. The GM-6001 control compound result appears to exhibit noise. Since the GM-6001 control experimental result is based upon a single replicate, firm conclusions about the effect of GM-6001 on Calu-3 monolayers may not be drawn.

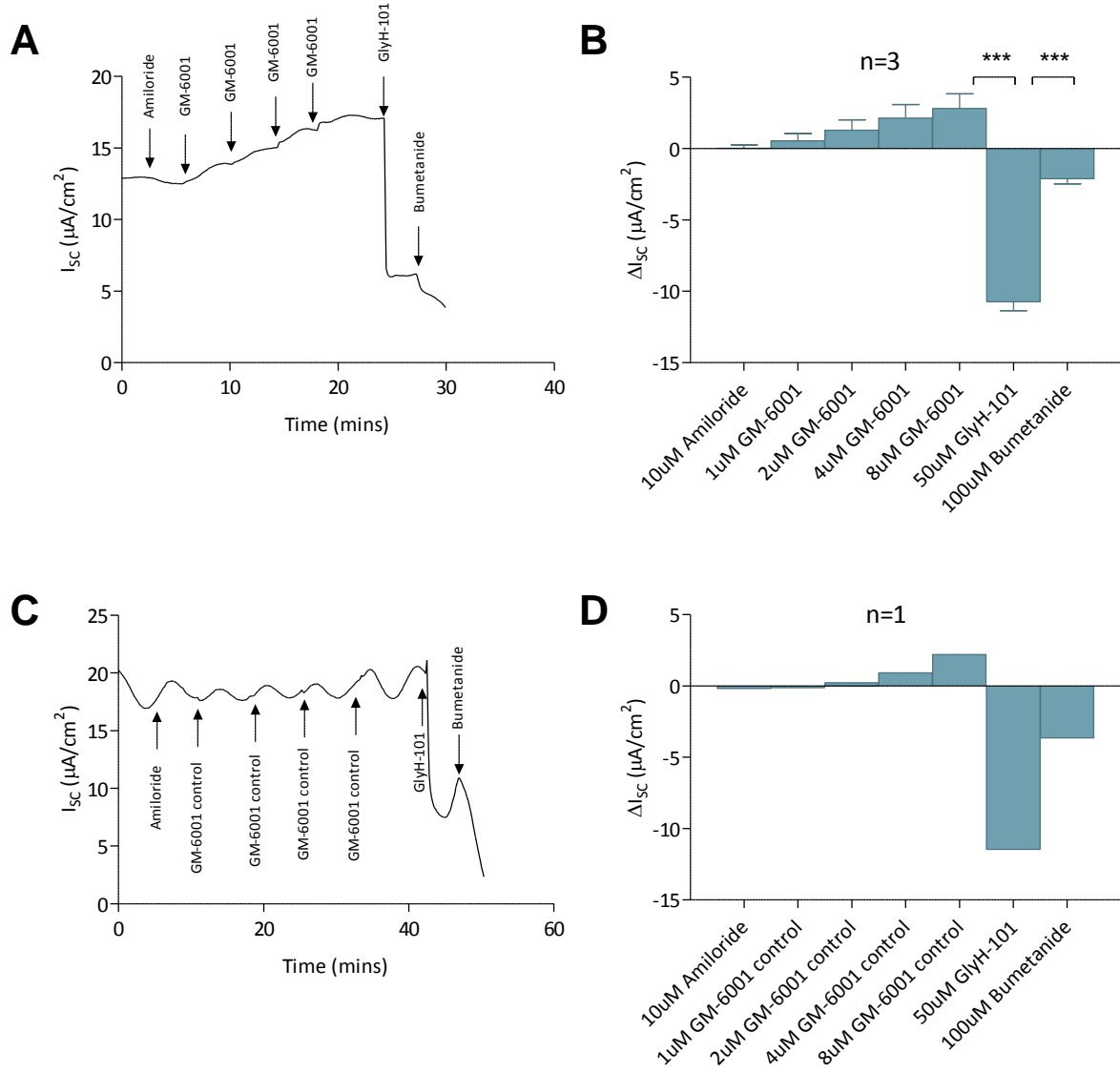


Figure 4.13 – GM-6001 acute response does not affect I_{SC} across Calu-3 monolayers.

Trace (A) and bar graph (B) to show the change in short circuit current across a Calu-3 epithelium in response to GM-6001 and compounds and their representative raw traces. There is a trend that GM-6001 increases the I_{SC} across the epithelium in a concentration dependent manner, and the increase is inhibited by 50 μM GlyH-101. Trace (C) and Bar graph (D) to show the change in short circuit current across a Calu-3 epithelium in response to GM-6001 Control. GM-6001 control does not increase the I_{SC} as much, and is also highly oscillated and exhibiting noise. Statistical analysis was performed using a one way ANOVA with Tukey's Multiple Comparison test, where $P<0.05$ was deemed statistically significant.

4.2.6 Negligible GM-6001 acute response in A549 monolayers

Similarly, a dose response experiment with apical application of GM-6001 was conducted using the A549 cell line (Figure 4.14, A and B). Unlike the previous experiment using Calu-3 monolayers shown in Figure 4.13, the results that were obtained were much more variable as shown in the size of the error bars. Some repeats generated a negative ΔI_{SC} after the addition of GM-6001, indicating an increasingly absorptive monolayer rather than a secretory one as exhibited by Calu-3 monolayers. Taken together, the result demonstrates that there was no evidence that the compound had a significant effect on ion transport in the A549 cell line.

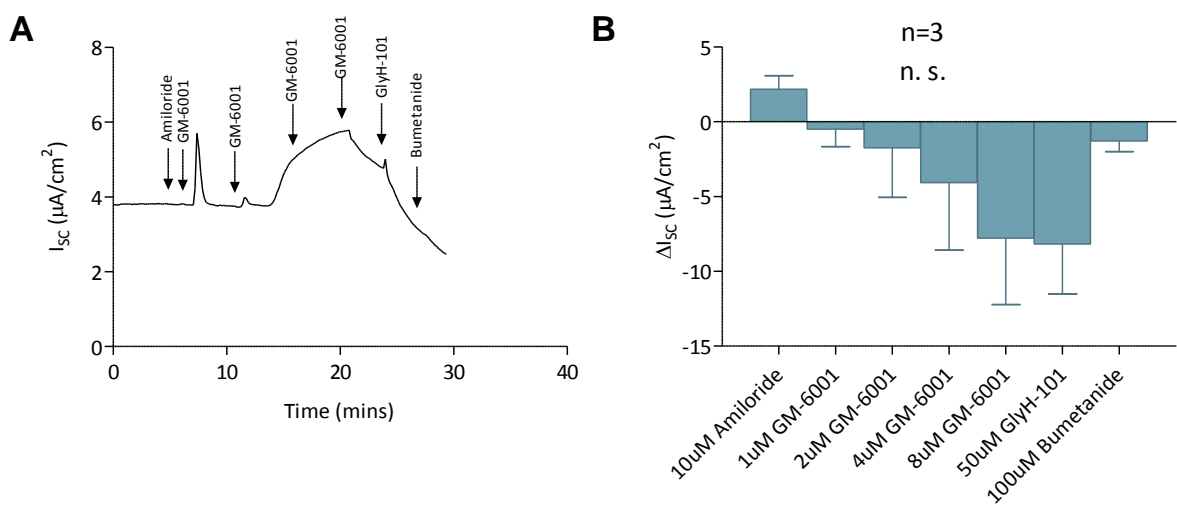


Figure 4.14 – Negligible GM-6001 acute response in A549 monolayers.

Trace (left) and bar graph (right) to show the change in short circuit current across an A549 epithelium in response to 1 – 8 μ M GM-6001. It is also seen that GM-6001 has little effect on I_{SC} . Statistical analysis was performed using a one way ANOVA with Tukey's Multiple Comparison test, where $P<0.05$ was deemed statistically significant.

4.2.7 Acute addition of recombinant MMP-2 does not decrease I_{SC} across Calu-3 monolayers

To assess the effects of MMPs on short circuit current across intact Calu-3 monolayers (Figure 4.15, A and B), 10 ng/ml recombinant MMP-2 was added to the apical side, leading to no significant change in short circuit current ($0.5 \pm 0.1 \mu\text{A cm}^{-2}$ ($n=3$)). Further additions of recombinant MMP-2 to the apical side did not significantly change the current. The Calu-3 monolayer was then treated with 10 μM forskolin on the basolateral side, leading to a large increase in I_{SC} to a peak of $33.4 \pm 1.5 \mu\text{A cm}^{-2}$ ($n=3$, $p<0.001$), followed by a baseline of $22.3 \pm 3.6 \mu\text{A cm}^{-2}$ ($n=3$). Apical application of 50 μM GlyH-101 led to a reduction in current of $12.5 \pm 1.4 \mu\text{A cm}^{-2}$ ($n=3$, $p<0.001$), which was not able to inhibit the response back to baseline, although it was statistically significant. Basolateral application of 100 μM bumetanide resulted in a further decrease of $11.2 \pm 2.9 \mu\text{A cm}^{-2}$ ($n=3$), which did fully inhibit the remaining increase due to forskolin. Taken together, it suggests that recombinant MMP-2 does not decrease ion transport across Calu-3 monolayers, but enhances either stimulated CFTR response, or increases current via basolateral potassium channels.

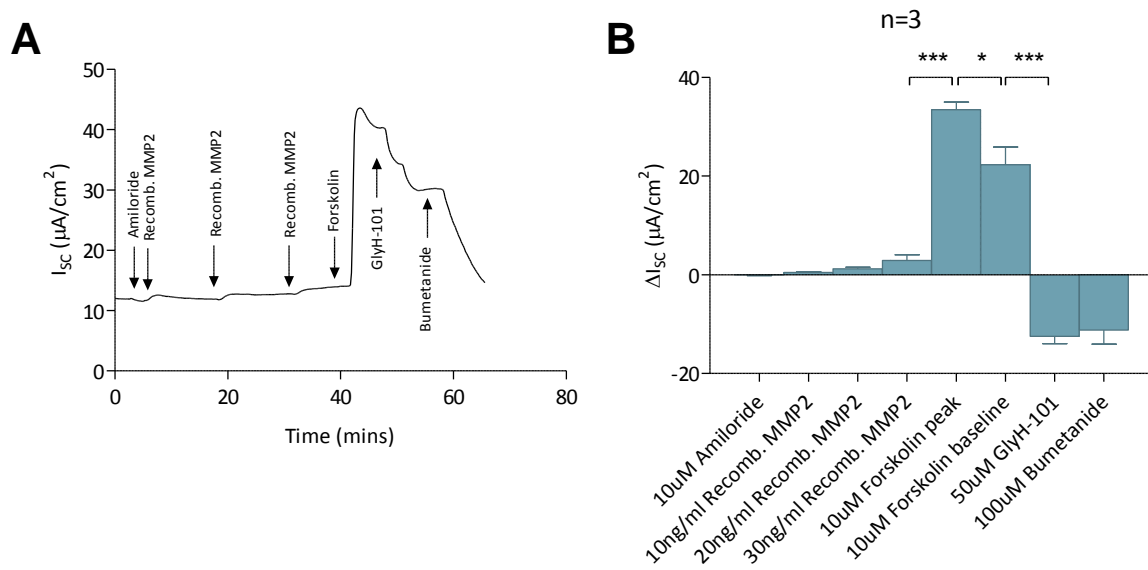


Figure 4.15 – Recombinant MMP-2 acute response does not affect I_{SC} across Calu-3 monolayers.

Trace (A) and bar graph (B) to show the change in short circuit current across a Calu-3 epithelium in response to 10 – 30 ng/ml recombinant MMP-2. Addition of recombinant MMP-2 itself causes little activation of current, however, it is seen that inhibition of CFTR by 50 μM GlyH-101 is reduced since the current fails to return to or below the baseline current. Statistical analysis was performed using a one way ANOVA with Tukey's Multiple Comparison test, where $P<0.05$ was deemed statistically significant.

4.2.8 Negligible recombinant MMP-2 response in A549 monolayers

Similarly, a dose response experiment with recombinant MMP-2 was conducted using the A549 cell line (Figure 4.16, A and B). The addition of recombinant MMP-2 to the apical surface of A549 monolayers led to increases in I_{SC} that were generally less than $1 \mu\text{A cm}^{-2}$. Subsequent stimulation with forskolin did not result in a large increase in I_{SC} that was seen in the Calu-3 cell line, but generally a small decrease was seen. Taken together, the results demonstrated that there was no evidence that the recombinant enzyme had a significant effect on ion transport in the A549 cell line. Subsequent attempts to stimulate the A549 monolayer with forskolin resulted in no increase in I_{SC} due to a lack of expression of CFTR.

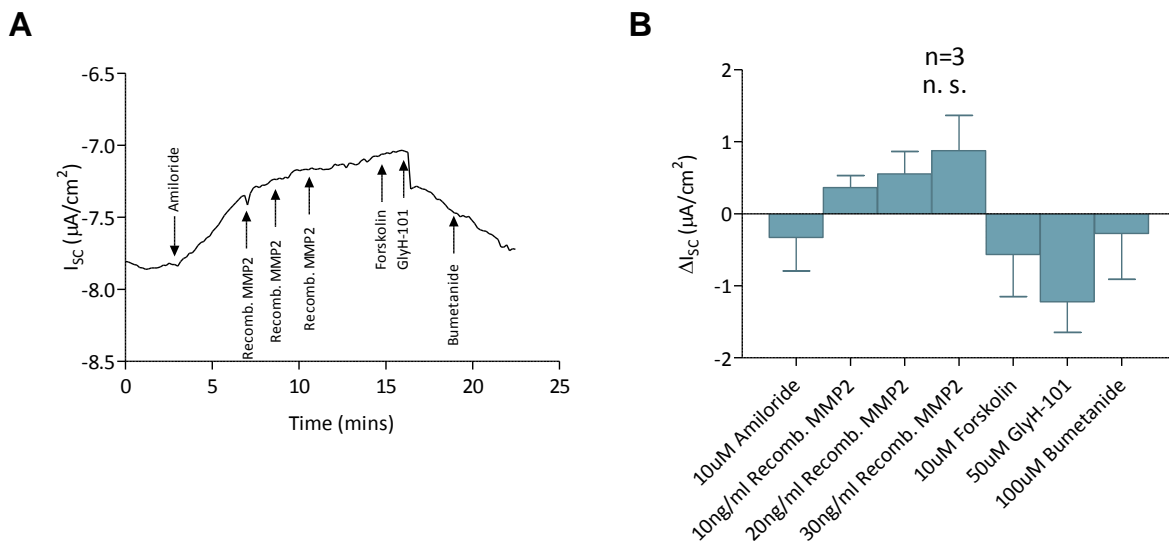


Figure 4.16 – Negligible recombinant MMP-2 response in A549 monolayers.

Trace (A) and bar graph (B) to show the change in short circuit current across an A549 epithelium in response to 10 – 30 ng/ml recombinant MMP-2. Recombinant MMP-2 has little effect on I_{SC} . Statistical analysis was performed using a one way ANOVA with Tukey's Multiple Comparison test, where $P<0.05$ was deemed statistically significant.

4.2.9 Acute addition of anti-MMP-2 does not affect I_{SC} across Calu-3 monolayers

To test whether antibodies raised against MMP-2 could inhibit MMP-2 activity and thus be able to affect short circuit current across intact Calu-3 monolayers, anti-MMP-2 was applied apically at 1:1000 dilution (Figure 4.17, A and B). This resulted in an increase in I_{SC} of $6.6 \pm 0.9 \mu\text{A cm}^{-2}$ ($n=3$). This increase was completely inhibited by apical application of 50 μM GlyH-101, leading to a decrease in I_{SC} of $11.0 \pm 1.8 \mu\text{A cm}^{-2}$ ($n=3$, $p<0.001$). Further inhibition of the remaining I_{SC} was achieved using 100 μM bumetanide on the basolateral side, leading to a decrease of $10.7 \pm 1.4 \mu\text{A cm}^{-2}$ ($n=3$).

In a similar experiment, mixed anti-IgG antibodies kindly provided by Dr Darren Sexton, University of East Anglia, were used as a control to test if antibodies in general can raise short circuit current (Figure 4.17, C and D). Apical application of IgG control antibodies were added apically at 1:1000 dilution. This resulted in an increase in I_{SC} of $7.4 \pm 0.6 \mu\text{A cm}^{-2}$ ($n=3$, $p<0.05$). This increase was completely inhibited by apical application of 50 μM GlyH-101, leading to a decrease in I_{SC} of $14.1 \pm 2.1 \mu\text{A cm}^{-2}$ ($n=3$, $p<0.001$). Further inhibition of the remaining I_{SC} was achieved using 100 μM bumetanide on the basolateral side, leading to a decrease of $5.6 \pm 0.5 \mu\text{A cm}^{-2}$ ($n=3$, $p<0.01$). Taken together, these data suggest that both anti-MMP-2 and anti-IgG antibodies raise I_{SC} , likely due to an effect of the antibodies themselves rather than effect of blocking MMPs.

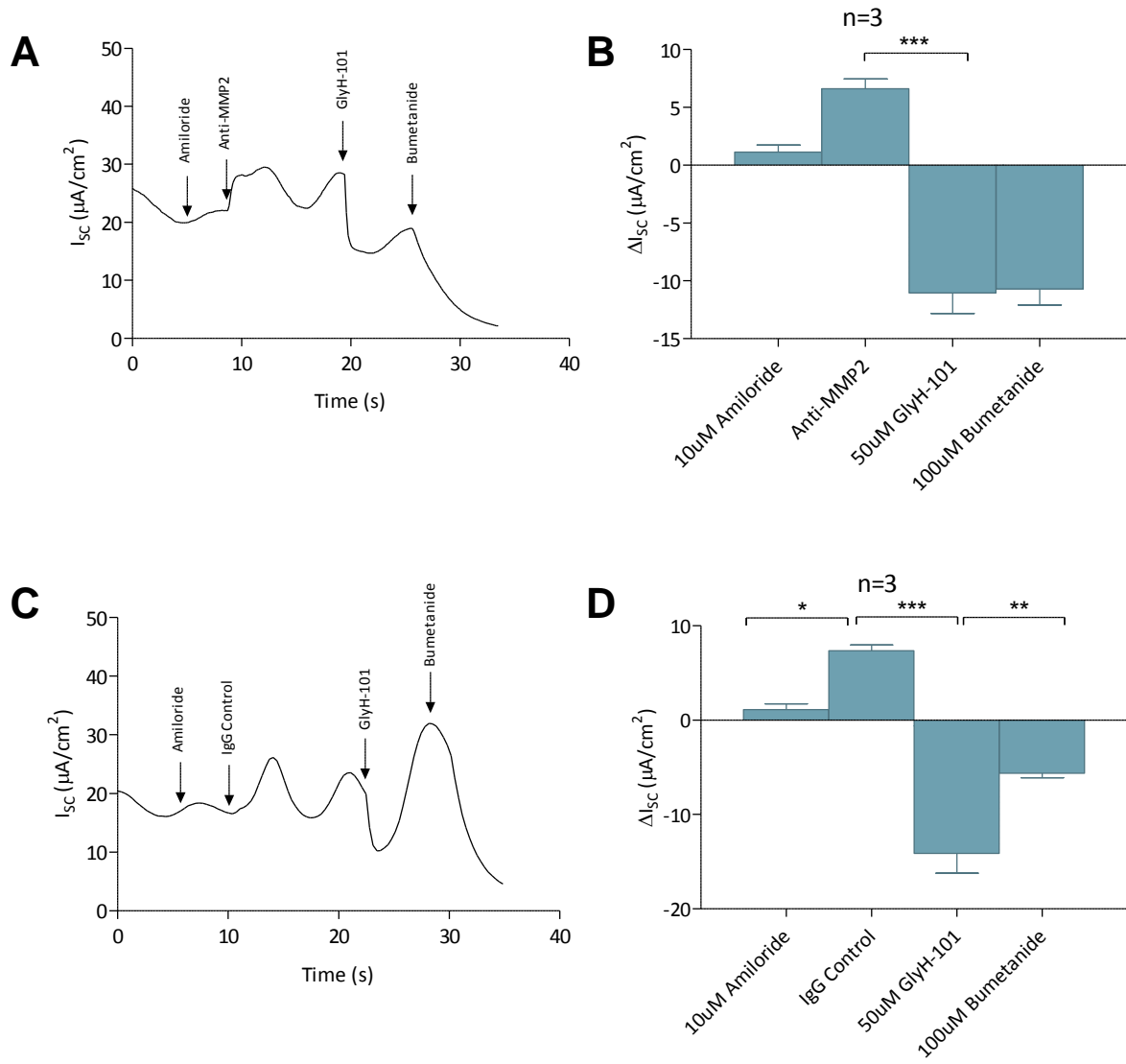


Figure 4.17 – Anti-MMP-2 acute response does not affect I_{sc} across Calu-3 monolayers.

Trace (A) and bar graph (B) to show the change in short circuit current across a Calu-3 epithelium in response to Anti-MMP-2 at 1:1000 dilution. Acute addition of Anti-MMP-2 leads to an increase in I_{sc} , which can be inhibited by GlyH-101. Trace (C) and bar graph (D) to show the change in short circuit current across a Calu-3 epithelium in response to IgG control at 1:1000 dilution. Mixed IgG antibodies exhibited a nearly identical result as with anti-MMP-2. Statistical analysis was performed using a one way ANOVA with Tukey's Multiple Comparison test, where $P<0.05$ was deemed statistically significant.

4.2.10 Negligible anti-MMP-2 and anti-IgG response in A549

Similarly, an experiment with apical application of anti-MMP-2 at a 1:1000 dilution was conducted using the A549 cell line (Figure 4.18, A and B). Unlike the experiments shown in Figure 4.17, A549 monolayers did not exhibit any significant increases in I_{SC} (less than $1 \mu\text{A cm}^{-2}$) when anti-MMP-2 antibodies were applied to the apical surface.

Furthermore, when anti-IgG control antibodies were applied to the apical surface of A549 monolayers at a 1:1000 dilution (Figure 4.18, C and D), it was seen that there were no significant increases in I_{SC} . Taken together, these results demonstrated that there was no evidence that the antibodies had a significant effect on ion transport in the A549 cell line. It may be possible that application of antibodies to Calu-3 monolayers leads to an activation of CFTR, and that due to the lack of expression of CFTR in A549 monolayers, a similar effect is not seen.

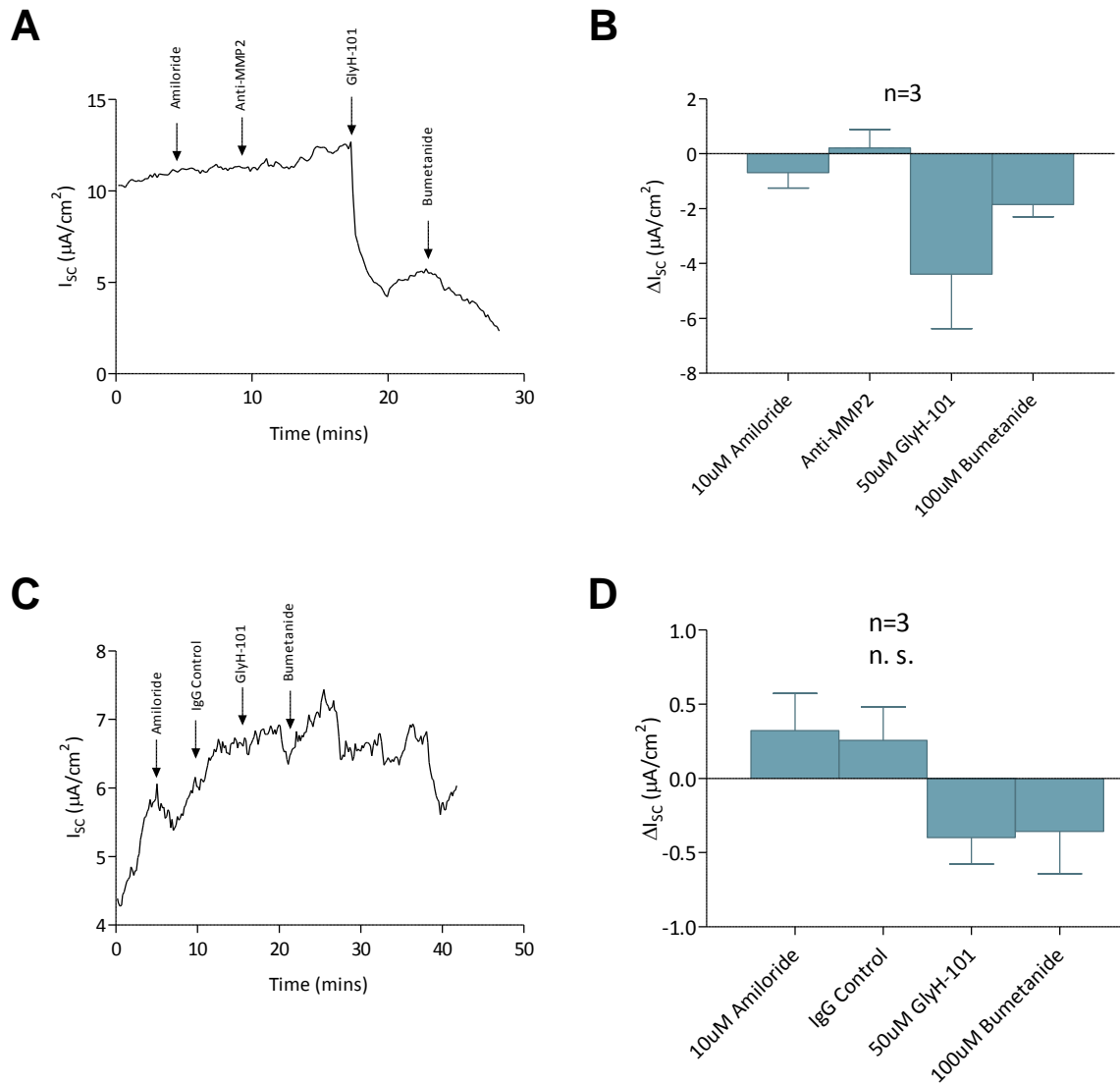


Figure 4.18 – Negligible anti-MMP-2 response in A549.

Trace (A) and bar graph (B) to show the change in short circuit current across an A549 epithelium in response to anti-MMP-2 at 1:1000 dilution. Anti-MMP-2 did not increase I_{SC} significantly, compared to the Calu-3 cell line. Trace (C) and bar graph (D) to show the change in short circuit current across an A549 epithelium in response to IgG control at 1:1000 dilution. Mixed IgG antibodies did not increase I_{SC} significantly, compared to the Calu-3 cell line. Statistical analysis was performed using a one way ANOVA with Tukey's Multiple Comparison test, where $P<0.05$ was deemed statistically significant.

4.2.11 Acute addition EGF increases I_{SC} across Calu-3 monolayers

Acute addition of 5 ng/ml EGF to the apical side of the monolayer resulted in a biphasic response (Figure 4.19, A and B). There was an initial transient increase (peak) in I_{SC} of $2.7 \pm 1.8 \mu\text{A cm}^{-2}$ (n=2), followed by a reduced but greater than baseline plateau phase (increase in I_{SC} of $1.5 \pm 0.8 \mu\text{A cm}^{-2}$, n=2). Increasing the EGF concentration to 50 ng/ml resulted in no further significant increase in I_{SC} . Apically applied 50 μM GlyH-101 inhibited by 257% (n=2) the increase in I_{SC} due to 5 ng/ml EGF.

In a similar experiment, pre-incubation of Calu-3 cells with the EGF receptor inhibitor, AG1478, followed by stimulation with 5ng/ml EGF on the apical side (Figure 4.19, C and D) resulted in complete inhibition of the EGF stimulated I_{SC} . Taken together, these data suggests that EGF may increase I_{SC} via EGFR when added acutely. This observation led to more experimentation with longer term preincubations detailed in later chapters.

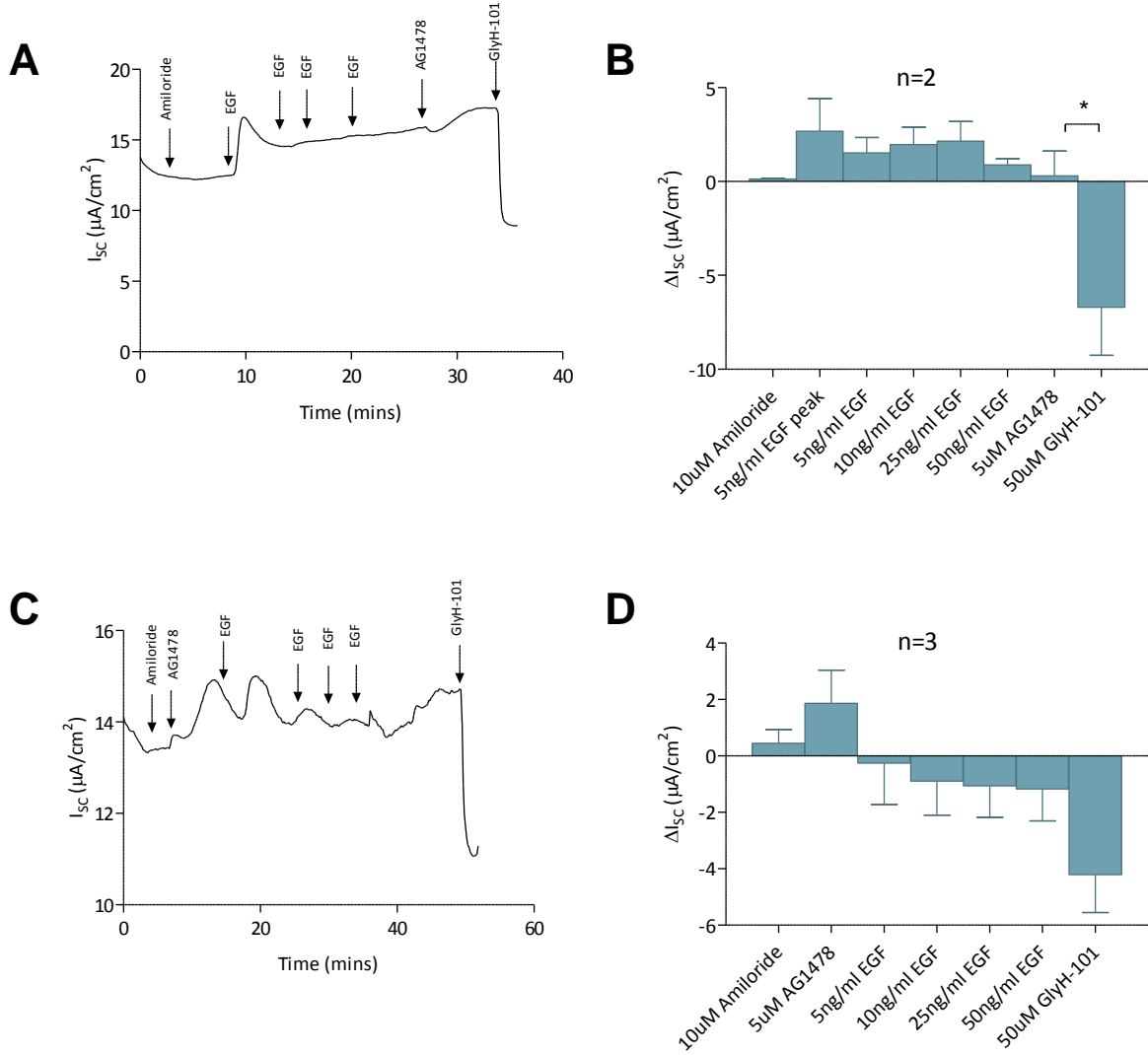


Figure 4.19 – EGF acute response increases I_{SC} across Calu-3 monolayers.

Trace (A) and bar graph (B) to show the change in short circuit current across a Calu-3 epithelium in response to 5 – 50 ng/ml EGF. EGF increases I_{SC} at concentrations of 5 ng/ml, and further additions produce no additional peaks. Trace (C) and Bar graph (D) to show the change in short circuit current across a Calu-3 epithelium in response to 5 μM AG1478 (before EGF). With the addition of EGF inhibitor before EGF, it is seen that the EGF peak is reduced. Statistical analysis was performed using a one way ANOVA with Tukey's Multiple Comparison test, where $P < 0.05$ was deemed statistically significant.

4.2.12 Negligible EGF response in A549 monolayers

Similarly, an experiment with EGF was conducted using the A549 cell line (Figure 4.20, A and B). Unlike what was seen with the Calu-3 cell line (shown in Figure 4.19), apical application of 5ng/ml EGF did not result in a significant change in I_{SC} . Subsequent application of tyrosine kinase inhibitor, AG1478, also did not result in any change in I_{SC} . Taken together, these results demonstrate that there was no evidence that the EGFR signalling pathway has a significant effect on ion transport in the A549 cell line.

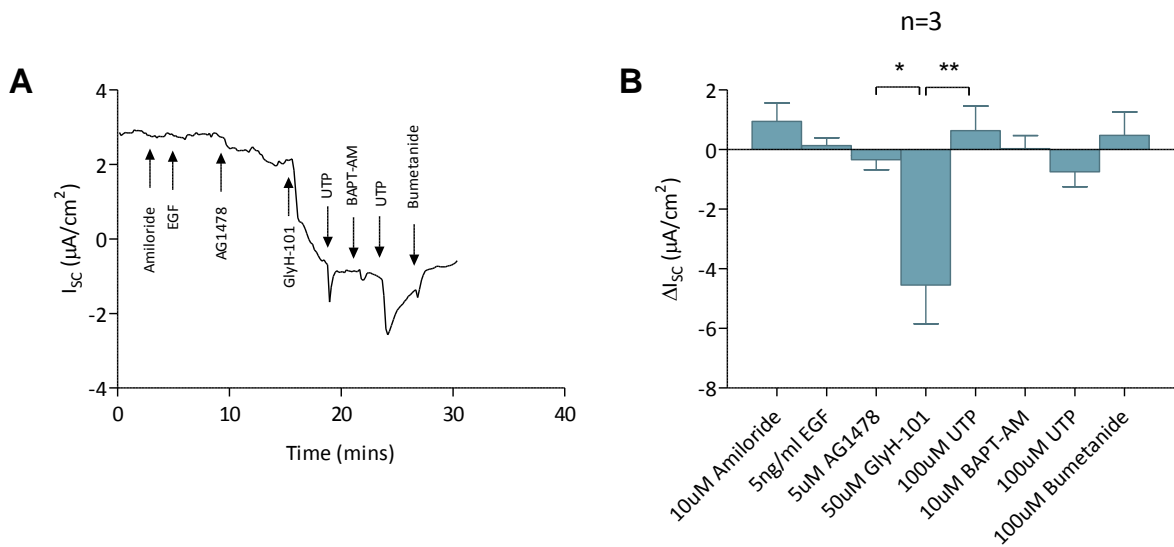


Figure 4.20 – Negligible EGF response in A549 monolayers.

Trace (left) and bar graph (right) to show the change in short circuit current across an A549 epithelium in response to 5 ng/ml EGF. It is also seen that EGF has little effect on I_{SC} . Statistical analysis was performed using a one way ANOVA with Tukey's Multiple Comparison test, where $P<0.05$ was deemed statistically significant.

4.2.13 Blocking Potassium Channels and EGF acute addition in Calu-3 monolayers

General potassium channel blocker barium chloride is applied on the basolateral side of intact Calu-3 monolayers to test the effects on acute EGF induced stimulation of I_{SC} (Figure 4.21, A and B). After addition of 5mM barium chloride, 5 ng/ml EGF is added to the apical side, resulting in an increase in I_{SC} of $13.3 \pm 2.1 \mu\text{A cm}^{-2}$, $n=3$, $p<0.001$). Sequential additions of EGF to the apical side did not provide further increases in I_{SC} .

When the basolateral membrane was permeabilised using 0.36 mg/ml nystatin and a basolateral to apical chloride gradient applied (Figure 4.21, C and D), 5 ng/ml EGF added to the apical side increased the I_{SC} by $11.0 \pm 0.3 \mu\text{A cm}^{-2}$ ($n=3$, $p<0.001$). Sequential additions of EGF do not provide further increases in I_{SC} as before. Taken together, this suggests that blocking potassium channels increases acute EGF response across Calu-3 monolayers, and that stimulation of CFTR by forskolin produced an additive effect that suggests that EGF may be activating a response independent of CFTR. This initial data was followed up by looking at long term EGF preincubation and the effect on I_{SC} in relation to potassium channels in later chapters.

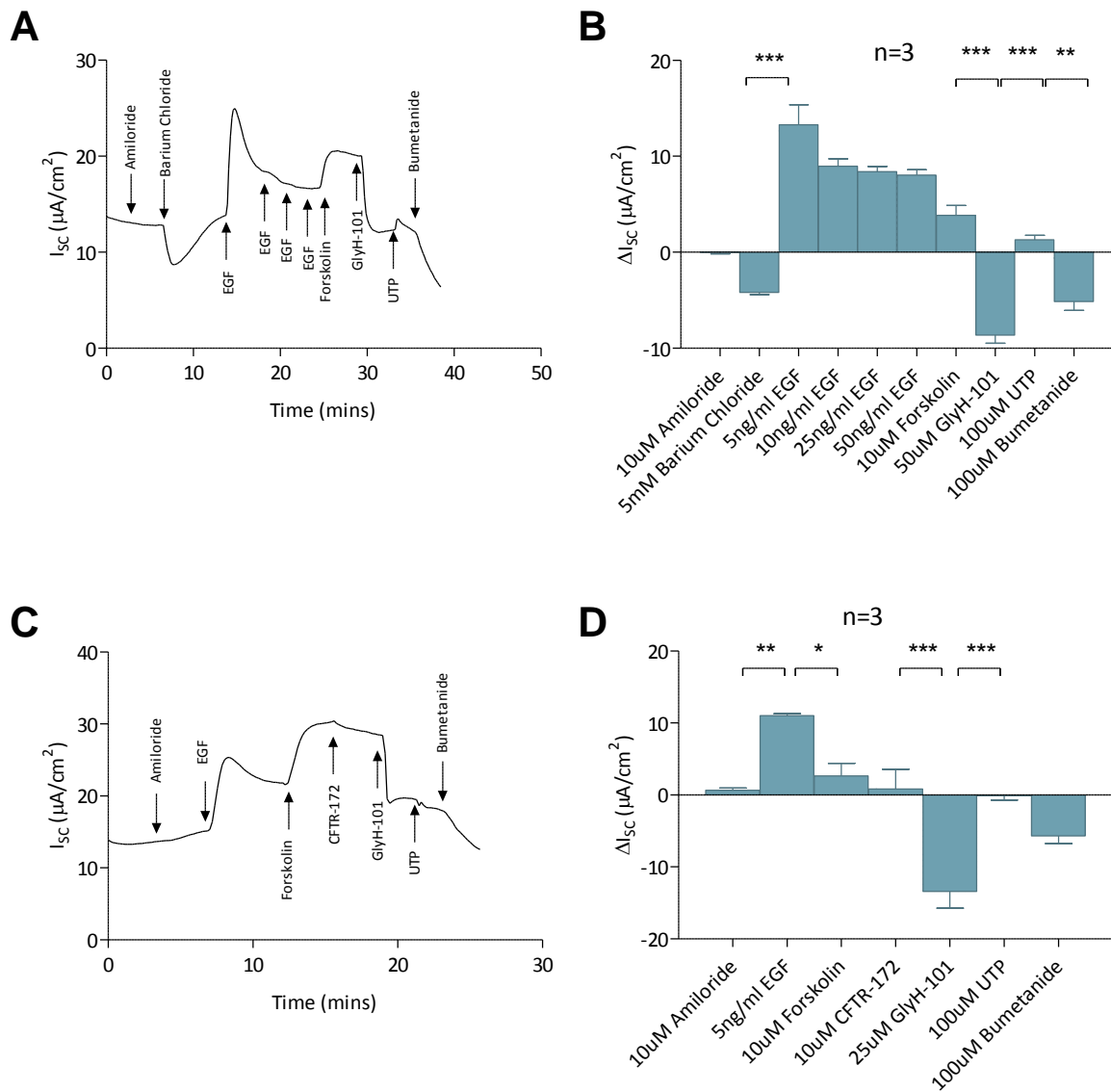


Figure 4.21 – Blocking potassium channels and EGF acute response in Calu-3 monolayers.

Trace (A) and bar graph (B) to show the change in short circuit current across a Calu-3 epithelium in response to 5 mM barium chloride. The addition of barium chloride, a basolateral potassium channel blocker, does not affect the increase in I_{SC} due to 5 ng/ml EGF. Trace (C) and bar graph (D) to show the change in short circuit current across a Calu-3 epithelium in response to basolateral membrane permeabilisation then 5 ng/ml EGF. By permeabilising the basolateral membrane with nystatin in order to eliminate all the basolateral channels from the equation, it is seen that despite this, EGF still increases I_{SC} . Statistical analysis was performed using a one way ANOVA with Tukey's Multiple Comparison test, where $P<0.05$ was deemed statistically significant.

4.2.14 Blocking Potassium Channels and EGF acute addition in A549 monolayers

Similarly, experiments with EGF and barium chloride (Figure 4.22, A and B) and basolateral membrane permeabilisation with a chloride gradient applied (Figure 4.22, C and D) was conducted using the A549 cell line. In contrast to the enhanced effect of barium chloride on apical EGF treatment seen in intact Calu-3 monolayers (Figure 4.21, A and B), it was seen that with barium chloride pretreatment that the effect of 5 ng/ml EGF was still not significant.

Furthermore, it was also seen that after basolateral membrane permeabilisation and application of a basolateral to apical chloride gradient applied, the effect of 5 ng/ml EGF was generally negligible at approximately $1 \mu\text{A cm}^{-2}$. This was in contrast to the effect of acute addition of 5 ng/ml EGF seen in Calu-3 monolayers (Figure 4.21, C and D) where a significant increase was seen. Taken together, the results demonstrate that there was no evidence that blocking potassium channels and stimulating with EGF had a significant effect on ion transport in the A549 cell line.

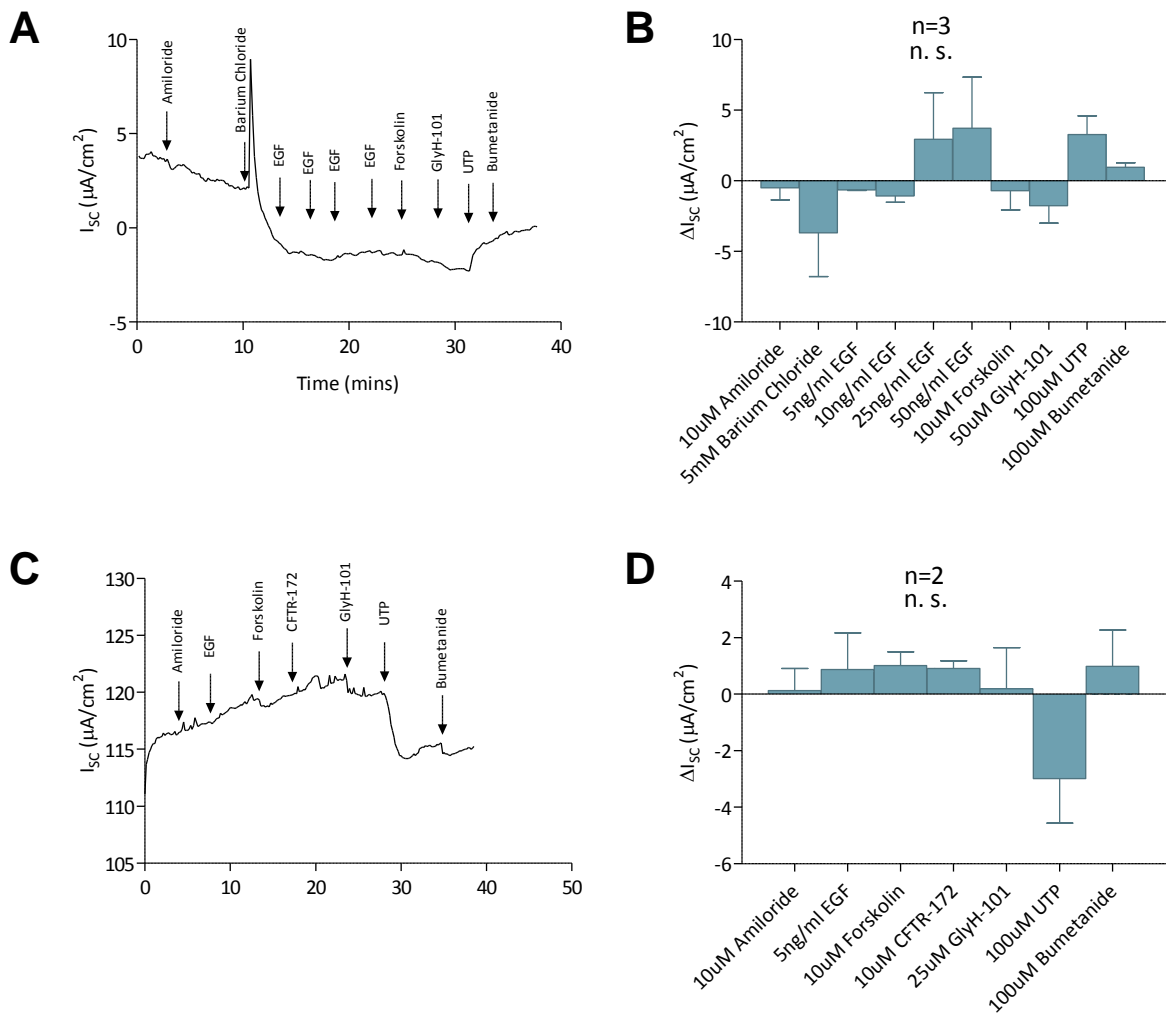


Figure 4.22 – Negligible EGF response in barium chloride treated A549 monolayers and permeabilised A549 monolayers.

Trace (A) and bar graph (B) to show the change in short circuit current across an A549 epithelium in response to 5 mM barium chloride. 5 ng/ml EGF also has no significant effect on I_{SC} after the addition of 5 mM barium chloride. Trace (C) and Bar graph (D) to show the change in short circuit current across an A549 epithelium in response to basolateral membrane permeabilisation then 5 ng/ml EGF. Basolateral membrane permeabilisation did not significantly affect the EGF response. Statistical analysis was performed using a one way ANOVA with Tukey's Multiple Comparison test, where $P<0.05$ was deemed statistically significant.

4.2.15 A549 Vehicle Controls

In order to determine that the vehicles used in the A549 experiments were not causing large changes in I_{SC} (Figure 4.23), vehicles were added to their corresponding chambers where they were generally applied (apical for DMSO, basolateral for ethanol). It was seen that each vehicle led to a change in I_{SC} that was less than $1 \mu\text{A cm}^{-2}$. Taken together, this result suggests that the vehicles used for A549 based experiments did not change the I_{SC} significantly.

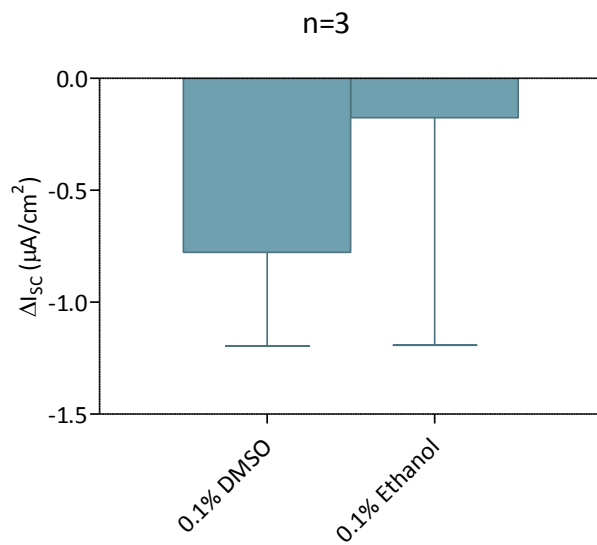


Figure 4.23 – Vehicle control data for A549 monolayers.

Bar graph showing the change in short circuit current across an A549 epithelium in response to 0.1% DMSO and 0.1% ethanol. The concentrations of vehicles used during the experiments do not affect I_{SC} . Statistical analysis was performed using a one way ANOVA with Tukey's Multiple Comparison test, where $P<0.05$ was deemed statistically significant.

4.2.16 Negligible Forskolin response in A549 monolayers

As a comparison to the Calu-3 data shown earlier in Chapter 3 (Figure 3.3), experiments with forskolin were conducted using the A549 cell line (Figure 4.24, A and B). The results demonstrate that there was no evidence that basolateral application of 10 μ M forskolin had a statistically significant effect on ion transport in the A549 cell line. This was in marked contrast to the effects of forskolin seen in the Calu-3 cell line, where an increase of $15.5 \pm 2.1 \mu\text{A cm}^{-2}$ was seen (Figure 3.3). Taken together, this result indicates that negligible functional CFTR is expressed in the A549 cell line.

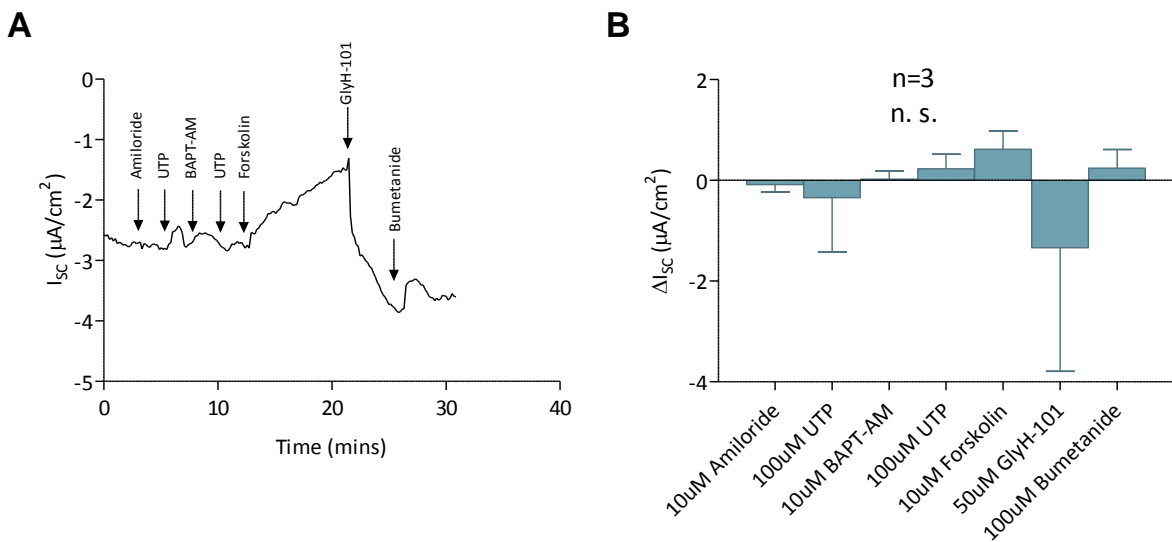


Figure 4.24 – Negligible forskolin response in A549 monolayers.

Trace (A) and bar graph (B) and to show the change in short circuit current across an A549 epithelium in response to 10 μ M forskolin. With A549 epithelia, it is seen that forskolin has little effect on I_{SC}. Statistical analysis was performed using a one way ANOVA with Tukey's Multiple Comparison test, where P<0.05 was deemed statistically significant.

4.3 Discussion

4.3.1 Calu-3 cells can grow at high seeding densities

The use of CFSE based probes to study cell proliferation is widely and successfully used in immunological studies in the airway. Specifically, CFSE probe based methodologies have been previously used to track cell proliferation of airway smooth muscle cells (Sukkar *et al.*, 2004), DO11.10 T cells (Stock *et al.*, 2005; Wang *et al.*, 2006) and human lung mast cells (HLMC) (Hollins *et al.*, 2008). In this study, it has been shown that there were greater shifts in mean fluorescence of the CFSE growth assays for the A549 cells than the Calu-3 cells is due to A549 cells growing at a much faster rate than Calu-3 cells. This finding is in agreement with a previous study that used both A549 and Calu-3 cell lines where split ratios of 1:5 to 1:3 were used respectively (Baba *et al.*, 1987). From the growth assays, of interest is the statistically significant decrease in growth within A549 cells at a seeding density of 50,000, shown during both experiments, most likely due to the rapid growth and subsequent quiescence of the A549 cells due to contact inhibition before the end of the incubation period. This is likely to be the case since in a previous study, A549 cells have been grown to confluence purposefully to cause contact inhibition to better investigate events in the cell cycle (Ray *et al.*, 1999). Calu-3 cells do not have the same issue; higher seeding densities do not inhibit normal growth and that a high seeding density has a similar growth rate as lower ones. It was also seen that the growth rate of the Calu-3 cell line was not affected by low serum conditions. In a previous study, Calu-3 cells have been grown in serum free media to investigate their metabolic capacity (Foster *et al.*, 2000). Calu-3s are best seeded at higher densities and can tolerate low or no serum well. The slow growth rate of Calu-3 cells can be compensated with higher seeding densities. In contrast, a 20,000 cell seeding density is the most optimal for growth for A549s within the 12-well plate format, as it provided the best growth rate in both experiments. Since A549s are a relatively fast growing cell line (Baba *et al.*, 1987), the decrease in cell growth in low or no serum is not crucial, as plenty of growth is observed compared to the initial sample as seen in the representative histograms.

4.3.2 Calu-3 cells are viable in low serum

Figure 4.5 shows that 72 hours in serum-free media has no statistically significant detrimental effect on A549 cell viability compared with the earlier time points, and that PMA does not have a detrimental effect on cell viability at the concentrations used. Figure 4.6 showing Calu-3 cell viability over 24 and 72 hours also shows no detrimental effect with either PMA or leaving in serum-free media. As a result, this validates the protocol for the gelatin zymography showing that the cells do survive in significant number. Propidium iodide has previously been used to access Calu-3 viability upon challenge with *Pseudomonas aeruginosa* (Lee *et al.*, 1999) and with house dust mite proteinases (Winton *et al.*, 1998b)

4.3.3 MMP-2 and 9 are functional in the conditioned media of Calu-3

Gelatin zymography has previously been used to demonstrate the function of MMP-2 and MMP-9 in melb-a cells, which is an immortal line of melanoblasts isolated from neonatal mouse epidermis (Lei *et al.*, 2002). The gelatinases present putatively correspond to active MMP-2 (66 kDa), proMMP-2 (72 kDa) and MMP-9 (93 kDa). Calu-3 cells produce the maximal amount of MMPs at 48 hours with 5 ng/ml PMA and A549 cells produce the maximal amount of MMPs at 48 hours with 10-20 ng/ml PMA. The results obtained in this chapter are in agreement with earlier studies where gelatinase function have previously been demonstrated in the Calu-3 cell line with the zymography technique (Duszyk *et al.*, 1999). It was seen in this study that Calu-3 cells generally secrete more MMP-2, while A549 cells secrete more MMP-9 (Figure 4.7). This is in agreement with a previous study using both cell lines and others where it was seen that high levels of MMP-2 function inversely correlated with MMP-9 function (Roomi *et al.*, 2009).

Epidermal growth factor (EGF) as well as another EGFR substrate, TGF- α , has previously been used in zymographic analysis to stimulate the expression of MMPs in normal human bronchial epithelial cells (NHBEC) in order to see its effect on the activity of collagenases in breaking down casein (Lavigne *et al.*, 2004). With our studies, EGF increases production of MMPs more strongly at 24 hours in both cell lines, and is seen to be a more potent stimulator than the synthetic stimulator PMA at the concentrations used in this study. 1,10-phenanthroline was used previously as an

MMP inhibitor by Duszyk *et al.*, 1999 to study the effect of MMP inhibitors on the gating of the CFTR channel. In this study, GM-6001, a potent (Galardy *et al.*, 1994), non-specific MMP inhibitor (Bendeck *et al.*, 1996; Santiskulvong & Rozengurt, 2003; Mirastschijski *et al.*, 2004) was used to further investigate this link. GM-6001 was chosen in this study over the previously used 1,10-phenanthroline since the former is more specific for MMPs, while the latter is a non-specific divalent metal ion chelating agent that can inhibit MMPs (Wallace *et al.*, 1996). It was seen in this study that GM-6001 is able to knockdown the expression of the gelatinases in Figure 4.10, which validates the use of the compound as an MMP inhibitor for use in the Ussing chamber.

4.3.4 MMP-2 protein is present in Calu-3 and A549 cells

The fact that MMP-2 was present in the conditioned media (as shown in Figure 4.12) would be expected as MMP-2 is a secreted enzyme (Lei *et al.*, 2002). The presence of MMP-2 only in Calu-3 cells correlates with the zymography data which show that A549 cells produce much more MMP-9 rather than MMP-2 (Figure 4.7). The results from this chapter are in agreement with previous studies where MMP-2 had been identified from cell homogenates obtained from both the Calu-3 and A549 cell lines (Duszyk *et al.*, 1999).

4.3.5 Effect of MMP-2 and EGF on I_{sc}

The data obtained in this study regarding the effect of GM-6001 on Calu-3 monolayers (Figure 4.13, A and B) suggests that GM-6001 is not having a significant effect on short circuit current. Similarly, the inactive GM-6001 control compound exhibited very similar results to the active inhibitor (Figure 4.13, C and D); further suggesting that GM-6001 was not affecting CFTR gating. The result suggests that the increase in short circuit current with 1,10-phenanthroline seen in Duszyk *et al.*, 1999 was more likely to be due to compound itself having a direct effect on the CFTR channel rather than due to it being an MMP inhibitor.

Addition of recombinant MMP-2 to Calu-3 monolayers may have some effect on the apical surface of the epithelium (Figure 4.15). MMP-2 is widely known to be involved in the remodelling of the extracellular matrix (ECM) (Stamenkovic, 2003). This clearing of ECM deposition on the surface of the monolayer may be responsible for

causing forskolin to have an apparent enhanced effect and for GlyH-101 to have a consistently reduced effect. This explanation is however highly speculative without further investigation. Further, previous reports of increased forskolin responses following recombinant MMP-2 addition has not been previously demonstrated in the literature in any cell line. Since anti-IgG control antibodies produce a very similar effect on I_{SC} as the anti-MMP-2 antibodies in the Calu-3 cell line (Figure 4.17), it suggests that the increase in I_{SC} is not specific to anti-MMP-2. It is likely an effect of applying antibodies to the apical membrane in general.

The fact that further acute stimulation with EGF on Calu-3 monolayers did not lead to a dose dependent response (Figure 4.19, A and B) may be due to oversaturation of the EGFR receptor at higher concentrations. The EGF response is likely working through EGFR as AG1478 inhibits the EGF peak (Figure 4.19, C and D). The results for acute addition of EGF to the apical membrane following barium chloride treatment and basolateral membrane permeabilisation (Figure 4.21) suggest that these increases in I_{SC} are due to EGF working independently of potassium channels. It is known that EGF can lead to an increase in the expression of MMPs as seen in this chapter and in previous studies (Atkinson & Senior, 2003; Poitras *et al.*, 2003; Lin *et al.*, 2008). If the addition of EGF led to induction of MMP activity, which then in turn had an effect on CFTR, one would expect the effect to take a longer period of time since a transcription event would be necessary for this to occur. However, the responses seen in this investigation suggest that the effect occurs within seconds. HB-EGF involvement also seemed unlikely, as the elimination of basolateral potassium channels by barium chloride and basolateral membrane permeabilisation did not remove the peak seen from acute EGF addition. In intestinal epithelia, it has been shown that transactivation of EGFR by Src can likely induce basolateral potassium and/or apical chloride secretion via protease activated receptor 2 (PAR-2) via both cAMP and calcium ion dependent mechanisms, so it may be possible that a similar mechanism is happening in the Calu-3 cell line (van der Merwe *et al.*, 2008).

It is possible that the anti-MMP-2, anti-IgG, and EGF bring about changes in short circuit current through CFTR. A549 cells are widely known not to express CFTR (Mohammad-Panah *et al.*, 1998; Carreiras *et al.*, 1999; Bossard *et al.*, 2007; Xu *et al.*, 2010), so you would expect that the addition of these compounds to A549

monolayers used in this study would not increase the short circuit current if the compounds work via CFTR. This was shown consistently to be the case in our results. In general, Calu-3 epithelia produced more stable I_{SC} recordings than A549 epithelia. With A549 epithelia, it is clear that the baseline current is highly variable, so that it is either a positive or negative current – indicating absorptive and secretive characteristics. This is supported by studies that have used the A549 cell line to model pulmonary absorption (Kobayashi *et al.*, 1995). The transepithelial resistance is also low in A549 cells (data not shown), which has been shown to be the case in previous studies (Blank *et al.*, 2007).

In summary, the data obtained in this study did not agree with previous literature by Duszyk *et al.*, 1999 that there was a link between MMPs and CFTR. However, it was seen in this part of the study that EGF on the other hand did exhibit properties of regulating secretion in the Calu-3 cell line that had not been previously investigated. Therefore the focus of the study shifted from looking at MMPs to looking at EGF in more detail, leading onto further investigations that explored the effects of EGF and the mechanisms behind these effects.

Chapter 5 Effects of EGF Treatment on Initial Short Circuit Current

5.1 Introduction

Previous data in this investigation suggested that EGF may increase ion transport independent of CFTR. The effect of EGF on ion transport has been previously studied in some depth using intestinal epithelial cells. Treatment of T84 cells with EGF led to activation of EGFR and hence, an inhibition of basolateral potassium channels via a signalling mechanism consisting of phosphatidylinositol 3-kinase (PI3K) and protein kinase C- ϵ (PKC- ϵ) (McCole & Barrett, 2009). Lower EGF/EGFR signalling led to a 40–70% reduction in K^+ currents and KvLQT1, ATP-sensitive potassium (K_{ATP}), and Ca^{2+} -activated K^+ (KCNN4) channel expression in CuFi cells (Trinh *et al.*, 2008) and that coupling between EGFR signalling and potassium channels is important for alveolar repair (Trinh *et al.*, 2007). While the effects of EGF on ion transport in cells within the gut has been previously demonstrated (McCole & Barrett, 2009), no similar study to date has been performed using Calu-3 cells. If EGF treatment can be demonstrated to cause an increase in ion transport within lung tissue, then this could allow for potential therapeutics for cystic fibrosis.

In order to address this current gap in knowledge, the aim of this investigation was to see how EGF affects the initial current as measured by the Ussing chamber at the start of the experiment. Untreated cells were compared to cells that were treated with 10 ng/ml EGF on the basolateral side over a time scale of 1, 2, 3 and 24 hours. These time points were selected since they were manageable in our experimental setup and gave an indication of both short term and longer term changes. The maximal value for initial starting current seen in this investigation is used in experiments utilising further manipulations later on.

Once an effect of EGF on ion transport has been demonstrated, discovering the downstream mechanisms of this effect would increase current understanding of the underlying biology of the process. This could in turn lead to the development of new avenues to augment the treatment of cystic fibrosis still further. Thus, in order to determine the mechanism behind the increases in initial starting current, experiments

were designed so that the Calu-3 monolayers were treated with inhibitors of a number of pathways before an hour of EGF treatment (previously determined to be the maximal response). The pathways of interest initially were PI3K, PKC and potassium channels, based on work with EGF conducted previously with gut cells (McCole & Barrett, 2009). With this investigation, we intended to also identify which type of potassium channel was involved. The expression of selected potassium channels in the Calu-3 cell line were also of interest due to their potential to influence chloride transport via increases in chloride driving force. The KCNN4, KCNA2, KCNA3 and KCNQ1 channels were selected since they are inhibited using charybdotoxin, iberiotoxin and chromanol 293B, which are later used in the functional analysis.

5.2 Results

5.2.1 Addition of Epidermal Growth Factor (EGF) to the Calu-3 monolayers leads to an increase in initial I_{SC}

Initially, a time course experiment was performed. Interestingly, as shown in Figure 5.1 (A), a 1 hour pretreatment of the Calu-3 monolayers with 10 ng/ml EGF added to the basolateral side of intact monolayers resulted in a starting I_{SC} of $24.8 \pm 3.0 \mu\text{A cm}^{-2}$ ($n=10$) compared to $12.1 \pm 0.7 \mu\text{A cm}^{-2}$ ($n=98$) observed in untreated controls. After a 24 hour pretreatment of the Calu-3 cells with 10 ng/ml EGF on the basolateral side of intact monolayers, the initial starting current had reduced back down to approximately pretreatment levels ($12.6 \pm 1.2 \mu\text{A cm}^{-2}$ ($n=8$)).

The increase in I_{SC} on EGF treatment could be due to an effect on the basolateral membrane or the apical membrane. In order to try to identify which membrane was responsible for this increase in I_{SC} , a series of experiments were carried out that treated the basolateral side of Calu-3 monolayers with 10 ng/ml EGF for one hour, followed by basolateral membrane permeabilisation, using 0.36 mg/ml nystatin, in the Ussing chamber. A chloride gradient was applied across the membrane from basal to apical. As shown in Figure 5.1 (B), following this treatment the initial I_{SC} of Calu-3 cells did not significantly change after EGF preincubation for one hour ($n=3$), suggesting that EGF was acting predominantly on ion channels or ion transporters on the basolateral membrane.

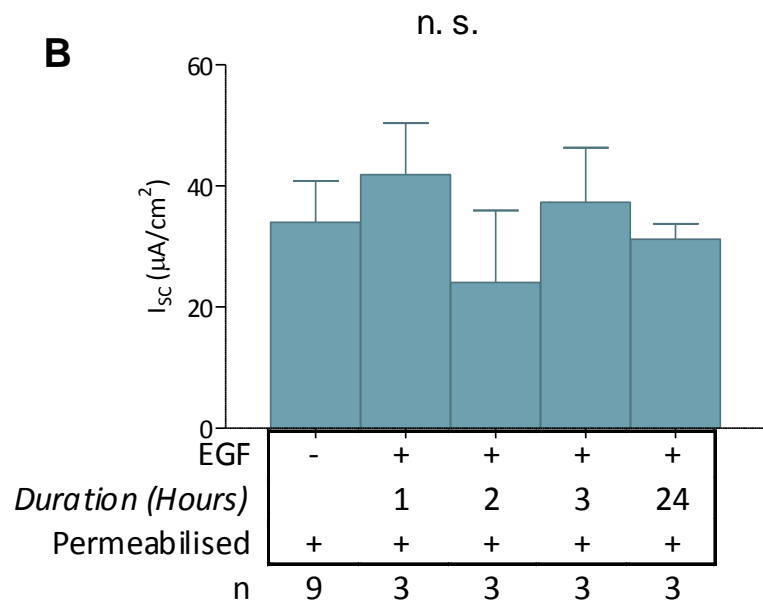
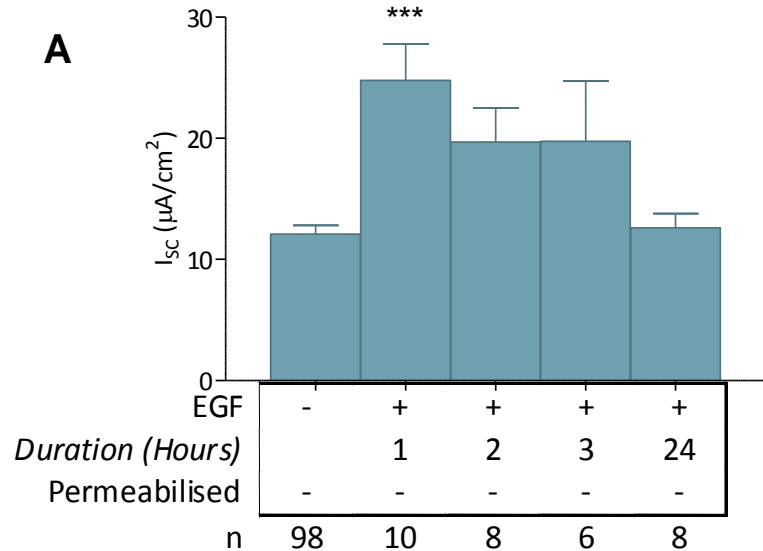


Figure 5.1 – EGF preincubation for 1 hour significantly increases initial I_{sc} in intact, but not permeabilised, Calu-3 monolayers.

Summary bar graphs showing (A) the initial I_{sc} across an intact Calu-3 epithelium in response to 10ng/ml EGF pretreatment over time, and (B) showing the initial I_{sc} across a Calu-3 epithelium in response to basolateral membrane permeabilisation upon 10ng/ml EGF preincubation. Statistical analysis was performed using a one way ANOVA with Tukey's Multiple Comparison test, where $P<0.05$ was deemed statistically significant.

5.2.2 The EGF stimulated increase in initial I_{SC} is prevented by inhibition of the EGF receptor (EGFR)

EGF brings about its physiological actions through its receptor the EGF receptor (EGFR). In order to determine whether the EGF-stimulated increase in the initial I_{SC} that occurred after 1 hour preincubation in Calu-3 monolayers was due to EGF working through the EGFR, the inhibitor AG1478 was used (Levitzki & Gazit, 1995). The intact Calu-3 monolayers were pretreated with the 5 μ M AG1478 on the basolateral side for 10 minutes, followed by addition of 10 ng/ml EGF to the basolateral side of the monolayers for 1 hour. The AG1478 inhibitor was present in the solution throughout the duration of the experiment. As shown in Figure 5.2, the initial I_{SC} was reduced to $5.2 \pm 1.3 \mu$ A cm^{-2} ($n=5$, $P<0.001$), significantly lower than the intact monolayers treated with 10ng/ml EGF on the basolateral side alone ($24.8 \pm 3.0 \mu$ A cm^{-2} , $n=10$). Thus EGF would seem to be working through the EGFR to increase ion transport across intact Calu-3 monolayers.

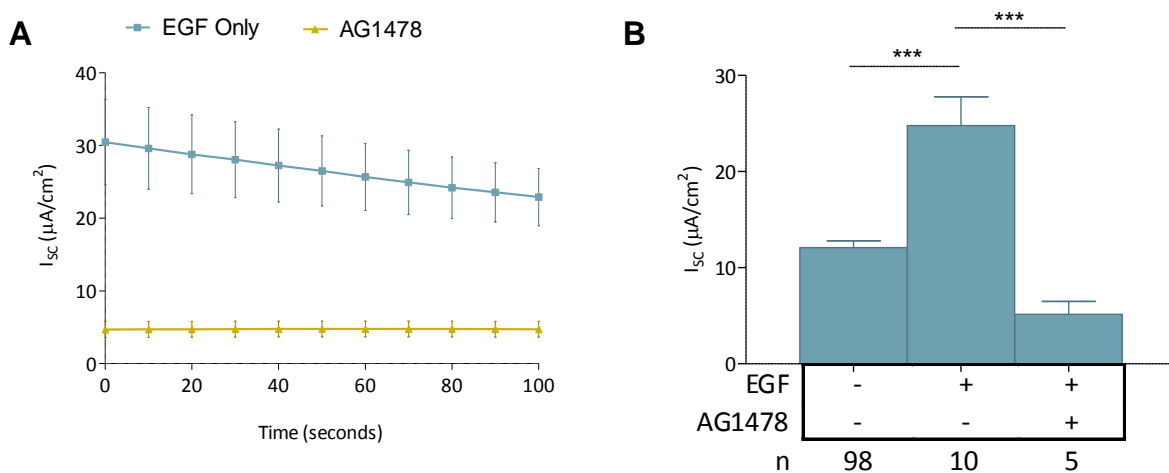


Figure 5.2 – EGFR inhibitor AG1478 reduces EGF induced increases in starting current.

Combined traces for the first 100 seconds (A) and a bar graph (B) showing the starting I_{SC} across a Calu-3 epithelium following basolateral treatment with 5 μ M AG1478 the EGFR inhibitor, followed subsequently by 10ng/ml EGF stimulation for 1 hour. Statistical analysis was performed using a one way ANOVA with Tukey's Multiple Comparison test, where $P<0.05$ was deemed statistically significant.

5.2.3 Protein kinase inhibitors prevent EGF-stimulated increases in initial I_{SC}

EGFR activation can result in the activation of a number of signalling pathways (Oda *et al.*, 2005), including phosphoinositol-3-kinase (PI3K) and mitogen-activated protein kinase (MAPK) related pathways. In order to determine if protein kinases were involved in the EGF induced increases in ion transport, intact Calu-3 monolayers were pretreated on the basolateral membrane as shown in Figure 5.3. Pretreatment with the PI3K inhibitor, wortmannin (50 μ M) for 10 minutes followed by 10 ng/ml EGF on the basolateral side for 1 hour, resulted in an initial starting I_{SC} of $5.7 \pm 1.5 \mu$ A cm^{-2} ($n=4$) which was significantly lower than the EGF-stimulated initial I_{SC} ($24.8 \pm 3.0 \mu$ A cm^{-2} , $n=8$, $P<0.001$). To further investigate the signalling pathways involved in this EGF-stimulated increase in the initial I_{SC} , other protein kinase inhibitors were used that targeted kinases known to be downstream to PI3K. Staurosporine is a non-specific protein kinase inhibitor that can inhibit both PKC and PKA. Pretreatment with staurosporine (0.1 μ M) for 10 minutes on the basolateral side of intact Calu-3 monolayers followed by 10 ng/ml EGF on the basolateral side for 1 hour reduced the EGF-stimulated initial I_{SC} to $5.3 \pm 0.8 \mu$ A cm^{-2} ($n=4$) significantly lower than the EGF-stimulated initial I_{SC} ($24.8 \pm 3.0 \mu$ A cm^{-2} , $n=8$, $P<0.001$). These data suggest that PKC and / or PKA were involved in EGF induced increases in ion transport. To further investigate the effect of inhibiting protein kinases, the PKC specific inhibitor chelerythrine chloride was used. Pretreatment with 10 μ M chelerythrine chloride for 10 minutes on the basolateral side of intact Calu-3 monolayers followed by 10 ng/ml EGF treatment for 1 hour reduced the EGF-stimulated initial I_{SC} to $4.3 \pm 0.9 \mu$ A cm^{-2} ($n=4$) significantly lower than the EGF-stimulated initial I_{SC} ($24.8 \pm 3.0 \mu$ A cm^{-2} , $n=8$, $P<0.001$). These data suggest that PKC was involved in the pathway. In order to try to identify the specific isoform of PKC that was involved in the signalling pathway, rottlerin was used. Pretreatment of intact Calu-3 monolayers with rottlerin (5 μ M), a PKC δ isoform specific inhibitor, on the basolateral side for 10 minutes followed by 10 ng/ml EGF on the basolateral side for 1 hour reduced the EGF-stimulated initial I_{SC} to $7.8 \pm 0.8 \mu$ A cm^{-2} ($n=5$) significantly lower than the EGF-stimulated initial I_{SC} ($24.8 \pm 3.0 \mu$ A cm^{-2} , $n=8$, $P<0.001$). Taken together these data suggest that the EGF-stimulated increase in initial I_{SC} is mediated through a PI3K and protein kinase C δ (PKC- δ) intracellular signalling pathway.

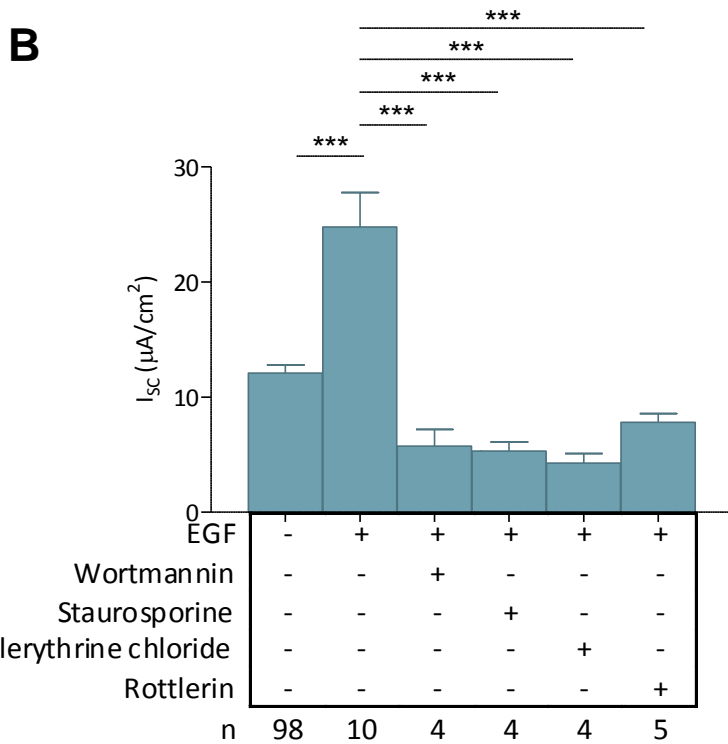
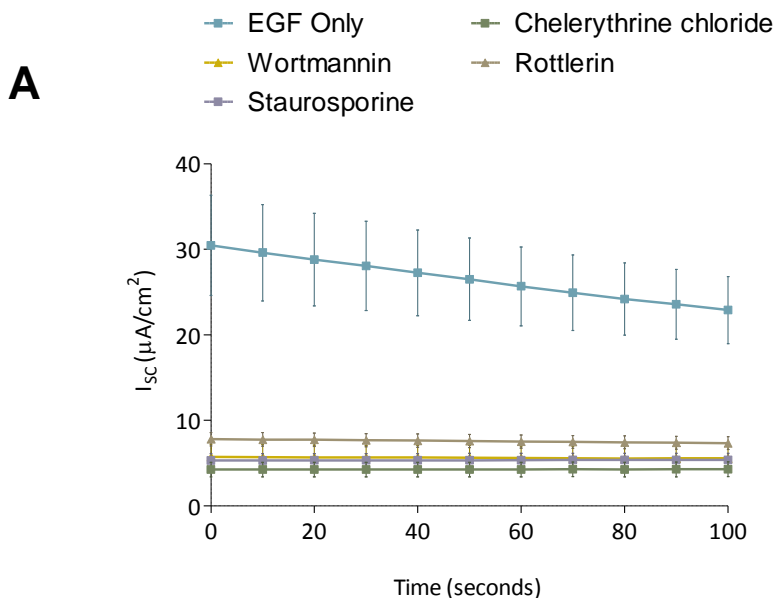


Figure 5.3 – Kinase inhibitors reduce EGF induced increases in starting current.

Combined traces for the first 100 seconds (A) and a bar graph (B) showing the initial I_{SC} across Calu-3 epithelia following basolateral treatment with inhibitors including 50 μ M wortmannin, 0.1 μ M staurosporine, 10 μ M chelerythrine chloride and 5 μ M rottlerin, followed subsequently by 10 ng/ml EGF stimulation for 1 hour. Statistical analysis was performed using a one way ANOVA with Tukey's Multiple Comparison test, where $P<0.05$ was deemed statistically significant.

5.2.4 Potassium channel blockers reduce EGF-stimulated increases in initial I_{SC}

In order to determine if basolateral potassium channels, which are known to be expressed in Calu-3 cells, are activated downstream of protein kinases, intact Calu-3 monolayers were pretreated on the basolateral membrane with potassium channel inhibitors as shown in Figure 5.4. Non-specific calcium activated potassium channel inhibitor charybdotoxin (1 μ M) for 10 minutes followed by 10 ng/ml EGF on the basolateral side for 1 hour reduced the EGF-stimulated initial I_{SC} to $11.3 \pm 1.2 \mu$ A cm^{-2} ($n=5$), significantly lower than the EGF-stimulated initial I_{SC} ($24.8 \pm 3.0 \mu$ A cm^{-2} , $n=8$, $P<0.01$). These data suggest that basolateral potassium channels were downstream of protein kinases. To further determine if the potassium channel KCNN4 was responsible for the EGF-induced increases in ion transport, intact Calu-3 monolayers were pretreated with KCNN4 specific inhibitor iberiotoxin (10 nM) on the basolateral side for 10 minutes followed by 10ng/ml EGF on the basolateral side for 1 hour. This reduced the EGF-stimulated initial I_{SC} to $4.3 \pm 0.6 \mu$ A cm^{-2} ($n=4$), significantly lower than the EGF-stimulated initial I_{SC} ($24.8 \pm 3.0 \mu$ A cm^{-2} , $n=8$, $P<0.001$). These data suggest that KCNN4 channels were activated by EGF and the subsequent PI3K / PKC- δ pathway. To further determine if the potassium channel KCNQ1 was also responsible for the EGF-induced increases in ion transport, intact Calu-3 monolayers were pretreated with KCNQ1 specific inhibitor chromanol 293B (10 μ M) on the basolateral side for 10 minutes followed by 10 ng/ml EGF on the basolateral side for 1 hour. This reduced the EGF-stimulated initial I_{SC} to $10.1 \pm 3.2 \mu$ A cm^{-2} ($n=5$), significantly lower than the EGF-stimulated initial I_{SC} ($24.8 \pm 3.0 \mu$ A cm^{-2} , $n=8$, $P<0.01$). Since these results were all significantly lower than the control ($24.8 \pm 3.0 \mu$ A cm^{-2} , $n=8$), it suggests that the EGF-stimulated increase in initial I_{SC} results from an increased ion transport via both KCNN4 and KCNQ1 channels.

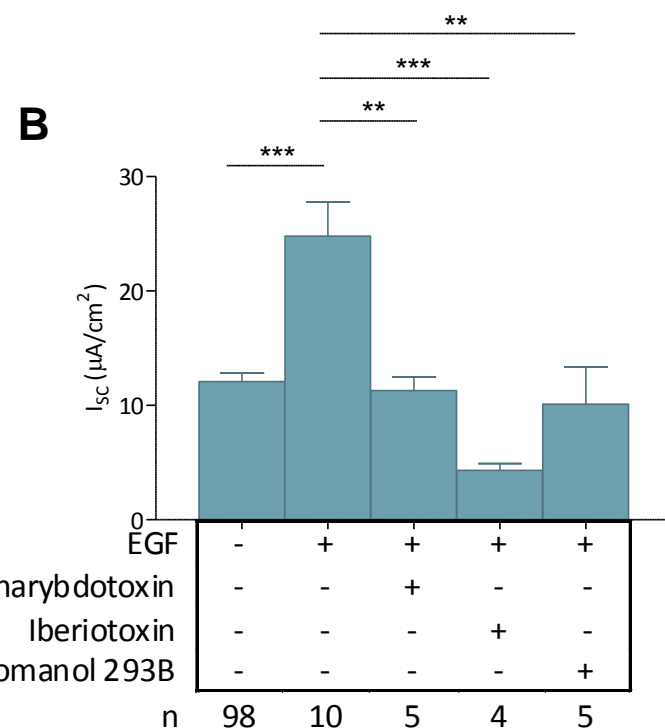
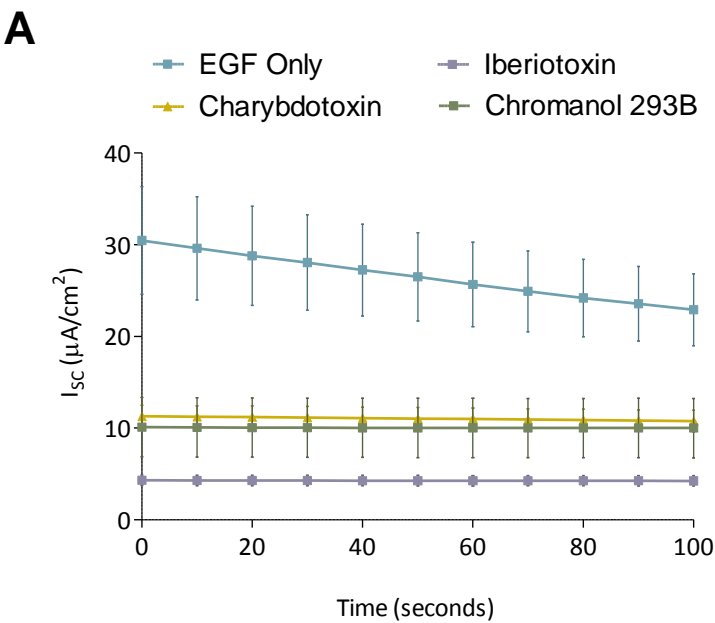


Figure 5.4 – Potassium channel inhibitors reduce EGF induced starting current.

Combined traces for the first 100 seconds (A) and a bar graph (B) showing the starting I_{sc} across Calu-3 epithelia following basolateral treatment with inhibitors including 1 μM charybdotoxin, 10 nM Iberiotoxin and 10 μM chromanol 293B, followed subsequently by 10 ng/ml EGF stimulation for 1 hour. Statistical analysis was performed using a one way ANOVA with Tukey's Multiple Comparison test, where $P<0.05$ was deemed statistically significant.

5.2.5 The potassium channels KCNQ1, KCNA2, KCNA3 and KCNN4 are expressed in the Calu-3 cell line

The potassium channel inhibitors used in this investigation together block a number of different potassium channels. Chromanol 293B blocks KCNQ1 only (Bett *et al.*, 2006), iberiotoxin blocks KCNN4 only (Candia *et al.*, 1992), and charybdotoxin blocks KCNA2, KCNA3 and KCNN4 (Rauer *et al.*, 2000). The expression of these channels in the Calu-3 cell line was therefore of interest to determine which channels are likely to be involved in increasing EGF stimulated initial short circuit current. The expression of the potassium channels genes KCNQ1, KCNA2, KCNA3 and KCNN4 was tested in the untreated Calu-3 cell line with three repeats using a different RNA sample each time (Figure 5.5). Each time, there was a strong signal for KCNA2, KCNA3 and KCNN4 channels, and with one of the repeats, there was also expression of KCNQ1.

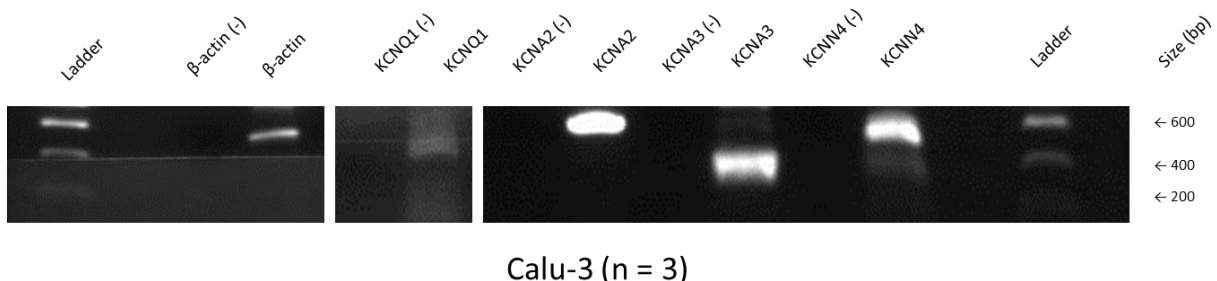


Figure 5.5 – KCNQ1, KCNA2, KCNA3 and KCNN4 channel expression in Calu-3 cells

Another repeat with a different RNA sample showed KCNQ1 expression. RT-PCR consisted of 3 repeats using different RNA samples.

5.2.6 U0126 pretreatment reduces initial EGF stimulated I_{SC} in EGF preincubated Calu-3 monolayers

The EGF signalling pathway is complex and can activate multiple downstream signalling pathways. Other than the PI3K pathway, the EGFR signalling pathway can also activate MAPK. To determine if MAPK signalling has an effect on chloride secretion, a time course experiment was conducted in both intact and permeabilised Calu-3 monolayers pretreated with 25 μ M U0126 (inhibitor of the ERK signalling messenger of the MAPK pathway) and 10ng/ml EGF on the basolateral side. These data are shown in Figure 5.6. As shown in Figure 5.6 (A), cells were pretreated with 25 μ M U0126 on the basolateral side alone for an hour, resulting in an initial current of $11.0 \pm 2.1 \mu$ A cm^{-2} (n=3). Treatment with U0126 on the basolateral side for 10 minutes followed by 10 ng/ml EGF on the basolateral side for 1 hour, 2 hours, 3 hours and 24 hours resulted in short circuit currents of $10.3 \pm 1.4 \mu$ A cm^{-2} (n=3), $17.6 \pm 3.3 \mu$ A cm^{-2} (n=3), $11.0 \pm 3.5 \mu$ A cm^{-2} (n=3) and $11.7 \pm 2.5 \mu$ A cm^{-2} (n=3) respectively. These results suggest that the ERK inhibitor U0126 causes an overall inhibition of EGF induced increases in short circuit current. To isolate chloride secretion in Calu-3 monolayers, the basolateral membrane was permeabilised with nystatin and a chloride gradient applied from basal to apical. As shown in Figure 5.6 (B), treatment with 25 μ M U0126 on the basolateral side for 10 minutes alone resulted in an initial current of $53.3 \pm 16.1 \mu$ A cm^{-2} (n=3). Treatment with 25 μ M U0126 on the basolateral side for 10 minutes followed by 10 ng/ml EGF on the basolateral side for 1 hour resulted in an initial current of $36.5 \pm 11.5 \mu$ A cm^{-2} (n=3). Treatment with 25 μ M U0126 on the basolateral side for 10 minutes followed by 10 ng/ml EGF on the basolateral side for 2 hours resulted in an initial current of $67.6 \pm 5.3 \mu$ A cm^{-2} (n=3). Treatment with 25 μ M U0126 on basolateral side for 10 minutes followed by 10 ng/ml EGF on the basolateral side for 3 hours resulted in an initial current of $28.7 \pm 9.3 \mu$ A cm^{-2} (n=3). Treatment with 25 μ M U0126 on the basolateral side for 10 minutes followed by 10 ng/ml EGF on the basolateral side for 24 hours resulted in an initial current of $48.2 \pm 9.4 \mu$ A cm^{-2} (n=3). None of these results were statistically significant from one another and very similar to the results of EGF alone.

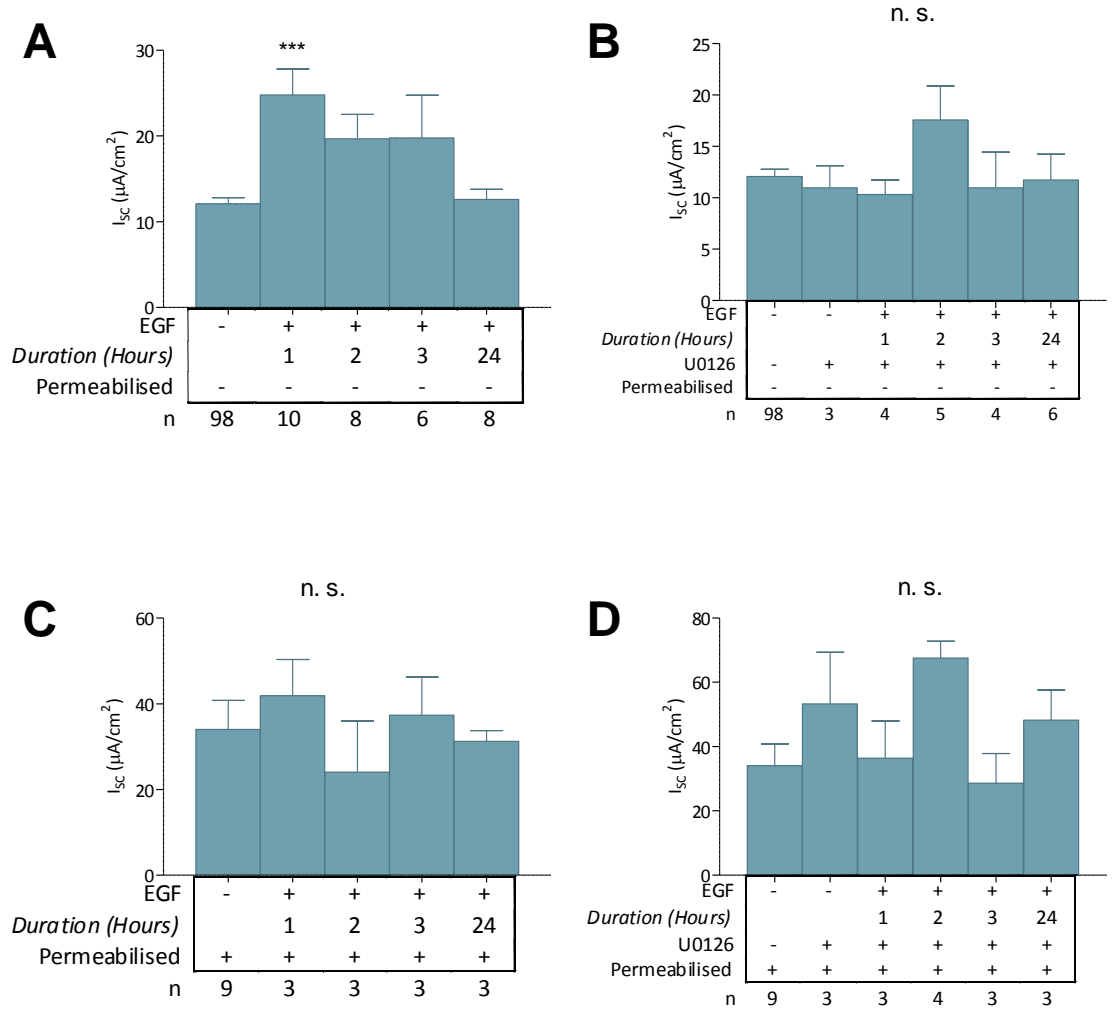


Figure 5.6 – ERK inhibitor U0126 reduces EGF induced starting current.

Summary bar graphs showing (A) the initial I_{SC} across an intact Calu-3 epithelium in response to 10 ng/ml EGF pretreatment over time, (B) the initial I_{SC} across an intact Calu-3 epithelium in response to 25 μM U0126 and 10 ng/ml EGF pretreatment over time, (C) showing the initial I_{SC} across a Calu-3 epithelium in response to basolateral membrane permeabilisation upon EGF preincubation and (D) showing the initial I_{SC} across a Calu-3 epithelium in response to basolateral membrane permeabilisation upon 25 μM U0126 and 10 ng/ml EGF preincubation. Statistical analysis was performed using a one way ANOVA with Tukey's Multiple Comparison test, where $P < 0.05$ was deemed statistically significant.

5.3 Discussion

5.3.1 EGF increases initial I_{SC} in intact Calu-3 monolayers

It was initially determined that 1 hour incubation of 10 ng/ml EGF produced a maximal response, and was thus chosen for comparison in all subsequent experiments. While to date no data looking at EGF treatment and the Calu-3 cell line has been acquired, our data are in agreement with investigations using the T84 colonic epithelial cell line that showed increases in I_{SC} when chronically treated with EGF (O'Mahony *et al.*, 2008). The increase due to EGF at 1 hour ties in with data showing that changes in intracellular calcium can affect the resting membrane potential in human astrocytoma cells (Bordey *et al.*, 2000). Further support in the literature for this finding includes a study by Borok *et al.* (1996) where it was shown in rat type II alveolar epithelial cells that treatment with EGF on the basolateral side results in increases in short circuit current at subacute (less than one day) time periods, which could be blocked using reversible tyrosine kinase inhibitor, tyrphostin RG-50864 (Borok *et al.*, 1996). In terms of possible delivery systems for introducing EGF into the lungs, aerosols generated from 20 μ g EGF in saline have been previously shown to increase lung liquid clearance and increase active sodium transport and Na^+-K^+ -ATPase activity in adult Sprague-Dawley male rats (Sznajder *et al.*, 1998).

5.3.2 EGF increases initial I_{SC} in Calu-3 via PI3K-PKC- δ -KCNN4/KCNQ1 dependent pathway

Activation of EGFR can trigger at least three different intracellular signalling pathways, which include mitogen-activated protein kinases ERK-1/2 (MAPK-ERK), phospholipase C γ 1 (PLC γ 1) and phosphatidylinositol-3-kinase (PI3K), and the JNK pathway. Other than EGF, five other EGFR ligands have been identified, which includes amphiregulin, TGF-alpha, betacellulin, HB-EGF (heparin binding EGF-like growth factor), and epiregulin (Sweeney & Carraway, 2000). The EGF pathway seen in the results of this chapter is likely to be one of these three signalling pathways.

Once stimulated, EGFR can recruit PI3K via an adapter protein such as c-Cbl, GAB1, IRS-1 and IRS-2 (Fujioka *et al.*, 2001; Onishi-Haraikawa *et al.*, 2001). Downstream of EGFR is the enzyme PLC- γ 1 (Yarden & Sliwkowski, 2001). Once phosphorylated, PLC- γ 1 converts PtdIns(4,5)P₂ into diacylglycerol (DAG) and inositol-1,4,5-

trisphosphate (IP₃) (Tkaczyk *et al.*, 2003). DAG is then able to activate PKC α , PKC β , PKC γ , PKC θ and PKC ϵ . PLC γ 1 can activate protein kinase C (PKC) and PI3K activates protein kinase B (PKB, or Akt) that in turn can activate PKCs (Koyama *et al.*, 2003). There is some crosstalk with the MAPK signalling pathway as PKC α , PKC β , PKC γ and PKC ϵ can activate Raf-1, which is a MAPK signalling messenger (Sozeri *et al.*, 1992; Hamilton *et al.*, 2001). PKC θ activates inhibitor of nuclear factor kappa-B kinase subunit beta (IKK- β), which in turn activates Nuclear factor NF-kappa-B (NF- κ B) (Altman & Villalba, 2003).

Upon dimerisation of EGFR, autophosphorylation of the tyrosine residues on the C-terminal domain leads to the creation of docking sites for various signalling messengers. These include the adaptor proteins SHC transforming protein 1 (Shc), Growth factor receptor-bound protein 2 (GRB2), Cas-Br-M ecotropic retroviral transforming sequence (c-Cbl), Docking protein 2 (DOK2) and NCK adaptor protein 1 (NCK1) (Jones & Dumont, 1999). These sites can also interact with enzymes, including Phospholipase C gamma 1 (PLC- γ 1), v-Src sarcoma viral oncogene homolog (c-Src) and PTK2 protein tyrosine kinase 2 (FAK1). Of the adaptor proteins, Shc and GRB2 recruit Son of sevenless homolog 1 (SOS), forming a protein complex. Once activated, SOS activates v-Ha-ras Harvey rat sarcoma viral oncogene homolog (H-Ras) by converting the inactive GDP-bound state to an active GTP-bound state. Activated H-Ras then activates the v-Raf-1 murine leukemia viral oncogene homolog 1 / Mitogen-activated protein kinase kinase 1 and 2 / Mitogen-activated protein kinase 1 and 3 kinase cascade (c-Raf-1 / MEK1 and MEK2 / ERK1/2 signalling pathway). This pathway leads to the activation of the transcription factors ELK1 member of ETS oncogene family (Elk-1), v-Myc myelocytomatosis viral oncogene homolog (c-Myc), and v-Fos FBJ murine osteosarcoma viral oncogene homolog (c-Fos) (Prenzel *et al.*, 2001).

The NCK1 adaptor of EGFR leads to the activation of the JNK signalling cascade. NCK1 can recruit p21-Activated kinase 1 (PAK1), forming a protein complex that binds Mitogen-activated protein kinase kinase kinase 10 (MLK2). This complex triggers a signalling cascade of proteins that include Mitogen-activated protein kinase kinase 4 and 7 (MEK4 and MKK7) / Mitogen-activated protein kinase 8 and 9 (JNK1

and JNK2). These activated JNKs translocate to the nucleus, activating transcription factors such as Elk-1 and Jun oncogene (c-Jun) (Poitras *et al.*, 2003).

Our results suggest that EGF signals through EGFR to increase initial short circuit current in Calu-3 cells and that PI3K is signalled downstream of EGFR (Figure 5.3). EGF is known to cause tyrosine phosphorylation of p85 of PI3K in T84 cells, leading to its activation (Uribe *et al.*, 1996; Chow & Barrett, 2007). Our results also suggest that PKC- δ is likely to be signalled downstream of PI3K (Figure 5.3), whereas previously, it was suggested that the PKC- ϵ isoform was involved in EGF signalling in the gut (McCole & Barrett, 2009). However, it was demonstrated in more recent studies carried out Mroz & Keely (2012) that EGF signals through a very similar mechanism involving both PI3K and PKC- δ in T84 cells in a similar way as described in this chapter for Calu-3 cells. Their study demonstrated that EGF signals through PI3K and PKC- δ to lead to an increase in activation of the calcium activated chloride channel ANO1 after 24 hours rather than potassium channels (Mroz & Keely, 2012). The result from this chapter shares some similarities with work previously carried out on skin, where potassium channel activation by EGF through PKC aids wound repair (Kang *et al.*, 2008). Furthermore, in the A431 human epithelial carcinoma cell line, it was found that activation of the EGF receptor resulted in an activation of voltage-independent calcium channels, which then leads to an activation of calcium activated potassium channels (Macara, 1986; Moolenaar *et al.*, 1986). The data in this chapter suggests that PKC is a positive regulator of calcium activated potassium channels in the Calu-3 cell line, whereas previous data from Peppelenbosch *et al.* (1991) show that PKC activation negatively regulated these channels (Peppelenbosch *et al.*, 1991).

The experiments shown in Figure 5.4 using potassium channel inhibitors suggest that this EGF signalling pathway results in a stimulation of basolateral potassium channels in a similar way as reported in rat basilar arteries (Ivanov *et al.*, 2006) and contrary to the mechanisms proposed in the gut (McCole & Barrett, 2009). Activation of EGFR leading to activation of basolateral potassium channels (primarily KCNN4) would increase chloride driving force for exit as described previously (Wang *et al.*, 2008). This increase in potassium ion transport would increase chloride driving force and thus the starting current.

Permeabilisation of the basolateral membrane bypasses the basolateral charybdotoxin / iberiotoxin -sensitive potassium channels and thus removes the EGF stimulated increases in starting current seen in intact membranes with EGF preincubation. These findings are in line with data which suggest that activation of tyrosine kinases can increase intracellular calcium (Munaron, 2002), and thus may play a role in the modulation of calcium activated potassium channels (Weaver *et al.*, 2004). The KCNN4 channel has also been previously identified as a potential target for inhibition to ameliorate the symptoms of asthma (Bradding & Wulff, 2009). Our data also allows for the possibility that the activation of PKC- δ may lead to an activation of the basolateral Na-K-2Cl cotransporter, which could allow more chloride into the cell, further increasing chloride transport as reported previously (Liedtke *et al.*, 2003). In intestinal epithelia, it was found that EGF upregulated the basolateral Na-K-2Cl cotransporter leading to chronic potentiation of chloride secretion (O'Mahony *et al.*, 2008). Inhibitors of the K_{ATP} and K_v LQT1 channels, glibenclamide and clofilium, have been shown to reduce basal transepithelial current, amiloride-sensitive sodium current, and forskolin-activated chloride currents while the K_{ATP} activator, pinacidil, had the reverse effect in rat type II alveolar epithelial cells. The potassium channel inhibitors were also found to decrease ENaC and CFTR mRNA and proteins (Leroy *et al.*, 2006). It has been demonstrated that stimulation of KCNQ1 and K_{ATP} currents by EGF promoted cell repair in rat type II alveolar epithelia (Trinh *et al.*, 2007). Similarly, it has been shown previously that TNF- α enhances KCNQ1 and K_{ATP} currents, promoting wound repair in primary cultures of airway epithelial cells from non-CF and CF patients. The effect of TNF- α is thought to be mediated through EGFR transactivation and subsequent K^+ channel stimulation (Maille *et al.*, 2011a). The study by Maille *et al.* (2011a) suggests that EGF treatment could have other beneficial effects in CF patients in airway repair in addition to the potential benefits in increased airway secretion highlighted by the data presented in this chapter. The data presented in this chapter allows us to construct a model for EGF signalling in the Calu-3 cell line shown in Figure 5.7.

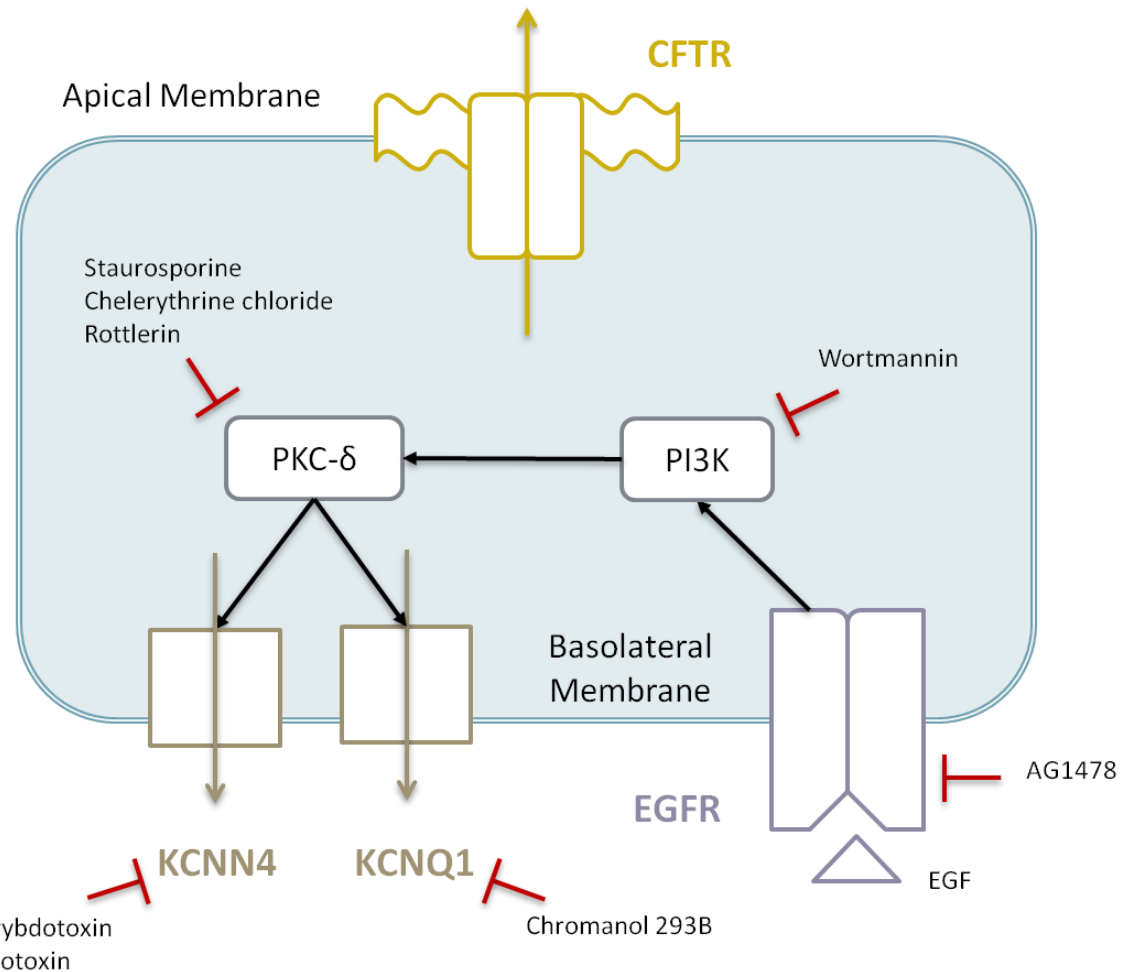


Figure 5.7 – Proposed signalling pathways involved in the regulation of chloride transport via EGF.

Activation of EGFR leads to an activation of phosphatidylinositol 3-kinase (PI3K) and protein kinase C δ that can be blocked by wortmannin and rottlerin, respectively. This in turn leads to an activation of potassium channels that include KCNN4 and KCNQ1, which can be blocked by iberiotoxin and chromanol 293B, respectively. Activation of this pathway ultimately leads to an increase in driving force for apical chloride exit and increased initial short circuit current. Based on information presented in this study. Statistical analysis was performed using a one way ANOVA with Tukey's Multiple Comparison test, where $P < 0.05$ was deemed statistically significant.

5.3.3 EGF increases in initial I_{SC} in intact Calu-3 monolayers are abolished by U0126 pretreatment

Our data suggests that there is possible involvement of the MAPK pathway in regulating ion transport across Calu-3 monolayers that potentially also involves basolateral potassium channels. While to date no similar study has been conducted in the Calu-3 cell line, our data are in agreement with previous studies in other cell lines such as the T84 colonic epithelial cell line which show that a MAPK pathway is involved in the regulation of chloride secretion. Specifically, it was shown that the JNK MAPK pathway in T84 cells regulates calcium dependent chloride secretion rather than cAMP dependent chloride secretion (Keely *et al.*, 1998). This effect is mediated through an inhibition of basolateral potassium channels and as a result, a decrease in driving force for apical chloride exit (Donnellan *et al.*, 2010). Another example of MAPK regulation of potassium channels that shares similarities with the data presented in this chapter can be found in the cortical collecting duct of the kidney. It has been shown that inhibition of the MAPK pathway can bring about stimulation of Ca^{2+} -dependent large-conductance K^+ channels (Li *et al.*, 2006).

5.3.4 Potassium channels are expressed in Calu-3

The fact that the KCNQ1 and KCNN4 genes were expressed in our study is in agreement with earlier work carried out using the Calu-3 cell line which identified the expression of KCNN4 and KCNQ1 (Cowley & Linsdell, 2002; Moser *et al.*, 2008). KCNA2 and KCNA3 expression has not been previously demonstrated in the Calu-3 cell line, but both have been found to be expressed in the smooth muscle in the human airways (Adda *et al.*, 1996). While it is possible that KCNA2 and KCNA3 are stimulated by EGF and cause increases in initial starting current, there is no evidence in the literature that this might be the case. Additionally, iberiotoxin, the KCNN4 blocker, reduced the short circuit current more than charybdotoxin, which can block KCNA2 and KCNA3 as well as KCNN4.

Chapter 6 Effects of EGF Treatment on UTP Response

6.1 Introduction

It has been demonstrated using intestinal epithelial cells that activation of Gq, which includes the m₃ muscarinic receptor, by agonists such as carbachol (CCh), initially causes calcium mobilisation that can in turn lead to an activation of calcium activated chloride channels that leads to an increase in chloride secretion. However, this is subsequently followed by a reduction in secretion since calcium mobilisation also ultimately leads to activation of EGFR by ligands such as EGF and TGF- α . This in turn can lead to an activation of ERK, which negatively regulates chloride secretion in the gut (McCole & Barrett, 2009). In contrast to what occurs in gut epithelia, EGF activates calcium activated chloride channels via p60c-src in human bronchial epithelial cell line 16HBE14o⁻, which could be blocked by tyrosine kinase inhibitor AG1478 (Jeulin *et al.*, 2008). Furthermore, EGF upregulated ANO1 expression and Ca²⁺ currents in T84 intestinal epithelia by a mechanism involving sequential activation of PI3K and PKC δ (Mroz & Keely, 2012).

While the relationship between calcium activated chloride channels and EGFR signalling has been previously studied in other tissues such as the gut (McCole & Barrett, 2009) and using 16HBE14o⁻ cells (Jeulin *et al.*, 2008), no similar studies have been conducted in the Calu-3 cell line. Studies of the link between EGF and calcium activated chloride channels in Calu-3 cells could lead to new avenues for potential therapeutics for CF since EGF could theoretically augment the response to P2Y agonists and increase ion transport. Thus, in order to address this gap in knowledge, the aim of this investigation was to determine the effect of 10 ng/ml treatment of EGF on acute stimulation with 100 μ M UTP. This was to determine if EGF was able to upregulate calcium activated chloride channels over a period of time. The impact of basolateral permeabilisation will also determine which conductance is likely to be causing effects on ion transport (if any).

The effect of EGF on message and/or protein levels of chloride channels has to date not been previously investigated in Calu-3 cells. EGF could also potentially increase

message and/or protein levels for chloride channels and thus boost ion transport through an increase in the amount of channels at the cell membrane. Therefore to address this current gap in knowledge, the change in expression of BEST1-4, Anoctamins 1-10 and CFTR when preincubated with 10 ng/ml EGF was investigated to see if EGF acts at the message level. Also of interest is whether 1 hour of preincubation of 10 ng/ml of EGF affects BEST1 protein expression.

6.2 Results

6.2.1 Addition of Epidermal Growth Factor (EGF) to the Calu-3 monolayers leads to an increase in UTP-stimulated I_{sc}

To investigate the effect of EGF preincubation on UTP response, Calu-3 monolayers were preincubated with EGF for 1, 2, 3 and 24 hours and compared to UTP stimulation without EGF treatment shown in Figure 6.1. With untreated monolayers, the response to UTP is small at $1.0 \pm 0.1 \mu\text{A cm}^{-2}$ (n=5). The response with EGF at 1 hour did not increase substantially at $1.6 \pm 0.7 \mu\text{A cm}^{-2}$ (n=5), and 2 hours at $0.5 \pm 0.5 \mu\text{A cm}^{-2}$ (n=5). With 3 hours of EGF treatment, the response to UTP was still low at $0.3 \pm 0.1 \mu\text{A cm}^{-2}$ (n=5). However, at 24 hour EGF treatment, the situation was different, with the UTP response increasing to $3.2 \pm 0.6 \mu\text{A cm}^{-2}$ (n=6), which is greater than the untreated monolayers by a statistically significant amount (p<0.5). These results suggest that EGF is able to regulate ion channels over a 24 period, and as such increases the response to UTP. These data suggest that CFTR, CaCCs or basolateral potassium channels may be involved in this process. Moreover, as a result of these data, stimulation of Calu-3 monolayers for 24 hours with EGF was treated as maximal and used for subsequent experiments.

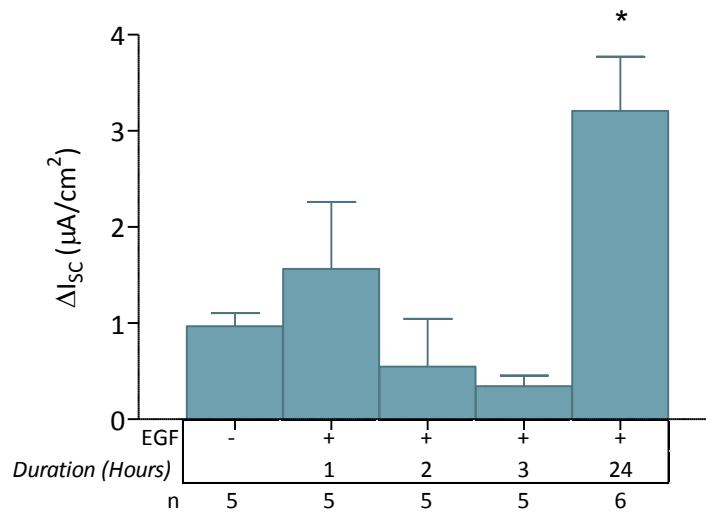


Figure 6.1 – Addition of EGF to the Calu-3 monolayers leads to an increase in UTP-stimulated I_{sc} .

Summary bar graph to show 100 μM UTP response following 10 ng/ml EGF preincubation over a 24 hour time period. Statistical analysis was performed using a one way ANOVA with Tukey's Multiple Comparison test, where $P<0.05$ was deemed statistically significant.

6.2.2 Permeabilisation removes EGF-induced UTP stimulated I_{sc} in Calu-3

In order to determine if the EGF-induced UTP spike in I_{sc} at 24 hours was due to CFTR, CaCCs or basolateral potassium channels, the basolateral membrane was permeabilised and a basolateral to apical chloride gradient applied. This method was used to eliminate the influence of basolateral potassium channels on ion transport so that only CFTR and CaCC responses were investigated. As seen in Figure 6.2 (A and B), if the monolayers are preincubated with 10 ng/ml EGF for 24 hours (seen to give a maximal response previously), it is seen that the response to UTP is effectively eliminated $0.5 \pm 0.4 \mu\text{A cm}^{-2}$ ($n=3$). Taken together, it is likely that basolateral calcium activated potassium channels are responsible for the UTP response seen across Calu-3 monolayers. This work is in line with similar work carried out previously investigating the response to adenosine in Calu-3 cells (Wang *et al.*, 2008).

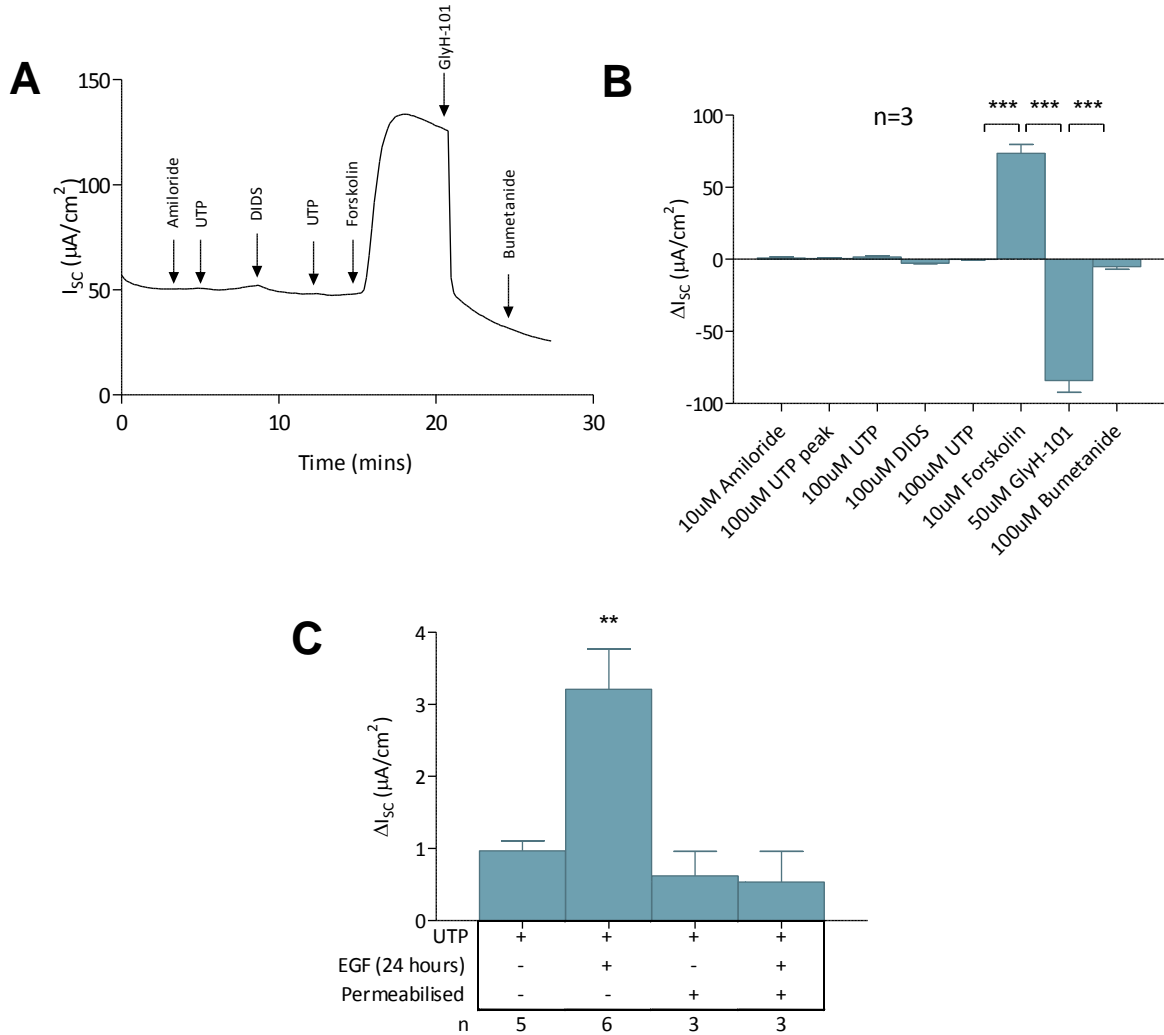


Figure 6.2 – Permeabilisation removes UTP induced I_{sc} in Calu-3.

Trace (A) and bar graph (B) to show permeabilised 100 μM UTP response following 10 ng/ml EGF preincubation for 24 hours, and summary bar graph (C) showing control 100 μM UTP response shown previously in Calu-3 monolayers compared to 10 ng/ml EGF treatment for 24 hours and permeabilised monolayers with and without 10 ng/ml EGF treatments 24 hour. Statistical analysis was performed using a one way ANOVA with Tukey's Multiple Comparison test, where $P<0.05$ was deemed statistically significant.

In summary, if the basolateral membrane is permeabilised, the response to UTP is effectively eliminated with or without 10 ng/ml EGF stimulation for 24 hours as shown in Figure 6.2 (C). The response to UTP with basolateral membrane permeabilisation without EGF pretreatment is $0.6 \pm 0.3 \mu\text{A cm}^{-2}$ (n=3), while the response with monolayers pretreated with EGF was $0.5 \pm 0.4 \mu\text{A cm}^{-2}$ (n=3). Taken together, this result shows that the increase in UTP response, albeit small, is likely to be highly tied to calcium activated potassium channels on the basolateral membrane.

6.2.3 EGF treatment and chloride channel gene expression in Calu-3 cells

Calu-3 cells were preincubated with 10 ng/ml EGF for set periods of time and RNA was extracted for RT-PCR analysis. The gene expression of bestrophins 1 – 4 and CFTR in response to EGF treatment is shown in Figure 6.3, and the gene expression of anoctamins 1 – 10 in response to EGF treatment is shown in Figure 6.4. In Figure 6.5 and Figure 6.6, the effect of EGF treatment on the expression of chloride channels and candidates was estimated with semi-quantitative densitometry. It was seen that the expression of bestrophin, CFTR, ANO1 and ANO4 genes appeared down regulated with EGF treatment, while ANO6, ANO8 and ANO10 were up regulated at three hours. ANO5 appeared equal regardless of treatment.

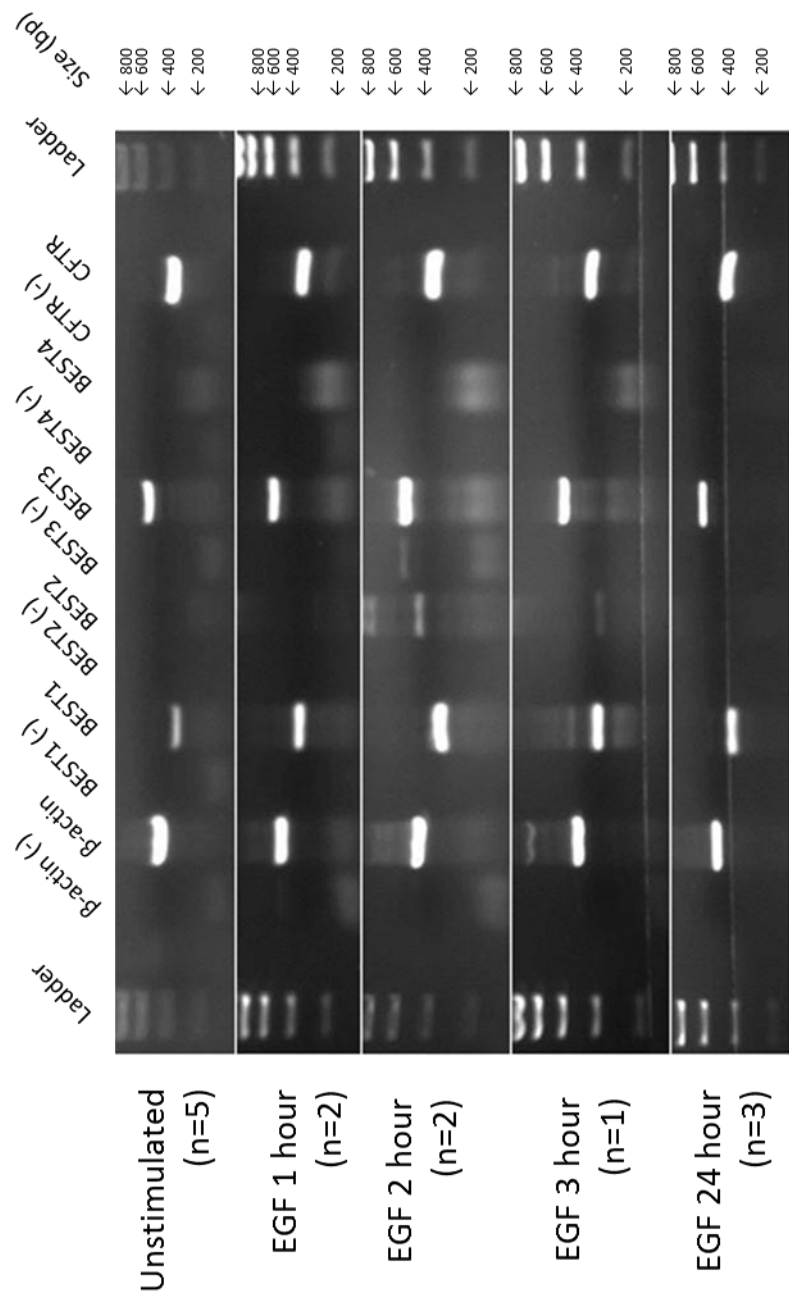


Figure 6.3 – Bestrophin and CFTR channel expression in response to EGF treatment in Calu-3 cells.

Number of repeats indicated with each using unique RNA sample. Ladder is the same for each experiment. Instances were bands appeared in the negative controls were not seen in repeats for that particular gene. Number of repeats indicated in brackets.

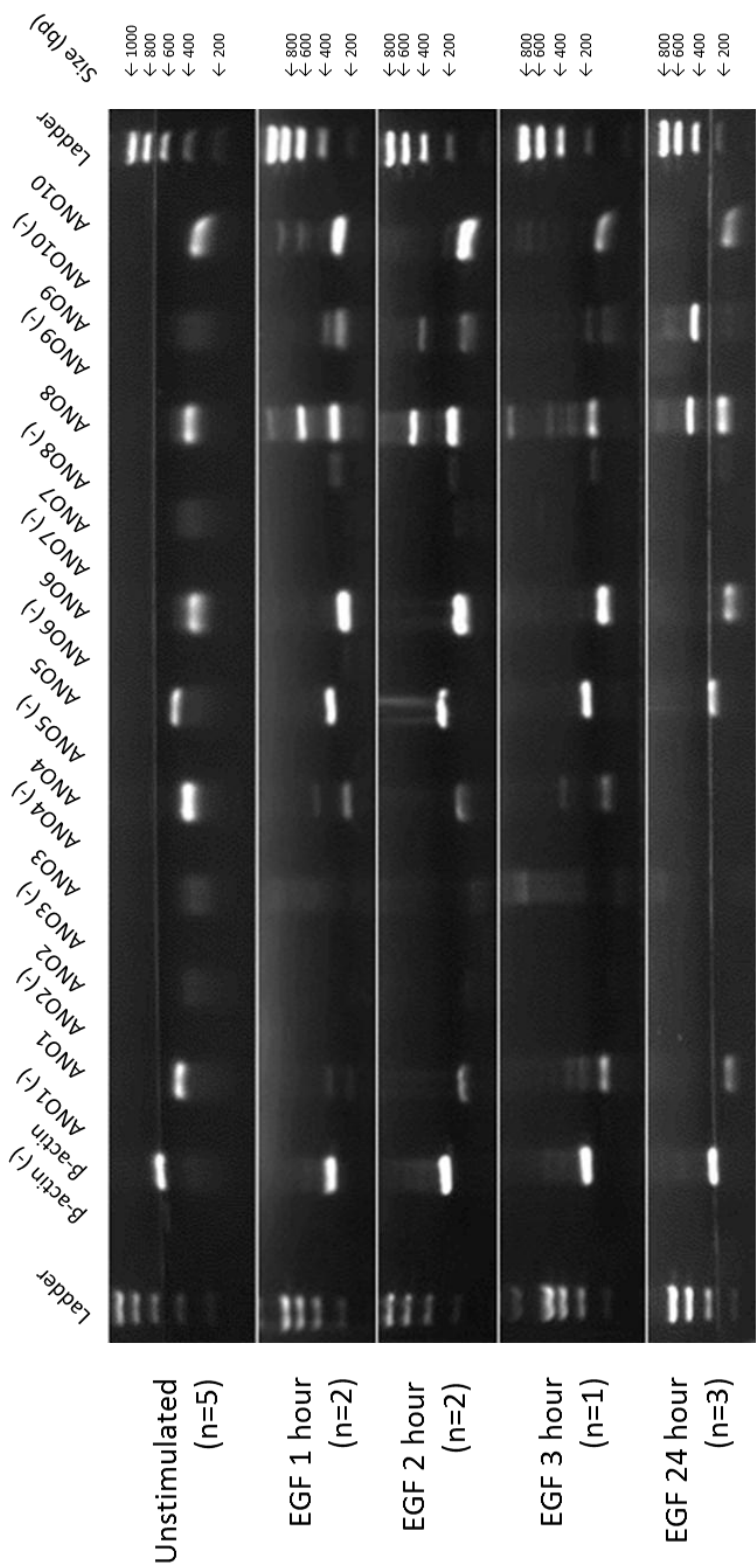


Figure 6.4 – Anoctamin expression in response to EGF treatment in Calu-3 cells.

Number of repeats indicated with each using unique RNA sample. Ladder is the same for each experiment. Instances were bands appeared in the negative controls were not seen in repeats for that particular gene. Number of repeats indicated in brackets.

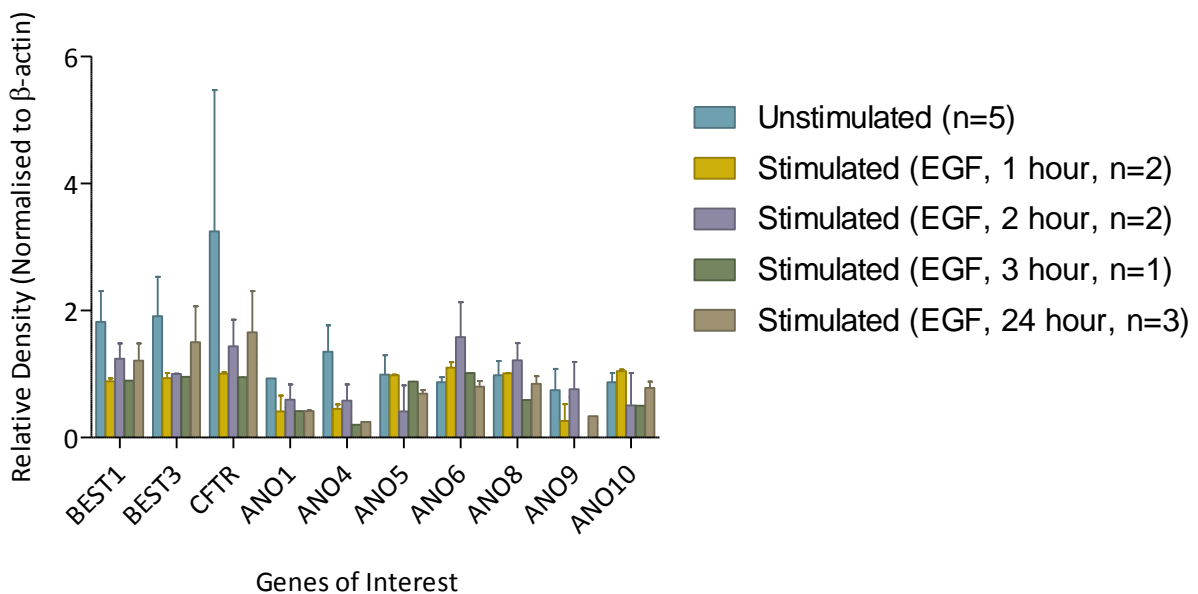


Figure 6.5 – Densitometry of chloride channel mRNA in response to EGF preincubation normalised to β -actin.

Calu-3 cells were preincubated with 10 ng/ml EGF for 1, 2, 3 and 24 hour time periods, the RNA extracted, and RT-PCR performed. The mRNA expression of bestrophins and anoctamins was analysed using densitometry of the band intensity and then normalised to β -actin. Numbers of repeats are indicated in brackets.

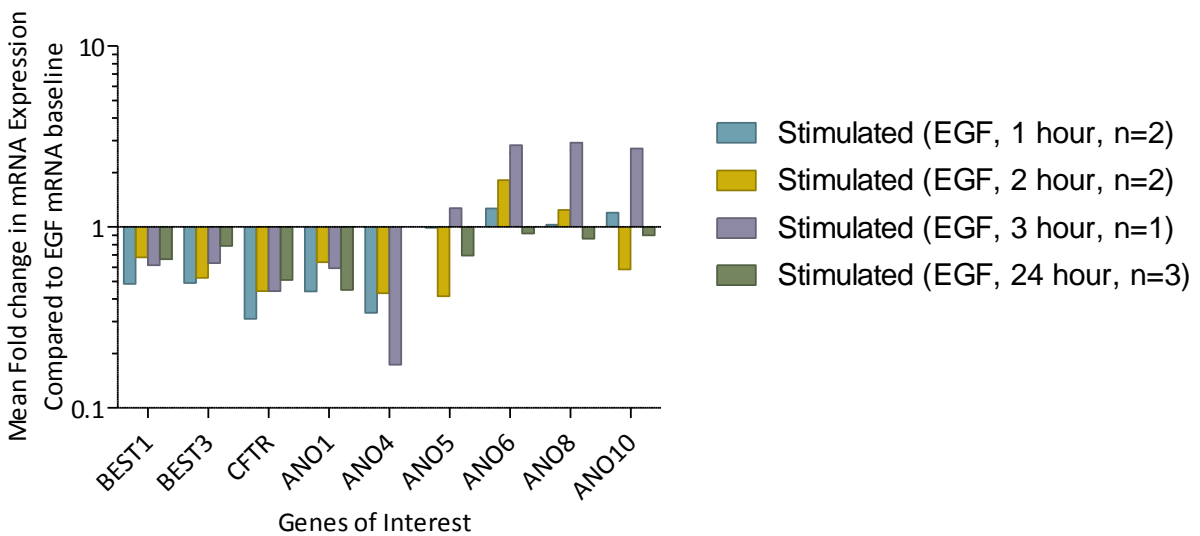


Figure 6.6 – Mean fold change in mRNA expression of chloride channels compared to the unstimulated mRNA baseline.

The data in Figure 6.5 is further normalised to the unstimulated control sample, giving a value for the mean fold change in mRNA expression due to 10 ng/ml EGF pretreatment for 1, 2, 3 and 24 hour time periods. Numbers of repeats are indicated in brackets.

6.2.4 EGF treatment and chloride channel gene expression in Calu-3 cells

To study the effects of EGF on CFTR expression on the protein level, a time course Western blot was performed (Figure 6.7). Cells were grown to confluence and preincubated with 10 ng/ml EGF where appropriate. 10 µg of protein was loaded into each well that was extracted the RIPA extraction technique described in the Materials and Methods. Despite a good β -actin signal, the bands for CFTR protein were either faint or not present. Taken together, these results show that our implementation of the RIPA method was not extracting CFTR protein effectively from the cell membrane, leading to poor detection. As a result, other extraction techniques were generally used.

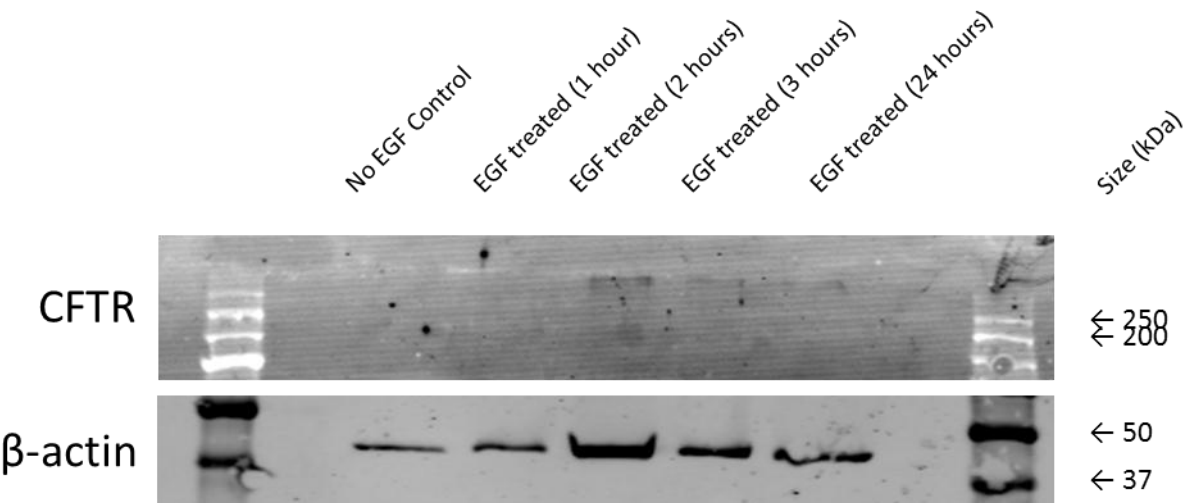


Figure 6.7 – Characterisation of CFTR protein expression in the Calu-3 cell line.

The Calu-3 cell line was treated with 10 ng/ml EGF over a period of 24 hours. The total protein content acquired using the RIPA extraction method. Representative of a single successful Western blot.

It was then of interest to see if EGF could affect BEST1 expression. Tissue culture flasks were grown to confluence and extracted using the NP-40 technique as described in the Materials and Methods. Each lane was loaded with 20 µg of protein. The first lane was loaded with protein obtained from a lysate of CHO cells transfected with BEST1 as a positive control kindly provided by Kirsty Kirk (Winpenny Lab, University of East Anglia). Subsequent lanes are loaded with protein lysates of unstimulated and 1 hour 10 ng/ml EGF stimulated Calu-3 cells. All the lanes were duplicated as an internal replicate, and the experiment was repeated successfully three times. As shown in Figure 6.8, it was seen that BEST1 was well expressed in all samples corresponding to a dark band at 68 kDa (Milenkovic *et al.*, 2009), and that

densitometry performed on the unstimulated and EGF stimulated bands showed no significant difference in protein expression. Taken together, it shows that BEST1 is expressed in Calu-3 cells, and that treatment with 10 ng/ml EGF for one hour does not have an affect the protein expression.

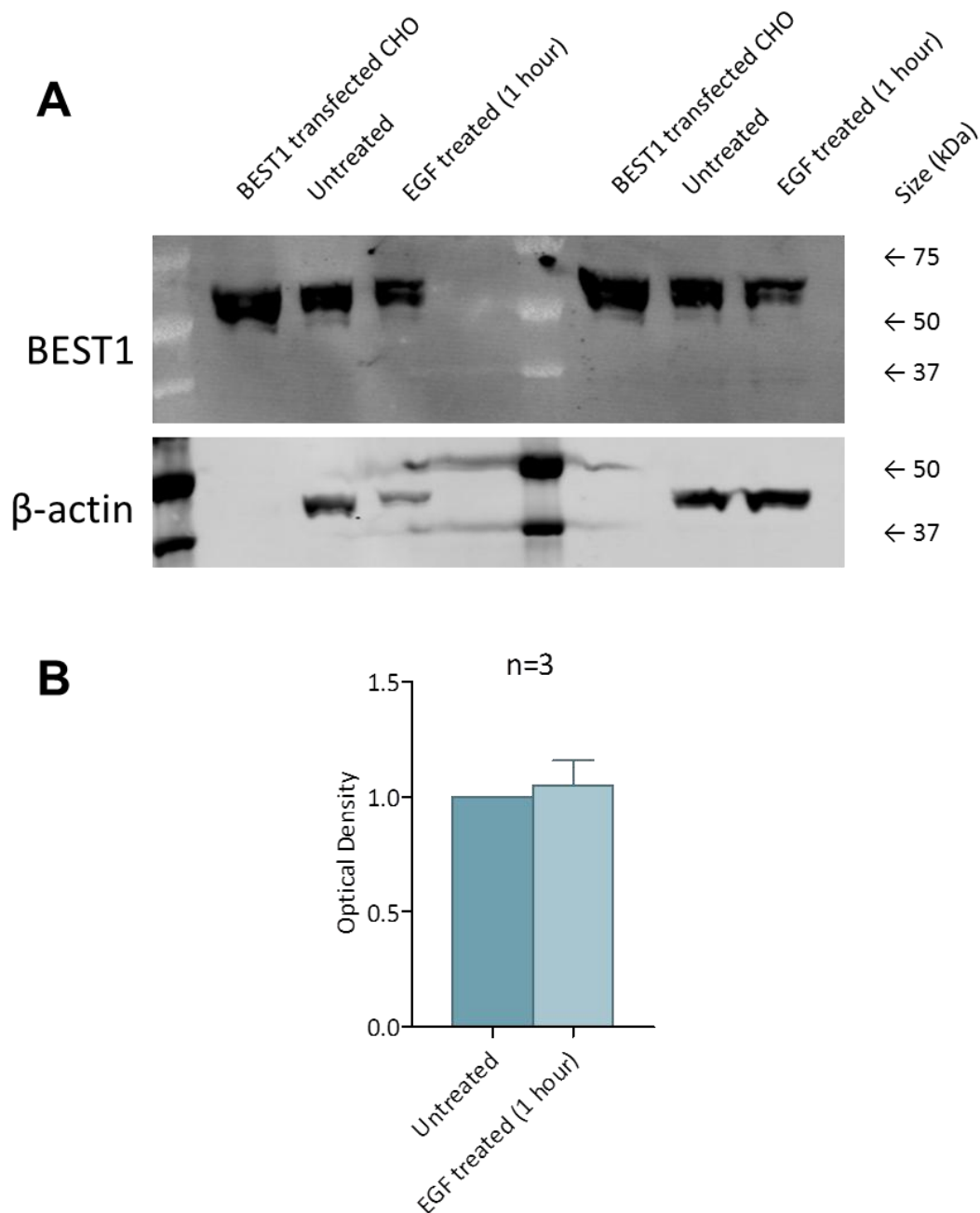


Figure 6.8 – BEST1 protein expression is not affected by EGF treatment.

Western blot showing the effect of 10 ng/ml EGF treatment for 1 hour on BEST1 protein expression (A) and bar graph to show the effect of 10 ng/ml EGF treatment for 1 hour on BEST1 protein expression using densitometry (B). Statistical analysis was performed using a one way ANOVA with Tukey's Multiple Comparison test, where $P < 0.05$ was deemed statistically significant.

6.3 Discussion

6.3.1 EGF increases intracellular Ca^{2+} over 24 hours and UTP induced CaCC activation

EGF is known to raise levels of intracellular Ca^{2+} in tumour cells (Dittmar *et al.*, 2002). High levels of intracellular Ca^{2+} may not necessarily keep calcium activated chloride channels open, as they can become inactivated by calmodulin-dependent kinase II (CaMKII) (Wang & Kotlikoff, 1997). From this experimental set alone, it is hard to say which ion channel(s) is responsible for the statistically significant higher spike when treated with EGF for 24 hours. However, there are several possible candidates, which include CaCCs, CFTR or potassium channels such as KCNN4, which the subsequent experiment attempted to answer. CaCCs are activated via P2Y receptors triggering calcium mobilisation. Our data potentially corresponds to data that has been previously published by Jeulin *et al.* (2008), where EGF was shown to activate calcium activated chloride channels in another lung derived cell line, 16HBE14o⁻ (Jeulin *et al.*, 2008). CaCCs have also been previously demonstrated to be upregulated by chronic EGF treatment in the gut. Recent studies using T84 monolayers found that when chronically stimulated with EGF, the response to carbachol was increased compared to control cells. This increase in carbachol response could be abolished using the ANO1 inhibitor, T16_{inh}-A01 (Mroz & Keely, 2012). This increase could similarly be inhibited by rottlerin (PKC- δ inhibitor) and LY290042 (PI3K inhibitor). LY290042 also inhibited EGF-induced phosphorylation of PKC- δ . Taken together, this suggested that EGF led to an upregulation of ANO1 response through sequential activation of PI3K and PKC- δ (Mroz & Keely, 2012). Moreover, CFTR can be activated indirectly via ATP being converted to ADO in the cytosol activating G protein coupled receptor A_{2B} that would increase levels of cAMP (Lazarowski & Boucher, 2009), making CFTR another potential candidate for the spike seen in our data. Calcium activated potassium channels on the basolateral membrane can be activated by both apical adenosine and calcium (Wang *et al.*, 2008), suggesting that EGF could be activating basolateral potassium channels and thus increasing the chloride driving force.

6.3.2 EGF elevates UTP induced CaCC responses via Ca^{2+} activated potassium channels

As a result of basolateral membrane permeabilisation, pretreatment with EGF for 24 hours and subsequent UTP stimulation, the current spike was greatly reduced. This suggests that a basolateral conductance is responsible for the increased spike seen previously. Apical adenosine is already known to activate calcium activated potassium channels through PLC/ Ca^{2+} via $\text{A}_{2\text{B}}$ adenosine receptors on the apical membrane (Wang *et al.*, 2008). Similarly, in human macrophages, application of 10 μM UTP or 10 μM ATP induces cytosolic calcium oscillations and changes in membrane potential. These calcium oscillations are caused by the activation of P2Y₂ receptors that are coupled to PLC, while the membrane potential oscillations are due to the opening of calcium activated potassium channels (Hanley *et al.*, 2004). As shown in this study and previous studies, KCNN4 is a dominant calcium activated potassium channel in Calu-3 cells (Cowley & Linsdell, 2002), so is a likely candidate. A proposed model is shown in Figure 6.9 based on data generated from this study in combination with previously known information (Lazarowski & Boucher, 2009). Our proposed model suggests that stimulation of EGFR leads to an increase in calcium mobilisation over a period of 24 hours that enhances the response by calcium dependent ion channels such as CaCCs and calcium activated potassium channels. EGF has been previously shown to enhance calcium mobilisation in mouse mammary epithelial cells (Ichikawa & Kiyohara, 2001) and rabbit corneal epithelial cells (Yang *et al.*, 2003). Addition of UTP leads to an activation of P2Y receptors, leading to a surge of intracellular calcium that is greatly enhanced by the EGF treatment. Permeabilisation of the basolateral membrane removes the effect of basolateral calcium activated potassium channels, and therefore removes a significant component of the response. This model is in agreement with our data and prior work looking at the relationship between EGF and GPCRs in the regulation of CaCCs (Liebmann, 2011).

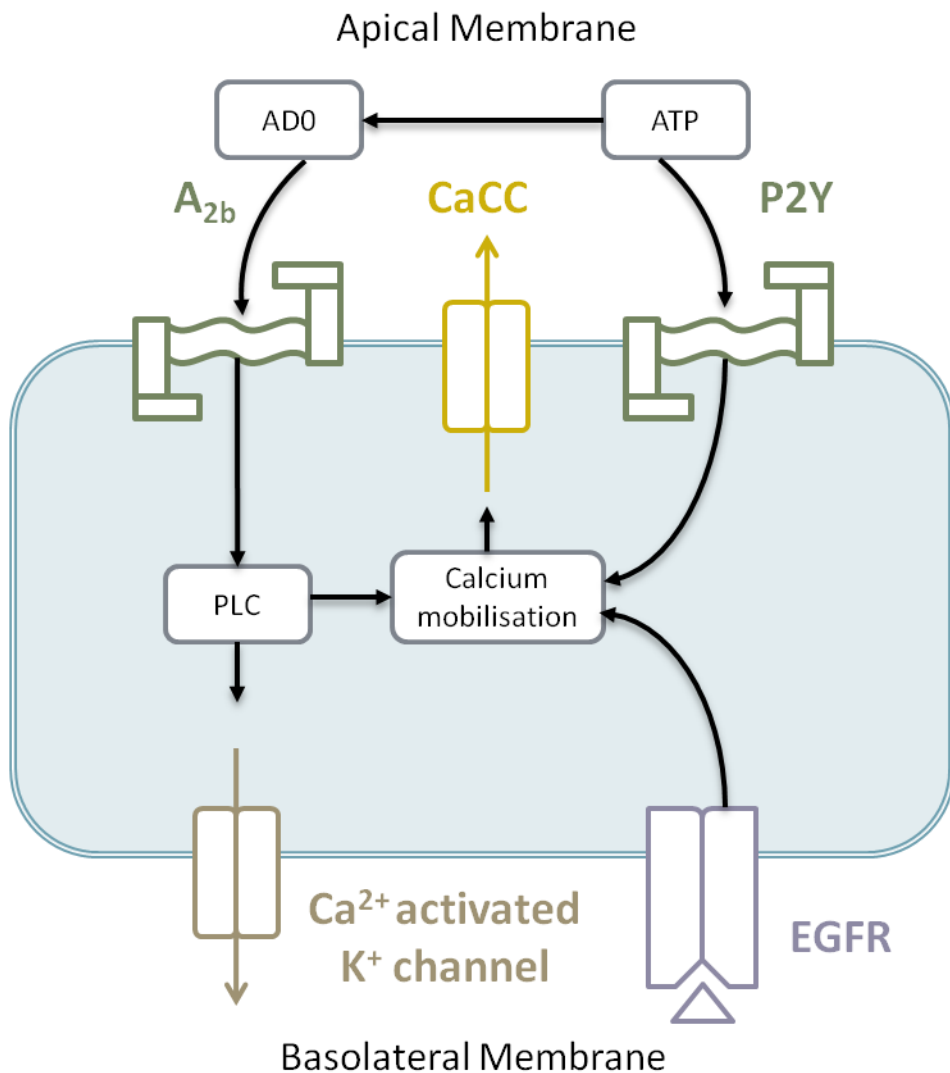


Figure 6.9 – Proposed model of EGF regulation of UTP response in Calu-3 cells.

Activation of EGFR with EGF over a 24 hour period leads to an increase in calcium mobilisation in the cytosol. Subsequent activation of P2Y receptors on the apical surface with UTP or ATP leads to a sharp increase in calcium mobilisation. ATP is broken down in the extracellular environment to ADO, which activates a G protein coupled receptor (GPCR) such as the adenosine A_{2B} receptor. The GPCR can then activate calcium activated potassium channels via phospholipase C (PLC). Based on information from data presented in this chapter and material from: (Hanley *et al.*, 2004; Lazarowski & Boucher, 2009)

6.3.3 Effect of EGF on chloride channel transcription

The EGF signalling pathway can eventually lead to the activation of a number of transcription factors, which include c-myc, c-jun, c-fos, STAT1, STAT3, Elk-1 and NF- κ B (Prenzel *et al.*, 2001; Altman & Villalba, 2003; Poitras *et al.*, 2003; Andl *et al.*, 2004). This creates a wide variety of candidates that could be responsible for affecting transcription of chloride channels. The fact that CFTR message decreases from EGF preincubation has been found previously in the gills of the striped bass *Morone saxatilis* (Madsen *et al.*, 2007), but no current literature addresses the effect of EGF on CFTR transcription in the mammalian airway. Recent studies in T84 cells demonstrated increased ANO1 and unchanged CFTR mRNA expression by 24 hour EGF preincubation (Mroz & Keely, 2012), which was in contrast to our studies in the Calu-3 cell line where EGF appeared to decrease both ANO1 and CFTR expression.

6.3.4 BEST1 protein is present in Calu-3 cells

BEST1 protein has previously been found in 16HBE cells (Barro Soria *et al.*, 2009) and in the nasal epithelial cells of Δ F508 homozygous CF patients (Martins *et al.*, 2011) as well as Calu-3 cells (Milenkovic *et al.*, 2009). The data obtained in this study concerning endogenous expression of BEST1 are in agreement with the studies of Milenkovic *et al.* (2009). The effect of EGF preincubation on BEST1 protein translation has not been previously studied. It was found that EGF does not appear to affect BEST1 protein translation. This suggests that the spike seen in the short circuit current data at 24 hours treatment with EGF (Figure 6.1) was not due to an upregulation of BEST1 protein. It is possible that EGF may be upregulating protein expression of other calcium activated chloride channel candidates, however at the time of writing effective antibodies for these proteins were not available for testing (see Further work, Section 8.4).

Chapter 7 Effects of EGF on Forskolin Stimulation

7.1 Introduction

The effect of forskolin on ion transport in Calu-3 cells has been widely reported (Shen *et al.*, 1994). However, the effect of preincubating EGF on the magnitude of the forskolin response has not been previously studied. In other cell types, such as rat cardiac myocytes, EGFR is coupled to adenylate cyclase, and EGFR signalling causes an accumulation of cAMP (Yu *et al.*, 1992). However, the interplay between EGF and forskolin in the Calu-3 cell line has not been previously studied.

To understand this effect could lead to a higher understanding of the underlying processes involved and help develop new avenues of research to aid the treatment of CF. Therefore, the effect of EGF treatment on the forskolin response was investigated to see how EGF influences chloride transport. This was accomplished by preincubating Calu-3 monolayers with 10 ng/ml EGF over a time scale of 1, 2, 3 and 24 hours, and then treating them firstly with 10 μ M amiloride (to remove the influence of ENaC on the results), and then stimulating with 10 μ M forskolin. Of interest was the initial peak size shortly following forskolin stimulation.

Further, the mechanism that links EGF and forskolin response is of importance since it could reveal new targets with which to develop new therapeutics. In order to determine the mechanism behind the EGF induced decreases in forskolin stimulated short circuit current, experiments were designed so that the Calu-3 monolayers were treated with inhibitors of a number of pathways before an hour of EGF treatment (previously determined to be statistically significant). As before, the pathways of interest initially were PI3K, PKC and potassium channels, based on work with EGF conducted previously with gut cells (McCole & Barrett, 2009).

From the literature, stimulation of β_2 adrenergic receptors, which are abundant in Calu-3 cells, can potentially induce EGF ligand shedding via the activation of sheddases and activate EGFR as a result (Liebmann, 2011). It has also been demonstrated in the T84 colonic epithelial cell line that agonists of GPCRs can rapidly

transactivate EGFR by a signalling pathway involving cAMP and PKA, and likely involves PI3K (Bertelsen *et al.*, 2004). It has also been demonstrated that carbachol activates ERK via EGFR transactivation, leading to inhibitory signalling of chloride secretion (Keely *et al.*, 1998). This transactivation process is thought to be mediated by a pathway that involves elevations in intracellular calcium, calmodulin, protein tyrosine kinase 2 (PYK-2) and p60src (Keely *et al.*, 2000). It was also demonstrated that the transactivation of EGFR is mediated through a metalloproteinase-dependent extracellular release of TGF-alpha and intracellular activation of Src (McCole *et al.*, 2002). However, it has not been previously demonstrated if a similar transactivation event upon stimulation of the β_2 receptor occurs in Calu-3 cells, and what the impact of such a process would be on ion transport. The release of EGF through a transactivation event could potentially lead to increased ion transport through the PI3K-PKC- δ -KCNN4/KCNQ1 pathway that I have previously demonstrated. This would be beneficial for treating CF if this is in fact the case. So, to address this current gap in knowledge, we hypothesised that a similar process could occur in our system. To test this, Calu-3 monolayers were preincubated with either GM-6001 or AG1478 and then stimulated with the β_2 agonist, salbutamol, with the results compared to that of salbutamol stimulation alone (Figure 7.1).

If EGF shedding does occur upon stimulation of the β_2 receptor with salbutamol, pretreatment with GM-6001 would inhibit the sheddases activity, and thus prevent the release of EGF ligand. No additional EGF release would lead to decreased ion transport compared to salbutamol alone since the PI3K-PKC- δ -KCNN4/KCNQ1 pathway previously described would not be activated. If shedding does not occur, there would be no difference in short circuit current between untreated and GM-6001 pretreated monolayers. Similarly, Calu-3 monolayers were also preincubated with AG1478 in the place of GM-6001 and similarly stimulated with salbutamol. If EGF ligand is released following stimulation of salbutamol, then AG1478 would prevent EGF signalling through EGFR and activating subsequent signalling pathways, so a reduced stimulated short circuit current from salbutamol would be expected. If no shedding of EGF ligand occurs, we would expect no difference from the control salbutamol response.

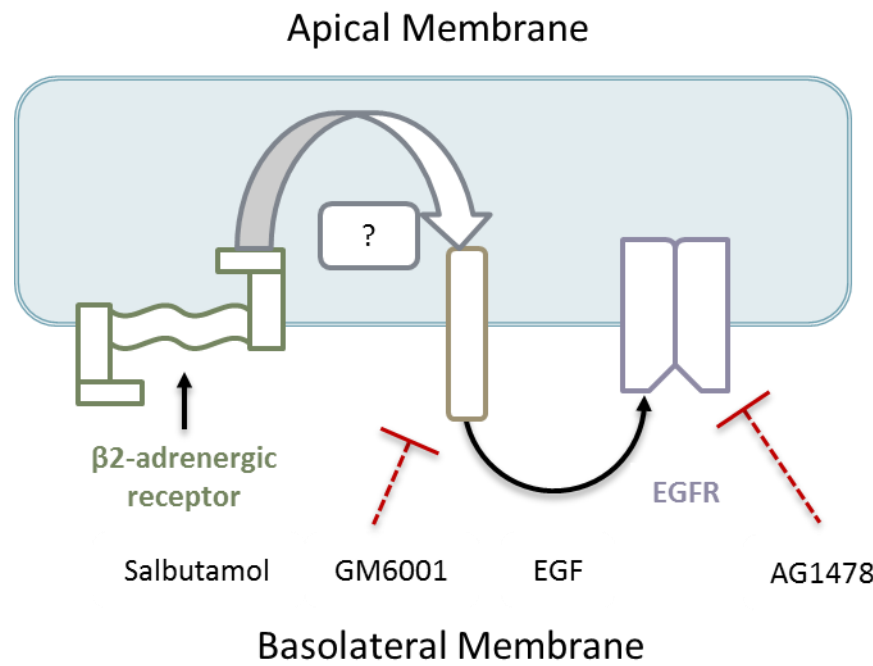


Figure 7.1 – Hypothesis of β_2 adrenergic receptor stimulation leading to transactivation of the EGF receptor by sheddases.
 Adapted from (Liebmann, 2011)

Following on from work on β_2 receptors, work on β_3 receptors in the airways is currently in its infancy. The effect of β_3 agonists on ion transport in wild-type lung tissue has not been previously demonstrated. Thus, to address this gap in knowledge, our focus was to characterise the functional response in Calu-3 cells using short circuit current since it was confirmed in this investigation that the gene for β_3 receptor was expressed in Calu-3 cells (Figure 7.10). To do this we used the specific β_3 agonist, CGP-12177, which has been used in previous studies (Robay *et al.*, 2005). Once the optimal concentration and side of the membrane is determined, preincubations with inhibitors on the basolateral side including MDL-12330A, wortmannin, U0126 and L-748,337 were used to block adenylate cyclase, PI3K, ERK1/2 and the β_3 receptor itself, respectively. This was conducted in both intact and permeabilised monolayers.

7.2 Results

7.2.1 EGF preincubation decreases forskolin response in intact Calu-3 monolayers

As shown in Figure 7.2 (A and B), the standard response to 10 μM forskolin on the basolateral side in intact Calu-3 monolayers produced an increase in short circuit current of $15.5 \pm 2.1 \mu\text{A cm}^{-2}$, $n=5$). When preincubated with 10 ng/ml EGF on the basolateral side for 1 hour, this increase in short circuit current was reduced to $6.9 \pm 1.5 \mu\text{A cm}^{-2}$ ($n=5$), which was statistically significant compared to the untreated result ($p<0.01$). After preincubation with 10 ng/ml EGF on the basolateral side of intact Calu-3 monolayers for two hours, the acute forskolin stimulated short circuit current is further reduced to $5.2 \pm 0.6 \mu\text{A cm}^{-2}$ ($n=5$), which was statistically significant compared to the untreated result ($p<0.001$). After 10 ng/ml EGF treatment on the basolateral side of intact Calu-3 monolayers for 3 hours, it is again further reduced to $4.3 \pm 0.7 \mu\text{A cm}^{-2}$ ($n=4$). However, after 10 ng/ml EGF treatment on the basolateral side of intact Calu-3 monolayers 24 hours, the forskolin stimulated short circuit result was restored to $12.5 \pm 1.9 \mu\text{A cm}^{-2}$ ($n=5$).

In permeabilised monolayers, the situation changes slightly (Figure 7.2, C and D). In permeabilised Calu-3 monolayers with a basal to apical chloride gradient, the acute response to 10 μM forskolin with no pretreatments was $39.4 \pm 7.1 \mu\text{A cm}^{-2}$ ($n=3$). 1 hour pretreatment with 10 ng/ml EGF resulted in a somewhat reduced increase in current in response to basolateral acute 10 μM forskolin treatment at $21.8 \pm 14.8 \mu\text{A cm}^{-2}$ ($n=3$). This was not statistically significant due to wider variation within the results. At 2 hours of 10 ng/ml EGF treatment on the basolateral side, the increase from 10 μM forskolin on the basolateral side was $29.1 \pm 6.3 \mu\text{A cm}^{-2}$ ($n=3$), and similarly at 3 hours, the increase from 10 μM forskolin was $29.4 \pm 20.8 \mu\text{A cm}^{-2}$ ($n=3$). By 24 hours of 10 ng/ml EGF treatment, the response is closer to untreated monolayers at $45.5 \pm 5.5 \mu\text{A cm}^{-2}$ ($n=3$). The result shares a similar pattern as before, but much less pronounced and with more variation within the results. This would indicate that there may be some potassium channel influence in the results, but not as strong as it is with initial starting current.

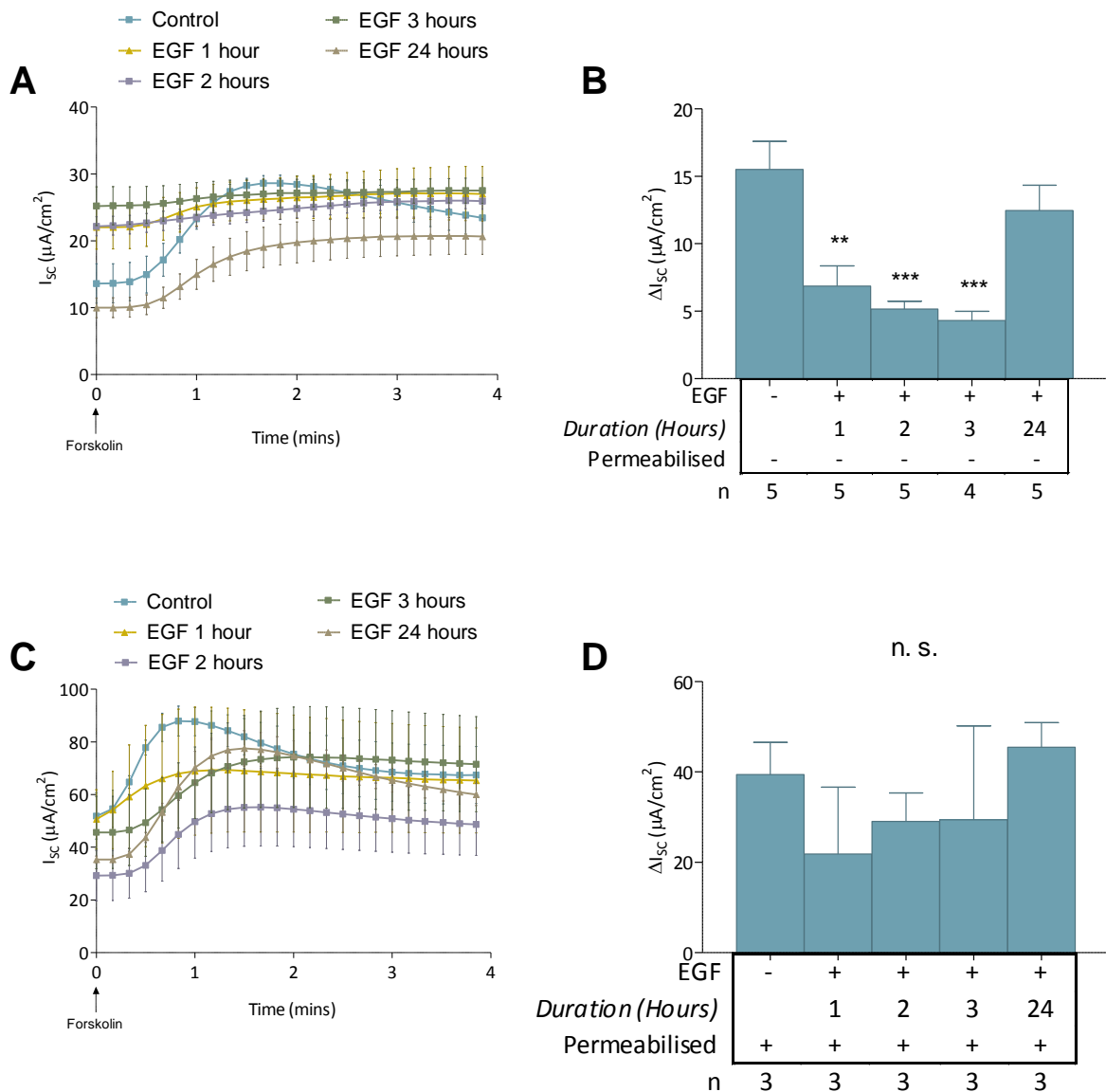


Figure 7.2 – Short term EGF preincubation decreases forskolin response in intact Calu-3 monolayers.
 Combined trace (A) and bar graph (B) showing the effect of 10 ng/ml EGF on forskolin peak current, and a combined trace (C) and bar graph (D) showing the effect of 10 ng/ml EGF on permeabilised monolayers. Statistical analysis was performed using a one way ANOVA with Tukey's Multiple Comparison test, where $P<0.05$ was deemed statistically significant.

7.2.2 EGFR inhibition does not prevent EGF-induced decreases in forskolin stimulated I_{SC}

In order to determine whether the EGF-induced decrease in the forskolin stimulated I_{SC} in Calu-3 monolayers was due to EGF working through the EGFR, the intact Calu-3 monolayers were pretreated with the EGFR inhibitor, AG1478 (Levitzki & Gazit, 1995) for 10 minutes followed by addition of 10 ng/ml EGF to the basolateral side of the monolayers for 1 hour. As shown in Figure 7.3, the forskolin stimulated I_{SC} was reduced to $7.2 \pm 1.7 \mu\text{A cm}^{-2}$ ($n=5$, $P<0.05$), significantly less than monolayers treated with forskolin alone ($15.5 \pm 2.1 \mu\text{A cm}^{-2}$, $n=5$), but not significantly different from monolayers preincubated with 10 ng/ml EGF for 1 hour alone ($6.9 \pm 1.5 \mu\text{A cm}^{-2}$, $n=5$). Thus EGF would seem to not be working through the EGFR to decrease forskolin stimulated current.

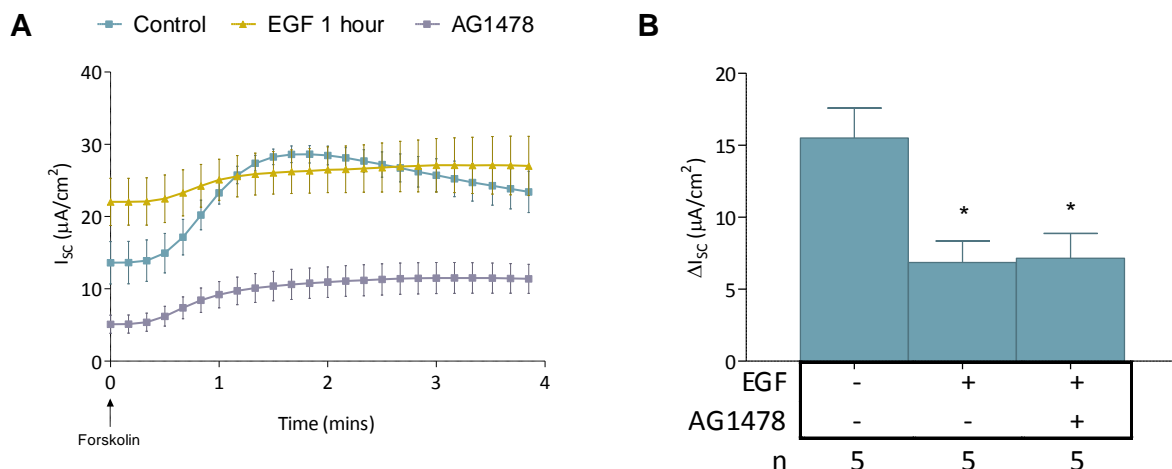


Figure 7.3 – EGFR inhibitor AG1478 does not significantly change EGF induced decreases in forskolin stimulated I_{SC} across Calu-3 monolayers.

Combined traces for the first 4 minutes after forskolin application (A) and a summary bar graph (B) showing the change in I_{SC} across Calu-3 epithelia following 10 μM forskolin treatment in response to basolateral treatment with 5 μM AG1478, a EGFR inhibitor, followed subsequently by 10 ng/ml EGF stimulation for 1 hour. Statistical analysis was performed using a one way ANOVA with Tukey's Multiple Comparison test, where $P<0.05$ was deemed statistically significant.

7.2.3 Protein kinase inhibitors do not prevent EGF-induced decreases in forskolin stimulated I_{SC}

As shown in Figure 7.4 (A and B), pretreatment of Calu-3 monolayers with the PI3K inhibitor, wortmannin (50 μ M), resulted in a forskolin stimulated I_{SC} of $1.4 \pm 0.5 \mu$ A cm^{-2} ($n=4$) which was significantly less than monolayers treated with forskolin alone ($15.5 \pm 2.1 \mu$ A cm^{-2} , $n=5$), but not significantly lower than monolayers preincubated with EGF for one hour alone ($6.9 \pm 1.5 \mu$ A cm^{-2} , $n=5$). To further investigate the signalling pathways involved in this EGF-induced decrease in forskolin stimulated I_{SC} , staurosporine a non-specific protein kinase inhibitor was used. Staurosporine (0.1 μ M) reduced the forskolin stimulated I_{SC} to $4.1 \pm 0.9 \mu$ A cm^{-2} ($n=4$, $P<0.001$) which was significantly less than monolayers treated with forskolin alone ($15.5 \pm 2.1 \mu$ A cm^{-2} , $n=5$), but not significantly different from monolayers preincubated with EGF for 1 hour alone ($6.9 \pm 1.5 \mu$ A cm^{-2} , $n=5$). The PKC specific inhibitor chelerythrine chloride (10 μ M), reduced the forskolin stimulated I_{SC} to $4.1 \pm 0.2 \mu$ A cm^{-2} ($n=4$, $P<0.001$) which was significantly less than monolayers treated with forskolin alone ($15.5 \pm 2.1 \mu$ A cm^{-2} , $n=5$), but not significantly different from monolayers preincubated with EGF for one hour alone ($6.9 \pm 1.5 \mu$ A cm^{-2} , $n=5$). Rottlerin (5 μ M), a PKC δ isoform specific inhibitor reduced the forskolin stimulated I_{SC} to $4.3 \pm 0.9 \mu$ A cm^{-2} ($n=5$, $P<0.001$) which was significantly less than monolayers treated with forskolin alone ($15.5 \pm 2.1 \mu$ A cm^{-2} , $n=5$), but not significantly different from monolayers preincubated with EGF for one hour alone ($6.9 \pm 1.5 \mu$ A cm^{-2} , $n=5$). Taken together these data suggest that the EGF-induced decrease in forskolin stimulated I_{SC} is not mediated through either PI3K or protein kinase C intracellular signalling pathways.

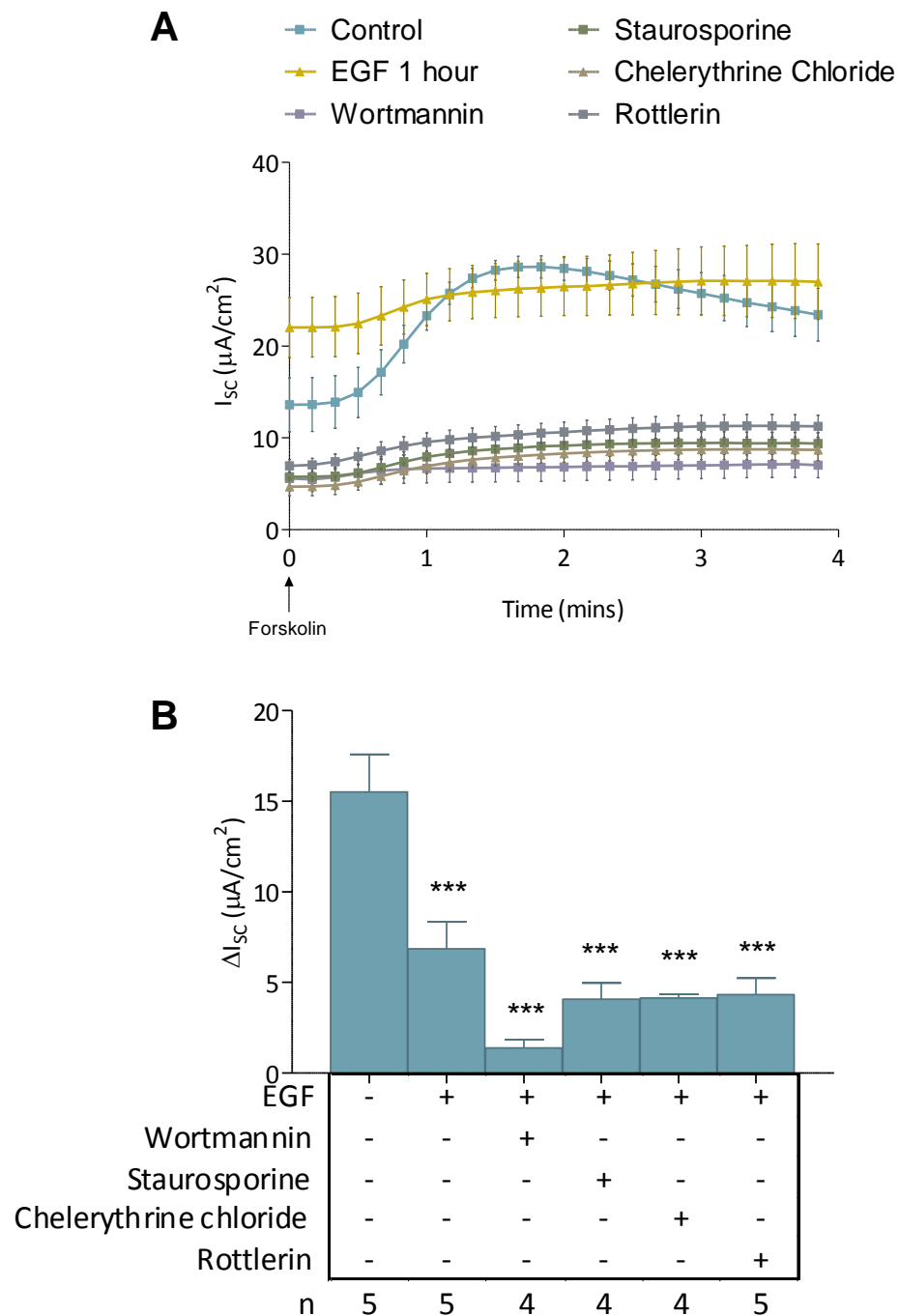


Figure 7.4 – Kinase inhibitors do not significantly change EGF induced decreases in forskolin stimulated Isc across Calu-3 monolayers.

Combined traces for the first 4 minutes after 10 μ M forskolin application (A) and a summary bar graph (B) showing the change in Isc across Calu-3 epithelia following 10 μ M forskolin treatment in response to basolateral treatment with inhibitors including 50 μ M wortmannin, 0.1 μ M staurosporine, 10 μ M chelerythrine chloride and 5 μ M rottlerin, followed subsequently by 10 ng/ml EGF stimulation for 1 hour. Statistical analysis was performed using a one way ANOVA with Tukey's Multiple Comparison test, where $P < 0.05$ was deemed statistically significant.

7.2.4 Chromanol 293B rescues EGF-induced decreases in forskolin stimulated I_{SC}

As shown in Figure 7.5 (A and B), basolateral pretreatment of intact Calu-3 monolayers with non-specific calcium activated potassium channel inhibitor charybdotoxin (1 μ M) for 10 minutes followed by 10 ng/ml EGF treatment for 1 hour reduced the forskolin stimulated I_{SC} to $3.9 \pm 0.7 \mu$ A cm^{-2} (n=5), which was significantly less than monolayers treated with forskolin alone ($15.5 \pm 2.1 \mu$ A cm^{-2} , n=5, P<0.05), but not significantly different from monolayers preincubated with EGF for one hour alone ($6.9 \pm 1.5 \mu$ A cm^{-2} , n=5). Basolateral pretreatment of intact Calu-3 monolayers with KCNN4 specific inhibitor iberiotoxin (10 nM) for 10 minutes followed by 10 ng/ml EGF treatment for 1 hour reduced the forskolin stimulated I_{SC} to $7.4 \pm 1.8 \mu$ A cm^{-2} (n=4), which was not significantly less than monolayers treated with forskolin alone ($15.5 \pm 2.1 \mu$ A cm^{-2} , n=5), but not significantly different from monolayers preincubated with EGF for one hour alone ($6.9 \pm 1.5 \mu$ A cm^{-2} , n=5). Basolateral pretreatment of intact Calu-3 monolayers with KCNQ1 specific inhibitor chromanol 293B (10 μ M) for 10 minutes followed by 10 ng/ml EGF treatment for 1 hour reduced the forskolin stimulated I_{SC} to $13.5 \pm 4.9 \mu$ A cm^{-2} (n=5), which was not significantly different from monolayers treated with forskolin alone ($15.5 \pm 2.1 \mu$ A cm^{-2} , n=5), but not significantly different from monolayers preincubated with EGF for one hour alone ($6.9 \pm 1.5 \mu$ A cm^{-2} , n=5). Taken together these data suggest that the EGF-induced decrease in forskolin stimulated I_{SC} is most likely mediated through KCNQ1 channels. The effects of charybdotoxin excludes KCNN4, KCNA2 and KCNA3, contradicting the iberiotoxin result, thus casting doubt over KCNN4's involvement in the process.

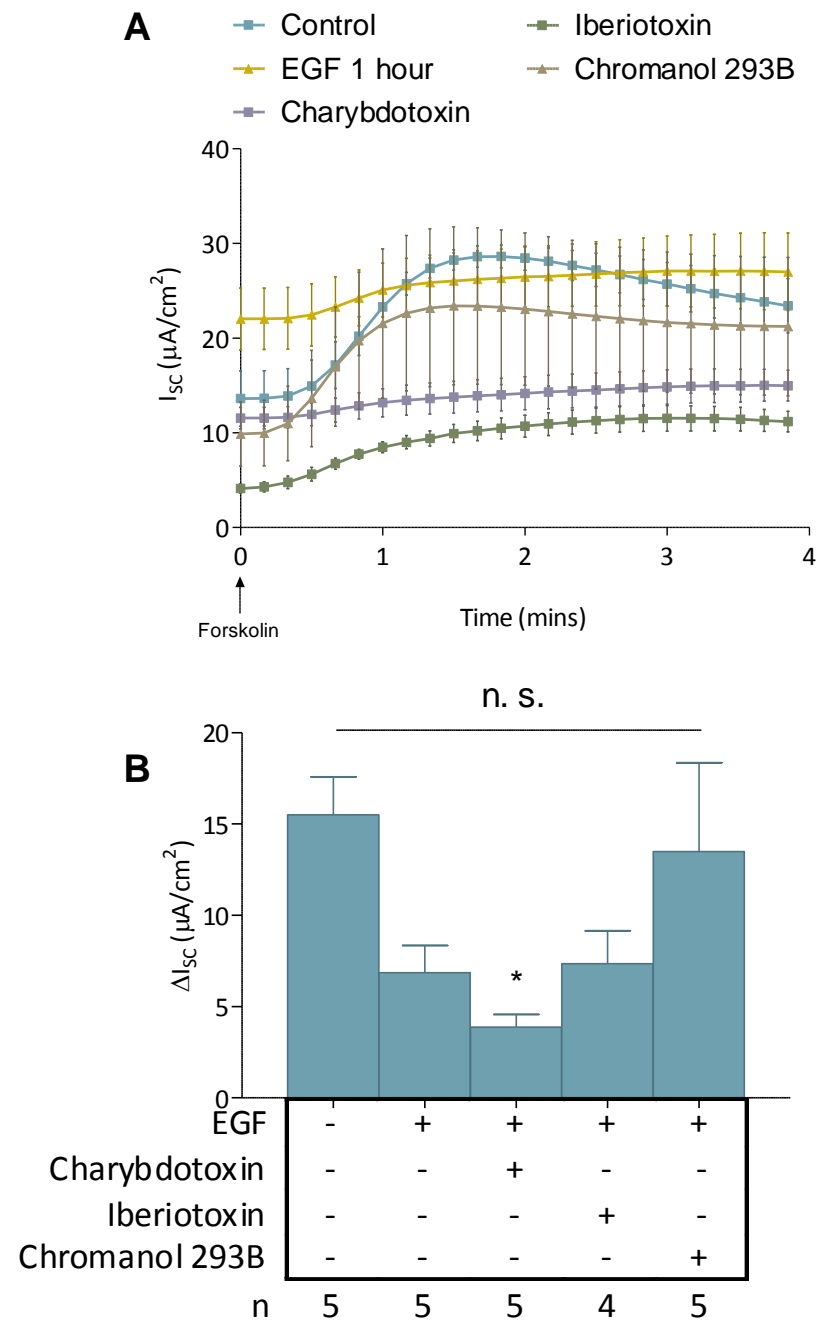


Figure 7.5 – Potassium channel inhibitor chromanol 293B rescues EGF induced decreases in forskolin stimulated I_{SC} across Calu-3 monolayers back to control levels.

Combined traces for the first 4 minutes after 10 μM forskolin application (A) and a bar graph (B) showing the change in I_{SC} across Calu-3 epithelia following forskolin treatment in response to basolateral treatment with inhibitors including 1 μM charybdotoxin, 10 nM Iberiotoxin and 10 μM chromanol 293B, followed subsequently by 10 ng/ml EGF stimulation for 1 hour. Statistical analysis was performed using a one way ANOVA with Tukey's Multiple Comparison test, where $P<0.05$ was deemed statistically significant.

7.2.5 U0126 prevents recovery of EGF induced decreases in forskolin stimulated I_{SC} at 24 hours

To find out if ERK signalling is involved in the EGF induced decreases in forskolin stimulated I_{SC} in Calu-3 cells, the monolayers were treated with U0126 over a period of 24 hours (Figure 7.6, A and B). With 25 μ M U0126 treatment alone on the basolateral side of intact Calu-3 monolayers for 10 minutes, the 10 μ M forskolin response was just $5.9 \pm 0.6 \mu\text{A cm}^{-2}$ ($n=3$) which is significantly different from untreated cells ($15.5 \pm 2.1 \mu\text{A cm}^{-2}$, $n=5$, $p<0.05$). Pretreatment with 25 μ M U0126 for 10 minutes and then 10 ng/ml EGF treatment for 1 hour, 2 hours and 3 hours led to responses of $6.8 \pm 1.0 \mu\text{A cm}^{-2}$ ($n=3$), $14.3 \pm 1.6 \mu\text{A cm}^{-2}$ ($n=3$) and $6.5 \pm 2.0 \mu\text{A cm}^{-2}$ ($n=3$) respectively. With 25 μ M U0126 pretreatment for 10 minutes and then 10 ng/ml EGF treatment for 24 hours, the current increase had not recovered, and remained at $4.0 \pm 1.4 \mu\text{A cm}^{-2}$ ($n=3$). This suggests that in intact membranes, blocking ERK signalling reduces forskolin response and prevents recovery at 24 hours as seen with EGF treatment alone.

In permeabilised membranes with a basal to apical chloride gradient applied, the situation changes (Figure 7.6, C and D). With 25 μ M U0126 treatment on the basolateral side of permeabilised Calu-3 monolayers, the increase in short circuit current due to 10 μ M forskolin on the basolateral side was $106.2 \pm 26.7 \mu\text{A cm}^{-2}$ ($n=3$). With a 10 minute pretreatment of 25 μ M U0126 followed by a 1 hour pretreatment with 10 ng/ml EGF on the basolateral side, the current increase due to 10 μ M forskolin treatment is less at $55.8 \pm 12.9 \mu\text{A cm}^{-2}$ ($n=3$). Similarly after 2 hours, the increase from 10 μ M forskolin treatment was $72.1 \pm 8.3 \mu\text{A cm}^{-2}$ ($n=3$), and at 3 hours, the increase is $47.6 \pm 23.0 \mu\text{A cm}^{-2}$ ($n=3$). By 24 hours, the increase in current from 10 μ M forskolin has somewhat recovered to $89.2 \pm 11.5 \mu\text{A cm}^{-2}$ ($n=3$). These results are not statistically significant however due to large variation in the results. Taken together, these permeabilised results suggest that inhibiting ERK with U0126 appears to overall increase short circuit current in EGF treated Calu-3 monolayers compared to without U0126 treatment (seen previously in Figure 7.2), suggesting that the ERK signalling which subsequently occurs after EGF signalling negatively regulates ion transport in permeabilised Calu-3 monolayers.

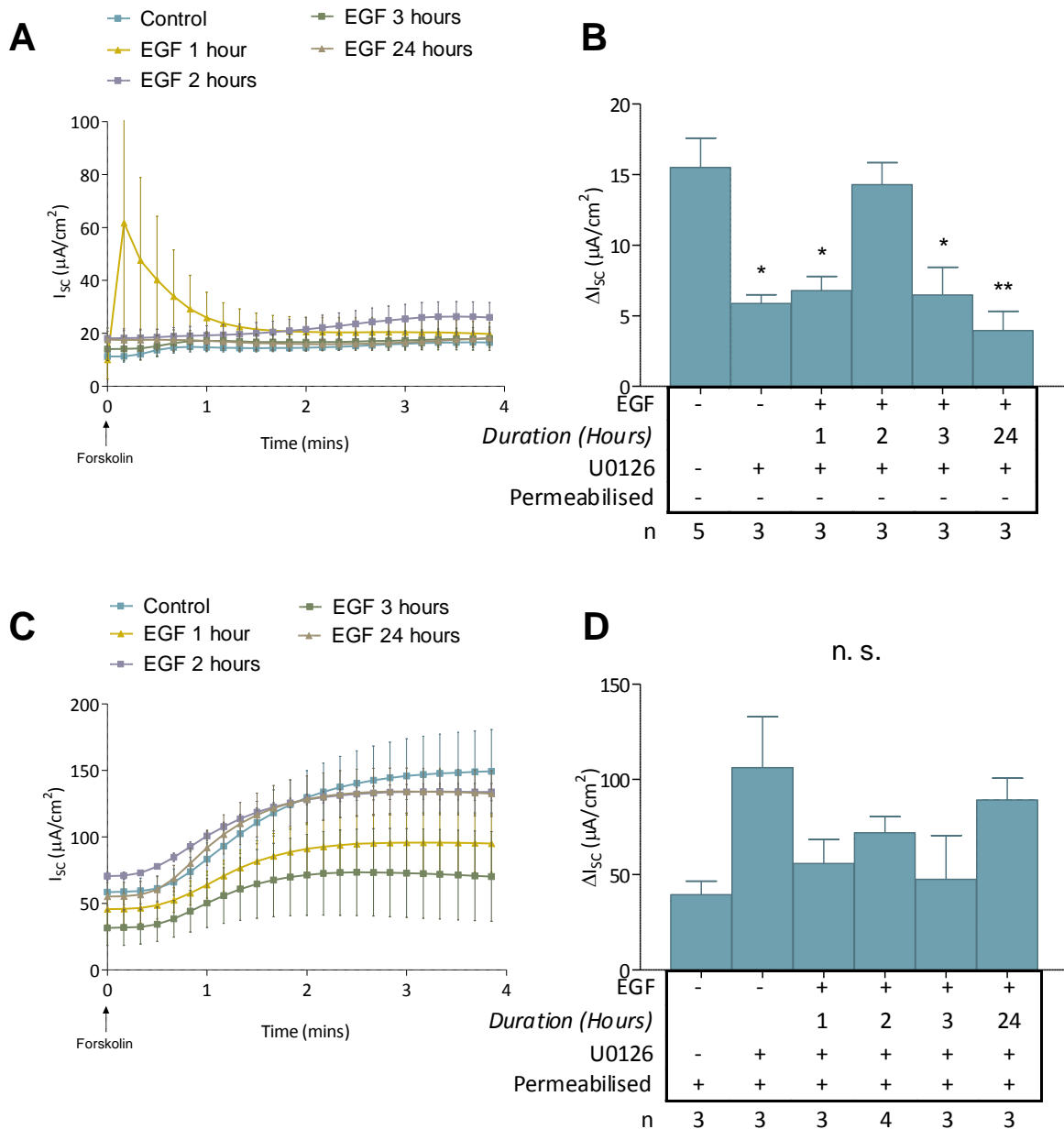


Figure 7.6 – U0126 further decreases EGF induced decreases in forskolin stimulated I_{sc} .

Combined trace (A) and summary bar graph (B) showing the effects of 25 μ M U0126 and 10 ng/ml EGF on 10 μ M forskolin peak current, and a combined trace (C) and bar graph (D) showing the effect of U0126 and EGF on permeabilised monolayers. Statistical analysis was performed using a one way ANOVA with Tukey's Multiple Comparison test, where $P<0.05$ was deemed statistically significant.

7.2.6 Does EGF work via transactivation of the β_2 adrenergic receptor?

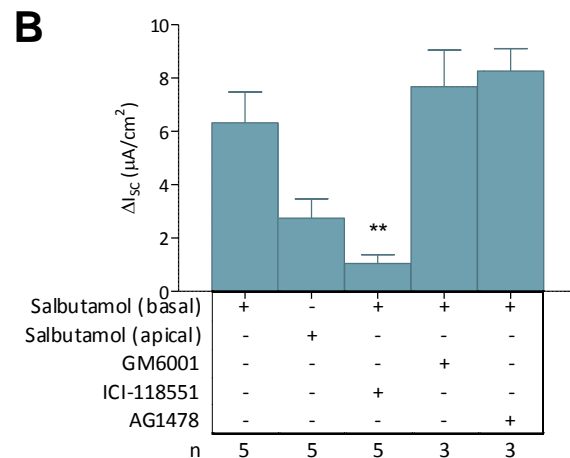
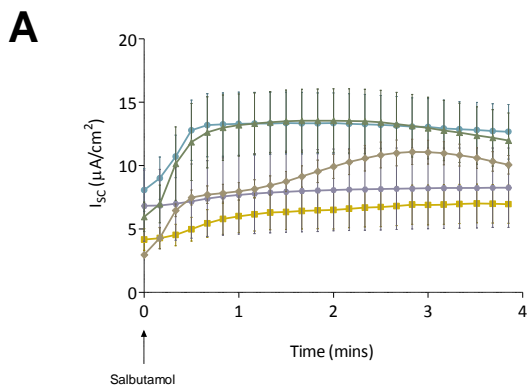
Firstly, to determine whether the apical or basolateral side of the Calu-3 monolayer had the greatest amount of β_2 adrenergic receptors, the monolayers were treated with β_2 agonist salbutamol on each side (Figure 7.7, A and B). Basolateral treatments of 1 μM salbutamol resulted in an increase of $6.3 \pm 1.2 \mu\text{A cm}^{-2}$ ($n=5$), whereas apical treatment only resulted in an increase of $2.7 \pm 0.7 \mu\text{A cm}^{-2}$ ($n=5$). Since treating the basolateral membrane consistently gave the biggest response, further experiments conducted involved only the treatment of the basolateral side. To determine if salbutamol was working through the β_2 adrenergic receptor as expected, β_2 antagonist ICI-118551 (10 μM) was preincubated on the basolateral side for 10 minutes prior to experiment. The salbutamol response was reduced to $1.0 \pm 0.3 \mu\text{A cm}^{-2}$ ($n=5$), which was statistically different from basolateral treatment with salbutamol alone ($p<0.01$). Taken together, this result shows that salbutamol stimulation in Calu-3 cells leads to an activation of the β_2 adrenergic receptor.

To determine whether the effect of EGF is a direct effect or whether it involves transactivation of EGFR via metalloproteinase induced HB-EGF shedding (Figure 7.7, A and B), cells were pretreated on the basolateral side with metalloproteinase inhibitor GM6001 (1 μM). Subsequent treatment with salbutamol resulted in a current of $7.7 \pm 1.4 \mu\text{A cm}^{-2}$ ($n=3$), a similar magnitude to salbutamol alone and not statistically significant. To further clarify if EGFR was involved in β_2 induced CFTR signalling, EGFR inhibitor AG1478 (5 μM) was preincubated on the basolateral side of intact Calu-3 monolayers for 10 minutes, followed by 1 μM salbutamol. This resulted in a short circuit current of $8.3 \pm 0.8 \mu\text{A cm}^{-2}$ ($n=3$), a similar magnitude to salbutamol alone and not statistically significant. From these findings, transactivation of the EGFR was ruled out as a possibility for the regulation of CFTR via EGF.

To further investigate the effect of forskolin treatment, Calu-3 monolayers were stimulated with 10 μM forskolin on the basolateral and apical sides alone, to see which side produced the biggest response (Figure 7.7, C and D). Basolateral treatment alone resulted in an increase in short circuit current of $15.5 \pm 2.1 \mu\text{A cm}^{-2}$ ($n=5$), whereas treatment on the apical side alone resulted in a response of just $8.1 \pm 1.3 \mu\text{A cm}^{-2}$ ($n=3$), the difference between the two being statistically significant ($p<0.01$). 10 ng/ml EGF pretreatment for one hour on the basolateral side reduces the

basolateral forskolin response to $6.9 \pm 1.5 \mu\text{A cm}^{-2}$ (n=5, p<0.01). Pretreatment with both 10 ng/ml EGF and 10 μM ICI-118551 resulted in a response of $4.7 \pm 0.3 \mu\text{A cm}^{-2}$ (n=5) that was again smaller than the basolateral 10 μM forskolin response by a statistically significant amount (p<0.01). It was also smaller than the response of 10 ng/ml EGF treatment alone, but was not statistically significant. This was expected since forskolin does not act via the β_2 receptor, but via activation of adenylate cyclase directly. Basolateral pretreatment with adenylate cyclase inhibitor MDL-12330A (20 μM) resulted in a forskolin response of just $2.7 \pm 0.5 \mu\text{A cm}^{-2}$ (n=3), which was a reduction from the basolateral response to forskolin alone by a statistically significant amount (p<0.001). Taken together, this result demonstrates that forskolin is working through adenylate cyclase to increase I_{sc} in Calu-3 cells, and that basolateral forskolin stimulation leads to a bigger increase in I_{sc} compared to apical stimulation.

● Salbutamol (basolateral) ■ Salbutamol (apical)
▲ GM6001 + Salbutamol ◆ AG1478 + Salbutamol
● ICI-118551 + Salbutamol



● Forskolin (basolateral) ■ Forskolin (apical)
● EGF ◆ ICI-118551 + EGF
▲ MDL-12330A

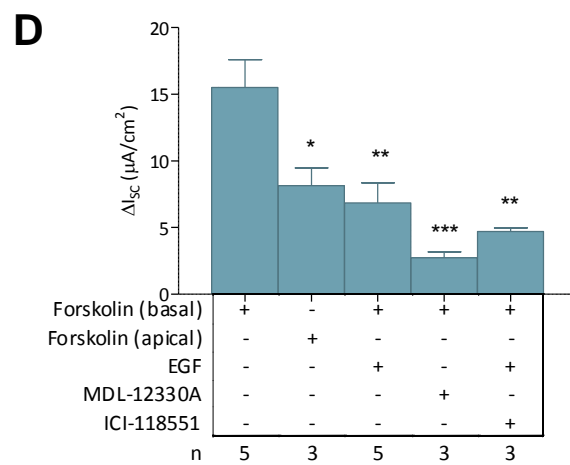
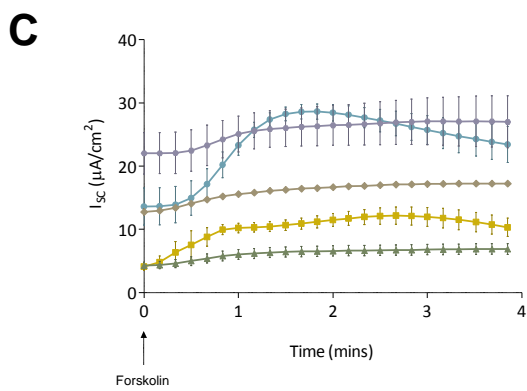


Figure 7.7 – Transactivation by the β_2 adrenergic receptor does not occur in Calu-3 monolayers.

Combined traces (A) and summary bar graph (B) depicting β_2 adrenergic receptor mechanisms, and combined traces (C) and summary bar graph (D) of forskolin related mechanisms. Statistical analysis was performed using a one way ANOVA with Tukey's Multiple Comparison test, where $P<0.05$ was deemed statistically significant.

7.2.7 β_3 adrenergic receptor - a minor regulator of ion transport in Calu-3?

The characterisation of the β_3 adrenergic receptor has not been previously demonstrated in the Calu-3 cell line. In order to go about this, specific β_3 agonist CGP-12177 was used to treat Calu-3 monolayers on the basolateral side in the Ussing chamber set up as described previously. CGP-12177 had not previously been used to stimulate Calu-3 cells; so firstly, a dose response experiment was conducted using different concentrations of the compound (Figure 7.8, A and B). A concentration of 0.1 μM resulted in a response of $0.8 \pm 0.3 \mu\text{A cm}^{-2}$ ($n=3$), 1 μM CGP-12177 resulted in a response of $1.1 \pm 0.6 \mu\text{A cm}^{-2}$ ($n=3$), and 10 μM CGP-12177 resulted in a response of $0.6 \pm 0.2 \mu\text{A cm}^{-2}$ ($n=3$). To determine which side of the membrane gave the biggest response, 1 μM CGP-12177 was applied to the apical side only, resulting in a negligible response of $0.2 \pm 0.2 \mu\text{A cm}^{-2}$ ($n=3$). Taken together, these results suggest that 1 μM CGP-12177 on the basolateral side gave a maximal response and was used for all subsequent experiments.

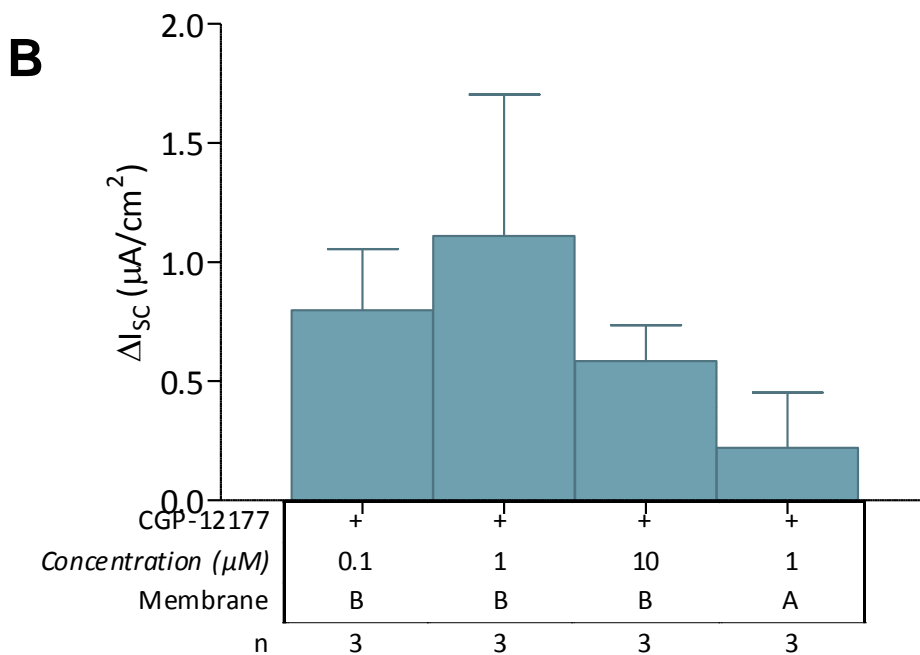
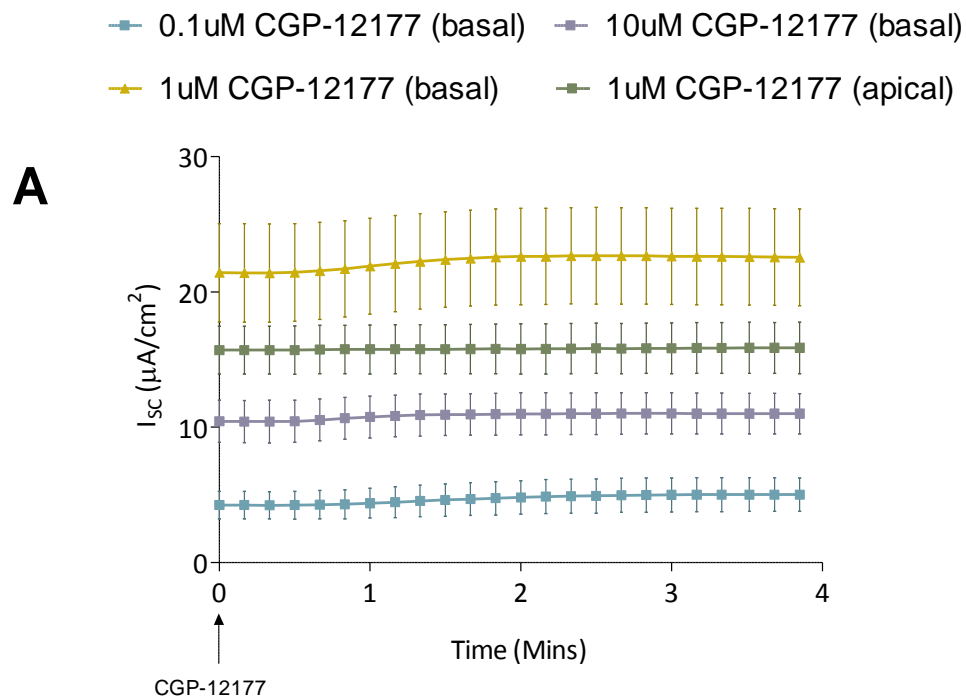


Figure 7.8 – Dose response to determine of the maximal response to CGP-12177.

Combined traces (A) and summary bar graph (B) showing a dose response curve of β_3 adrenergic receptor agonist CGP-12177. Statistical analysis was performed using a one way ANOVA with Tukey's Multiple Comparison test, where $P<0.05$ was deemed statistically significant.

7.2.8 How is the β_3 adrenergic receptor regulated in Calu-3?

To determine how the β_3 adrenergic receptor regulates ion transport, inhibitors were used of several common pathways, including wortmannin, MDL-12330A and U0126, as well as using β_3 receptor antagonist L-748,337 (Figure 7.9, A and B). Pretreatment with 50 μM wortmannin on the basolateral side resulted in a CGP-12177 response of just $0.1 \pm 0.0 \mu\text{A cm}^{-2}$ ($n=3$), effectively eliminating the response, although not statistically different (likely due to the small currents involved). It is very likely that PI3K is involved in the pathway. Pretreatment with 25 μM U0126 on the basolateral side resulted in a CGP-12177 response of $1.0 \pm 0.3 \mu\text{A cm}^{-2}$ ($n=3$), which was very similar to the control response, so it is likely that the response from stimulating the β_3 receptor is MAPK independent. Pretreatment with 20 μM MDL-12330A resulted in a CGP-12177 response of just $0.1 \pm 0.0 \mu\text{A cm}^{-2}$ ($n=3$), also eliminating the response, indicating that adenylate cyclase is likely activated in the response. Pretreatment with 10 μM L-748,337 on the basolateral side resulted in a CGP-12177 response of $0.5 \pm 0.2 \mu\text{A cm}^{-2}$ ($n=3$), reducing the response by approximately half.

To further explore the mechanisms behind β_3 receptor signalling, the basolateral membrane of the Calu-3 monolayers were permeabilised, and the same pretreatments of wortmannin, MDL-12330A, U0126 and L-748,337 were applied as before (Figure 7.9, C and D). Firstly, an initial experiment was performed by simply stimulating untreated permeabilised Calu-3 monolayers with 1 μM CGP-12177, resulting in a short circuit current of $9.4 \pm 5.0 \mu\text{A cm}^{-2}$ ($n=3$). Pretreatment with 50 μM wortmannin on the basolateral side followed by stimulation with 1 μM CGP-12177 resulted in a response of $21.9 \pm 7.6 \mu\text{A cm}^{-2}$ ($n=3$), greater than treatment with CGP-12177 alone, but not statistically significant. Pretreatment with 25 μM U0126 on the basolateral side followed by stimulation with 1 μM CGP-12177 resulted in a response of $5.2 \pm 2.3 \mu\text{A cm}^{-2}$ ($n=3$), less than treatment with CGP-12177 alone but not statistically significant. Pretreatment with 20 μM MDL-12330A on the basolateral side followed by stimulation with 1 μM CGP-12177 resulted in a response of $9.8 \pm 2.1 \mu\text{A cm}^{-2}$ ($n=3$), very similar to treatment with CGP-12177 alone. Pretreatment of permeabilised monolayers with 10 μM L-748,337 on the basolateral side and subsequent stimulation with 1 μM CGP-12177 resulted in a response of $9.3 \pm 3.2 \mu\text{A cm}^{-2}$ ($n=3$), again, very similar to that of CGP-12177 treatment alone.

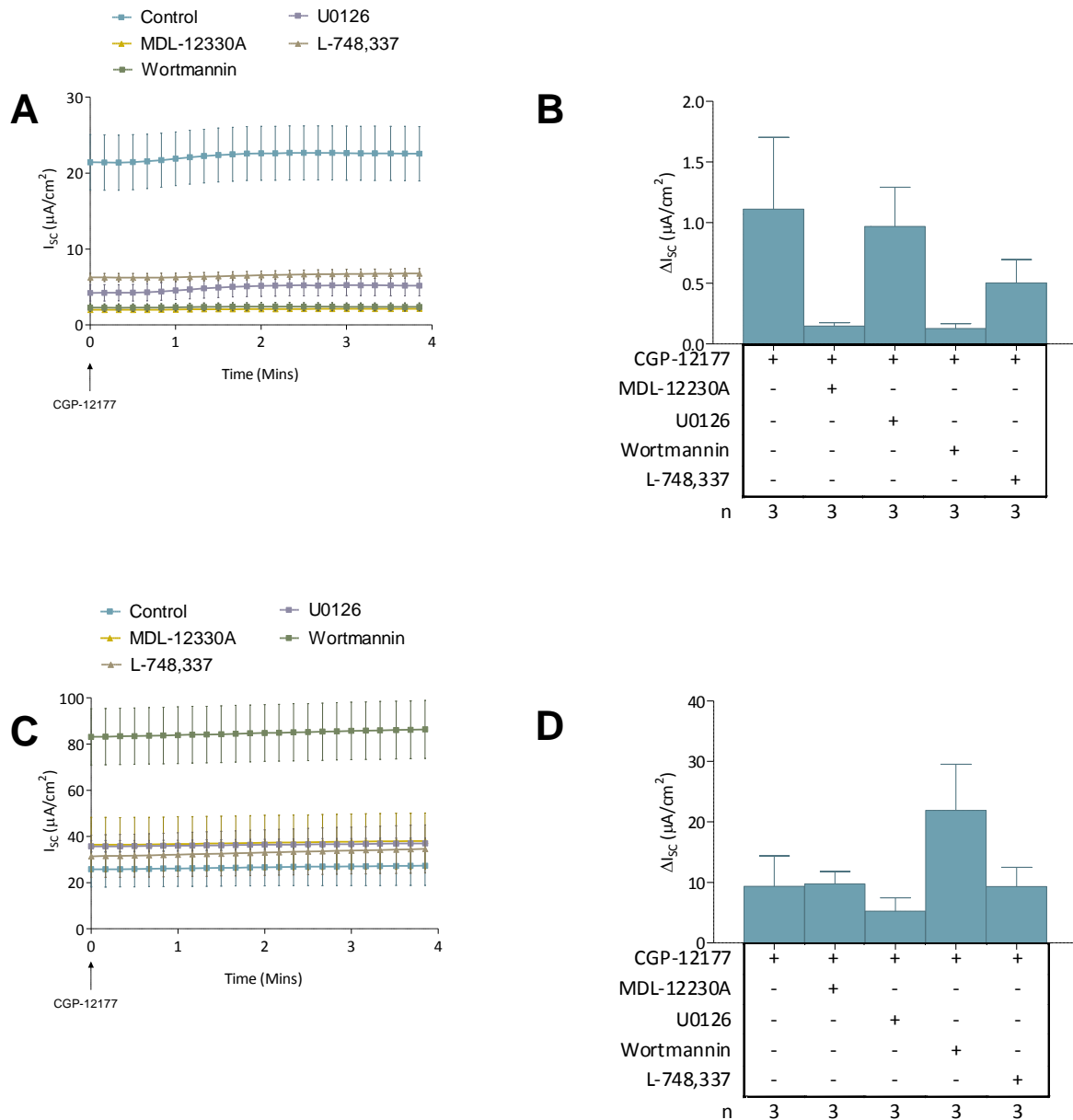


Figure 7.9 – β_3 adrenergic receptor is potentially regulated by adenylate cyclase and PI3K in Calu-3 cells.
 Combined traces and bar graphs to show β_3 adrenergic receptor mechanisms in intact (A, B) and permeabilised membranes (C, D). Statistical analysis was performed using a one way ANOVA with Tukey's Multiple Comparison test, where $P < 0.05$ was deemed statistically significant.

7.2.9 Beta Receptors 1, 2 and 3 are expressed in the Calu-3 cell line

The expression of Beta 1, 2 and 3 receptors was tested in the Calu-3 cell line with three repeats using a different RNA sample each time (Figure 7.10). It was seen that all three receptors were present, with the strongest signal being that of the β_2 receptor, and the weakest being the β_3 receptor.

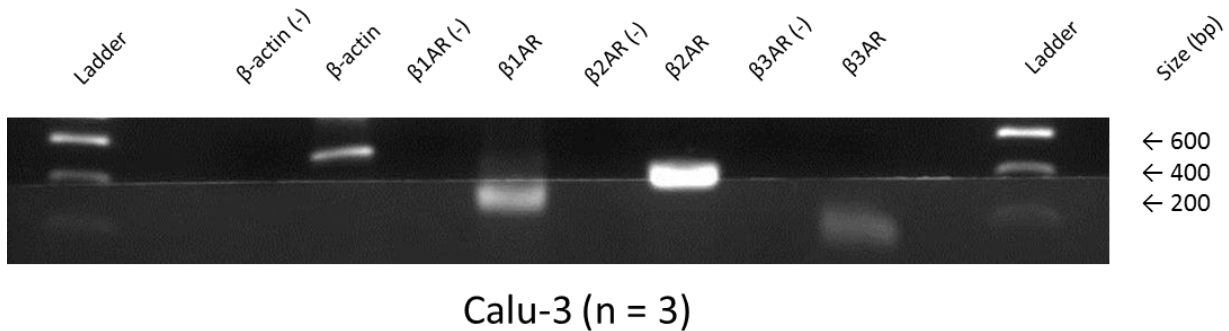


Figure 7.10 – Beta receptor expression in Calu-3 cells, showing expression of all three receptors.

Bands correspond to the correct band size for each gene (212bp for β_1 , 287bp for β_2 and 122 bp for β_3). RT-PCR consisted of 3 repeats using different RNA samples.

7.3 Discussion

7.3.1 EGF pretreatment suppresses forskolin stimulation in Calu-3 monolayers

It was noted that forskolin stimulation upon preincubation of EGF was reduced as the initial currents increased, before returning to normal at 24 hours. From the traces shown in Figure 7.2, it can be seen that the relationship between forskolin stimulation and EGF treatment is complex, with the data showing at least two processes involved at the same time. The first process that occurs is the increase in initial current from EGF treatment, as described in detail in Chapter 5. The second process is the suppression of forskolin stimulation by EGF. In isolated pancreatic acinar membranes, it was seen that forskolin, vasoactive intestinal peptide (VIP) and EGF were able to increase cAMP production. Treatment with anti- $G_s\alpha$ antibodies abolished both the EGF and VIP induced cAMP production but not forskolin-induced cAMP production. Importantly, when either VIP or forskolin is present, EGF inhibits both VIP and forskolin-induced cAMP production with an IC_{50} of 5 nM. These data suggested that in pancreatic acinar membranes, EGF regulates adenylate cyclase via the activation of G_s and G_i proteins and tyrosine phosphorylation (Stryjek-Kaminska *et al.*, 1996). In the heart, EGF stimulates adenylate cyclase via the activation of the G protein subunit G_s (Sun *et al.*, 1995). A region resembling the peptide sequence in the β_2 -adrenergic receptor that activates G_s has been found in rat EGFR. This 13-aa region spans Arg⁶⁴⁶-Arg⁶⁵⁸ with the sequence RRREIVRKRTLRR and immediately follows the transmembrane region that spans Ile⁶²³-Met⁶⁴⁵ (Okamoto *et al.*, 1991). Activated EGFR initially leads to stimulated GTP binding and GTPase activity of G_s and not the inhibitory G protein, G_i . At the same time, EGFR activation leads to phosphorylation of PKC, which in turn decreases the ability of EGFR to stimulate G_s . PKC also leads to an increase in the GTPase activity of the inhibitory G protein subunit, G_i . The G_i protein can then inhibit the activities of adenylate cyclase (Sun *et al.*, 1995). The data obtained in this chapter represented by Figure 7.2, this time in Calu-3 cells, agrees with this finding.

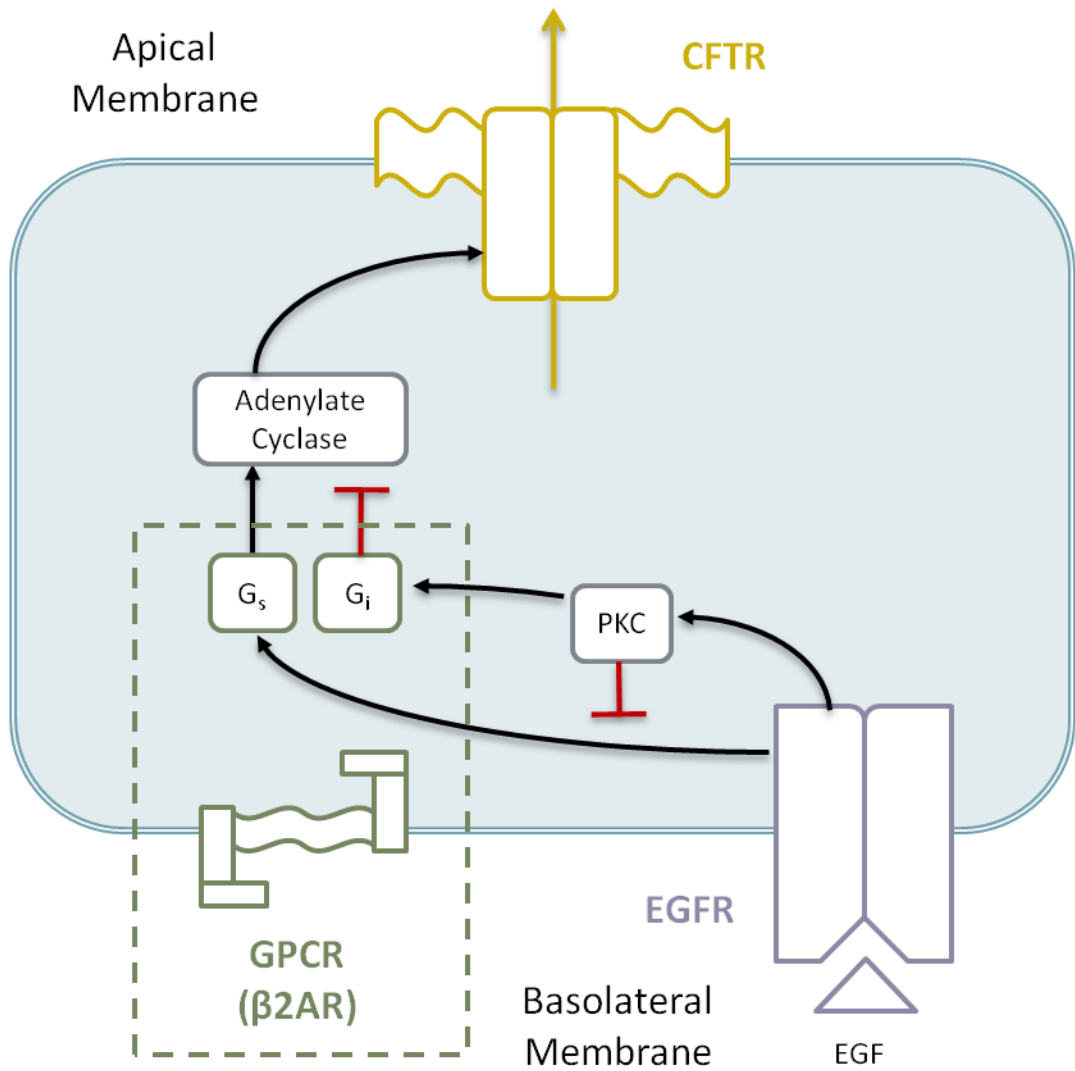


Figure 7.11 – Proposed model of the effect of EGF treatment on adenylate cyclase in Calu-3 cells.

Activation of EGFR leads to activation of G_s and protein kinase C (PKC). PKC activation leads to a decreased ability of EGFR to activate G_s and an increase in GTPase activity of G_i . G_i then inhibits adenylate cyclase, preventing chloride secretion through CFTR. Based on data from this investigation and data from: (Sun *et al.*, 1995; Stryjek-Kaminska *et al.*, 1996)

In our Calu-3 based system (Figure 7.11), activation of EGFR by EGF activates PKC (evidenced by data shown in Chapter 5). This in turn would lead to attenuation of G_s activity over the period of 1-3 hours EGF incubation and increase in G_i activation and adenylate cyclase inhibition. This ultimately leads to the decrease in stimulated forskolin response seen in the data of this chapter. Further work could use the G_i inhibitor, pertussis toxin (PTX), to investigate the effects of the G_i subunit in more detail (See Further work, Section 8.4).

7.3.2 Chromanol 293B pretreatment restores forskolin response in EGF treated Calu-3 monolayers

It was seen that EGFR inhibitors did not restore the control forskolin response, suggesting that the effect of EGF was independent of EGFR. Protein kinase inhibitors such as wortmannin and various PKC inhibitors appeared to further decrease the short circuit current rather than restore the current back to the control level of stimulation seen. This suggests that PI3K and PKC are important regulators of ion transport, likely via multiple processes. Inhibition of these proteins leads to a large reduction in both initial current and forskolin stimulated short circuit current, so may or may not conflict with work carried out previously in the heart (Sun *et al.*, 1995). The data in this study concerning forskolin and PKC inhibitors are in agreement with a previous study where responses to forskolin plus CPT-cAMP in Calu-3 cells were also found to be markedly sensitive to preincubation with the PKC inhibitor, chelerythrine (Liedtke & Cole, 1998). In their study, chelerythrine reduced peak Cl^- efflux to rates observed in cells treated only with the vehicle. Inhibition by chelerythrine was found to remove 69.4% of the peak Cl^- efflux in CHO-wtCFTR cells and 79.2% of peak Cl^- efflux in Calu-3 cells (Liedtke & Cole, 1998). Our novel data differs from this study in that EGF was preincubated with the inhibitor as well. In terms of potassium channels, it was clear that inhibiting KCNQ1 in the presence of EGF restored forskolin response to near control levels, indicating that the channel is affected by EGF and decreases forskolin response by an as yet unknown mechanism. In a normal situation with no other treatments, forskolin is known to raise intracellular cAMP by adenylate cyclase and thus can activate KCNQ1, increasing ion transport (Boucherot *et al.*, 2001). Blocking KCNQ1 could only decrease ion transport after activation of forskolin in this situation due to decreased driving force for anion exit in this simplified situation. Our system however has EGF present on the basolateral membrane for 1 hour in addition

to the above. With our results, we do not see a decrease, but an increase in forskolin response. Perhaps since EGF can activate both KCNN4 channels as well as KCNQ1 channels, raising the initial current, inhibiting KCNQ1 could prevent a raise in initial current allowing forskolin to have a larger effect by activating CFTR. Iberiotoxin and charybdotoxin treatment may eliminate more channels overall as KCNN4 is highly expressed in Calu-3, thus decreasing chloride channel driving force rather than increasing it like chromanol 293B. It is very likely that additional processes or signalling pathways are involved in the process that are not investigated here.

7.3.3 The EGF induced decrease in forskolin stimulated I_{SC} at 24 hours is blocked by U0126

Moreover, pretreatment with U0126 prevents the recovery following treatment of Calu-3 monolayers with EGF for 24 hours. This suggests that ERK signalling after pretreatment with EGF may be responsible for the recovery of forskolin stimulation over 24 hours. In a study that bears similarities to data presented in this chapter, it has been demonstrated previously in rabbit colonocytes that EGF acts via EGFR and the MAPK signalling pathway to increase chloride transport. Inhibitors of this pathway (genistein, AG1478, and PD98059) prevented chloride stimulation (Carlos *et al.*, 2007).

7.3.4 EGFR transactivation via stimulation of β_2 adrenergic receptor does not occur in Calu-3 monolayers

It has been previously demonstrated that TNF- α induces MMP-9 release, EGF ligand shedding and EGFR transactivation in airway epithelial cells. TNF- α treatment increases wound closure rates in NuLi and CuFi cells, which can be prevented by GM-6001, anti-EGF antibodies and tyrosine kinase inhibitors (Maille *et al.*, 2011a). However, our data does not follow these results. Given that the magnitude of the salbutamol response is virtually identical for AG1478, GM-6001 and the control response, transactivation likely does not occur. The trace for AG1478 pretreatment does show some delay in reaching the same ΔI_{SC} after treatment with salbutamol, which may suggest that some endogenous EGFR activity may possibly be present, which would require further testing to explore in more detail. The transactivation process described in detail in the literature appears not to occur in Calu-3 (Liebmann, 2011).

7.3.5 Adenylate cyclase and PI3K blockers prevent β_3 adrenergic receptor induced ion transport in Calu-3 monolayers

A previous study utilised A549 cells that had been simultaneously transfected with β_3 adrenergic receptor and CFTR (Robay *et al.*, 2005). In this artificial system, of interest was to investigate the effect of β_3 adrenergic receptor on CFTR response using microcytometry. It was discovered that CGP-12177 response could be inhibited in this system by the $G_{i/o}$ inhibitor pertussis toxin (PTX), PI3K inhibitors wortmannin and LY-294002 and ERK1/2 inhibitors including PD-98059 and U0126. It was not seen that PKA was involved in the process. From this, the authors concluded that transfected β_3 adrenergic receptors could activate CFTR response through $G_{i/o}$ -PI3K-ERK-MAPK pathway (Robay *et al.*, 2005). Our system does not involve transfection and is only looking at endogenous levels of β_3 receptors and CFTR in Calu-3 cells in a short circuit current set up. Our results suggested that PI3K was also involved, however, we determined that there was also likelihood of involvement of adenylate cyclase, but probably not ERK1/2 as found previously.

7.3.6 Beta adrenergic receptors are expressed in Calu-3

Beta 2 adrenergic receptors are shown to be expressed in our data and have been known to be expressed in Calu-3 cells from previous studies (Abraham *et al.*, 2004). Beta 1 and 3 adrenergic receptors have not been previously been shown to be expressed in Calu-3 cells, but have previously been shown to be expressed in other airway epithelial cell lines such as 16HBE14o⁻ as well as from explanted samples of CF and non-CF bronchi from patients (Bossard *et al.*, 2011).

Chapter 8 Final Discussion

8.1 Overview

Mutations in the CFTR channel can lead to decreased chloride ion transport in epithelial tissues resulting in disease conditions such as CF (The Cystic Fibrosis Genetic Analysis Consortium, 1994). As a result, novel pharmacological strategies have been proposed to increase chloride secretion to treat the disease.

Recent strategies involve high-throughput screening of compounds to find correctors and potentiators of the CFTR channel (Van Goor *et al.*, 2009; Van Goor *et al.*, 2011). This strategy has already proved to be successful in clinical trials with the approval of VX-770 to treat CF children 6 years or younger with the G551D mutation, and with combination treatments of VX-770 and VX-809 currently in phase 2 for Δ F508 mutations (See section 1.3.5.2 for further details). Other strategies employed involve increasing the transport of other channels such as calcium activated chloride channels to increase chloride ion transport. Moreover, it was seen that EGF was present and elevated during lung disease conditions (Mercer *et al.*, 2006), and that it may affect ion transport in the lung. EGF has been shown to induce the gelatinase, MMP-9, via the JNK signalling pathway (Poitras *et al.*, 2003). MMP-9 is involved in tissue remodelling and repair in the airway (Bove *et al.*, 2007). While the effect of EGF and its related signalling pathways on chloride secretion in the gut have been widely studied (McCole *et al.*, 2002; McCole & Barrett, 2009), the effect of EGF on ion transport in the airway has yet to be investigated. Currently, there are no studies that have used the Calu-3 cell line to study EGF and its effects on chloride transport. In order to address this gap in knowledge, this study looked principally into the effects of EGF on chloride transport using Ussing chamber studies. Experiments involved the preincubation of Calu-3 monolayers with EGF over a period of hours to 1 day and the short circuit currents measured. Areas of study included:

- (i) Characterisation of the effects of stimulants and determining the expression of chloride channels and candidates in the Calu-3 cell line (Chapter 3)
- (ii) The effect of MMPs on ion transport (Chapter 4)
- (iii) The effect of EGF on initial short circuit current (Chapter 5)

- (iv) The effect of EGF on UTP stimulated ion transport (Chapter 6)
- (v) The effect of EGF on forskolin and beta receptor stimulated short circuit current and possible transactivation of EGFR (Chapter 7).

8.2 Summary of Findings

8.2.1 Characterisation of chloride channels in the Calu-3 cell line

In order to understand the processes which can regulate ion transport in the Calu-3 cell line, it was necessary to determine baseline levels upon stimulation with forskolin and UTP with and without basolateral membrane permeabilisation and application of a chloride gradient. The important outcomes generated from this data set include the fact that forskolin generated a short circuit current in Calu-3 cells, which is increased further when the basolateral membrane is permeabilised. This is strong evidence that the Calu-3 cells used in our experiments were responding normally to the adenylate cyclase activator. Calcium chelator BAPTA-AM appeared to remove the peak phase of the standard response curve from forskolin, indicating that the peak phase may be calcium-dependent. In contrast, UTP responses were so small that they were not considered to be statistically significant from baseline readings, and basolateral membrane permeabilisation did not change this. This is important since it shows that receptors that respond to UTP (such as P2Y) are not major transporters in Calu-3 cells under unstimulated conditions.

Since the results from short circuit current indicated that channels such as CaCCs may not be major transporters in Calu-3 cells, this may have been due to little to no expression of CaCC candidates at the message and protein levels. Therefore the question was to determine which CaCC candidate genes were expressed in Calu-3 cells, with A549 and CFPAC cell lines used as a comparison. Despite the fact that expression of CaCCs in the cell lines Calu-3, A549 and CFPAC have been studied in some depth previously (Kunzelmann *et al.*, 2009), there were some gaps in knowledge, such as the expression of bestrophins 1 – 4 in the A549 cell line has not been shown. To address these gaps in current knowledge, the expression of all bestrophins and anoctamins was carried out in all three cell lines. It has been demonstrated in this study that there is expression of a wide array of chloride

channels and candidates in Calu-3 cells, suggesting that the CaCC candidates could potentially remain inside the cell and not expressed on the cell membrane.

8.2.2 Effect of MMPs on ion transport in the Calu-3 cell line

It has been previously been demonstrated that MMP inhibitors such as 1,10-phenanthroline could act as CFTR openers in the Calu-3 cell line (Duszyk *et al.*, 1999; Duszyk *et al.*, 2001), but the mechanism involved in this process was unknown. To address this gap in knowledge, experiments were designed with the intention of verifying results using other inhibitors such as GM-6001 and then extend the investigation to influences of EGF and basolateral potassium channels for potential signalling pathways potentially involved in the process.

It was discovered that metalloproteinases were unlikely to be involved in modulating chloride currents such as those transmissible through CFTR. Broad spectrum MMP inhibitor GM-6001 did not activate chloride currents in the Calu-3 cell line, and addition of recombinant MMP-2 did not inhibit chloride currents. These data appeared to directly contradict prior work by Duszyk *et al.*, 1999, suggesting that the inhibitor used previously (1,10-phenanthroline) may have had a direct effect on the CFTR channel rather than inhibiting MMPs that were in turn inhibiting the channel. This information is significant in that it shows that MMP inhibitors in general may in fact not be CFTR openers and thus be a means for treating cystic fibrosis.

8.2.3 EGF signalling increases chloride driving force in the Calu-3 cell line

The effect of EGF on ion transport in the gut has been widely reported and the mechanisms involved are comparatively well understood (McCole & Barrett, 2009). However in the airway, the effect of EGF treatment on ion transport is largely unknown, especially in the submucosal cell line Calu-3 where no studies have been previously conducted. We hypothesised that EGF would have a similar effect on ion transport as seen in the gut, so in order to address this gap in knowledge, experiments were designed so that Calu-3 monolayers were preincubated with EGF over a period of time up to 24 hours and the initial currents measured.

It was seen that EGF raised initial current at 1 hour compared to controls, suggesting that EGF was activating a signalling pathway or activating channels directly. This was

a very important discovery since this was a completely novel means of increasing ion transport across the Calu-3 monolayers and so warranted further investigation. The important question then became that of how EGF was bringing about these effects, as at this early point, there were many potential candidates. By performing experiments with Calu-3 monolayers and basolateral membrane permeabilisation combined with EGF treatment, it suggested that this increase was likely due to activation of basolateral potassium channels since the pattern of stimulation seen in intact monolayers was abolished. With potassium channels implicated, the next question was to determine the signalling pathway that linked EGF to potassium channel activation, and which potassium channels were actually affected. Further investigation using inhibitors of EGF signalling pathways known to be involved in other tissues showed that EGF was working through the EGFR receptor and that the PI3K – PKC- δ signalling messengers were involved. Inhibition of potassium channels showed that KCNN4 played a major role in generating the current, and that KCNQ1 also contributed. This result is very significant since it provides many potential targets for which to treat CF that have not been previously considered, as well as shedding new insight on how the EGF signalling pathway affects ion transport in the Calu-3 cell line. Aerosols have been previously made using 20 μ g EGF in saline and administered to rat models, where improvements in lung liquid clearance was seen (Sznajder *et al.*, 1998). It may be possible to similarly administer aerosolised EGF to human patients to aid mucus clearance in cystic fibrosis sufferers.

8.2.4 EGF signalling increases UTP response in the Calu-3 cell line

While the effects of UTP on Calu-3 cells produced no significant effect, it was possible that this could change under the treatment of EGF. The effect of EGF on calcium activated chloride channels (CaCCs) in the gut has been widely reported and the mechanisms involved are comparatively well understood (McCole & Barrett, 2009). However in the airway, the effect of EGF treatment on CaCCs has yet to be investigated. We hypothesised that EGF would have a similar effect on stimulated CaCC transport, so in order to address this gap in knowledge, experiments were designed so that Calu-3 monolayers were preincubated with EGF over a period of time up to 24 hours and the response to UTP measured.

While shorter time points indicated that UTP was not having a different effect when combined with EGF treatment, stimulating with UTP resulted in a statistically significant spike where intact Calu-3 monolayers were treated with EGF for the longer period of 24 hours, which did not occur when the basolateral membrane was permeabilised. These data suggested that potassium channels on the basolateral membrane were involved, and we suggest that these are likely to be calcium activated potassium channels since UTP stimulation is known to lead to elevated levels of intracellular calcium. This finding was considered significant since EGF treatment not only increases ion transport by itself, but also enhances the effects of at least one stimulator of ion transport as well. This could prove to be a useful avenue for combination treatments to tackle CF.

8.2.5 Reduction in stimulated I_{sc} after EGF treatment in the Calu-3 cell line

While it was demonstrated that EGF could enhance UTP stimulation over a period of 24 hours, the effect of EGF treatment on forskolin stimulation was also of interest. The link between EGF related mechanisms and stimulated ion transport in the gut has been widely reported and the mechanisms involved are comparatively well understood (Keely *et al.*, 1998; Keely *et al.*, 2000). However in the airway, the effect of EGF treatment on stimulated ion transport is largely unknown, especially in the submucosal cell line Calu-3 where no studies have been previously conducted. In order to address this gap in knowledge, experiments were designed so that Calu-3 monolayers were preincubated with EGF over a period of time up to 24 hours and the response to adenylate cyclase agonist measured.

It was seen that responses to forskolin were almost reciprocal to elevations caused by EGF treatment over the 24 hour time period used. Based on information from previous studies (Sun *et al.*, 1995; Stryjek-Kaminska *et al.*, 1996) and the data collected in this study, it was proposed that activation of EGFR led to an activation of PKC (as similarly reported in Chapter 5). Activation of PKC subsequently leads to an activation of G_i and an attenuation of EGFR's ability to activate G_s . This in turn leads to an inhibition of adenylate cyclase and reduced forskolin response. Once the effect of EGF dissipates at 24 hours, forskolin regains its ability to increase the current.

Following on from this result, we were interested in investigating if it was possible to restore the reduced effect of forskolin with EGF back to control levels. Through the use of inhibitors, it was seen that inhibitors of PI3K and PKC were not able to do so, suggesting that these signalling molecules were not suppressing the forskolin response. Upon inhibiting KCNN4, again, this was not able to rescue the reduced effect of forskolin by EGF. However, inhibition of KCNQ1 by chromanol 293B did rescue the response so that it was no longer statistically significant from the response to forskolin alone. This result was seen as significant since it ties in with the knowledge that KCNQ1 is potentially involved in raising the initial short circuit current and that inhibition of the channel allows forskolin to produce a larger effect. Inhibition of PI3K and PKC likely inhibited other ion channels, leading to a greatly decreased chloride driving force and therefore a greatly reduced short circuit current.

When intact Calu-3 monolayers were preincubated first with U0126 and then EGF, it prevented the recovery of the forskolin stimulated short circuit current at 24 hours as seen with EGF treated monolayers without U0126 treatment. This suggested that the recovery process through which responses from EGF return to the resting state are mediated through an ERK signalling pathway. This finding provides additional in depth understanding of the underlying signalling pathways that regulate secretion in Calu-3 cells.

8.2.6 Effect of EGF in the Calu-3 cell line is independent of a transactivation process

From the literature, it is clear that activation of the β_2 adrenergic receptor is able to induce shedding of EGF ligands and transactivate the EGF receptor (Liebmann, 2011). The effect of β_2 agonists on chloride transport in the Calu-3 cell line is widely understood (Cobb *et al.*, 2002). However, it is not understood if the β_2 adrenergic receptor is able to transactivate EGFR when it is stimulated in the Calu-3 cell line. In order to address this gap in knowledge, experiments were designed experiments were designed to initially characterise the response to β_2 agonist salbutamol, and then to see how response could be altered using inhibitors of both metalloproteinases (to prevent shedding) and EGFR (to prevent EGF ligand activating EGFR).

It was found that basolateral pretreatment with neither AG1478 nor GM-6001 could significantly reduce the size of the standard response to acute basolateral treatment with salbutamol, suggesting that a transactivation was not involved. This is significant since it shows that drugs such as salbutamol do not act via metalloproteinases to release EGF ligand and increase short circuit current.

8.2.7 β_3 agonists have negligible effects on Calu-3 monolayers

Very few studies looking at the β_3 adrenergic receptor in the airway have been conducted and as such, the effects (if any) of the receptor is poorly understood, especially in non-transfected cell lines. Studies in the Calu-3 cell line have yet to be published. In order to address this gap in knowledge, experiments were designed to characterise the response of β_3 agonist CGP-12177 on the β_3 adrenergic receptor, with the intention of discovering another possible regulator of ion transport in the Calu-3 cell line.

RT-PCR results suggested that the β_3 adrenergic receptor was weakly expressed in the Calu-3 cell line. The resulting currents generated by stimulation with CGP-12177 were very small but measurable. It was not expected for these currents to be large since it was previously seen that β_3 adrenergic receptors were not greatly expressed in Calu-3 cells, which was also in agreement with data gathered during this investigation. It was possible to completely inhibit the response using wortmannin and adenylate cyclase inhibitor MDL-12330A, and reduce the response using selective β_3 blocker L-748,337. When repeated with basolateral membrane permeabilisation, the responses to CGP-12177 were greater, but the inhibitors used bar ERK inhibitor U0126 did not decrease the current, suggesting that there may be an effect of basolateral potassium channels, which once removed, invalidates the actions of inhibitors such as wortmannin. It is however more difficult to make firm conclusions when the increases are slight and the number of repeats low, which would explain why other groups have transfected excess β_3 receptors in cell lines to examine the responses rather than our approach that only looked at endogenous levels of β_3 . While our investigation may have failed to demonstrate a statistically significant increase from the β_3 agonist used, it nevertheless demonstrated the presence of the β_3 adrenergic receptor, which is a novel finding.

8.3 Concluding Remarks

In conclusion, the data obtained during this investigation suggest that activation of basolateral potassium channels via the EGFR receptor and subsequent signalling pathway implicated in this study would be a desirable outcome for ion transport in the lung in disease conditions such as CF. It has been previously shown in rat lungs that EGF increases lung liquid clearance when administered as an aerosol (Sznajder *et al.*, 1998). In this study, the activation of basolateral potassium channels was accomplished by preincubating Calu-3 monolayers with EGF for a period of 1 hour, and in other studies such as those carried out by Roth *et al.*, 2011 and Devor *et al.*, 1996, it has been accomplished by treatment with 1-EBIO in rectal biopsies (Roth *et al.*, 2011) and Calu-3 cells (Devor *et al.*, 1996). There is good potential for effective treatments for CF through combination therapy of basolateral potassium activation and CFTR activation and potentiation with drugs such as VX-770 (Van Goor *et al.*, 2009; Accurso *et al.*, 2010) and VX-809 (Clancy *et al.*, 2012), of which VX-770 has been approved (G551D mutation in children) and combination therapy of the two are already in phase 2 clinical trials. While these drugs have been shown to be effective in improving lung function in CF patients, there is still scope for restoring CFTR currents in patients with CF.

8.4 Future Work

During this investigation, there have been various findings which have yet to be studied to determine further mechanisms. One such finding is the return of initial currents, and forskolin stimulated responses to normal after being stimulated by EGF for 24 hours. While we speculate that at 24 hours the EGFR receptor may be internalised by the cell and thus return the cell ion transport status to normal, we did not demonstrate this experimentally. It should be possible to use inhibitors of internalisation such as baflomycin A₁ or chloroquine to simultaneously preincubate with EGF for 24 hours and compare the results to the control (Storey *et al.*, 2002). It would be expected for the initial current not to return to baseline levels with these inhibitors if internalisation of the EGFR is in fact the case.

Another possible explanation is that there is in fact a transmodulation of the EGF receptor, leading to an eventual decrease in ion transport (Figure 8.1). The model for

transmodulation of the EGF receptor would involve stimulation of the β_2 adrenergic receptor leading to the activation of PKA. PKA is able to negatively regulate EGFR signalling (Liebmann, 2011). If the initial current and forskolin stimulated current recovers at 24 hours, then if cells were preincubated with EGF and a PKA inhibitor such as 14-22 amide simultaneously for 24 hours, our hypothesis would suggest that PKA being present would prevent the return of current back to the resting state if transmodulation is occurring.

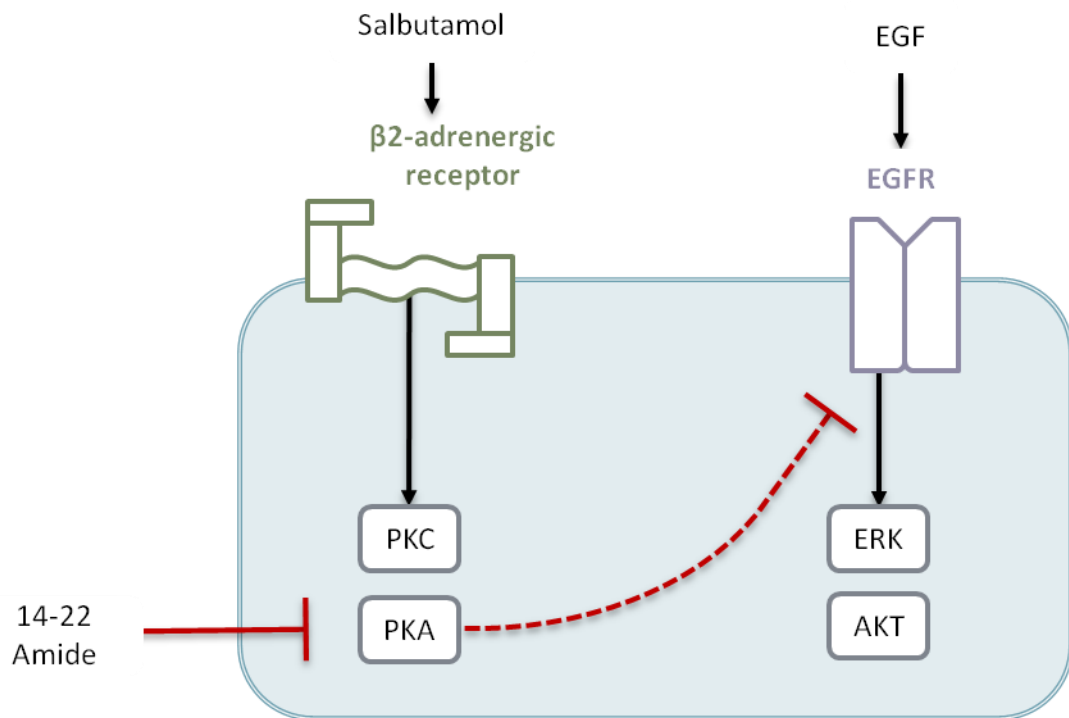


Figure 8.1 – Model for the transmodulation of the EGFR receptor.

Simultaneous treatment of intact Calu-3 monolayers with EGF and specific protein kinase A (PKA) inhibitor, 14-22 amide, would prevent the return in short circuit current to unstimulated levels if transmodulation of EGFR occurs in this manner. Based on a schematic by (Liebmann, 2011)

Activation of the EGFR receptor led to an inhibition of forskolin stimulated short circuit current, which was suggested to be due to an inhibition of adenylate cyclase via G_i proteins. However, this explanation is untested; therefore an investigation could be carried out using Calu-3 monolayers treated with EGF as detailed before, with the addition of pertussis toxin to inhibit G_i activity. For our proposed model to be true, it would be expected that activation of CFTR via forskolin treatment would be rescued.

Moreover, there is some evidence in the literature that activation of tyrosine kinases such as EGFR can lead to activation of Na^+/K^+ -ATPase activity in the rat proximal

convoluted tubule (Feraille *et al.*, 1997). It may be the case that there is an increase in Na^+/K^+ -ATPase activity in Calu-3 cells when they are treated with EGF. Na^+/K^+ -ATPase are known to be present in Calu-3 cells (Devor *et al.*, 1999). Future studies could look at the effect of EGF on the Na^+/K^+ -ATPase. This could be better studied by permeabilising the apical membrane and using a potassium gradient. The default response to EGF treatment could be compared to a combined treatment of EGF and ouabain (a Na^+/K^+ -ATPase inhibitor) to see if the increase in short circuit current was reduced in the latter, which would suggest Na^+/K^+ -ATPase involvement.

This investigation looked at the gene expression of bestrophins and anoctamins in three epithelial cell lines. Protein expression of BEST1 was investigated in the Calu-3 cell line, but not other bestrophins and anoctamins. This was due to a lack of availability of reliable antibodies to detect these proteins. Future work could entail using new antibodies that are currently being developed in an attempt to determine their expression in the Calu-3 cell line. Subsequently, it may be possible to see if their expression is upregulated by EGF to see if there is a link between EGFR signalling and expression of calcium activated chloride channel proteins. Such a link has yet to be described.

References

Abraham G, Kneuer C, Ehrhardt C, Honscha W & Ungemach FR. (2004). Expression of functional beta2-adrenergic receptors in the lung epithelial cell lines 16HBE14o(-), Calu-3 and A549. *Biochim Biophys Acta* **1691**, 169-179.

Accurso FJ, Moss RB, Wilmott RW, Anbar RD, Schaberg AE, Durham TA & Ramsey BW. (2011). Denufosal tetrasodium in patients with cystic fibrosis and normal to mildly impaired lung function. *Am J Respir Crit Care Med* **183**, 627-634.

Accurso FJ, Rowe SM, Clancy JP, Boyle MP, Dunitz JM, Durie PR, Sagel SD, Hornick DB, Konstan MW, Donaldson SH, Moss RB, Pilewski JM, Rubenstein RC, Uluer AZ, Aitken ML, Freedman SD, Rose LM, Mayer-Hamblett N, Dong Q, Zha J, Stone AJ, Olson ER, Ordonez CL, Campbell PW, Ashlock MA & Ramsey BW. (2010). Effect of VX-770 in persons with cystic fibrosis and the G551D-CFTR mutation. *N Engl J Med* **363**, 1991-2003.

Adda S, Fleischmann BK, Freedman BD, Yu M, Hay DW & Kotlikoff MI. (1996). Expression and function of voltage-dependent potassium channel genes in human airway smooth muscle. *J Biol Chem* **271**, 13239-13243.

Agnel M, Vermat T & Culoscou JM. (1999). Identification of three novel members of the calcium-dependent chloride channel (CaCC) family predominantly expressed in the digestive tract and trachea. *FEBS Lett* **455**, 295-301.

Almaca J, Tian Y, Aldehni F, Ousingsawat J, Kongsuphol P, Rock JR, Harfe BD, Schreiber R & Kunzelmann K. (2009). TMEM16 proteins produce volume-regulated chloride currents that are reduced in mice lacking TMEM16A. *J Biol Chem* **284**, 28571-28578.

Altman A & Villalba M. (2003). Protein kinase C-theta (PKC θ): it's all about location, location, location. *Immunol Rev* **192**, 53-63.

Amour A, Slocombe PM, Webster A, Butler M, Knight CG, Smith BJ, Stephens PE, Shelley C, Hutton M, Knauper V, Docherty AJ & Murphy G. (1998). TNF-alpha converting enzyme (TACE) is inhibited by TIMP-3. *FEBS Lett* **435**, 39-44.

Amsler K & Kinne R. (1986). Photoinactivation of sodium-potassium-chloride cotransport in LLC-PK1/Cl 4 cells by bumetanide. *Am J Physiol* **250**, C799-806.

Anderson MP & Welsh MJ. (1991). Calcium and cAMP activate different chloride channels in the apical membrane of normal and cystic fibrosis epithelia. *Proc Natl Acad Sci U S A* **88**, 6003-6007.

Andl CD, Mizushima T, Oyama K, Bowser M, Nakagawa H & Rustgi AK. (2004). EGFR-induced cell migration is mediated predominantly by the JAK-STAT pathway in primary esophageal keratinocytes. *Am J Physiol Gastrointest Liver Physiol* **287**, G1227-1237.

Ao M, Venkatasubramanian J, Boonkaewwan C, Ganesan N, Syed A, Benya RV & Rao MC. (2011). Lubiprostone activates Cl⁻ secretion via cAMP signaling and increases membrane CFTR in the human colon carcinoma cell line, T84. *Dig Dis Sci* **56**, 339-351.

Araujo FG, Novaes FC, Santos NP, Martins VC, Souza SM, Santos SE & Ribeiro-dos-Santos AK. (2005). Prevalence of deltaF508, G551D, G542X, and R553X mutations among cystic fibrosis patients in the North of Brazil. *Braz J Med Biol Res* **38**, 11-15.

Atkinson JJ & Senior RM. (2003). Matrix metalloproteinase-9 in lung remodeling. *Am J Respir Cell Mol Biol* **28**, 12-24.

Auer J & Meltzer SJ. (1911). The Status of Respiration in the Methods of Differential Pressure Compared with That under the Method of Intratracheal Insufflation. *J Exp Med* **14**, 569-593.

Baba M, Klein-Szanto AJ, Trono D, Obara T, Yoakum GH, Masui T & Harris CC. (1987). Preneoplastic and neoplastic growth of xenotransplanted lung-derived human cell lines using deepithelialized rat tracheas. *Cancer Res* **47**, 573-578.

Ballard ST & Inglis SK. (2004). Liquid secretion properties of airway submucosal glands. *J Physiol* **556**, 1-10.

Barman SA, Zhu S, Han G & White RE. (2003). cAMP activates BKCa channels in pulmonary arterial smooth muscle via cGMP-dependent protein kinase. *Am J Physiol Lung Cell Mol Physiol* **284**, L1004-1011.

Barnes PJ. (2001). Neurogenic inflammation in the airways. *Respir Physiol* **125**, 145-154.

Barro-Soria R, Aldehni F, Almaca J, Witzgall R, Schreiber R & Kunzelmann K. (2010). ER-localized bestrophin 1 activates Ca2+-dependent ion channels TMEM16A

and SK4 possibly by acting as a counterion channel. *Pflugers Arch* **459**, 485-497.

Barro Soria R, Spitzner M, Schreiber R & Kunzelmann K. (2009). Bestrophin-1 enables Ca²⁺-activated Cl⁻ conductance in epithelia. *J Biol Chem* **284**, 29405-29412.

Baudouin-Legros M, Brouillard F, Tondelier D, Hinzpeter A & Edelman A. (2003). Effect of ouabain on CFTR gene expression in human Calu-3 cells. *Am J Physiol Cell Physiol* **284**, C620-626.

Becq F, Mall MA, Sheppard DN, Conese M & Zegarra-Moran O. (2011). Pharmacological therapy for cystic fibrosis: from bench to bedside. *J Cyst Fibros* **10 Suppl 2**, S129-145.

Bendeck MP, Irvin C & Reidy MA. (1996). Inhibition of matrix metalloproteinase activity inhibits smooth muscle cell migration but not neointimal thickening after arterial injury. *Circ Res* **78**, 38-43.

Bergin DA, Greene CM, Sterchi EE, Kenna C, Geraghty P, Belaaouaj A, Taggart CC, O'Neill SJ & McElvaney NG. (2008). Activation of the epidermal growth factor receptor (EGFR) by a novel metalloprotease pathway. *J Biol Chem* **283**, 31736-31744.

Bernard K, Bogliolo S, Soriano O & Ehrenfeld J. (2003). Modulation of calcium-dependent chloride secretion by basolateral SK4-like channels in a human bronchial cell line. *J Membr Biol* **196**, 15-31.

Bertelsen LS, Barrett KE & Keely SJ. (2004). Gs protein-coupled receptor agonists induce transactivation of the epidermal growth factor receptor in T84 cells: implications for epithelial secretory responses. *J Biol Chem* **279**, 6271-6279.

Bett GC, Morales MJ, Beahm DL, Duffey ME & Rasmussen RL. (2006). Ancillary subunits and stimulation frequency determine the potency of chromanol 293B block of the KCNQ1 potassium channel. *J Physiol* **576**, 755-767.

Bijvelds MJ, Bot AG, Escher JC & De Jonge HR. (2009). Activation of intestinal Cl⁻ secretion by lubiprostone requires the cystic fibrosis transmembrane conductance regulator. *Gastroenterology* **137**, 976-985.

Blank F, Rothen-Rutishauser B & Gehr P. (2007). Dendritic cells and macrophages form a transepithelial network against foreign particulate antigens. *Am J Respir Cell Mol Biol* **36**, 669-677.

Bompadre SG, Sohma Y, Li M & Hwang TC. (2007). G551D and G1349D, two CF-associated mutations in the signature sequences of CFTR, exhibit distinct gating defects. *J Gen Physiol* **129**, 285-298.

Bordey A, Sontheimer H & Trouslard J. (2000). Muscarinic activation of BK channels induces membrane oscillations in glioma cells and leads to inhibition of cell migration. *J Membr Biol* **176**, 31-40.

Borok Z, Hami A, Danto SI, Lubman RL, Kim KJ & Crandall ED. (1996). Effects of EGF on alveolar epithelial junctional permeability and active sodium transport. *Am J Physiol* **270**, L559-565.

Bossard F, Robay A, Toumaniantz G, Dahimene S, Becq F, Merot J & Gauthier C. (2007). NHE-RF1 protein rescues DeltaF508-CFTR function. *Am J Physiol Lung Cell Mol Physiol* **292**, L1085-1094.

Bossard F, Silantieff E, Lavazais-Blancou E, Robay A, Sagan C, Rozec B & Gauthier C. (2011). beta1, beta2, and beta3 adrenoceptors and Na⁺/H⁺ exchanger regulatory factor 1 expression in human bronchi and their modifications in cystic fibrosis. *Am J Respir Cell Mol Biol* **44**, 91-98.

Boucherot A, Schreiber R & Kunzelmann K. (2001). Regulation and properties of KCNQ1 (K(V)LQT1) and impact of the cystic fibrosis transmembrane conductance regulator. *J Membr Biol* **182**, 39-47.

Bove PF, Wesley UV, Greul AK, Hristova M, Dostmann WR & van der Vliet A. (2007). Nitric oxide promotes airway epithelial wound repair through enhanced activation of MMP-9. *Am J Respir Cell Mol Biol* **36**, 138-146.

Bowlby MR, Fadool DA, Holmes TC & Levitan IB. (1997). Modulation of the Kv1.3 potassium channel by receptor tyrosine kinases. *J Gen Physiol* **110**, 601-610.

Bradding P & Wulff H. (2009). The K⁺ channels K(Ca)3.1 and K(v)1.3 as novel targets for asthma therapy. *Br J Pharmacol* **157**, 1330-1339.

Brdickova N, Brdicka T, Andera L, Spicka J, Angelisova P, Milgram SL & Horejsi V. (2001). Interaction between two adapter proteins, PAG and EBP50: a possible link between membrane rafts and actin cytoskeleton. *FEBS Lett* **507**, 133-136.

Brew K, Dinakarpandian D & Nagase H. (2000). Tissue inhibitors of metalloproteinases: evolution, structure and function. *Biochim Biophys Acta* **1477**, 267-283.

Brouillard F, Bouthier M, Leclerc T, Clement A, Baudouin-Legros M & Edelman A. (2001). NF-kappa B mediates up-regulation of CFTR gene expression in Calu-3 cells by interleukin-1beta. *J Biol Chem* **276**, 9486-9491.

Buscher R, Eilmes KJ, Grasemann H, Torres B, Knauer N, Sroka K, Insel PA & Ratjen F. (2002). beta2 adrenoceptor gene polymorphisms in cystic fibrosis lung disease. *Pharmacogenetics* **12**, 347-353.

Candia S, Garcia ML & Latorre R. (1992). Mode of action of iberiotoxin, a potent blocker of the large conductance Ca(2+)-activated K+ channel. *Biophysical journal* **63**, 583-590.

Caputo A, Caci E, Ferrera L, Pedemonte N, Barsanti C, Sondo E, Pfeffer U, Ravazzolo R, Zegarra-Moran O & Galietta LJ. (2008). TMEM16A, a membrane protein associated with calcium-dependent chloride channel activity. *Science* **322**, 590-594.

Carlos MA, Nwagwu C, Ao M, Venkatasubramanian J, Boonkaewwan C, Prasad R, Chowdhury SA, Vidyasagar D & Rao MC. (2007). Epidermal growth factor stimulates chloride transport in primary cultures of weanling and adult rabbit colonocytes. *Journal of pediatric gastroenterology and nutrition* **44**, 300-311.

Carreiras F, Cruet S, Staedel C, Sichel F & Gauduchon P. (1999). Human ovarian adenocarcinoma cells synthesize vitronectin and use it to organize their adhesion. *Gynecologic oncology* **72**, 312-322.

Carstairs JR, Nimmo AJ & Barnes PJ. (1985). Autoradiographic visualization of beta-adrenoceptor subtypes in human lung. *Am Rev Respir Dis* **132**, 541-547.

Chang MH, Plata C, Sindic A, Ranatunga WK, Chen AP, Zandi-Nejad K, Chan KW, Thompson J, Mount DB & Romero MF. (2009). Slc26a9 is inhibited by the R-region of the cystic fibrosis transmembrane conductance regulator via the STAS domain. *J Biol Chem* **284**, 28306-28318.

Chappe V, Hinkson DA, Howell LD, Evangelidis A, Liao J, Chang XB, Riordan JR & Hanrahan JW. (2004). Stimulatory and inhibitory protein kinase C consensus sequences regulate the cystic fibrosis transmembrane conductance regulator. *Proc Natl Acad Sci U S A* **101**, 390-395.

Chappe V, Hinkson DA, Zhu T, Chang XB, Riordan JR & Hanrahan JW. (2003). Phosphorylation of protein kinase C sites in NBD1 and the R domain control CFTR channel activation by PKA. *J Physiol* **548**, 39-52.

Chappe V, Irvine T, Liao J, Evangelidis A & Hanrahan JW. (2005). Phosphorylation of CFTR by PKA promotes binding of the regulatory domain. *EMBO J* **24**, 2730-2740.

Chen MF & Chen TY. (2001). Different fast-gate regulation by external Cl(-) and H(+) of the muscle-type CIC chloride channels. *J Gen Physiol* **118**, 23-32.

Chen P, Yuan Y, Wang S, Zhan L & Xu J. (2006). Serum matrix metalloproteinase 9 as a marker for the assessment of severe acute pancreatitis. *Tohoku J Exp Med* **208**, 261-266.

Cheng SH, Gregory RJ, Marshall J, Paul S, Souza DW, White GA, O'Riordan CR & Smith AE. (1990). Defective intracellular transport and processing of CFTR is the molecular basis of most cystic fibrosis. *Cell* **63**, 827-834.

Chillon M, Casals T, Mercier B, Bassas L, Lissens W, Silber S, Romey MC, Ruiz-Romero J, Verlingue C, Claustres M & et al. (1995). Mutations in the cystic fibrosis gene in patients with congenital absence of the vas deferens. *N Engl J Med* **332**, 1475-1480.

Choi JY, Muallem D, Kiselyov K, Lee MG, Thomas PJ & Muallem S. (2001). Aberrant CFTR-dependent HCO3- transport in mutations associated with cystic fibrosis. *Nature* **410**, 94-97.

Chow JY & Barrett KE. (2007). Role of protein phosphatase 2A in calcium-dependent chloride secretion by human colonic epithelial cells. *Am J Physiol Cell Physiol* **292**, C452-459.

Chow JY, Uribe JM & Barrett KE. (2000). A role for protein kinase cepsilon in the inhibitory effect of epidermal growth factor on calcium-stimulated chloride secretion in human colonic epithelial cells. *J Biol Chem* **275**, 21169-21176.

Chung KF. (2001). Cytokines in chronic obstructive pulmonary disease. *Eur Respir J Suppl* **34**, 50s-59s.

Chung L, Shimokawa K, Dinakarpandian D, Grams F, Fields GB & Nagase H. (2000). Identification of the (183)RWTNNFREY(191) region as a critical segment of

matrix metalloproteinase 1 for the expression of collagenolytic activity. *J Biol Chem* **275**, 29610-29617.

Clancy JP, Rowe SM, Accurso FJ, Aitken ML, Amin RS, Ashlock MA, Ballmann M, Boyle MP, Bronsveld I, Campbell PW, De Boeck K, Donaldson SH, Dorkin HL, Dunitz JM, Durie PR, Jain M, Leonard A, McCoy KS, Moss RB, Pilewski JM, Rosenbluth DB, Rubenstein RC, Schechter MS, Botfield M, Ordonez CL, Spencer-Green GT, Vernallet L, Wisseh S, Yen K & Konstan MW. (2012). Results of a phase IIa study of VX-809, an investigational CFTR corrector compound, in subjects with cystic fibrosis homozygous for the F508del-CFTR mutation. *Thorax* **67**, 12-18.

Clemo HF, Stambler BS & Baumgarten CM. (1999). Swelling-activated chloride current is persistently activated in ventricular myocytes from dogs with tachycardia-induced congestive heart failure. *Circ Res* **84**, 157-165.

Cobb BR, Ruiz F, King CM, Fortenberry J, Greer H, Kovacs T, Sorscher EJ & Clancy JP. (2002). A(2) adenosine receptors regulate CFTR through PKA and PLA(2). *Am J Physiol Lung Cell Mol Physiol* **282**, L12-25.

Cohn JA, Melhus O, Page LJ, Dittrich KL & Vigna SR. (1991). CFTR: development of high- affinity antibodies and localization in sweat gland. *Biochem Biophys Res Commun* **181**, 36-43.

Colombo C, Faelli N, Tirelli AS, Fortunato F, Biffi A, Claut L, Cariani L, Dacco V, Prato R & Conese M. (2011). Analysis of inflammatory and immune response biomarkers in sputum and exhaled breath condensate by a multi-parametric biochip array in cystic fibrosis. *Int J Immunopathol Pharmacol* **24**, 423-432.

Corey M, McLaughlin FJ, Williams M & Levison H. (1988). A comparison of survival, growth, and pulmonary function in patients with cystic fibrosis in Boston and Toronto. *J Clin Epidemiol* **41**, 583-591.

Cowley EA & Linsdell P. (2002). Characterization of basolateral K⁺ channels underlying anion secretion in the human airway cell line Calu-3. *J Physiol* **538**, 747-757.

Cuppoletti J, Malinowska DH, Tewari KP, Li QJ, Sherry AM, Patchen ML & Ueno R. (2004a). SPI-0211 activates T84 cell chloride transport and recombinant human CIC-2 chloride currents. *Am J Physiol Cell Physiol* **287**, C1173-1183.

Cuppoletti J, Tewari KP, Sherry AM, Ferrante CJ & Malinowska DH. (2004b). Sites of protein kinase A activation of the human ClC-2 Cl(-) channel. *J Biol Chem* **279**, 21849-21856.

Currid A, Ortega B & Valverde MA. (2004). Chloride secretion in a morphologically differentiated human colonic cell line that expresses the epithelial Na⁺ channel. *J Physiol* **555**, 241-250.

Cuthbert AW. (2001). Assessment of CFTR chloride channel openers in intact normal and cystic fibrosis murine epithelia. *Br J Pharmacol* **132**, 659-668.

Cuthbert AW. (2011a). Lubiprostone targets prostanoid EP receptors in ovine airways. *Br J Pharmacol* **162**, 508-520.

Cuthbert AW. (2011b). New horizons in the treatment of cystic fibrosis. *Br J Pharmacol* **163**, 173-183.

Cuthbert AW, Hickman ME, MacVinish LJ, Evans MJ, Colledge WH, Ratcliff R, Seale PW & Humphrey PP. (1994). Chloride secretion in response to guanylin in colonic epithelial from normal and transgenic cystic fibrosis mice. *Br J Pharmacol* **112**, 31-36.

Danner I, Escande D & Gauthier C. (2001). Beta(3)-adrenoceptors control Cl(-) conductance in rabbit nasal epithelium. *Eur J Pharmacol* **422**, 203-207.

Davidson TM, Murphy C, Mitchell M, Smith C & Light M. (1995). Management of chronic sinusitis in cystic fibrosis. *Laryngoscope* **105**, 354-358.

Davies B, Brown PD, East N, Crimmin MJ & Balkwill FR. (1993). A synthetic matrix metalloproteinase inhibitor decreases tumor burden and prolongs survival of mice bearing human ovarian carcinoma xenografts. *Cancer Res* **53**, 2087-2091.

Davis AJ, Forrest AS, Jepps TA, Valencik ML, Wiwchar M, Singer CA, Sones WR, Greenwood IA & Leblanc N. (2010). Expression profile and protein translation of TMEM16A in murine smooth muscle. *Am J Physiol Cell Physiol* **299**, C948-959.

Davis KA & Cowley EA. (2006). Two-pore-domain potassium channels support anion secretion from human airway Calu-3 epithelial cells. *Pflugers Arch* **451**, 631-641.

Davis PB. (2006). Cystic fibrosis since 1938. *Am J Respir Crit Care Med* **173**, 475-482.

Denton J, Nehrke K, Yin X, Morrison R & Strange K. (2005). GCK-3, a newly identified Ste20 kinase, binds to and regulates the activity of a cell cycle-dependent CIC anion channel. *J Gen Physiol* **125**, 113-125.

Devor DC, Singh AK, Frizzell RA & Bridges RJ. (1996). Modulation of Cl⁻ secretion by benzimidazolones. I. Direct activation of a Ca(2+)-dependent K⁺ channel. *Am J Physiol* **271**, L775-784.

Devor DC, Singh AK, Lambert LC, DeLuca A, Frizzell RA & Bridges RJ. (1999). Bicarbonate and chloride secretion in Calu-3 human airway epithelial cells. *J Gen Physiol* **113**, 743-760.

Dittmar T, Husemann A, Schewe Y, Nofer JR, Niggemann B, Zanker KS & Brandt BH. (2002). Induction of cancer cell migration by epidermal growth factor is initiated by specific phosphorylation of tyrosine 1248 of c-erbB-2 receptor via EGFR. *FASEB J* **16**, 1823-1825.

Dixon WE. (1903). Contributions to the physiology of the lungs: Part I. The bronchial muscles, their innervation, and the action of drugs upon them. *J Physiol* **29**, 97-173.

Donnellan F, Keating N, Geoghegan P, Murray FE, Harvey BJ & Keely SJ. (2010). JNK mitogen-activated protein kinase limits calcium-dependent chloride secretion across colonic epithelial cells. *Am J Physiol Gastrointest Liver Physiol* **298**, G37-44.

Donnini S, Monti M, Roncone R, Morbidelli L, Rocchigiani M, Oliviero S, Casella L, Giachetti A, Schulz R & Ziche M. (2008). Peroxynitrite inactivates human-tissue inhibitor of metalloproteinase-4. *FEBS Lett* **582**, 1135-1140.

Duan D, Zhong J, Hermoso M, Satterwhite CM, Rossow CF, Hatton WJ, Yamboliev I, Horowitz B & Hume JR. (2001). Functional inhibition of native volume-sensitive outwardly rectifying anion channels in muscle cells and *Xenopus* oocytes by anti-CIC-3 antibody. *J Physiol* **531**, 437-444.

Ducroc R, Guilmeau S, Akasbi K, Devaud H, Buyse M & Bado A. (2005). Luminal leptin induces rapid inhibition of active intestinal absorption of glucose mediated by sodium-glucose cotransporter 1. *Diabetes* **54**, 348-354.

Dufour A, Sampson NS, Zucker S & Cao J. (2008). Role of the hemopexin domain of matrix metalloproteinases in cell migration. *J Cell Physiol* **217**, 643-651.

Duran C, Qu Z, Osunkoya AO, Cui Y & Hartzell HC. (2012). ANOs 3-7 in the anoctamin/Tmem16 Cl- channel family are intracellular proteins. *Am J Physiol Cell Physiol* **302**, C482-493.

Duszyk M, MacVinish L & Cuthbert AW. (2001). Phenanthrolines--a new class of CFTR chloride channel openers. *Br J Pharmacol* **134**, 853-864.

Duszyk M, Shu Y, Sawicki G, Radomski A, Man SF & Radomski MW. (1999). Inhibition of matrix metalloproteinase MMP-2 activates chloride current in human airway epithelial cells. *Can J Physiol Pharmacol* **77**, 529-535.

Dutzler R. (2006). The CIC family of chloride channels and transporters. *Curr Opin Struct Biol* **16**, 439-446.

Dutzler R. (2007). A structural perspective on CIC channel and transporter function. *FEBS Lett* **581**, 2839-2844.

Dzwonek J, Rylski M & Kaczmarek L. (2004). Matrix metalloproteinases and their endogenous inhibitors in neuronal physiology of the adult brain. *FEBS Lett* **567**, 129-135.

Elkins MR, Robinson M, Rose BR, Harbour C, Moriarty CP, Marks GB, Belousova EG, Xuan W & Bye PT. (2006). A controlled trial of long-term inhaled hypertonic saline in patients with cystic fibrosis. *N Engl J Med* **354**, 229-240.

Engelhardt JF, Yankaskas JR, Ernst SA, Yang Y, Marino CR, Boucher RC, Cohn JA & Wilson JM. (1992). Submucosal glands are the predominant site of CFTR expression in the human bronchus. *Nature genetics* **2**, 240-248.

Enomoto Y, Orihara K, Takamasu T, Matsuda A, Gon Y, Saito H, Ra C & Okayama Y. (2009). Tissue remodeling induced by hypersecreted epidermal growth factor and amphiregulin in the airway after an acute asthma attack. *J Allergy Clin Immunol* **124**, 913-920 e911-917.

Enz R & Cutting GR. (1998). Molecular composition of GABAC receptors. *Vision Res* **38**, 1431-1441.

Failes TW & Hambley TW. (2007). Towards bioreductively activated prodrugs: Fe(III) complexes of hydroxamic acids and the MMP inhibitor marimastat. *J Inorg Biochem* **101**, 396-403.

Faria D, Schreiber R & Kunzelmann K. (2009). CFTR is activated through stimulation of purinergic P2Y2 receptors. *Pflugers Arch* **457**, 1373-1380.

Farinas J, Kneen M, Moore M & Verkman AS. (1997). Plasma membrane water permeability of cultured cells and epithelia measured by light microscopy with spatial filtering. *J Gen Physiol* **110**, 283-296.

Feraille E, Carranza ML, Rousselot M & Favre H. (1997). Modulation of Na⁺,K(+)-ATPase activity by a tyrosine phosphorylation process in rat proximal convoluted tubule. *J Physiol* **498 (Pt 1)**, 99-108.

Ferrera L, Caputo A, Ubbi I, Bussani E, Zegarra-Moran O, Ravazzolo R, Pagani F & Galietta LJ. (2009). Regulation of TMEM16A chloride channel properties by alternative splicing. *J Biol Chem* **284**, 33360-33368.

Fielitz J, Leuschner M, Zurbrugg HR, Hannack B, Pregla R, Hetzer R & Regitz-Zagrosek V. (2004). Regulation of matrix metalloproteinases and their inhibitors in the left ventricular myocardium of patients with aortic stenosis. *J Mol Med* **82**, 809-820.

Fini ME, Girard MT, Matsubara M & Bartlett JD. (1995). Unique regulation of the matrix metalloproteinase, gelatinase B. *Invest Ophthalmol Vis Sci* **36**, 622-633.

Finkbeiner WE, Carrier SD & Teresi CE. (1993). Reverse transcription-polymerase chain reaction (RT-PCR) phenotypic analysis of cell cultures of human tracheal epithelium, tracheobronchial glands, and lung carcinomas. *Am J Respir Cell Mol Biol* **9**, 547-556.

Fischer H, Illek B, Sachs L, Finkbeiner WE & Widdicombe JH. (2010). CFTR and calcium-activated chloride channels in primary cultures of human airway gland cells of serous or mucous phenotype. *Am J Physiol Lung Cell Mol Physiol* **299**, L585-594.

Forstner GG, Kopelman HR, Durie PR & Corey ML. (1987). Pancreatic and intestinal dysfunction in cystic fibrosis. *Progress in clinical and biological research* **254**, 7-17.

Foster KA, Avery ML, Yazdanian M & Audus KL. (2000). Characterization of the Calu-3 cell line as a tool to screen pulmonary drug delivery. *Int J Pharm* **208**, 1-11.

Fujioka T, Kim JH, Adachi H, Saito K, Tsujimoto M, Yokoyama S & Ui M. (2001). Further evidence for the involvement of insulin receptor substrates in epidermal growth factor-induced activation of phosphatidylinositol 3-kinase. *Eur J Biochem* **268**, 4158-4168.

Gadsby DC & Nairn AC. (1999). Regulation of CFTR Cl- ion channels by phosphorylation and dephosphorylation. *Adv Second Messenger Phosphoprotein Res* **33**, 79-106.

Gaggar A, Hector A, Bratcher PE, Mall MA, Gries M & Hartl D. (2011). The role of matrix metalloproteinases in cystic fibrosis lung disease. *Eur Respir J* **38**, 721-727.

Galardy RE, Grobelny D, Foellmer HG & Fernandez LA. (1994). Inhibition of angiogenesis by the matrix metalloprotease inhibitor N-[2R-2-(hydroxamidocarbonylmethyl)-4-methylpentanoyl]-L-tryptophan methylamide. *Cancer Res* **54**, 4715-4718.

Galietta LJ, Pagesy P, Folli C, Caci E, Romio L, Costes B, Nicolis E, Cabrini G, Goossens M, Ravazzolo R & Zegarra-Moran O. (2002). IL-4 is a potent modulator of ion transport in the human bronchial epithelium in vitro. *J Immunol* **168**, 839-845.

Garnett JP, Hickman E, Burrows R, Hegyi P, Tiszlavicz L, Cuthbert AW, Fong P & Gray MA. (2011). Novel role for pendrin in orchestrating bicarbonate secretion in cystic fibrosis transmembrane conductance regulator (CFTR)-expressing airway serous cells. *J Biol Chem* **286**, 41069-41082.

Garnett JP, Hickman E, Tunkamnerdthai O, Cuthbert AW & Gray MA. (2012). Protein Phosphatase 1 Coordinates CFTR-Dependent Airway Epithelial HCO(3) (-) Secretion by Reciprocal Regulation of Apical and Basolateral Membrane Cl(-) HCO(3) (-) Exchangers. *Br J Pharmacol*.

Gavrilovic J, Moens G, Thiery JP & Jouanneau J. (1990). Expression of transfected transforming growth factor alpha induces a motile fibroblast-like phenotype with extracellular matrix-degrading potential in a rat bladder carcinoma cell line. *Cell Regul* **1**, 1003-1014.

Gett AV & Hodgkin PD. (1998). Cell division regulates the T cell cytokine repertoire, revealing a mechanism underlying immune class regulation. *Proc Natl Acad Sci U S A* **95**, 9488-9493.

Gibson A, Lewis AP, Affleck K, Aitken AJ, Meldrum E & Thompson N. (2005). hCLCA1 and mCLCA3 are secreted non-integral membrane proteins and therefore are not ion channels. *J Biol Chem* **280**, 27205-27212.

Gomez-Pinilla PJ, Gibbons SJ, Bardsley MR, Lorincz A, Pozo MJ, Pasricha PJ, Van de Rijn M, West RB, Sarr MG, Kendrick ML, Cima RR, Dozois EJ, Larson DW, Ordog T & Farrugia G. (2009). Ano1 is a selective marker of interstitial cells of Cajal in the human and mouse gastrointestinal tract. *Am J Physiol Gastrointest Liver Physiol* **296**, G1370-1381.

Grasemann H & Ratjen F. (1999). Cystic fibrosis lung disease: the role of nitric oxide. *Pediatr Pulmonol* **28**, 442-448.

Gray MA, Pollard CE, Harris A, Coleman L, Greenwell JR & Argent BE. (1990). Anion selectivity and block of the small-conductance chloride channel on pancreatic duct cells. *Am J Physiol* **259**, C752-761.

Greenlee KJ, Werb Z & Kheradmand F. (2007). Matrix metalloproteinases in lung: multiple, multifarious, and multifaceted. *Physiol Rev* **87**, 69-98.

Greger R. (2000). Role of CFTR in the colon. *Annu Rev Physiol* **62**, 467-491.

Gruber AD, Elble RC, Ji HL, Schreur KD, Fuller CM & Pauli BU. (1998). Genomic cloning, molecular characterization, and functional analysis of human CLCA1, the first human member of the family of Ca²⁺-activated Cl⁻ channel proteins. *Genomics* **54**, 200-214.

Gruber AD & Pauli BU. (1999). Molecular cloning and biochemical characterization of a truncated, secreted member of the human family of Ca²⁺-activated Cl⁻ channels. *Biochim Biophys Acta* **1444**, 418-423.

Gruber AD, Schreur KD, Ji HL, Fuller CM & Pauli BU. (1999). Molecular cloning and transmembrane structure of hCLCA2 from human lung, trachea, and mammary gland. *Am J Physiol* **276**, C1261-1270.

Ha HC & Snyder SH. (1999). Poly(ADP-ribose) polymerase is a mediator of necrotic cell death by ATP depletion. *Proc Natl Acad Sci U S A* **96**, 13978-13982.

Haghi M, Young PM, Traini D, Jaiswal R, Gong J & Bebawy M. (2010). Time- and passage-dependent characteristics of a Calu-3 respiratory epithelial cell model. *Drug Dev Ind Pharm* **36**, 1207-1214.

Hamann M, Gibson A, Davies N, Jowett A, Walhin JP, Partington L, Affleck K, Trezise D & Main M. (2009). Human ClCa1 modulates anionic conduction of calcium-dependent chloride currents. *J Physiol* **587**, 2255-2274.

Hamed SA. (2006). Drug evaluation: PTC-124--a potential treatment of cystic fibrosis and Duchenne muscular dystrophy. *IDrugs : the investigational drugs journal* **9**, 783-789.

Hamilton M, Liao J, Cathcart MK & Wolfman A. (2001). Constitutive association of c-N-Ras with c-Raf-1 and protein kinase C epsilon in latent signaling modules. *J Biol Chem* **276**, 29079-29090.

Hanley PJ, Musset B, Renigunta V, Limberg SH, Dalpke AH, Sus R, Heeg KM, Preisig-Muller R & Daut J. (2004). Extracellular ATP induces oscillations of intracellular Ca²⁺ and membrane potential and promotes transcription of IL-6 in macrophages. *Proc Natl Acad Sci U S A* **101**, 9479-9484.

Hansen CR, Pressler T, Koch C & Hoiby N. (2005). Long-term azitromycin treatment of cystic fibrosis patients with chronic *Pseudomonas aeruginosa* infection; an observational cohort study. *J Cyst Fibros* **4**, 35-40.

Harron SA, Clarke CM, Jones CL, Babin-Muise D & Cowley EA. (2009). Volume regulation in the human airway epithelial cell line Calu-3. *Can J Physiol Pharmacol* **87**, 337-346.

Hartmann K, Stief F, Draguhn A & Frahm C. (2004). Ionotropic GABA receptors with mixed pharmacological properties of GABAA and GABAC receptors. *Eur J Pharmacol* **497**, 139-146.

Hartzell C, Putzier I & Arreola J. (2005). Calcium-activated chloride channels. *Annu Rev Physiol* **67**, 719-758.

Hawkins ED, Hommel M, Turner ML, Battye FL, Markham JF & Hodgkin PD. (2007). Measuring lymphocyte proliferation, survival and differentiation using CFSE time-series data. *Nat Protoc* **2**, 2057-2067.

Haws C, Finkbeiner WE, Widdicombe JH & Wine JJ. (1994). CFTR in Calu-3 human airway cells: channel properties and role in cAMP-activated Cl⁻ conductance. *Am J Physiol* **266**, L502-512.

Henderson N, Markwick LJ, Elshaw SR, Freyer AM, Knox AJ & Johnson SR. (2007). Collagen I and thrombin activate MMP-2 by MMP-14-dependent and -independent pathways: implications for airway smooth muscle migration. *Am J Physiol Lung Cell Mol Physiol* **292**, L1030-1038.

Henriksen K, Sorensen MG, Nielsen RH, Gram J, Schaller S, Dziegel MH, Everts V, Bollerslev J & Karsdal MA. (2006). Degradation of the organic phase of bone by osteoclasts: a secondary role for lysosomal acidification. *J Bone Miner Res* **21**, 58-66.

Herbison AE & Moenter SM. (2011). Depolarising and hyperpolarising actions of GABA(A) receptor activation on gonadotrophin-releasing hormone neurones: towards an emerging consensus. *J Neuroendocrinol* **23**, 557-569.

Hetz M, Walcher D, Grub M, Bach H, Hombach V & Marx N. (2003). Inhibition of MMP-9 expression by PPARgamma activators in human bronchial epithelial cells. *Thorax* **58**, 778-783.

Hevers W & Luddens H. (1998). The diversity of GABA_A receptors. Pharmacological and electrophysiological properties of GABA_A channel subtypes. *Mol Neurobiol* **18**, 35-86.

Hirsh AJ, Zhang J, Zamurs A, Fleegle J, Thelin WR, Caldwell RA, Sabater JR, Abraham WM, Donowitz M, Cha B, Johnson KB, St George JA, Johnson MR & Boucher RC. (2008). Pharmacological properties of N-(3,5-diamino-6-chloropyrazine-2-carbonyl)-N'-4-[4-(2,3-dihydroxypropoxy)phenyl]butyl-guanidine methanesulfonate (552-02), a novel epithelial sodium channel blocker with potential clinical efficacy for cystic fibrosis lung disease. *J Pharmacol Exp Ther* **325**, 77-88.

Hochman HI, Feins NR, Rubin R & Gould J. (1976). Chloride losing diarrhoea and metabolic alkalosis in an infant with cystic fibrosis. *Arch Dis Child* **51**, 390-391.

Hollins F, Kaur D, Yang W, Cruse G, Saunders R, Sutcliffe A, Berger P, Ito A, Brightling CE & Bradding P. (2008). Human airway smooth muscle promotes human lung mast cell survival, proliferation, and constitutive activation: cooperative roles for CADM1, stem cell factor, and IL-6. *J Immunol* **181**, 2772-2780.

Hotary K, Allen E, Punturieri A, Yana I & Weiss SJ. (2000). Regulation of cell invasion and morphogenesis in a three-dimensional type I collagen matrix by membrane-type matrix metalloproteinases 1, 2, and 3. *J Cell Biol* **149**, 1309-1323.

Huang F, Rock JR, Harfe BD, Cheng T, Huang X, Jan YN & Jan LY. (2009). Studies on expression and function of the TMEM16A calcium-activated chloride channel. *Proc Natl Acad Sci U S A* **106**, 21413-21418.

Huang J, Shan J, Kim D, Liao J, Evangelidis A, Alper SL & Hanrahan JW. (2012). Basolateral chloride loading by the anion exchanger type 2: role in fluid secretion by the human airway epithelial cell line Calu-3. *J Physiol* **590**, 5299-5316.

Huang P, Lazarowski ER, Tarran R, Milgram SL, Boucher RC & Stutts MJ. (2001). Compartmentalized autocrine signaling to cystic fibrosis transmembrane conductance regulator at the apical membrane of airway epithelial cells. *Proc Natl Acad Sci U S A* **98**, 14120-14125.

Hwang SJ, Blair PJ, Britton FC, O'Driscoll KE, Hennig G, Bayguinov YR, Rock JR, Harfe BD, Sanders KM & Ward SM. (2009). Expression of anoctamin 1/TMEM16A by interstitial cells of Cajal is fundamental for slow wave activity in gastrointestinal muscles. *J Physiol* **587**, 4887-4904.

Hwang TC & Sheppard DN. (2009). Gating of the CFTR Cl- channel by ATP-driven nucleotide-binding domain dimerisation. *J Physiol* **587**, 2151-2161.

Iamaroon A, Tait B & Diewert VM. (1996). Cell proliferation and expression of EGF, TGF-alpha, and EGF receptor in the developing primary palate. *J Dent Res* **75**, 1534-1539.

Ianowski JP, Choi JY, Wine JJ & Hanrahan JW. (2007). Mucus secretion by single tracheal submucosal glands from normal and cystic fibrosis transmembrane conductance regulator knockout mice. *J Physiol* **580**, 301-314.

Ichikawa J & Kiyohara T. (2001). Suppression of EGF-induced cell proliferation by the blockade of Ca²⁺ mobilization and capacitative Ca²⁺ entry in mouse mammary epithelial cells. *Cell Biochem Funct* **19**, 213-219.

Ignoul S & Eggermont J. (2005). CBS domains: structure, function, and pathology in human proteins. *Am J Physiol Cell Physiol* **289**, C1369-1378.

Illman SA, Lohi J & Keski-Oja J. (2008). Epilysin (MMP-28)--structure, expression and potential functions. *Exp Dermatol* **17**, 897-907.

Imai K & Okada Y. (2008). Purification of matrix metalloproteinases by column chromatography. *Nat Protoc* **3**, 1111-1124.

Inglis SK, Corboz MR, Taylor AE & Ballard ST. (1997). In situ visualization of bronchial submucosal glands and their secretory response to acetylcholine. *Am J Physiol* **272**, L203-210.

Ingvarsen S, Madsen DH, Hillig T, Lund LR, Holmbeck K, Behrendt N & Engelholm LH. (2008). Dimerization of endogenous MT1-MMP is a regulatory step in the activation of the 72-kDa gelatinase MMP-2 on fibroblasts and fibrosarcoma cells. *Biol Chem* **389**, 943-953.

Ivanov A, Gerzanich V, Ivanova S, Denhaese R, Tsymbalyuk O & Simard JM. (2006). Adenylate cyclase 5 and KCa1.1 channel are required for EGFR up-regulation of PCNA in native contractile rat basilar artery smooth muscle. *J Physiol* **570**, 73-84.

Iyer S, Wei S, Brew K & Acharya KR. (2007). Crystal structure of the catalytic domain of matrix metalloproteinase-1 in complex with the inhibitory domain of tissue inhibitor of metalloproteinase-1. *J Biol Chem* **282**, 364-371.

Jansen M, Bali M & Akabas MH. (2008). Modular design of Cys-loop ligand-gated ion channels: functional 5-HT3 and GABA rho1 receptors lacking the large cytoplasmic M3M4 loop. *J Gen Physiol* **131**, 137-146.

Jentsch TJ, Gunther W, Pusch M & Schwappach B. (1995). Properties of voltage-gated chloride channels of the CIC gene family. *J Physiol* **482**, 19S-25S.

Jentsch TJ, Neagoe I & Scheel O. (2005). CLC chloride channels and transporters. *Curr Opin Neurobiol* **15**, 319-325.

Jentsch TJ, Steinmeyer K & Schwarz G. (1990). Primary structure of *Torpedo marmorata* chloride channel isolated by expression cloning in *Xenopus* oocytes. *Nature* **348**, 510-514.

Jeulin C, Seltzer V, Bailbe D, Andreau K & Marano F. (2008). EGF mediates calcium-activated chloride channel activation in the human bronchial epithelial cell line 16HBE14o-: involvement of tyrosine kinase p60c-src. *Am J Physiol Lung Cell Mol Physiol* **295**, L489-496.

Jia Y, Mathews CJ & Hanrahan JW. (1997). Phosphorylation by protein kinase C is required for acute activation of cystic fibrosis transmembrane conductance regulator by protein kinase A. *J Biol Chem* **272**, 4978-4984.

Jin NG, Kim JK, Yang DK, Cho SJ, Kim JM, Koh EJ, Jung HC, So I & Kim KW. (2003). Fundamental role of CIC-3 in volume-sensitive Cl- channel function and cell volume regulation in AGS cells. *Am J Physiol Gastrointest Liver Physiol* **285**, G938-948.

Johannesson M, Bogdanovic N, Nordqvist AC, Hjelte L & Schalling M. (1997). Cystic fibrosis mRNA expression in rat brain: cerebral cortex and medial preoptic area. *Neuroreport* **8**, 535-539.

Johannesson M, Landgren BM, Csemiczky G, Hjelte L & Gottlieb C. (1998). Female patients with cystic fibrosis suffer from reproductive endocrinological disorders despite good clinical status. *Hum Reprod* **13**, 2092-2097.

Johnson J. (1935). Effect of Superior Laryngeal Nerves on Tracheal Mucus: An Experimental Study on the Relationship. *Ann Surg* **101**, 494-499.

Jones AM & Helm JM. (2009). Emerging treatments in cystic fibrosis. *Drugs* **69**, 1903-1910.

Jones N & Dumont DJ. (1999). Recruitment of Dok-R to the EGF receptor through its PTB domain is required for attenuation of Erk MAP kinase activation. *Curr Biol* **9**, 1057-1060.

Jung K. (2008). Measurement of matrix metalloproteinases and their tissue inhibitors in serum produces doubtful results. *J Infect Dis* **198**, 1722-1723; author reply 1723-1724.

Jurasz P, Sawicki G, Duszyk M, Sawicka J, Miranda C, Mayers I & Radomski MW. (2001). Matrix metalloproteinase 2 in tumor cell-induced platelet aggregation: regulation by nitric oxide. *Cancer Res* **61**, 376-382.

Kang D, Choi TH, Han K, Son D, Kim JH, Kim SH & Park J. (2008). Regulation of K(+) channels may enhance wound healing in the skin. *Med Hypotheses* **71**, 927-929.

Kaplan E, Shwachman H, Perlmutter AD, Rule A, Khaw KT & Holsclaw DS. (1968). Reproductive failure in males with cystic fibrosis. *N Engl J Med* **279**, 65-69.

Kassim SY, Gharib SA, Mecham BH, Birkland TP, Parks WC & McGuire JK. (2007). Individual matrix metalloproteinases control distinct transcriptional responses in airway epithelial cells infected with *Pseudomonas aeruginosa*. *Infect Immun* **75**, 5640-5650.

Keely SJ, Calandrella SO & Barrett KE. (2000). Carbachol-stimulated transactivation of epidermal growth factor receptor and mitogen-activated protein kinase in T(84) cells is mediated by intracellular Ca^{2+} , PYK-2, and p60(src). *J Biol Chem* **275**, 12619-12625.

Keely SJ, Uribe JM & Barrett KE. (1998). Carbachol stimulates transactivation of epidermal growth factor receptor and mitogen-activated protein kinase in T84 cells. Implications for carbachol-stimulated chloride secretion. *J Biol Chem* **273**, 27111-27117.

Kelley TJ, Thomas K, Milgram LJ & Drumm ML. (1997). In vivo activation of the cystic fibrosis transmembrane conductance regulator mutant deltaF508 in murine nasal epithelium. *Proc Natl Acad Sci U S A* **94**, 2604-2608.

Kim S & Nadel JA. (2009). Fibrinogen binding to ICAM-1 promotes EGFR-dependent mucin production in human airway epithelial cells. *Am J Physiol Lung Cell Mol Physiol* **297**, L174-183.

Knowles MR, Church NL, Waltner WE, Yankaskas JR, Gilligan P, King M, Edwards LJ, Helms RW & Boucher RC. (1990). A pilot study of aerosolized amiloride for the treatment of lung disease in cystic fibrosis. *N Engl J Med* **322**, 1189-1194.

Kobayashi S, Kondo S & Juni K. (1995). Permeability of peptides and proteins in human cultured alveolar A549 cell monolayer. *Pharm Res* **12**, 1115-1119.

Kobeticova K, Bezchlebova J, Lana J, Sochova I & Hofman J. (2008). Toxicity of four nitrogen-heterocyclic polycyclic aromatic hydrocarbons (NPAHs) to soil organisms. *Ecotoxicol Environ Saf*.

Koide M, Penar PL, Tranmer BI & Wellman GC. (2007). Heparin-binding EGF-like growth factor mediates oxyhemoglobin-induced suppression of voltage-dependent potassium channels in rabbit cerebral artery myocytes. *Am J Physiol Heart Circ Physiol* **293**, H1750-1759.

Koyama N, Kashimata M, Sakashita H, Sakagami H & Gresik EW. (2003). EGF-stimulated signaling by means of PI3K, PLCgamma1, and PKC isozymes regulates branching morphogenesis of the fetal mouse submandibular gland.

Kreda SM, Mall M, Mengos A, Rochelle L, Yankaskas J, Riordan JR & Boucher RC. (2005). Characterization of wild-type and deltaF508 cystic fibrosis transmembrane regulator in human respiratory epithelia. *Mol Biol Cell* **16**, 2154-2167.

Krouse ME, Talbott JF, Lee MM, Joo NS & Wine JJ. (2004). Acid and base secretion in the Calu-3 model of human serous cells. *Am J Physiol Lung Cell Mol Physiol* **287**, L1274-1283.

Kuhse J, Betz H & Kirsch J. (1995). The inhibitory glycine receptor: architecture, synaptic localization and molecular pathology of a postsynaptic ion-channel complex. *Curr Opin Neurobiol* **5**, 318-323.

Kuhse J, Laube B, Magalei D & Betz H. (1993). Assembly of the inhibitory glycine receptor: identification of amino acid sequence motifs governing subunit stoichiometry. *Neuron* **11**, 1049-1056.

Kunzelmann K. (2001). CFTR: interacting with everything? *News Physiol Sci* **16**, 167-170.

Kunzelmann K, Kongsuphol P, Aldehni F, Tian Y, Ousingsawat J, Warth R & Schreiber R. (2009). Bestrophin and TMEM16-Ca(2+) activated Cl(-) channels with different functions. *Cell Calcium* **46**, 233-241.

Kunzelmann K, Milenkovic VM, Spitzner M, Soria RB & Schreiber R. (2007). Calcium-dependent chloride conductance in epithelia: is there a contribution by Bestrophin? *Pflugers Arch* **454**, 879-889.

Kunzelmann K, Schreiber R, Kmit A, Jantarajit W, Martins JR, Faria D, Kongsuphol P, Ousingsawat J & Tian Y. (2012). Expression and function of epithelial anoctamins. *Exp Physiol* **97**, 184-192.

Kuroda M, Murakami K & Ishikawa Y. (1987). Role of hydroxyl radicals derived from granulocytes in lung injury induced by phorbol myristate acetate. *Am Rev Respir Dis* **136**, 1435-1444.

Lai H & Rogers DF. (2010). New pharmacotherapy for airway mucus hypersecretion in asthma and COPD: targeting intracellular signaling pathways. *J Aerosol Med Pulm Drug Deliv* **23**, 219-231.

Lavigne MC, Thakker P, Gunn J, Wong A, Miyashiro JS, Wasserman AM, Wei SQ, Pelker JW, Kobayashi M & Eppihimer MJ. (2004). Human bronchial epithelial cells express and secrete MMP-12. *Biochem Biophys Res Commun* **324**, 534-546.

Lazarowski ER & Boucher RC. (2009). Purinergic receptors in airway epithelia. *Curr Opin Pharmacol* **9**, 262-267.

Lazarowski ER, Tarran R, Grubb BR, van Heusden CA, Okada S & Boucher RC. (2004). Nucleotide release provides a mechanism for airway surface liquid homeostasis. *J Biol Chem* **279**, 36855-36864.

Leblais V, Demolombe S, Vallette G, Langin D, Baro I, Escande D & Gauthier C. (1999). beta3-adrenoceptor control the cystic fibrosis transmembrane conductance regulator through a cAMP/protein kinase A-independent pathway. *J Biol Chem* **274**, 6107-6113.

Lechapt-Zalcman E, Pruliere-Escabasse V, Advenier D, Galiacy S, Charriere-Bertrand C, Coste A, Harf A, d'Ortho MP & Escudier E. (2006). Transforming growth factor-beta1 increases airway wound repair via MMP-2 upregulation: a new pathway for epithelial wound repair? *Am J Physiol Lung Cell Mol Physiol* **290**, L1277-1282.

Lee A, Chow D, Haus B, Tseng W, Evans D, Fleiszig S, Chandy G & Machen T. (1999). Airway epithelial tight junctions and binding and cytotoxicity of *Pseudomonas aeruginosa*. *Am J Physiol* **277**, L204-217.

Lei TC, Vieira WD & Hearing VJ. (2002). In vitro migration of melanoblasts requires matrix metalloproteinase-2: implications to vitiligo therapy by photochemotherapy. *Pigment cell research / sponsored by the European Society for Pigment Cell Research and the International Pigment Cell Society* **15**, 426-432.

Leroy C, Prive A, Bourret JC, Berthiaume Y, Ferraro P & Brochiero E. (2006). Regulation of ENaC and CFTR expression with K⁺ channel modulators and effect on fluid absorption across alveolar epithelial cells. *Am J Physiol Lung Cell Mol Physiol* **291**, L1207-1219.

Levitzki A & Gazit A. (1995). Tyrosine kinase inhibition: an approach to drug development. *Science* **267**, 1782-1788.

Lewis HA, Buchanan SG, Burley SK, Conners K, Dickey M, Dorwart M, Fowler R, Gao X, Guggino WB, Hendrickson WA, Hunt JF, Kearns MC, Lorimer D, Maloney PC, Post KW, Rajashankar KR, Rutter ME, Sauder JM, Shriner S, Thibodeau PH, Thomas PJ, Zhang M, Zhao X & Emtage S. (2004). Structure of nucleotide-binding domain 1 of the cystic fibrosis transmembrane conductance regulator. *EMBO J* **23**, 282-293.

Li C, Ramjeesingh M, Wang W, Garami E, Hewryk M, Lee D, Rommens JM, Galley K & Bear CE. (1996). ATPase activity of the cystic fibrosis transmembrane conductance regulator. *J Biol Chem* **271**, 28463-28468.

Li D, Wang Z, Sun P, Jin Y, Lin DH, Hebert SC, Giebisch G & Wang WH. (2006). Inhibition of MAPK stimulates the Ca^{2+} -dependent big-conductance K-channels in cortical collecting duct. *Proc Natl Acad Sci U S A* **103**, 19569-19574.

Li X, Shimada K, Showalter LA & Weinman SA. (2000). Biophysical properties of CIC-3 differentiate it from swelling-activated chloride channels in Chinese hamster ovary-K1 cells. *J Biol Chem* **275**, 35994-35998.

Li XY, Ota I, Yana I, Sabeh F & Weiss SJ. (2008). Molecular dissection of the structural machinery underlying the tissue-invasive activity of membrane type-1 matrix metalloproteinase. *Mol Biol Cell* **19**, 3221-3233.

Liang L, MacDonald K, Schwiebert EM, Zeitlin PL & Guggino WB. (2009). Spiperone, identified through compound screening, activates calcium-dependent chloride secretion in the airway. *Am J Physiol Cell Physiol* **296**, C131-141.

Lieberman J. (1968). Dornase aerosol effect on sputum viscosity in cases of cystic fibrosis. *JAMA* **205**, 312-313.

Liebmann C. (2011). EGF receptor activation by GPCRs: an universal pathway reveals different versions. *Mol Cell Endocrinol* **331**, 222-231.

Liedtke CM & Cole TS. (1998). Antisense oligonucleotide to PKC-epsilon alters cAMP-dependent stimulation of CFTR in Calu-3 cells. *Am J Physiol* **275**, C1357-1364.

Liedtke CM, Hubbard M & Wang X. (2003). Stability of actin cytoskeleton and PKC-delta binding to actin regulate NKCC1 function in airway epithelial cells. *Am J Physiol Cell Physiol* **284**, C487-496.

Lin CC, Tseng HW, Hsieh HL, Lee CW, Wu CY, Cheng CY & Yang CM. (2008). Tumor necrosis factor-alpha induces MMP-9 expression via p42/p44 MAPK, JNK, and nuclear factor-kappaB in A549 cells. *Toxicol Appl Pharmacol* **229**, 386-398.

Lindstad RI, Sylte I, Mikalsen SO, Seglen PO, Berg E & Winberg JO. (2005). Pancreatic trypsin activates human promatrix metalloproteinase-2. *J Mol Biol* **350**, 682-698.

Linsdell P, Tabcharani JA, Rommens JM, Hou YX, Chang XB, Tsui LC, Riordan JR & Hanrahan JW. (1997). Permeability of wild-type and mutant cystic fibrosis transmembrane conductance regulator chloride channels to polyatomic anions. *J Gen Physiol* **110**, 355-364.

Loewen ME & Forsyth GW. (2005). Structure and function of CLCA proteins. *Physiol Rev* **85**, 1061-1092.

Macara IG. (1986). Activation of 45Ca²⁺ influx and 22Na⁺/H⁺ exchange by epidermal growth factor and vanadate in A431 cells is independent of phosphatidylinositol turnover and is inhibited by phorbol ester and diacylglycerol. *J Biol Chem* **261**, 9321-9327.

Mackenzie AB, Chirakkal H & North RA. (2003). Kv1.3 potassium channels in human alveolar macrophages. *Am J Physiol Lung Cell Mol Physiol* **285**, L862-868.

Madsen SS, Jensen LN, Tipsmark CK, Kiilerich P & Borsig RJ. (2007). Differential regulation of cystic fibrosis transmembrane conductance regulator and Na⁺,K⁺-ATPase in gills of striped bass, Morone saxatilis: effect of salinity and hormones. *J Endocrinol* **192**, 249-260.

Maille E, Trinh NT, Prive A, Bilodeau C, Bissonnette E, Grandvaux N & Brochiero E. (2011a). Regulation of normal and cystic fibrosis airway epithelial repair processes by TNF-alpha after injury. *Am J Physiol Lung Cell Mol Physiol* **301**, L945-955.

Maille E, Trinh NT, Prive A, Bilodeau C, Bissonnette E, Grandvaux N & Brochiero E. (2011b). Regulation of normal and cystic fibrosis airway epithelial repair processes by TNF{alpha} after injury. *Am J Physiol Lung Cell Mol Physiol*.

Mak JC, Chuang TT, Harris CA & Barnes PJ. (2002). Increased expression of G protein-coupled receptor kinases in cystic fibrosis lung. *Eur J Pharmacol* **436**, 165-172.

Mall M, Gonska T, Thomas J, Schreiber R, Seydewitz HH, Kuehr J, Brandis M & Kunzelmann K. (2003). Modulation of Ca²⁺-activated Cl⁻ secretion by basolateral K⁺ channels in human normal and cystic fibrosis airway epithelia. *Pediatr Res* **53**, 608-618.

Manoury B, Nenan S, Guenon I, Lagente V & Boichot E. (2007). Influence of early neutrophil depletion on MMPs/TIMP-1 balance in bleomycin-induced lung fibrosis. *Int Immunopharmacol* **7**, 900-911.

Manoury B, Tamuleviciute A & Tammaro P. (2010). TMEM16A/anoctamin 1 protein mediates calcium-activated chloride currents in pulmonary arterial smooth muscle cells. *J Physiol* **588**, 2305-2314.

Marino CR, Matovcik LM, Gorelick FS & Cohn JA. (1991). Localization of the cystic fibrosis transmembrane conductance regulator in pancreas. *J Clin Invest* **88**, 712-716.

Marsey LL & Winpenny JP. (2009). Bestrophin expression and function in the human pancreatic duct cell line, CFPAC-1. *J Physiol* **587**, 2211-2224.

Martins JR, Kongsuphol P, Sammels E, Dahimene S, Aldehni F, Clarke LA, Schreiber R, de Smedt H, Amaral MD & Kunzelmann K. (2011). F508del-CFTR increases intracellular Ca(2+) signaling that causes enhanced calcium-dependent Cl(-) conductance in cystic fibrosis. *Biochim Biophys Acta* **1812**, 1385-1392.

Massova I, Kotra LP, Fridman R & Mobashery S. (1998). Matrix metalloproteinases: structures, evolution, and diversification. *FASEB J* **12**, 1075-1095.

Matos JE, Sausbier M, Beranek G, Sausbier U, Ruth P & Leipziger J. (2007). Role of cholinergic-activated KCa1.1 (BK), KCa3.1 (SK4) and KV7.1 (KCNQ1) channels in mouse colonic Cl⁻ secretion. *Acta Physiol (Oxf)* **189**, 251-258.

Matsui H, Davis CW, Tarran R & Boucher RC. (2000). Osmotic water permeabilities of cultured, well-differentiated normal and cystic fibrosis airway epithelia. *J Clin Invest* **105**, 1419-1427.

Matsui H, Grubb BR, Tarran R, Randell SH, Gatzky JT, Davis CW & Boucher RC. (1998). Evidence for periciliary liquid layer depletion, not abnormal ion composition, in the pathogenesis of cystic fibrosis airways disease. *Cell* **95**, 1005-1015.

McCole DF & Barrett KE. (2009). Decoding epithelial signals: critical role for the epidermal growth factor receptor in controlling intestinal transport function. *Acta Physiol (Oxf)* **195**, 149-159.

McCole DF, Keely SJ, Coffey RJ & Barrett KE. (2002). Transactivation of the epidermal growth factor receptor in colonic epithelial cells by carbachol requires extracellular release of transforming growth factor-alpha. *J Biol Chem* **277**, 42603-42612.

McCoy KS, Quittner AL, Oermann CM, Gibson RL, Retsch-Bogart GZ & Montgomery AB. (2008). Inhaled aztreonam lysine for chronic airway *Pseudomonas aeruginosa* in cystic fibrosis. *Am J Respir Crit Care Med* **178**, 921-928.

Mercer BA, Lemaitre V, Powell CA & D'Armiento J. (2006). The Epithelial Cell in Lung Health and Emphysema Pathogenesis. *Curr Respir Med Rev* **2**, 101-142.

Merigo F, Benati D, Di Chio M, Osculati F & Sbarbati A. (2007). Secretory cells of the airway express molecules of the chemoreceptive cascade. *Cell Tissue Res* **327**, 231-247.

Meyer S & Dutzler R. (2006). Crystal structure of the cytoplasmic domain of the chloride channel CIC-0. *Structure* **14**, 299-307.

Meyrick B, Sturgess JM & Reid L. (1969). A reconstruction of the duct system and secretory tubules of the human bronchial submucosal gland. *Thorax* **24**, 729-736.

Miledi R. (1982). A calcium-dependent transient outward current in *Xenopus laevis* oocytes. *Proc R Soc Lond B Biol Sci* **215**, 491-497.

Milenkovic VM, Brockmann M, Stohr H, Weber BH & Strauss O. (2010). Evolution and functional divergence of the anoctamin family of membrane proteins. *BMC Evol Biol* **10**, 319.

Milenkovic VM, Soria RB, Aldehni F, Schreiber R & Kunzelmann K. (2009). Functional assembly and purinergic activation of bestrophins. *Pflugers Arch* **458**, 431-441.

Miller C. (1982). Open-state substructure of single chloride channels from Torpedo electroplax. *Philos Trans R Soc Lond B Biol Sci* **299**, 401-411.

Miller TL, Zhu Y, Markwardt S, Singhaus CJ, Chidekel AS & Shaffer TH. (2008). Dissociation between the effects of oxygen and pressure on matrix metalloproteinase-2, -7, and -9 expression in human airway epithelial cells. *Am J Perinatol* **25**, 481-489.

Mirastschijski U, Haaksma CJ, Tomasek JJ & Agren MS. (2004). Matrix metalloproteinase inhibitor GM 6001 attenuates keratinocyte migration, contraction and myofibroblast formation in skin wounds. *Exp Cell Res* **299**, 465-475.

Mohammad-Panah R, Demolombe S, Riochet D, Leblais V, Loussouarn G, Pollard H, Baro I & Escande D. (1998). Hyperexpression of recombinant CFTR in heterologous cells alters its physiological properties. *Am J Physiol* **274**, C310-318.

Moolenaar WH, Aerts RJ, Tertoolen LG & de Laat SW. (1986). The epidermal growth factor-induced calcium signal in A431 cells. *J Biol Chem* **261**, 279-284.

Moon S, Singh M, Krouse ME & Wine JJ. (1997). Calcium-stimulated Cl⁻ secretion in Calu-3 human airway cells requires CFTR. *Am J Physiol* **273**, L1208-1219.

Morse DM, Smullen JL & Davis CW. (2001). Differential effects of UTP, ATP, and adenosine on ciliary activity of human nasal epithelial cells. *Am J Physiol Cell Physiol* **280**, C1485-1497.

Mort JS & Billington CJ. (2001). Articular cartilage and changes in arthritis: matrix degradation. *Arthritis Res* **3**, 337-341.

Mortensen J, Hansen A, Falk M, Nielsen IK & Groth S. (1993). Reduced effect of inhaled beta 2-adrenergic agonists on lung mucociliary clearance in patients with cystic fibrosis. *Chest* **103**, 805-811.

Moser SL, Harron SA, Crack J, Fawcett JP & Cowley EA. (2008). Multiple KCNQ potassium channel subtypes mediate basal anion secretion from the human airway epithelial cell line Calu-3. *J Membr Biol* **221**, 153-163.

Mroz MS & Keely SJ. (2012). Epidermal Growth Factor Chronically Upregulates Ca²⁺-Dependent Cl⁻ Conductance and TMEM16A Expression in Intestinal Epithelial Cells. *J Physiol*.

Muanprasat C, Sonawane ND, Salinas D, Taddei A, Galietta LJ & Verkman AS. (2004). Discovery of glycine hydrazide pore-occluding CFTR inhibitors:

mechanism, structure-activity analysis, and in vivo efficacy. *J Gen Physiol* **124**, 125-137.

Munaron L. (2002). Calcium signalling and control of cell proliferation by tyrosine kinase receptors (review). *Int J Mol Med* **10**, 671-676.

Mundhenk L, Alfalah M, Elble RC, Pauli BU, Naim HY & Gruber AD. (2006). Both cleavage products of the mCLCA3 protein are secreted soluble proteins. *J Biol Chem* **281**, 30072-30080.

Murphy G, Knauper V, Atkinson S, Butler G, English W, Hutton M, Stracke J & Clark I. (2002). Matrix metalloproteinases in arthritic disease. *Arthritis Res* **4 Suppl 3**, S39-49.

Nakahara H, Howard L, Thompson EW, Sato H, Seiki M, Yeh Y & Chen WT. (1997). Transmembrane/cytoplasmic domain-mediated membrane type 1-matrix metalloprotease docking to invadopodia is required for cell invasion. *Proc Natl Acad Sci U S A* **94**, 7959-7964.

Namkung W, Finkbeiner WE & Verkman AS. (2010). CFTR-adenylyl cyclase I association responsible for UTP activation of CFTR in well-differentiated primary human bronchial cell cultures. *Mol Biol Cell* **21**, 2639-2648.

Namkung W, Phuan PW & Verkman AS. (2011). TMEM16A inhibitors reveal TMEM16A as a minor component of calcium-activated chloride channel conductance in airway and intestinal epithelial cells. *J Biol Chem* **286**, 2365-2374.

Naren AP, Cobb B, Li C, Roy K, Nelson D, Heda GD, Liao J, Kirk KL, Sorscher EJ, Hanrahan J & Clancy JP. (2003). A macromolecular complex of beta 2 adrenergic receptor, CFTR, and ezrin/radixin/moesin-binding phosphoprotein 50 is regulated by PKA. *Proc Natl Acad Sci U S A* **100**, 342-346.

Naruse S, Kitagawa M, Ishiguro H, Fujiki K & Hayakawa T. (2002). Cystic fibrosis and related diseases of the pancreas. *Best Pract Res Clin Gastroenterol* **16**, 511-526.

Nesti E, Everill B & Morielli AD. (2004). Endocytosis as a mechanism for tyrosine kinase-dependent suppression of a voltage-gated potassium channel. *Mol Biol Cell* **15**, 4073-4088.

Neussert R, Muller C, Milenkovic VM & Strauss O. (2010). The presence of bestrophin-1 modulates the Ca²⁺ recruitment from Ca²⁺ stores in the ER. *Pflugers Arch* **460**, 163-175.

Noel A, Gutierrez-Fernandez A, Sounni NE, Behrendt N, Maquoi E, Lund IK, Cal S, Hoyer-Hansen G & Lopez-Otin C. (2012). New and paradoxical roles of matrix metalloproteinases in the tumor microenvironment. *Frontiers in pharmacology* **3**, 140.

O'Mahony F, Toumi F, Mroz MS, Ferguson G & Keely SJ. (2008). Induction of Na⁺/K⁺/2Cl⁻ cotransporter expression mediates chronic potentiation of intestinal epithelial Cl⁻ secretion by EGF. *Am J Physiol Cell Physiol* **294**, C1362-1370.

O'Reilly PJ, Gaggar A & Blalock JE. (2008). Interfering with extracellular matrix degradation to blunt inflammation. *Curr Opin Pharmacol* **8**, 242-248.

Oda K, Matsuoka Y, Funahashi A & Kitano H. (2005). A comprehensive pathway map of epidermal growth factor receptor signaling. *Mol Syst Biol* **1**, 2005 0010.

Okamoto T, Murayama Y, Hayashi Y, Inagaki M, Ogata E & Nishimoto I. (1991). Identification of a Gs activator region of the beta 2-adrenergic receptor that is autoregulated via protein kinase A-dependent phosphorylation. *Cell* **67**, 723-730.

Oliynyk I, Varelogianni G, Roomans GM & Johannesson M. (2010). Effect of duramycin on chloride transport and intracellular calcium concentration in cystic fibrosis and non-cystic fibrosis epithelia. *APMIS* **118**, 982-990.

Onishi-Haraikawa Y, Funaki M, Gotoh N, Shibuya M, Inukai K, Katagiri H, Fukushima Y, Anai M, Ogihara T, Sakoda H, Ono H, Kikuchi M, Oka Y & Asano T. (2001). Unique phosphorylation mechanism of Gab1 using PI 3-kinase as an adaptor protein. *Biochem Biophys Res Commun* **288**, 476-482.

Oppenheimer EA, Case AL, Esterly JR & Rothberg RM. (1970). Cervical mucus in cystic fibrosis: a possible cause of infertility. *American journal of obstetrics and gynecology* **108**, 673-674.

Ousingsawat J, Martins JR, Schreiber R, Rock JR, Harfe BD & Kunzelmann K. (2009). Loss of TMEM16A causes a defect in epithelial Ca²⁺-dependent chloride transport. *J Biol Chem* **284**, 28698-28703.

Pai VB & Nahata MC. (2001). Efficacy and safety of aerosolized tobramycin in cystic fibrosis. *Pediatr Pulmonol* **32**, 314-327.

Palmer ML, Lee SY, Maniak PJ, Carlson D, Fahrenkrug SC & O'Grady SM. (2006). Protease-activated receptor regulation of Cl⁻ secretion in Calu-3 cells requires prostaglandin release and CFTR activation. *Am J Physiol Cell Physiol* **290**, C1189-1198.

Palosaari H, Pennington CJ, Larmas M, Edwards DR, Tjaderhane L & Salo T. (2003). Expression profile of matrix metalloproteinases (MMPs) and tissue inhibitors of MMPs in mature human odontoblasts and pulp tissue. *Eur J Oral Sci* **111**, 117-127.

Pawlowski K, Lepisto M, Meinander N, Sivars U, Varga M & Wieslander E. (2006). Novel conserved hydrolase domain in the CLCA family of alleged calcium-activated chloride channels. *Proteins* **63**, 424-439.

Pelletier M, Lavastre V & Girard D. (2002). Activation of human epithelial lung a549 cells by the pollutant sodium sulfite: enhancement of neutrophil adhesion. *Toxicol Sci* **69**, 210-216.

Peppelenbosch MP, Tertoolen LG & de Laat SW. (1991). Epidermal growth factor-activated calcium and potassium channels. *J Biol Chem* **266**, 19938-19944.

Pettit RS & Johnson CE. (2011). Airway-rehydrating agents for the treatment of cystic fibrosis: past, present, and future. *Ann Pharmacother* **45**, 49-59.

Pifferi S, Dibattista M & Menini A. (2009). TMEM16B induces chloride currents activated by calcium in mammalian cells. *Pflugers Arch* **458**, 1023-1038.

Pilewski JM & Frizzell RA. (1999). Role of CFTR in airway disease. *Physiol Rev* **79**, S215-255.

Pirila E, Korpi JT, Korkiamaki T, Jahkola T, Gutierrez-Fernandez A, Lopez-Otin C, Saarialho-Kere U, Salo T & Sorsa T. (2007). Collagenase-2 (MMP-8) and matrilysin-2 (MMP-26) expression in human wounds of different etiologies. *Wound Repair Regen* **15**, 47-57.

Poitras L, Jean S, Islam N & Moss T. (2003). PAK interacts with NCK and MLK2 to regulate the activation of jun N-terminal kinase. *FEBS Lett* **543**, 129-135.

Poulsen JH, Fischer H, Illek B & Machen TE. (1994). Bicarbonate conductance and pH regulatory capability of cystic fibrosis transmembrane conductance regulator. *Proc Natl Acad Sci U S A* **91**, 5340-5344.

Prenzel N, Fischer OM, Streit S, Hart S & Ullrich A. (2001). The epidermal growth factor receptor family as a central element for cellular signal transduction and diversification. *Endocr Relat Cancer* **8**, 11-31.

Puechal X, Fajac I, Bienvenu T, Desmazes-Dufeu N, Hubert D, Kaplan JC, Menkes CJ & Dusser DJ. (1999). Increased frequency of cystic fibrosis deltaF508 mutation in bronchiectasis associated with rheumatoid arthritis. *Eur Respir J* **13**, 1281-1287.

Pusch M, Ludewig U, Rehfeldt A & Jentsch TJ. (1995). Gating of the voltage-dependent chloride channel CIC-0 by the permeant anion. *Nature* **373**, 527-531.

Qu Z, Han X, Cui Y & Li C. (2010). A PI3 kinase inhibitor found to activate bestrophin 3. *J Cardiovasc Pharmacol* **55**, 110-115.

Qu Z & Hartzell HC. (2008). Bestrophin Cl⁻ channels are highly permeable to HCO₃⁻. *Am J Physiol Cell Physiol* **294**, C1371-1377.

Radpour R, Gourabi H, Dizaj AV, Holzgreve W & Zhong XY. (2008). Genetic investigations of CFTR mutations in congenital absence of vas deferens, uterus, and vagina as a cause of infertility. *J Androl* **29**, 506-513.

Ratjen F & Doring G. (2003). Cystic fibrosis. *Lancet* **361**, 681-689.

Ratjen F, Hartog CM, Paul K, Wermelt J & Braun J. (2002). Matrix metalloproteases in BAL fluid of patients with cystic fibrosis and their modulation by treatment with dornase alpha. *Thorax* **57**, 930-934.

Rauer H, Lanigan MD, Pennington MW, Aiyar J, Ghanshani S, Cahalan MD, Norton RS & Chandy KG. (2000). Structure-guided transformation of charybdotoxin yields an analog that selectively targets Ca(2+)-activated over voltage-gated K(+) channels. *J Biol Chem* **275**, 1201-1208.

Ray S, Misso NL, Lenzo JC, Robinson C & Thompson PJ. (1999). Gamma-glutamylcysteine synthetase activity in human lung epithelial (A549) cells: factors influencing its measurement. *Free radical biology & medicine* **27**, 1346-1356.

Remillard CV, Lupien MA, Crepeau V & Leblanc N. (2000). Role of Ca²⁺- and swelling-activated Cl⁻ channels in alpha1-adrenoceptor-mediated tone in pressurized rabbit mesenteric arterioles. *Cardiovasc Res* **46**, 557-568.

Restrepo-Hartwig MA & Ahlquist P. (1996). Brome mosaic virus helicase- and polymerase-like proteins colocalize on the endoplasmic reticulum at sites of viral RNA synthesis. *J Virol* **70**, 8908-8916.

Riordan JR, Rommens JM, Kerem B, Alon N, Rozmahel R, Grzelczak Z, Zielenski J, Lok S, Plavsic N, Chou JL & et al. (1989). Identification of the cystic fibrosis gene: cloning and characterization of complementary DNA. *Science* **245**, 1066-1073.

Robay A, Toumaniantz G, Leblais V & Gauthier C. (2005). Transfected beta3- but not beta2-adrenergic receptors regulate cystic fibrosis transmembrane conductance regulator activity via a new pathway involving the mitogen-activated protein kinases extracellular signal-regulated kinases. *Mol Pharmacol* **67**, 648-654.

Rock JR, O'Neal WK, Gabriel SE, Randell SH, Harfe BD, Boucher RC & Grubb BR. (2009). Transmembrane protein 16A (TMEM16A) is a Ca²⁺-regulated Cl⁻ secretory channel in mouse airways. *J Biol Chem* **284**, 14875-14880.

Rodgers HC & Knox AJ. (1999). The effect of topical benzamil and amiloride on nasal potential difference in cystic fibrosis. *Eur Respir J* **14**, 693-696.

Roomi MW, Monterrey JC, Kalinovsky T, Rath M & Niedzwiecki A. (2009). Patterns of MMP-2 and MMP-9 expression in human cancer cell lines. *Oncol Rep* **21**, 1323-1333.

Rosenfeld MA, Yoshimura K, Trapnell BC, Yoneyama K, Rosenthal ER, Dalemans W, Fukayama M, Bargon J, Stier LE, Stratford-Perricaudet L & et al. (1992). In vivo transfer of the human cystic fibrosis transmembrane conductance regulator gene to the airway epithelium. *Cell* **68**, 143-155.

Roth EK, Hirtz S, Duerr J, Wenning D, Eichler I, Seydewitz HH, Amaral MD & Mall MA. (2011). The K⁺ channel opener 1-EBIO potentiates residual function of mutant CFTR in rectal biopsies from cystic fibrosis patients. *PLoS One* **6**, e24445.

Roux J, Carles M, Koh H, Goolaerts A, Ganter MT, Chesebro BB, Howard M, Houseman BT, Finkbeiner W, Shokat KM, Paquet AC, Matthay MA & Pittet JF.

(2010). Transforming growth factor beta1 inhibits cystic fibrosis transmembrane conductance regulator-dependent cAMP-stimulated alveolar epithelial fluid transport via a phosphatidylinositol 3-kinase-dependent mechanism. *J Biol Chem* **285**, 4278-4290.

Sagel SD, Kapsner RK & Osberg I. (2005). Induced sputum matrix metalloproteinase-9 correlates with lung function and airway inflammation in children with cystic fibrosis. *Pediatr Pulmonol* **39**, 224-232.

Sampson HM, Robert R, Liao J, Matthes E, Carlile GW, Hanrahan JW & Thomas DY. (2011). Identification of a NBD1-binding pharmacological chaperone that corrects the trafficking defect of F508del-CFTR. *Chemistry & biology* **18**, 231-242.

Santiskulvong C & Rozengurt E. (2003). Galardin (GM 6001), a broad-spectrum matrix metalloproteinase inhibitor, blocks bombesin- and LPA-induced EGF receptor transactivation and DNA synthesis in rat-1 cells. *Exp Cell Res* **290**, 437-446.

Santos MC, de Souza AP, Gerlach RF, Trevilatto PC, Scarel-Caminaga RM & Line SR. (2004). Inhibition of human pulpal gelatinases (MMP-2 and MMP-9) by zinc oxide cements. *J Oral Rehabil* **31**, 660-664.

Savitski AN, Mesaros C, Blair IA, Cohen NA & Kreindler JL. (2009). Secondhand smoke inhibits both Cl⁻ and K⁺ conductances in normal human bronchial epithelial cells. *Respir Res* **10**, 120.

Schneider F, Kemmner W, Haensch W, Franke G, Gretschel S, Karsten U & Schlag PM. (2001). Overexpression of sialyltransferase CMP-sialic acid:Galbeta1,3GalNAc-R alpha6-Sialyltransferase is related to poor patient survival in human colorectal carcinomas. *Cancer Res* **61**, 4605-4611.

Schreiber R, Uliyakina I, Kongsuphol P, Warth R, Mirza M, Martins JR & Kunzelmann K. (2010). Expression and function of epithelial anoctamins. *J Biol Chem* **285**, 7838-7845.

Schroeder BC, Cheng T, Jan YN & Jan LY. (2008). Expression cloning of TMEM16A as a calcium-activated chloride channel subunit. *Cell* **134**, 1019-1029.

Schwake M, Friedrich T & Jentsch TJ. (2001). An internalization signal in CIC-5, an endosomal Cl⁻ channel mutated in dent's disease. *J Biol Chem* **276**, 12049-12054.

Scott-Ward TS, Li H, Schmidt A, Cai Z & Sheppard DN. (2004). Direct block of the cystic fibrosis transmembrane conductance regulator Cl(-) channel by niflumic acid. *Mol Membr Biol* **21**, 27-38.

Seavilleklein G, Amer N, Evangelidis A, Chappe F, Irvine T, Hanrahan JW & Chappe V. (2008). PKC phosphorylation modulates PKA-dependent binding of the R domain to other domains of CFTR. *Am J Physiol Cell Physiol* **295**, C1366-1375.

Sermet-Gaudelus I, Boeck KD, Casimir GJ, Vermeulen F, Leal T, Mogenet A, Roussel D, Fritsch J, Hanssens L, Hirawat S, Miller NL, Constantine S, Reha A, Ajayi T, Elfring GL & Miller LL. (2010). Ataluren (PTC124) induces cystic fibrosis transmembrane conductance regulator protein expression and activity in children with nonsense mutation cystic fibrosis. *Am J Respir Crit Care Med* **182**, 1262-1272.

Shamsuddin AK, Reddy MM & Quinton PM. (2008). Iontophoretic beta-adrenergic stimulation of human sweat glands: possible assay for cystic fibrosis transmembrane conductance regulator activity in vivo. *Exp Physiol* **93**, 969-981.

Shan J, Liao J, Huang J, Robert R, Palmer ML, Fahrenkrug SC, O'Grady SM & Hanrahan JW. (2012). Bicarbonate-dependent chloride transport drives fluid secretion by the human airway epithelial cell line Calu-3. *J Physiol* **590**, 5273-5297.

Shen BQ, Finkbeiner WE, Wine JJ, Mrsny RJ & Widdicombe JH. (1994). Calu-3: a human airway epithelial cell line that shows cAMP-dependent Cl- secretion. *Am J Physiol* **266**, L493-501.

Shen BQ, Mrsny RJ, Finkbeiner WE & Widdicombe JH. (1995). Role of CFTR in chloride secretion across human tracheal epithelium. *Am J Physiol* **269**, L561-566.

Sheppard DN & Welsh MJ. (1999). Structure and function of the CFTR chloride channel. *Physiol Rev* **79**, S23-45.

Shimada K, Li X, Xu G, Nowak DE, Showalter LA & Weinman SA. (2000). Expression and canalicular localization of two isoforms of the CIC-3 chloride channel from rat hepatocytes. *Am J Physiol Gastrointest Liver Physiol* **279**, G268-276.

Shute J, Marshall L, Bodey K & Bush A. (2003). Growth factors in cystic fibrosis - when more is not enough. *Paediatr Respir Rev* **4**, 120-127.

Smith JJ, Travis SM, Greenberg EP & Welsh MJ. (1996). Cystic fibrosis airway epithelia fail to kill bacteria because of abnormal airway surface fluid. *Cell* **85**, 229-236.

Smith JJ & Welsh MJ. (1992). cAMP stimulates bicarbonate secretion across normal, but not cystic fibrosis airway epithelia. *J Clin Invest* **89**, 1148-1153.

Sozeri O, Vollmer K, Liyanage M, Frith D, Kour G, Mark GE, 3rd & Stabel S. (1992). Activation of the c-Raf protein kinase by protein kinase C phosphorylation. *Oncogene* **7**, 2259-2262.

Springman EB, Angleton EL, Birkedal-Hansen H & Van Wart HE. (1990). Multiple modes of activation of latent human fibroblast collagenase: evidence for the role of a Cys73 active-site zinc complex in latency and a "cysteine switch" mechanism for activation. *Proc Natl Acad Sci U S A* **87**, 364-368.

Srivastava A, Romanenko VG, Gonzalez-Begne M, Catalan MA & Melvin JE. (2008). A variant of the Ca²⁺-activated Cl⁻ channel Best3 is expressed in mouse exocrine glands. *J Membr Biol* **222**, 43-54.

Stamenkovic I. (2003). Extracellular matrix remodelling: the role of matrix metalloproteinases. *J Pathol* **200**, 448-464.

Stanich JE, Gibbons SJ, Eisenman ST, Bardsley MR, Rock JR, Harfe BD, Ordog T & Farrugia G. (2011). Ano1 as a regulator of proliferation. *Am J Physiol Gastrointest Liver Physiol* **301**, G1044-1051.

Stanton JB, Goldberg AF, Hoppe G, Marmorstein LY & Marmorstein AD. (2006). Hydrodynamic properties of porcine bestrophin-1 in Triton X-100. *Biochim Biophys Acta* **1758**, 241-247.

Stephan AB, Shum EY, Hirsh S, Cygnar KD, Reisert J & Zhao H. (2009). ANO2 is the ciliary calcium-activated chloride channel that may mediate olfactory amplification. *Proc Natl Acad Sci U S A* **106**, 11776-11781.

Stobrawa SM, Breiderhoff T, Takamori S, Engel D, Schweizer M, Zdebik AA, Bosl MR, Ruether K, Jahn H, Draguhn A, Jahn R & Jentsch TJ. (2001). Disruption of CIC-3, a chloride channel expressed on synaptic vesicles, leads to a loss of the hippocampus. *Neuron* **29**, 185-196.

Stock P, Akbari O, DeKruyff RH & Umetsu DT. (2005). Respiratory tolerance is inhibited by the administration of corticosteroids. *J Immunol* **175**, 7380-7387.

Stohr H, Heisig JB, Benz PM, Schoberl S, Milenkovic VM, Strauss O, Aartsen WM, Wijnholds J, Weber BH & Schulz HL. (2009). TMEM16B, a novel protein with calcium-dependent chloride channel activity, associates with a presynaptic protein complex in photoreceptor terminals. *J Neurosci* **29**, 6809-6818.

Storey N, Latchman D & Bevan S. (2002). Selective internalization of sodium channels in rat dorsal root ganglion neurons infected with herpes simplex virus-1. *J Cell Biol* **158**, 1251-1262.

Stryjek-Kaminska D, Piiper A & Zeuzem S. (1996). Epidermal growth factor regulates adenylate cyclase activity via Gs and Gi1-2 proteins in pancreatic acinar membranes. *Biochem J* **316 (Pt 1)**, 87-91.

Sugrue RJ, Brown C, Brown G, Aitken J & Mc LRHW. (2001). Furin cleavage of the respiratory syncytial virus fusion protein is not a requirement for its transport to the surface of virus-infected cells. *J Gen Virol* **82**, 1375-1386.

Sukkar MB, Stanley AJ, Blake AE, Hodgkin PD, Johnson PR, Armour CL & Hughes JM. (2004). 'Proliferative' and 'synthetic' airway smooth muscle cells are overlapping populations. *Immunol Cell Biol* **82**, 471-478.

Sun H, Seyer JM & Patel TB. (1995). A region in the cytosolic domain of the epidermal growth factor receptor antithetically regulates the stimulatory and inhibitory guanine nucleotide-binding regulatory proteins of adenylyl cyclase. *Proc Natl Acad Sci U S A* **92**, 2229-2233.

Sun H, Tsunenari T, Yau KW & Nathans J. (2002). The vitelliform macular dystrophy protein defines a new family of chloride channels. *Proc Natl Acad Sci U S A* **99**, 4008-4013.

Sun Y, Chen M, Lowentritt BH, Van Zijl PS, Koch KR, Keay S, Simard JM & Chai TC. (2007). EGF and HB-EGF modulate inward potassium current in human bladder urothelial cells from normal and interstitial cystitis patients. *Am J Physiol Cell Physiol* **292**, C106-114.

Sweeney C & Carraway KL, 3rd. (2000). Ligand discrimination by ErbB receptors: differential signaling through differential phosphorylation site usage. *Oncogene* **19**, 5568-5573.

Szkotak AJ, Murthy M, MacVinish LJ, Duszyk M & Cuthbert AW. (2004). 4-Chlorobenzo[F]isoquinoline (CBIQ) activates CFTR chloride channels and KCNN4 potassium channels in Calu-3 human airway epithelial cells. *Br J Pharmacol* **142**, 531-542.

Sznajder JI, Ridge KM, Yeates DB, Ilekis J & Olivera W. (1998). Epidermal growth factor increases lung liquid clearance in rat lungs. *J Appl Physiol* **85**, 1004-1010.

Tai CF & Baraniuk JN. (2002). Upper airway neurogenic mechanisms. *Curr Opin Allergy Clin Immunol* **2**, 11-19.

Takeyama K, Tamaoki J, Chiyotani A, Sakai N, Kanemura T & Konno K. (1993). [Stimulation of ciliary motility by beta 3-adrenoceptor agonist rabbit tracheal epithelium]. *Kokyū To Jūkan* **41**, 993-997.

Tamaoki J, Chiyotani A, Sakai N & Konno K. (1993). Stimulation of ciliary motility mediated by atypical beta-adrenoceptor in canine bronchial epithelium. *Life Sci* **53**, 1509-1515.

Tanaka H, Miyazaki N, Oashi K, Tanaka S, Ohmichi M & Abe S. (2000). Sputum matrix metalloproteinase-9: tissue inhibitor of metalloproteinase-1 ratio in acute asthma. *J Allergy Clin Immunol* **105**, 900-905.

Tavee J & Zhou L. (2009). Small fiber neuropathy: A burning problem. *Cleve Clin J Med* **76**, 297-305.

The Cystic Fibrosis Genetic Analysis Consortium. (1994). Population variation of common cystic fibrosis mutations. The Cystic Fibrosis Genetic Analysis Consortium. *Hum Mutat* **4**, 167-177.

Thiemann A, Grunder S, Pusch M & Jentsch TJ. (1992). A chloride channel widely expressed in epithelial and non-epithelial cells. *Nature* **356**, 57-60.

Tian YC, Chen YC, Chang CT, Hung CC, Wu MS, Phillips A & Yang CW. (2007). Epidermal growth factor and transforming growth factor-beta1 enhance HK-2 cell migration through a synergistic increase of matrix metalloproteinase and sustained activation of ERK signaling pathway. *Exp Cell Res* **313**, 2367-2377.

Timmreck LS, Gray MR, Handelin B, Allito B, Rohlfis E, Davis AJ, Gidwani G & Reindollar RH. (2003). Analysis of cystic fibrosis transmembrane conductance

regulator gene mutations in patients with congenital absence of the uterus and vagina. *Am J Med Genet A* **120A**, 72-76.

Tizzano EF, Chitayat D & Buchwald M. (1993). Cell-specific localization of CFTR mRNA shows developmentally regulated expression in human fetal tissues. *Hum Mol Genet* **2**, 219-224.

Tkaczyk C, Beaven MA, Brachman SM, Metcalfe DD & Gilfillan AM. (2003). The phospholipase C gamma 1-dependent pathway of Fc epsilon RI-mediated mast cell activation is regulated independently of phosphatidylinositol 3-kinase. *J Biol Chem* **278**, 48474-48484.

Tod H. (1917). Pin in Bronchiole of Posterior Lobe of Right Lung. *Proc R Soc Med* **10**, 90-93.

Tos M. (1966). Development of the tracheal glands in man. Number, density, structure, shape, and distribution of mucous glands elucidated by quantitative studies of whole mounts. *Acta Pathol Microbiol Scand* **68**, Suppl 185:183+.

Toumi F, Frankson M, Ward JB, Kelly OB, Mroz MS, Bertelsen LS & Keely SJ. (2011). Chronic regulation of colonic epithelial secretory function by activation of G protein-coupled receptors. *Neurogastroenterol Motil* **23**, 178-186, e143.

Trinh NT, Prive A, Kheir L, Bourret JC, Hijazi T, Amraei MG, Noel J & Brochiero E. (2007). Involvement of KATP and KvLQT1 K⁺ channels in EGF-stimulated alveolar epithelial cell repair processes. *Am J Physiol Lung Cell Mol Physiol* **293**, L870-882.

Trinh NT, Prive A, Maille E, Noel J & Brochiero E. (2008). EGF and K⁺ channel activity control normal and cystic fibrosis bronchial epithelia repair. *Am J Physiol Lung Cell Mol Physiol* **295**, L866-880.

Tsunenari T, Nathans J & Yau KW. (2006). Ca²⁺-activated Cl⁻ current from human bestrophin-4 in excised membrane patches. *J Gen Physiol* **127**, 749-754.

Uribe JM, Keely SJ, Traynor-Kaplan AE & Barrett KE. (1996). Phosphatidylinositol 3-kinase mediates the inhibitory effect of epidermal growth factor on calcium-dependent chloride secretion. *J Biol Chem* **271**, 26588-26595.

Uribe JM, McCole DF & Barrett KE. (2002). Interferon-gamma activates EGF receptor and increases TGF-alpha in T84 cells: implications for chloride secretion. *Am J Physiol Gastrointest Liver Physiol* **283**, G923-931.

van der Merwe JQ, Hollenberg MD & MacNaughton WK. (2008). EGF receptor transactivation and MAP kinase mediate proteinase-activated receptor-2-induced chloride secretion in intestinal epithelial cells. *Am J Physiol Gastrointest Liver Physiol* **294**, G441-451.

van der Schans C, Prasad A & Main E. (2000). Chest physiotherapy compared to no chest physiotherapy for cystic fibrosis. *Cochrane Database Syst Rev*, CD001401.

Van Goor F, Hadida S, Grootenhuis PD, Burton B, Cao D, Neuberger T, Turnbull A, Singh A, Joubran J, Hazlewood A, Zhou J, McCartney J, Arumugam V, Decker C, Yang J, Young C, Olson ER, Wine JJ, Frizzell RA, Ashlock M & Negulescu P. (2009). Rescue of CF airway epithelial cell function in vitro by a CFTR potentiator, VX-770. *Proc Natl Acad Sci U S A* **106**, 18825-18830.

Van Goor F, Hadida S, Grootenhuis PD, Burton B, Stack JH, Straley KS, Decker CJ, Miller M, McCartney J, Olson ER, Wine JJ, Frizzell RA, Ashlock M & Negulescu PA. (2011). Correction of the F508del-CFTR protein processing defect in vitro by the investigational drug VX-809. *Proc Natl Acad Sci U S A* **108**, 18843-18848.

Vastiau A, Cao L, Jaspers M, Owsianik G, Janssens V, Cuppens H, Goris J, Nilius B & Cassiman JJ. (2005). Interaction of the protein phosphatase 2A with the regulatory domain of the cystic fibrosis transmembrane conductance regulator channel. *FEBS Lett* **579**, 3392-3396.

Vergani P, Lockless SW, Nairn AC & Gadsby DC. (2005). CFTR channel opening by ATP-driven tight dimerization of its nucleotide-binding domains. *Nature* **433**, 876-880.

Verkman AS. (2001). Lung disease in cystic fibrosis: is airway surface liquid composition abnormal? *Am J Physiol Lung Cell Mol Physiol* **281**, L306-308.

Visse R & Nagase H. (2003). Matrix metalloproteinases and tissue inhibitors of metalloproteinases: structure, function, and biochemistry. *Circ Res* **92**, 827-839.

Walker LC, Venglarik CJ, Aubin G, Weatherly MR, McCarty NA, Lesnick B, Ruiz F, Clancy JP & Sorscher EJ. (1997). Relationship between airway ion transport and a mild pulmonary disease mutation in CFTR. *Am J Respir Crit Care Med* **155**, 1684-1689.

Wallace RJ, Newbold CJ & McKain N. (1996). Inhibition by 1,10-phenanthroline of the breakdown of peptides by rumen bacteria and protozoa. *The Journal of applied bacteriology* **80**, 425-430.

Wang D, Sun Y, Zhang W & Huang P. (2008). Apical adenosine regulates basolateral Ca²⁺-activated potassium channels in human airway Calu-3 epithelial cells. *Am J Physiol Cell Physiol* **294**, C1443-1453.

Wang H, Peters N & Schwarze J. (2006). Plasmacytoid dendritic cells limit viral replication, pulmonary inflammation, and airway hyperresponsiveness in respiratory syncytial virus infection. *J Immunol* **177**, 6263-6270.

Wang L, Chen L & Jacob TJ. (2000). The role of CIC-3 in volume-activated chloride currents and volume regulation in bovine epithelial cells demonstrated by antisense inhibition. *J Physiol* **524 Pt 1**, 63-75.

Wang YX & Kotlikoff MI. (1997). Inactivation of calcium-activated chloride channels in smooth muscle by calcium/calmodulin-dependent protein kinase. *Proc Natl Acad Sci U S A* **94**, 14918-14923.

Ward CL, Omura S & Kopito RR. (1995). Degradation of CFTR by the ubiquitin-proteasome pathway. *Cell* **83**, 121-127.

Weaver AK, Liu X & Sontheimer H. (2004). Role for calcium-activated potassium channels (BK) in growth control of human malignant glioma cells. *J Neurosci Res* **78**, 224-234.

West JB. (1995). *Respiratory physiology-- the essentials*. Williams & Wilkins, Baltimore.

Westerman EM, Le Brun PP, Touw DJ, Frijlink HW & Heijerman HG. (2004). Effect of nebulized colistin sulphate and colistin sulphomethate on lung function in patients with cystic fibrosis: a pilot study. *J Cyst Fibros* **3**, 23-28.

Weston SA & Parish CR. (1990). New fluorescent dyes for lymphocyte migration studies. Analysis by flow cytometry and fluorescence microscopy. *Journal of immunological methods* **133**, 87-97.

Weylandt KH, Valverde MA, Nobles M, Raguz S, Amey JS, Diaz M, Nastrucci C, Higgins CF & Sardini A. (2001). Human CIC-3 is not the swelling-activated chloride channel involved in cell volume regulation. *J Biol Chem* **276**, 17461-17467.

Widdicombe JG. (2003). Overview of neural pathways in allergy and asthma. *Pulm Pharmacol Ther* **16**, 23-30.

Wilschanski M, Miller LL, Shoseyov D, Blau H, Rivlin J, Aviram M, Cohen M, Armoni S, Yaakov Y, Pugatch T, Cohen-Cymberknob M, Miller NL, Reha A, Northcutt VJ, Hirawat S, Donnelly K, Elfring GL, Ajayi T & Kerem E. (2011). Chronic ataluren (PTC124) treatment of nonsense mutation cystic fibrosis. *Eur Respir J* **38**, 59-69.

Wine JJ. (1999). The genesis of cystic fibrosis lung disease. *J Clin Invest* **103**, 309-312.

Winton HL, Wan H, Cannell MB, Gruenert DC, Thompson PJ, Garrod DR, Stewart GA & Robinson C. (1998a). Cell lines of pulmonary and non-pulmonary origin as tools to study the effects of house dust mite proteinases on the regulation of epithelial permeability. *Clin Exp Allergy* **28**, 1273-1285.

Winton HL, Wan H, Cannell MB, Thompson PJ, Garrod DR, Stewart GA & Robinson C. (1998b). Class specific inhibition of house dust mite proteinases which cleave cell adhesion, induce cell death and which increase the permeability of lung epithelium. *Br J Pharmacol* **124**, 1048-1059.

Xu J, Benyon RC, Leir SH, Zhang S, Holgate ST & Lackie PM. (2002). Matrix metalloproteinase-2 from bronchial epithelial cells induces the proliferation of subepithelial fibroblasts. *Clin Exp Allergy* **32**, 881-888.

Xu X, Chen Z, Wang Y, Bonewald L & Steffensen B. (2007). Inhibition of MMP-2 gelatinolysis by targeting exodomain-substrate interactions. *Biochem J* **406**, 147-155.

Xu Y, Krause A, Hamai H, Harvey BG, Worgall TS & Worgall S. (2010). Proinflammatory phenotype and increased caveolin-1 in alveolar macrophages with silenced CFTR mRNA. *PLoS One* **5**, e11004.

Xue H, Zhang YL, Liu GS & Wang H. (2005). A new ATP-sensitive potassium channel opener protects the kidney from hypertensive damage in spontaneously hypertensive rats. *J Pharmacol Exp Ther* **315**, 501-509.

Yang H, Sun X, Wang Z, Ning G, Zhang F, Kong J, Lu L & Reinach PS. (2003). EGF stimulates growth by enhancing capacitative calcium entry in corneal epithelial cells. *J Membr Biol* **194**, 47-58.

Yang YD, Cho H, Koo JY, Tak MH, Cho Y, Shim WS, Park SP, Lee J, Lee B, Kim BM, Raouf R, Shin YK & Oh U. (2008). TMEM16A confers receptor-activated calcium-dependent chloride conductance. *Nature* **455**, 1210-1215.

Yarden Y & Sliwkowski MX. (2001). Untangling the ErbB signalling network. *Nature reviews Molecular cell biology* **2**, 127-137.

Yerxa BR, Sabater JR, Davis CW, Stutts MJ, Lang-Furr M, Picher M, Jones AC, Cowlen M, Dougherty R, Boyer J, Abraham WM & Boucher RC. (2002). Pharmacology of INS37217 [P(1)-(uridine 5')-P(4)-(2'-deoxycytidine 5')tetraphosphate, tetrasodium salt], a next-generation P2Y(2) receptor agonist for the treatment of cystic fibrosis. *J Pharmacol Exp Ther* **302**, 871-880.

Yu Y, Nair BG & Patel TB. (1992). Epidermal growth factor stimulates cAMP accumulation in cultured rat cardiac myocytes. *J Cell Physiol* **150**, 559-567.

Zhao KQ, Xiong G, Wilber M, Cohen NA & Kreindler JL. (2011). A role for two-pore K⁺ channels in modulating Na⁺ absorption and Cl⁻ secretion in normal human bronchial epithelial cells. *Am J Physiol Lung Cell Mol Physiol*.

Zhou JG, Ren JL, Qiu QY, He H & Guan YY. (2005). Regulation of intracellular Cl⁻ concentration through volume-regulated CIC-3 chloride channels in A10 vascular smooth muscle cells. *J Biol Chem* **280**, 7301-7308.

Zhu MH, Kim TW, Ro S, Yan W, Ward SM, Koh SD & Sanders KM. (2009). A Ca(2+)-activated Cl(-) conductance in interstitial cells of Cajal linked to slow wave currents and pacemaker activity. *J Physiol* **587**, 4905-4918.